"Low Temperature Calorimetric Studies of Inclusion Compounds".

A thesis submitted for the Degree of Doctor of Philosophy of the University of London.

by

ROBERT CHARLES PEMBERTON

B.Sc., A.R.C.S.

Physical Chemistry (Cryogenics Laboratory),
Royal College of Science,
Imperial College,
London, S.W. 7.

March, 1965.

ACKNOWLEDGEMENTS.

I wish to express my sincere thanks to Dr. N.G.Parsonage for supervising this work and particularly for his assistance with heat capacity measurements.

I am also indebted to the College Technical Staff for their co-operation in the construction of certain items of apparatus and to my fellow students for useful discussions.

British Petroleum Ltd., also provided hydrocarbon samples of high purity for which I thank them, and a maintainance grant from the Department of Scientific and Industrial Research over the period 1961 - 1964 is gratefully acknowledged.

Robert C. Pemberton.



ABSTRACT

The heat capacities (Cp) of the n-decane, n-dodecane, n-hexadecane, n-eicosane, n-pentadecane and 2 -methyl-pentadecane adducts of urea have been measured between 12^{o} - 300^{o} K. All these adducts show a small excess heat absorption with a maximum at 16.2 $\pm$ o.1 K and, with the exception of the 2-methyl-pentadecane compound, a sharp co-operative transition having a maximum in the temperature range 110^{o} to 190^{o}K. The transition temperatures (Tc), enthalpies(Δ H) and entropies (Δ S) of transitionper mole of adducted hydrocarbon are reported. These increase with the length of the hydrocarbon chain along smooth curves except for the odd membered C_{15} H_{32} homologuefor which Tc is higher and ΔH and Δ S lower than expected from the even hydrocarbon series. The hexadecane adduct is also found to be exceptional in showing a subsidiary maximum below the main anomaly peak.

A possible interpretation of the cause of these transitions is given and a pseudo 3-dimensional model of the system proposed which treats the end-end interactions of hydrocarbon molecules along the urea channels exactly by the Ising model and the weaker lateral hydrocarbon-hydrocarbon interactions by the Weiss approximation,

The reorientation of the hydrocarbon molecules between two energetically favourable sites is considered in the presence of a helical crystaline field arising from the urea lattice.

Computed values of the configurational partition function and long range order parameters for this system as a function of temperature were obtained and values of the theoretical transition temperatures, free energies and heat capacities are presented.

Prior to heat capacity measurements two platinum resistance thermometers were constructed and calibrated by the intercomparison method against a standard thermometer (A) on the National Bureau of Standards Provisional Temperature Scale from 12° - 90° K and on the International Temperature Scale (1955) from 90° - 312°K.

The reliability of (A) and of the temperature scale established for the working thermometer (C) has been confirmed by determinations of the ice point and oxygen boiling point resistances, the latter being found by oxygen vapour pressure measurements in the range 73° - 91°K.

As a check on the absolute accuracy of heat capacity measurements Cp determinations for a standard thermochemical substance (benzoic acid) have been made

over six temperature ranges between 12° to 286°K. The results are compared with data from the National Bureau of Standards and other laboratories.

CONTENTS

Page

Title

Acknowledgements 1

Abstract 2

Contents 5

PART A: Introduction

Chapter I:

I(a) General historical background. 9
I(b) The urea and thiourea inclusion compounds. 11
I(c) The objects of this thesis. 13
I( ) X-ray structure determination of the urea adducts. 14
I(e) The position of the hydrocarbon molecules in the hexagonal urea lattice. 22
I(f) Composition of the urea adducts. 23
I(g) Thermodynamic studies. 24
I(h) Nuclear magnetic resonance studies. 29
I(i) Dielectric absorption studies. 34
I(j) Infra red spectra. 40
I(k) Investigations of molecular motion in inclusion compounds other than the urea adducts. 43

PART B: Experimental
Chapter II: Apparatus

II(a) The adiabatic calorimeter. 48
II(b) The cryostat and calorimeter. 50
II(c) Filling the calorimeter. 57
II(d) The calorimeter heater. 58
II(e) The platinum resistance thermometers. 59
II(f) The radiation shield assembly. 61
II(g) The differential thermocouples. 62
II(h) The electric leads to the measuring circuits. 65

Page

Chapter III: Apparatus (Continued). The electrical measuring circuits.

III(a) The differential thermocouple circuit. 66
III(b) Differential thermocouple control during runs. 68
III(c) The thermometer circuit. 69
III(d) The calorimeter heater circuit. 75
III(e) The shield heater circuits. 78

Chapter IV: Apparatus (Continued).

IV(a) The vacuum line and auxillary apparatus. 81
IV(b) The vibration free manometer used in the oxygen vapour pressure measurements. 83

Chapter V: The platinum resistance thermometer calibration.

V(a) Note on temperature scales. 85
V(b) Calibration of platinum resistance thermometers (B) and (C). 89
V(c) Technique of calibration. 91
V(d) Treatment of the intercomparison results. 92
V(e) Determination of the ice point resistance of the standard thermometer(A) and working thermometers (B) and (C). 96

Chapter VI: Oxygen vapour pressure measurements

VI(a) Apparatus. 100
VI(b) Experimental procedure. 100
VI(c) The reliability of the temperature scale established for thermometer (C). 104

Chapter VII: The technique of heat capacity measurement.

VII(a) Experimental procedure. 108
VII(b) The energy input measurements. 117
VII(c) The calculation of energy input. 119
VII(d) Evaluation of heat capacity from experimental data for a specimen point. 122

Page

Chapter VIII: The heat capacity of the empty calorimeter.

VIII(a) The determination and results of the empty calorimeter heat capacity. 131

Chapter IX: Heat capacity measurements on a standard thermodynamic substance.

IX(a) The heat capacity of benzoic acid. 141
IX(b) The factors affecting the accuracy of the calorimetric measurements. 150

Chapter X: The urea adduct samples

X(a) Preparation. 158
X(b) Analysis of the adducts. 162

PART C: Results

Chapter XI: Results of the heat capacity determinations.

XI(a) Results for six urea-hydrocarbon adducts. 171

PART D: Discussion

Chapter XII:

XII(a) General description of the experimental heat capacity curves. 201
XII(b) The low temperature anomaly. 208
XII(c) The co-operative "high temperature" anomalies. 214
XII(d) The origin of the "high temperature" anomalies. 233
XII(e) The excess energy absorption in the region 220-250° K. 236

Page

Chapter XIII: The Intermolecular forces present in the adducts.

XIII(a) The interaction between the urea crystaline field and the adducted n-paraffins. 238

XIII(b) Characteristics of the computed urea-hydrocarbon potential energy. 261

XIII(c) The interaction between neighbouring hydrocarbon molecules in the same channel of the urea lattice. 263

XIII(d) The interaction between hydrocarbon molecules in neighbouring channels of the hexagonal urea lattice. 266

Chapter XIV: The theoretical treatment of the co-operative transitions.

XIV(a) Introduction. 277

XIV(b) The Ising-Weiss model for the n-paraffin adducts of urea. 282

XIV(c) Computed results of the Ising-Weiss model and conclusions. 292

References: 324

PART A : INTRODUCTION.

CHAPTER I.

SECTION I.(a). General Historical Background.

The preparation of the chlorine hydrate $6H_2O.(\sim)Cl_2$ by Davy[1] in 1811, in which the two component molecules are not united in whole number ratio, marked the true beginning of a wide and interesting field of chemical research - the study of non stoichiometric and inclusion compounds. Many other "complex" or "adduct" compounds as they were called in the formative years of organic chemistry were discovered in the nineteenth and early twentieth centuries including those between deoxycholic acid and other fatty acids[2], the H_2S [3], SO_2 [4], and H.COOH [5] - hydroquinone systems, nickel cyanide ammine [6] and further gas hydrates. Since then many other ß - quinol complexes with O_2 [7], HCl [8], HBr [9] and some of the rare gases [10][11] have been reported together with the picrates of polynuclear hydrocarbons[12], the triphenyl-methyl free radical compounds with paraffins [13], phenol complexes with HCl, A, Xe, CH_3Br [14] and a large number of inorganic complexes of the zeolite, fibrous clay and layer silicate types.

The nature of the majority of these compounds was not well understood until X-ray studies had been made. Among the notable contributions in this field are the

elucidation of the gas hydrate structures by Pauling and Marsh [15] and von Stackelberg and Muller[16][17] showing the presence of two types of cavity in which the "guest" molecules were held, and Palin and Powell's[18][19][20] work on the hydroquinone complexes which were shown to consist of two interpenetrating three dimensional networks with the quinol molecules hydrogen bonded to form approximately spherical cages. The molecules of the second component are imprisoned in this open lattice. Substances of this type were called clathrate compounds by Powell.

Further research has shown all these complex compounds to consist of a host lattice with the guest molecules contained in cavities, parallel channels, channel networks or between parallel chains or layers. The general term "inclusion compound" has been designated to such substances but the labels complex and adduct still linger and are to be found in the literature.

Possible forms of bonding between the constituent atoms of the cage structure of these compounds include, covalent bonds, metallic bonds, hydrogen bonds, dispersion or van der Waals bonds or combinations of these types. However, the binding between guest and host molecular species will depend on the nature and bonding present in each component.

SECTION I. (b). The Urea and Thiourea Inclusion compounds:

The discovery that urea forms crystalline adducts with long straight-chain hydrocarbons was made by Bengen[21] [22] in 1940 while experimenting on the use of urea to determine the fat content of milk. The closely related class of thiourea adducts formed with branched-chain paraffins, carbon tetrachloride, naphthene, camphene, etc., was reported by Fetterly[23] in 1947. The chief difference between the two series of adducts lies in the size of the cavities in the host lattice. In the urea adducts the guest molecules are situated in channels 5·3 Å in diameter running through the lattice framework whereas the thiourea has a canal of greater cross-section (6·1 Å) which is divided into zones by the large sulphur atoms. Straight-chain substances will not form stable thiourea complexes unless the chain is sufficiently long (e.g. n-paraffins with 16 or more carbon atoms form weak complexes at 0°C [24]).

The unbranched n-paraffins above hexane readily form urea adducts abeve 25° C although at lower temperatures and under pressure even n-propane[25] will form a complex. There is however, no theeretical upper limit to the length of n-paraffin chains that will complex. Bailey and France[26] have prepared urea adducts with poly etheylene oxide in which the included component has a molecular weight as high

as 4,000,000. Certain ketones, fatty acids, alcohols, esters, ethers and alkyl halides will give inclusion compounds providing the cross-sectional dimensions of the molecules are close to the channel diameter of 5·3 Å. Molecules with marginally larger cross-section, arising from a methyl side group for example, may adduct with difficulty by causing some distortion of the urea lattice. However, if the n-alkyl chain in such molecules is sufficiently long, 10-13 carbon-atoms for a single 2 - methyl side group[27] and 24 for a 2-ethyl branched species, the presence of certain side groups or even terminal cyclysation will not prevent adduction. In general, groups such as halide, phenyl, ester or carbon - carbon double bond will distort the urea lattice less when sited at the end of the paraffin chain rather than as a centrally located group or side chain. Components which form adducts with great difficulty however, (e.g. 3-methyl-heptane) can frequently be drawn into the host channels by solid solution formation in the presence of a second component which readily gives an adduct (e.g. n-decane).

Since the recognition of the importance of urea complex formation as a method of separation for branched and unsaturated hydrocarbons from straight chain components[28][29], the dewaxing of oils[30] and the commercial

separation of hydrocarbon fractions[31][32], a considerable amount of work has been reported. Other applications include the "molecular packaging" of chemicals, by which the guest molecules may be protected against reaction (i.e. oxidation or spontaneous polymerisation)[33][34], the separation of optical isomers[35], and the initiation of stereospecific polymerisations in the channels induced by high energy irradiation[36]. Their use as molecular sieves[37] and to determine the lengths and configurations of adducted molecules through analysis and comparison of their X-ray diffraction patterns with those of known configurations[38] has also been considered.

Reviews of the uses and physical and chemical properties of these and other inclusion compounds have been published by Kolbe[39], Schlenk[40], Staveley[41], McLaughlin[42], Mandelcorn[43], Child[44], Fetterly[45][46], and Cramer[47].

SECTION I.(c). The Objects of this thesis.

In this thesis the thermodynamic properties of some adducts of urea with certain paraffin hydrocarbons are studied with special reference to the inter-component bonding in so far as it affects the degrees of freedom of the included molecules.

The specific objects of the work were:

(1) To establish a temperature scale from 12° - 300° K and test its reliability.

(2) To measure the heat capacity of a standard substance (benzoic acid) and compare the results with those of the National Bureau of Standards (Washington) and thereby to establish the precision and accuracy of such determinations.

(3) To measure the heat capacities over the range 12°- 300°K of the urea adducts of n-decane, n-dodecane, n-pentadecane, n-hexadecane, eicosane and 2-methyl pentadecane and from this data to find the entropies at 298·15°K.

(4) To determine the nature and degree of interaction between the constituent molecules and the size of the resulting barriers to rotation of the guest molecules in the urea lattice channels.

(5) To interpret any transitions found during heat capacity measurements.

Various physical methods for the determination of the urea lattice structure and elucidation of the bonding between the guest and host molecules in those complexes have been reported and these are reviewed below.

SECTION I. (d). X-ray Structure Determination of the urea adducts.

X-ray investigations of the urea - n-paraffin hydrocarbon complexes have been made by Smith[48][49], Herman and

Lenné[50], Schlenk[51], Lenné[52] and Kutzelnigg et al[53].

Smith's work included both powder diagrams of adducts for a range of n-hydrocarbon chain lengths C_8-C_{50}, various straight-chain alcohols, acids, esters and a detailed structure investigations of single crystals of n-hexadecane and 1,10 - dibromodecane complexes. Similar powder patterns were obtained with each adduct. This observation has been confirmed by the present research as the powder pattern technique was used to check the absence of uncomplexed urea in the adducts prepared.

Such studies have established that urea which normally crystallises in a tetragonal form exists in these adducts as a hexagonal modification containing channels with a cross-section just sufficient to accommodate the unbranched paraffin molecules in the planar zig-zag configuration.

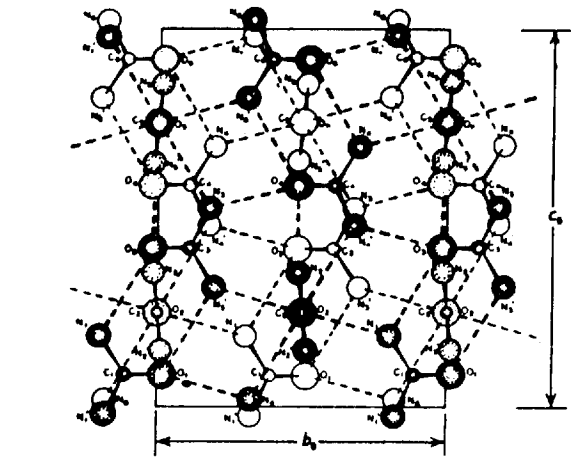
The hexagonal unit cell contains six urea molecules with a = b = 8·230 ± 0·004 Å and c = 11·005 ± 0·005 Å. Guest hydrocarbon molecules with a chain length slightly greater than an integral multiple of the urea lattice repeat unit of 11·01 Å along the channel may effectively adopt a length which is an integral multiple of this value. This occurs with the C_7, C_{16} and C_{24} hydrocarbons where the terminal methyl groups are slightly distorted by rotation

from the plane of the remaining carbon atoms thereby shortening the chain length to a multiple of 11·01 Å. This effect has been confirmed by compound analysis, the molar ratio (m) of urea to guest molecule is found to be decreased in these instances. Thus for hexadecane of chain length 22·84 Å, which is quite close to twice the "c" repeat of 11·01 Å, the adduct analysis gives m = 12·0 instead of the expected value of 12·57.

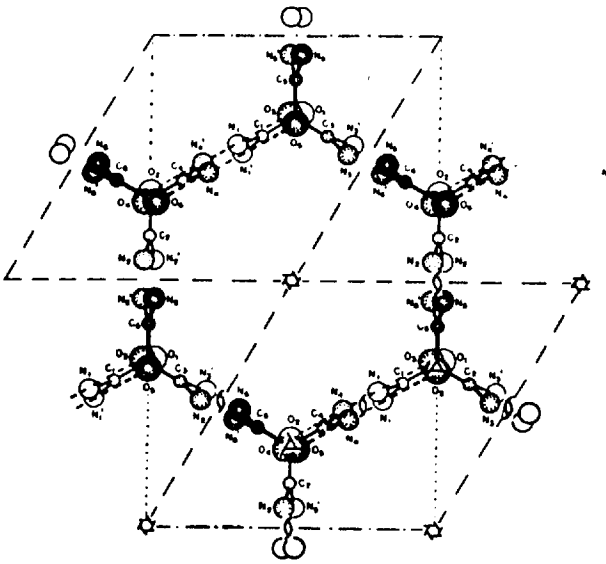
The structure of the hexadecane complex, after Smith, is illustrated in FIG. (1). Plate (1) shows a model of this structure, looking along the "b" and "c" crystallographic axes, on a scale of 2 cm = 1 Å in the actual model while the Lebold model of a heptane molecule shown in the urea lattice channel was originally of scale 1·5 cm. = 1 Å. The packing arrangement along the "c" axis is shown, together with the van der Waals packing radii, in FIG. (2).

The urea channel consists of three interpenetrating spirals of urea molecules, which are randomly either right or left hand helices, hydrogen bonded through each oxygen atom to four nitrogen atoms and through each nitrogen to two oxygen atoms. The arrangement of hydrogen bonds is shown by broken lines in FIG. (1).

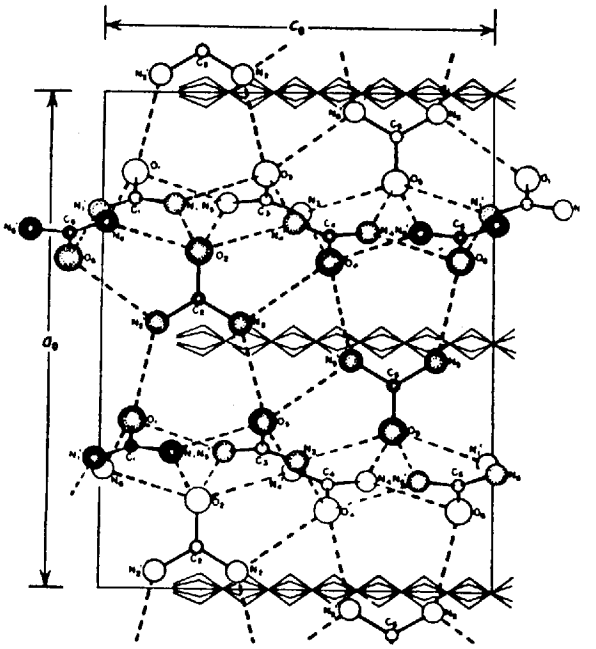
FIG. 1. The n-hexadecane - hexagonal urea structure. (After Smith 1952).



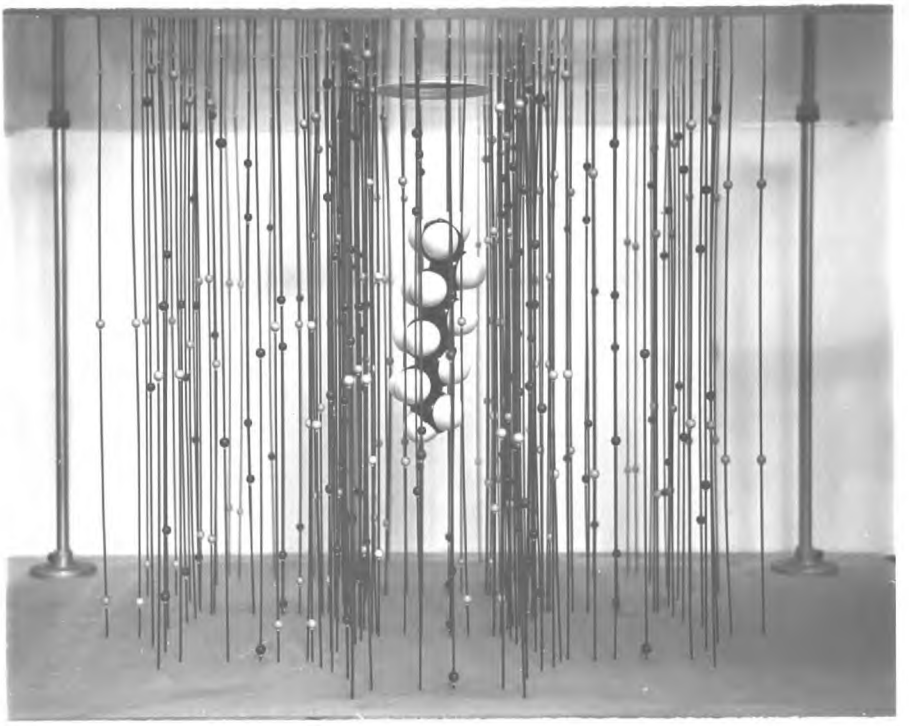
(a). Projection along the "a" axis.



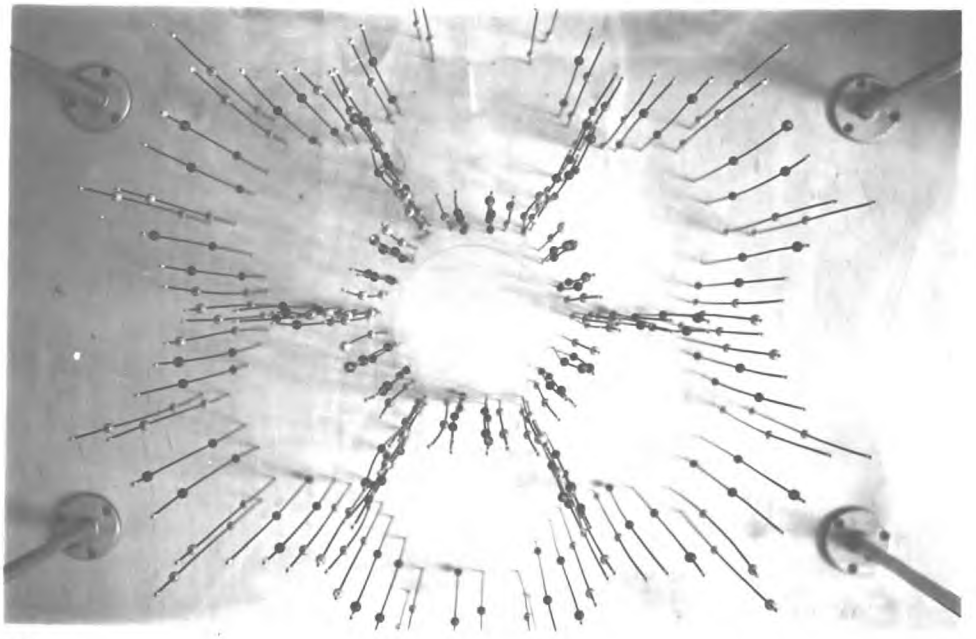
(b). Projection along the "c" axis.



(c). Projection along the "b" axis.



1.



2.

PLATE 1 .

A MODEL OF THE HEXAGONAL UREA LATTICE LOOKING ALONG (1) THE a AND (2) THE b CRYSTALOGRAPHIC AXIS.

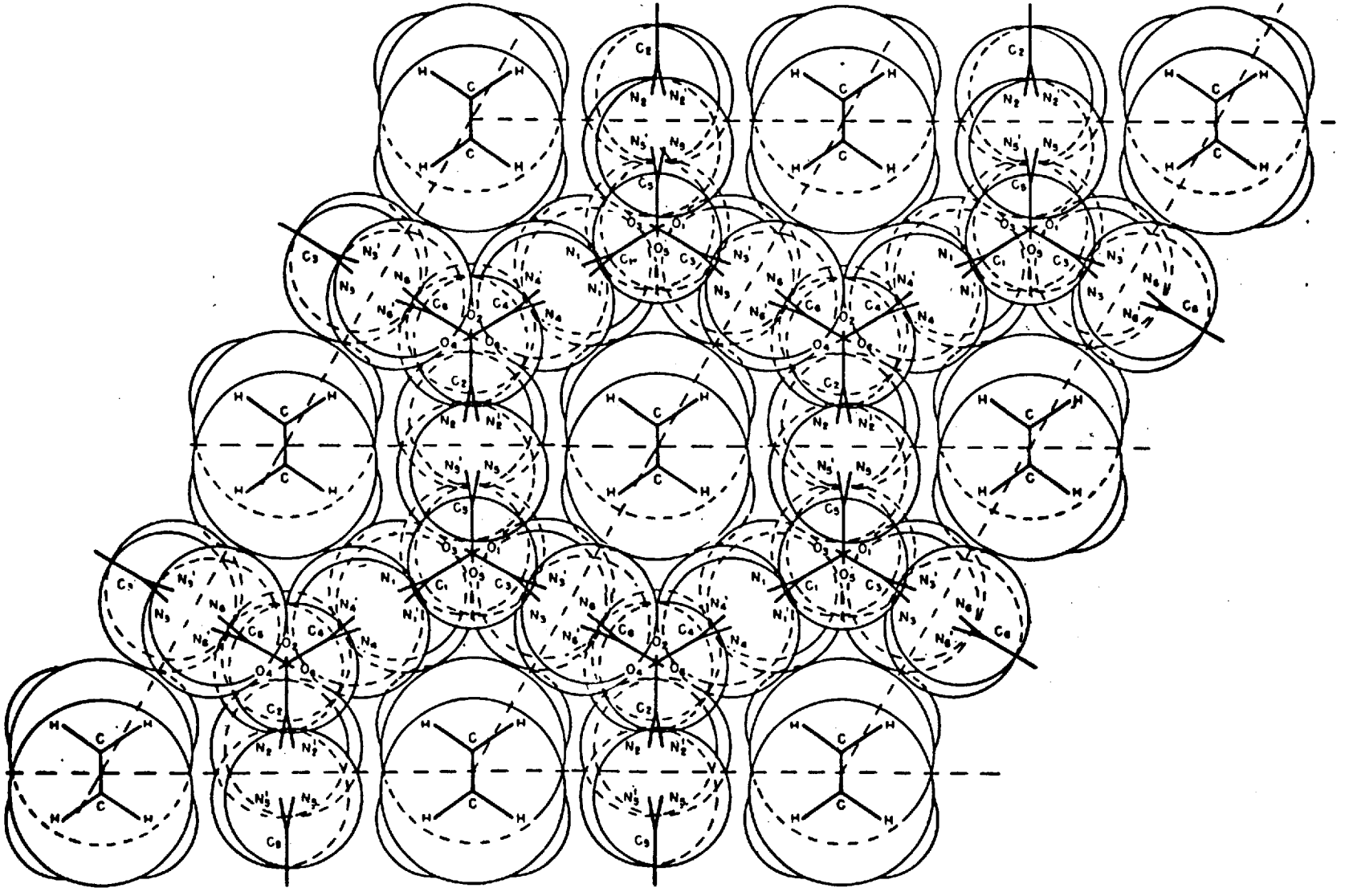


FIG. 2. VIEW ALONG THE 'c' AXIS OF THE HEXAGONAL UREA STRUCTURE SHOWING AN INCLUDED HYDROCARBON AND THE PACKING ARRANGEMENT.

The hydrogen bonds are of two types:

(a) $N_4 - H \ldots\ldots\ldots\ldots O_5$

$N_4' - H \ldots\ldots\ldots\ldots O_3$

Both 2·93 Å in length.

(b) $N_4 - H \ldots\ldots\ldots\ldots O_6$

$N_4' - H \ldots\ldots\ldots\ldots O_2$

Both 3·04 Å in length.

These hydrogen bonds are essentially coplanar with the urea molecules to which the bonded nitrogen atoms belong. This bonding arrangement results in the urea oxygen atoms being situated one above the other at a separation of 3·7 Å along each edge of the hexagonal unit cell. Further interatomic distances for the urea-hydrocarbon complex and tetragonal urea (after Wyckoff and Corey[54]) are shown in Table (1) below:

TABLE (1).

Hexagonal urea complex.		Tetragonal urea	
C – O	1·28 Å	C – O	1·25 Å
C – N	1·33	C – N	1·37
$N_1 \ldots\ldots N_1$	2·30	N.....N	2·31
$N_1 \ldots\ldots N_3$	3·55		
$N_1 - H \ldots O_2$	2·93	N – H.....O	2·98
$N_1 - H \ldots O_3$	3·04	N – H.....O	3·03

The observed shortening of the N - H....O and C - N bonds in the complex, and the C^{N}H....O bond angles of 116° and 136° closer to 120° than those in tetragonal urea which are 99° and 128° respectively, apparently suggests that the complex arrangement is possibly the more stable. However, the hexagonal urea lattice is highly unstable when the guest molecules are not present, although some investigators[55], [56][57] have postulated the existence of the "free" hexagonal form. Kyriacou reported that a sample of the acetone-urea adduct when completely thermally decomposed at 55°C gave a urea residue containing up to 5% of the hexagonal structure.

The collapse of the hexagonal form has been attributed to[34] a constricting effect of the hydrogen bonds tending to stabilise the less open tetragonal lattice once the adducted molecules have been removed. The relative stability of the urea and thiourea complexes thus involves "strong" hydrogen bonding between adjacent urea molecules and van der Waals forces between urea and the guest hydrocarbon molecules. In cases where the adducted molecule possesses a polar group additional dipole-dipole forces will be present. However, the strong hydrogen bonds of the complex can only exist when an almost inert molecule is present; these additionally stabilised bonds have been

called "supported hydrogen bonds" by Fetterly[46]:

A bonding interaction of about 2800 cal. per CH_2 group of an included n-paraffin chain was suggested by Schlenk[58] and the presence of a strong co-ordination chemical bond was proposed by Angla[59] in the case of the thiourea - $C Cl_4$ complex to explain the stability of this compound. However, the existence of bonding of the type proposed by Angla is now thought to be highly unlikely. Schlenk's value lies close to that found in the present research ($\sim$ 3000 cals. per CH_2 group) from a computation of the van der Waals interaction of various paraffins with the urea lattice.

An estimate of the energy associated with the shortening of the N - H.....O hydrogen bond has been made by Smith[49] using the data for O - H.....O bonds which are similar in nature. The observed contraction of 0·05 Å would lead to an increased bond strength of approximately 3·0 K cal. per mole of urea. This value is undoubtedly too high due to the greater strength of the O - H.....O bond but is thought to be of the order of magnitude required to stabilise the structure.

SECTION I.(e). The position of the Hydrocarbon Molecules in the Hexagonal urea lattice

From the electron-density projection Smith deduced that the interpenetrating urea spiral lattice contained the

guest hydrocarbon chains situated centrally in the channels. The occurrence of discrete spots instead of diffuse bands from reflections attributed entirely to the hydrocarbon molecules possibly indicates that these molecules are not randomly distributed along the channel. It was also concluded that the hydrocarbon atoms were not freely rotating about their long axis but randomly occupy on a statistical time average basis one of three fixed positions perpendicular to the a-axis occurring at intervals of 120° from each other.

According to Smith the terminal methyl groups of two adjacent hydrocarbon chains in the same channel are separated by about 4·1 Å which is similar to the distance found for free hydrocarbons in the solid state. However, the reliability of this figure is in some doubt since it was obtained by comparison of calculated values of hydrocarbon length, from the diffuse-band repeat distance, and that deduced for an extended planar zig-zag hydrocarbon configuration.

SECTION I. (f). Composition of the urea Adducts:

Unlike the ß -quinol clathrates the urea adducts can only exist when guest molecules fill the lattice canals completely. Consequently these inclusion compounds have a unique composition. Smith[49] has calculated the composition as a function of hydrocarbon chain length directly from the

crystallographic data. Assuming a van der Waals radius of 2·0 Å for a CH_3 group and the length (l) of a hydrocarbon molecule of n carbon atoms in the extended zig-zag planar configuration is given by:

$$l = 1{\cdot}256\ (n - 1) + 4{\cdot}0\ \text{Å}$$

then the urea / hydrocarbon mole ration (m) was found to be

$$m = 0{\cdot}6848\ (n - 1) + 2{\cdot}181.$$

The theoretical values are in good agreement with the measured compositions as found by Schlenk[58], Zimmerschied et al.[60] and Redlich et al.[61] as shown in FIG. (3).

SECTION I. (g). Thermodynamic studies.

The heat of formation for the reaction:

Complex (s) = Urea (s) + hydrocarbon (liq)

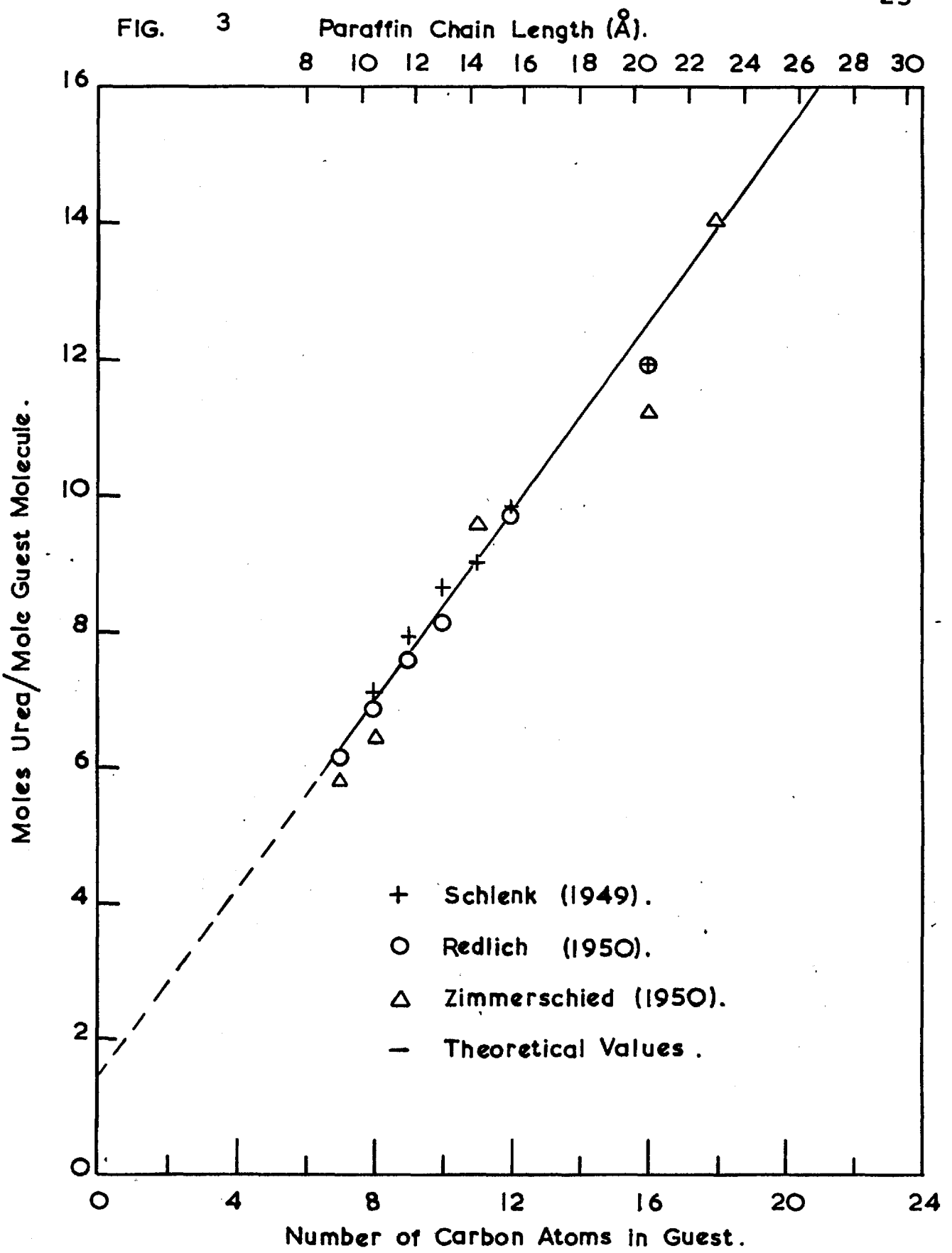
has been measured by Schlenk[62], Redlich et al.[61] and Zimmerschied et al.[60][63]. The data of Redlich are summarised in TABLE.2. below:

TABLE 2.

Adduct	Mole ratio (m) urea/reactant	ΔH K cal/Mole Hydrocarbon
n-heptane	6·1	7·3
n-octane	6·73	9·7
n-decane	8·1	13·1
n-dodecane	9·3	16·1
n-hexadecane	11·95	21·0

Similar values for the heat of decomposition were found by

FIG. 3


Paraffin Chain Length (Å).
8 10 12 14 16 18 20 22 24 26 28 30
16
14
12
10
8
6
4
2
0
Moles Urea/Mole Guest Molecule.
+ Schlenk (1949).
O Redlich (1950).
△ Zimmerschied (1950).
— Theoretical Values.
0 4 8 12 16 20 24
Number of Carbon Atoms in Guest.

McAdie[64] from differential thermal analysis measurements combined with the heat of fusion of urea[65].

Redlich postulated the approximately linear function:

$$\triangle H \text{ (liq.)} = -6{\cdot}5 + 2{\cdot}37\ m \quad \text{(K cal/mole reactant)}$$

to fit this data. However, exact proportionatity of $\triangle H$ to chain length is not found because of van der Waals end group effects and the absence of linearity of the heats of fusion and vapourisation. Subtracting the heat of fusion from $\triangle H$ (liq.) gives:

$$\triangle H \text{ (solid)} = 1{\cdot}5 + 0{\cdot}51\ m \quad \text{(K cal/mole)}$$

These results show an increase of approximately 0·5 K cal/mole of urea in the adduct or 0·3 K cal. for each additional CH_2 group with all the components in the solid state.

The equilibrium constant K for the reaction

$$\text{complex (solid)} \rightleftharpoons \text{hydrocarbon (H)} + m \text{ . urea (U)},$$

given by ,

$$K = aH \text{ . } aU^m$$

where "a" represents the activity of the various molecular species present, has been determined by Redlich et al[61].

The relationships between K and temperature and also with chain length in saturated urea solution for the n-paraffins up to and including hexadecane are shown respectively in FIG. (4) and (5). The thermal stability of the adducts increases

FIG. 4 Variation of urea adduct Equilibrium Constant with Temperature.

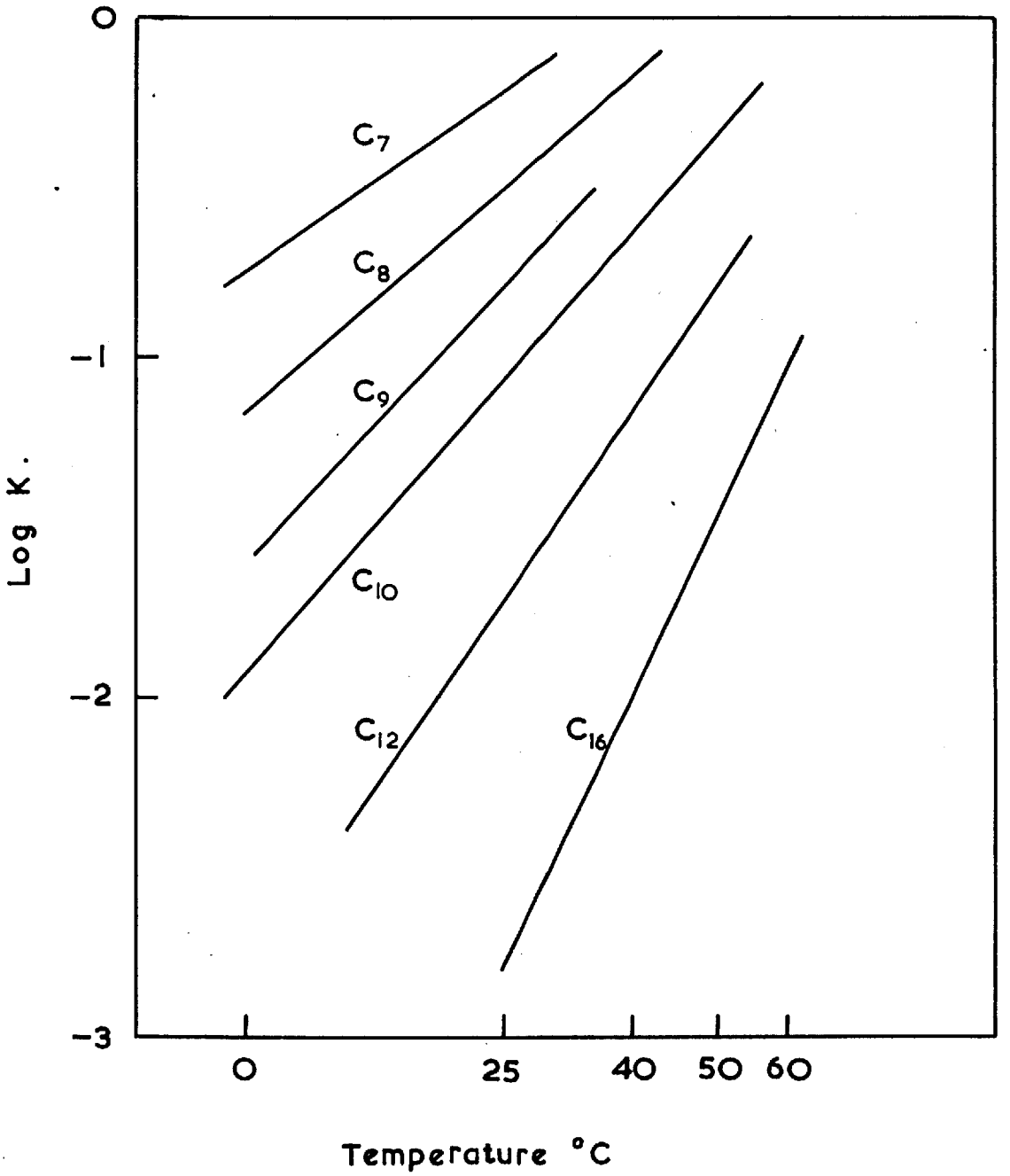
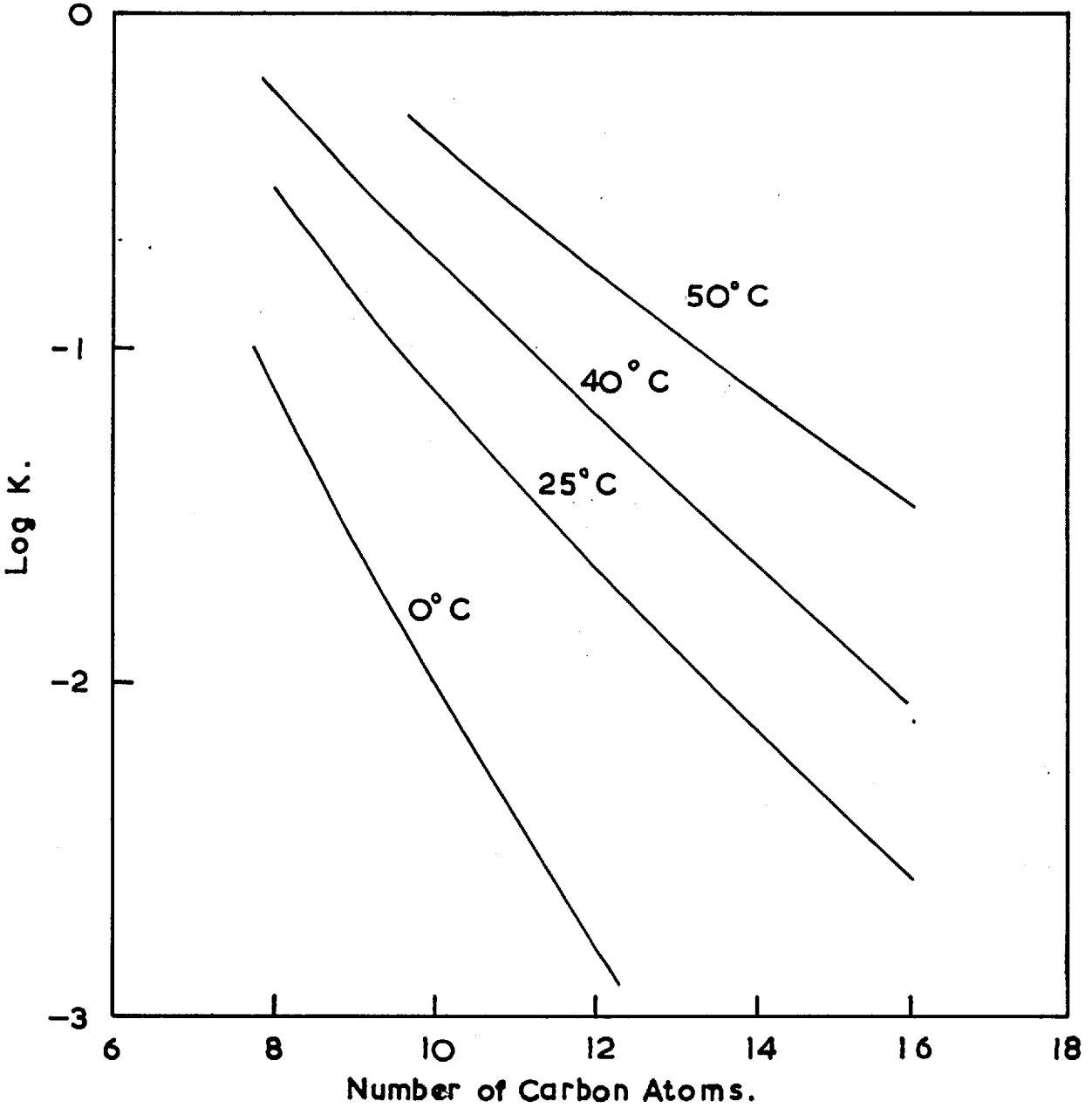


FIG. 5 Influence of Chain Length on the Equilibrium Constant of n-paraffin adducts in saturated urea solution.



concurrently with chain length and this variation is much more rapid at lower than at higher temperatures. For hydrocarbons containing fewer than seven carbon atoms adduct formation becomes rapidly thermodynamically unfavourable. The adducts below $C_{10}H_{22}$ lose hydrocarbon molecules increasingly rapidly on standing and for this reason were not included in the programme of calorimetric measurements.

SECTION I. (h). Nuclear Magnetic Resonance Studies

Gilson and McDowel[66] have studied the n.m.r. spectra of a number of urea - n-paraffin adducts, e.g. $C_7 - C_{13}$, C_{16} and C_{26} at 25°C. These adducts all had similar spectra showing a broad resonance line of 6·9 - 7·3 gauss in width due to protons of the urea cage and a narrow line 0·25 gauss wide from the enclathrated hydrocarbon molecules. Their more recent investigations[67] by wide line proton magnetic resonance on the fully deuterated urea adducts of n-tridecane and n-hexadecane from 77° to 298°K are however of greater interest as here the prime aim was to determine the degree and nature of molecular motion in those compounds.

The onset of molecular reorientation, even if only part of the molecule is involved, is revealed by a narrowing of the absorption line or decrease in the second moment when the frequency of reorientation approaches the frequency width

of the line (10^4 to 10^5 c.p.s.). However, for rotation to contribute to the heat capacity a much higher rate of re-orientation must occur (10^{10} c.p.s.). Thus the temperature at which molecular motion is detected by nuclear magnetic resonance measurements is not simply related to that found from calorimetric studies. The topic of n.m.r. studies of molecular motion in solids has been reviewed by Andrew[68][69].

The second moment for the tridecane adduct was observed to decrease from 12·6 gauss^2 at 77°K to 2·8 gauss^2 at 160°K when only a slow drop to 2·1 gauss^2 at 225°K occurred. However, a sharp fall to 0·7 gauss^2 was noticed above 225°K. Very similar behaviour was found for the hexadecane adduct (see FIG. 7.) the second moment being 15·5 gauss^2 at 77°K decreasing to 2·6 gauss^2 at 160°K and then to 1·3 gauss^2 at 200°K. Gilson and McDowell considered the following factors to contribute to the second moment:

(1) Intra-molecular interactions from the hydrocarbon chain.

(2) Inter-molecular interactions from terminal methyl groups of adjacent chains in the same channel.

(3) Inter-molecular interactions between chains in different channels.

(4) Other impurity nucleii possessing spins.

(5) Unexchanged protons in the urea lattice, unadducted hydrocarbon and occluded solvent.

On the basis of evidence from infra red investigations the presence of occluded solvent was discounted and only contributions from (1) and (2) were considered to be important. An estimate of 1 gauss^2 for contributions from terminal methyl group interactions at a separation of 4 Å and a total rigid lattice value of the second moment of 20·9 gauss^2 and 20·6 gauss^2 (from the van Vleck equation) for tridecane and hexadecane adducts respectively were made by Gilson and McDowell. As these values are far larger than those observed experimentally at 77°K a large degree of molecular freedom equivalent to an angular amptitude of oscillation of 45° and 30° for the two included hydrocarbon molecules was postulated. However, rotation of the terminal methyl groups, besides removing the inter-molecular contribution entirely, would reduce the intra-molecular second moment by 3·8 gauss^2 giving values of 16·1 gauss^2 and 15·8 gauss^2 not differing greatly from the experimental values at 77°K.

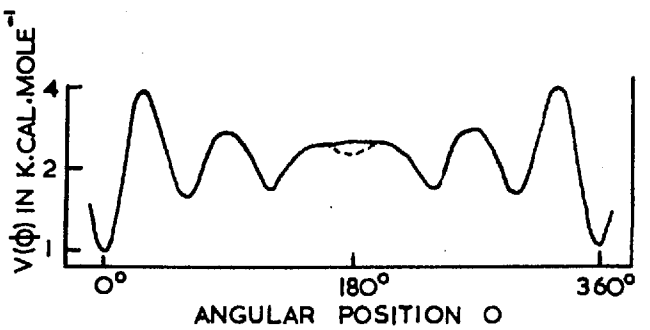
The gradual linear decrease with temperature of the second moment for pure tridecane and hexadecane, until the melting point is reached, is typical of hydrocarbons of similar chain length and some comparison can be drawn with the adducted hydrocarbons at 77°K. Here again the experimental values of 21·5 gauss^2 and 23·5 gauss^2 are well below the calculated rigid lattice second moments of 27·7 and 27·3

gauss^2 respectively and obviously the pure hydrocarbons also have a considerable degree of freedom at 77^{o}K.

The fairly rapid decrease in second moment for both adducts in the range 77^{o} to 160^{o}K has been related to an increasing degree of rotational oscillation until an amplitude of 60^{o} is reached when the motion is essentially "free". However, the motion can not be purely rotational since the intra-molecular contribution for a rotating chain is about 8·5 gauss^2 and above 100^{o}K both adduct hydrocarbons were shown by Gilson and McDowell to have moments smaller than this value. A combination of rotation, torsional oscillation, flexing and longitudinal and lateral motion in the channel was therefore suggested to account for the observed values. The discontinuity observed in the second moment for both adducts at 225^{o} - 230^{o}K is thought to result from an expansion of the urea lattice allowing greater freedom of motion for the guest hydrocarbon (see discussion).

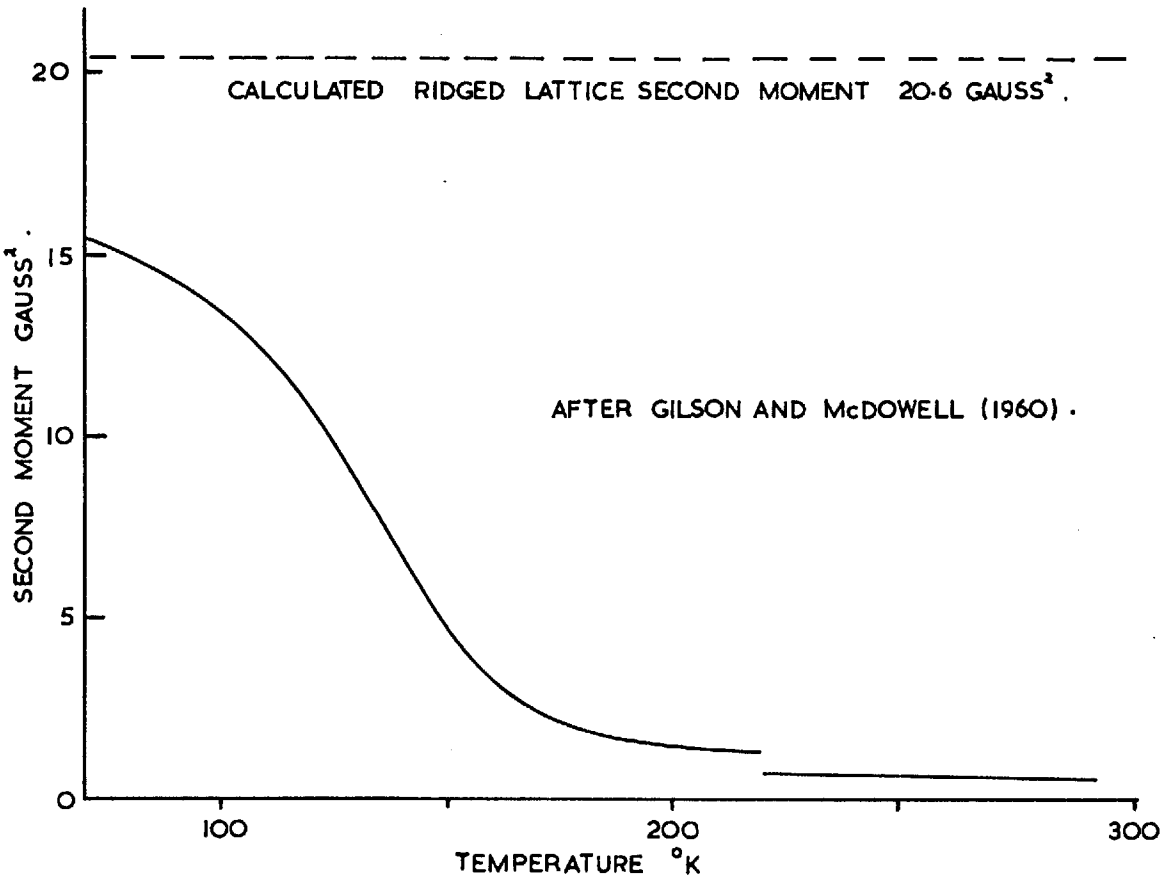
Estimation of the barrier to rotation from the variation of line width data with temperature, by the method of Gutowsky and Pake[70], gave values of 1·0 K cal/mole and 1·6 K cal/mole for the tridecane and hexadecane adducts respectively. This may be compared with the rotational barrier of approximately 3·3 K cals found for ethane and most substituted ethanes.

FIG. 6 .



POTENTIAL ENERGY V(ϕ) FOR THE POLAR GROUP OF 16 HENTRIACONTANONE IN THE HEXAGONAL UREA LATTICE AT Z=O AS A FUNCTION OF ANGULAR POSITION FROM THE EXPERIMENTAL DIELECTRIC DATA . LAURITZEN (1958) .

FIG. 7 .



VARIATION OF THE SECOND MOMENT WITH TEMPERATURE FOR THE PROTON MAGNETIC RESONANCE LINE FROM N-HEXADECANE-UREA-D_4 ADDUCT .

An extension of Gilson and McDowell's work to lower temperatures seems desirable as by 77° K the second moment is obviously already decreasing. Such measurements would give further information on the number and type of molecular interactions present by comparison with the calculated second moments for the rigid lattice.

Similar investigations for the thiourea - cyclohexane adduct show a variation of the second moment from 2·7 gauss^2 at 77°K to 0·3 gauss^2 at 298° K. That this small second moment arises largely from inter-molecular interactions and the observed decrease with temperature is due to isotropic reorientation is not doubted in this system, as the channels present are large a = 15·8 Å, c = 12·5 Å (71). However, the comparatively large sulphur atoms of the thiourea lattice produce a periodic van der Waals force along the channel and consequently the possibility of translational motion or "rattling" will be determined by the size of the guest molecule in this direction. The adducted molecule may thus become held at a potential minimum of the thiourea crystal field although oscillation and rotatory modes perpendicular to the channel may still be unhindered.

SECTION I. (i). Dielectric Absorption Studies

Meakins(72) has carried out measurements of the dielectric properties of the following urea adducts: 9-heptadecanone, 16-hentriacontanone, 18-pentatriacontanone,

methyl palmitate, didodecyl ether, 12-bromotricosane, 16-bromohentriacontane, n-octadecyl bromide, 1:10-dibromodecane and the non polar n-docosane. Large dielectric absorption at micro wave frequencies was found for all except the n-docosane adduct and therefore it was decided that the dielectric loss observed was due to reorientation of the dipoles within the retaining urea channel.

The absorption maxima occur at relatively high frequencies (between $\sim 1 \times 10^{9}$ and 3×10^{11} c.p.s.) which indicates that the potential barrier to reorientation is not large. From the similarity of the maximum absorption frequencies of the dielectric loss factors for the three ketones studied, although their chain lengths vary from 17 to 35 carbon atoms, it appears that the carbonyl group must effectively reorientate independently of the rest of the molecule. However, a second possibility arises - the almost complete restriction of interaction with the urea lattice to the region of the dipole - although this is thought to be unlikely.

The large absorption by the 1:10 dibromodecane adduct, which is known to be fully extended in the urea lattice from the X-ray measurements of Smith[49], and should therefore have an overall zero dipole moment is also unexpected. This result suggests the C-Br dipoles are capable of reorientating independently of the main carbon chain. Absorption in the 12-

bromotricosane adduct was abnormal. The absorption region was displaced to lower frequencies and this was attributed by Meakins to a greater relative barrier to dipole reorientation caused by the large area of cross-section in the region of the bromine atom. However, dielectric absorption occurred over a wide frequency range for each adduct studied and consequently Meakins proposed that more than one relaxation time was involved.

From a more detailed examination of the variation of dielectric loss with temperature in the range 197° to 293°K for some of the adducts mentioned above a partial separation into different frequency ranges was achieved. From the lower frequency part of the absorption the energy barrier to reorientation (H) was found using the equation,

$$\frac{1}{2\pi\tau} = f_{max} = A \exp(-H/kT)$$

where A is a frequency factor and T the absolute temperature. The barriers obtained are shown in the TABLE.3. below:

TABLE. 3.

Adduct	Frequency Factor (A)	Energy Barrier (K cal/Mole)
Didodecyl ether	$1\cdot0 \times 10^{10}$	1·0
Palmitone	$1\cdot6 \times 10^{10}$	1·4
9-heptadecanone	$3\cdot8 \times 10^{10}$	1·8
n-octadecyl bromide	$1\cdot6 \times 10^{11}$	2·4
1:10-dibromodecane	$1\cdot3 \times 10^{11}$	2·3

In general these barriers are approximately one tenth the size of those in pure crystalline long-chain compounds of similar molecular weight[73] and even smaller than the activation energies in the pure liquids. It can be concluded from Meakin's work that in the urea adducts the guest-host interactions are only small, particularly in the n-paraffin adducts where there is no dipole - dipole attraction.

A detailed analysis of Meakin's results for the 12-bromotridecane and 16-hentriacontanone adducts has since been made by Lauritzen[74]. This treatment represents the interaction between the crystalline field of the hexagonal urea lattice and the guest species by a potential energy function dependent on the orientation of the adducted molecule. By assuming that the interaction between adjacent included polar molecules is negligible and that the polar guest molecules are in an environment of known geometry, unaffected by dipole reorientation, Lauritzen was able to compute the interaction potential energy by summation of contributions from individual atom pairs using the Lennard-Jones (6-12) interaction potential,

$$V(r) = C\left[\tfrac{1}{2}\,(r^o/r)^{12} - (r^o/r)^6\right]$$

where r is the distance between the two interacting atoms and ro is the sum of their van der Waal's radii. As an alterna-

tive method Lauritzen assumed the potential V(r) to be proportional to the volume overlap of the van der Waal's spheres associated with the two atoms. Although this second method is simpler, due to the finite range of the forces imposed by the model, the Lennard-Jones function has greater theoretical justification. However, in both calculations the contributions from the hydrocarbon chains of the ketone molecules were negligible compared with the interaction between the lattice and the dipolar group.

The derived potential energy function for rotation of the ketonic dipole in the z = o plane, which contains the oxygen atoms of the urea lattice, was characterised by a symmetrical six fold energy barrier. However, this is effectively reduced to a five barrier potential as the energy difference of $\sim$ 0·1 K cal/mole between the two shallow maxima symmetrical about $\dot{\phi} = 180^{\circ}$, where $\dot{\phi}$ is the angle of rotation, is negligible compared with approximately 4 K cal/mole in 16-hentriacontanone and 2 K cal/mole in 12-bromotriacosane at $\dot{\phi} = 40^{\circ}$ resulting from the close approach of the rotating polar group and a single nitrogen atom of the urea lattice. The resulting four modes of relaxation and the size of the computed barriers agrees satisfactorily with Meakin's values and proposal of three relaxation times.

Lauritzen carried his analysis further by assuming the "single jump hypothesis" of Hoffman and Pheiffer[75], which restricts dipole reorientation to adjacent sites only. The probabilities of dipole reorientations were then given by,

$$k_1 = A \exp \left[- (W_1) / kT \right]$$

where W_1 is the energy barrier for the polar group to leave site 1 and enter site 2, A is a frequency factor and T the absolute temperature. By solving a series of differential equations to give the populations of each site and employing a procedure developed by Hoffmann et al[75] the four molecular relaxation times (τ_β) were expressed in terms of the probabilities k_1 etc. These in turn were related to the dielectric loss factor (ϵ'') by the Debye equation extended to the case of several relaxation modes:

$$\epsilon''(w) = \sum_{\beta} \frac{\Delta\epsilon_\beta \, w \, \tau_\beta}{1 + (w\tau_\beta)^2}$$

where w is the frequency of the applied field, $\beta = 1, 2, 3 \ldots\ldots\ldots$ and $\Delta\epsilon_\beta$ is the increment of dielectric constant associated with the β th relaxation mode.

To compare the calculated values with Meakin's experimental values of $\epsilon''(w)$ for 16-tentriacontanone it was necessary to assume a variation of energy barriers with temperature arising from a change in the urea lattice

dimensions. The barrier-adjusted in this way is shown in FIG. 6. The correspondence of the dielectric loss factors was then excellent over the range of temperatures reported by Meakins.

Lauritzen's theoretical treatment again confirms the comparatively weak nature of the interaction between the occluded molecules in urea adducts particularly for simple hydrocarbon chains.

SECTION I. (j). Infra Red Spectra:

The infra-red spectra of the urea n-paraffin adducts have been extensively investigated[76,77,78] but due to the low intensity of the absorption arising from the non polar hydrocarbon guest molecules most attention has been directed to the bands from the urea lattice. Fischer and McDowell have examined the spectra of the urea adducts, from n-heptane to n-hexadecane, in the region 600 cm^{-1} to 4000 cm^{-1}. All the spectra showed marked differences from that of tetragonal urea[70][80] although in varying degrees. The largest change is in the N-H stretching frequency region where absorption from out of phase stretching occurs at 3436 cm^{-1} in tetragonal urea while in the adducts this is lowered to 3420 cm^{-1}, correspondingly the in phase vibration moves from 3333 cm^{-1} to 3220 cm^{-1} showing an increase in hydrogen bond strength in the hexagonal lattice. Similar shifts from

1464 cm^{-1} to 1492 cm^{-1} arising from C-N shortening and an increase in the C-N frequency and intensity at 1014 cm^{-1} (instead of 1000 cm^{-1}) have also been observed. This has been attributed to the urea carbonyl group being more highly polarised as a result of hydrogen bonding and closer packing in the hexagonal form in agreement with the X-ray data of Smith[49].

Durie and Harrison[81] have examined the C_{12}, C_{16}, C_{22}, C_{28}, C_{34}, and C_{23} n-paraffin urea complexes with special regard to the contributions from interactions of the included molecules with the urea lattice at room temperature. The absorption due to the n-paraffin guest is largely restricted to a band at 2920 - 2850 cm^{-1} which has an analogous band in the pure hydrocarbons produced by C-H stretching. Bands also occur at 1465 cm^{-1} (CH_2 and CH_3 bending), 1375 cm^{-1} (CH_3 bending) and 720 cm^{-1} (CH_2 rocking).

To investigate the physical state of the adducted hydrocarbons comparisons between spectra of the pure hydrocarbons in 0·005 M solution (using carbon tetrachloride and carbon disulphide as solvents) and as solid and liquid were drawn. An intensification of the 720 cm^{-1} band relative to the 2920 cm^{-1} band was found in going from the solution to the solid state. Since the 720 cm^{-1} band is suppressed in the adducts the absorption characteristics of the paraffin in solution or as a liquid rather than the solid state were found to be more closely comparable with those of the adduct.

The CH stretching vibrations in the region 2800-3000 cm^{-1} have also been compared for the adducts and various states of the pure hydrocarbon. As this mode is sensitive to change of state these workers found a considerably higher change of $\sim$ 10 cm^{-1} for the assymetrical stretching $\nu_a(CH_2)$ and $\sim$ 5 cm^{-1} for the symmetrical $\nu_s(CH_2)$ frequencies in both liquid and solution than in the solid state. Again, the corresponding frequencies for the adduct, shown on TABLE. (4). below, were always closer to the liquid or solution values.

TABLE. 4.

Paraffin	Physical State	CH stretching frequency cm^{-1}	
		$\nu_a(CH_2)$	$\nu_s(CH_2)$
$n\text{-}C_{12}H_{26}$	liquid	2924	2852
	solid	2918	2847
	Urea Adduct	2925	2852
$n\text{-}C_{16}H_{34}$	Solution	2926	2852
	Liquid	2925	2854
	Solid	2916	2849
	Urea Adduct	2923	2851
$n\text{-}C_{22}H_{46}$	Solution	2927	2854
	Solid	2916	2849
	Urea Adduct	2924	2851
$n\text{-}C_{28}H_{58}$	Solid	2918	2850
	Urea Adduct	2925	2853

SECTION I. (k). Investigations of molecular motion in inclusion compounds other than the urea adducts.

Many physio-chemical investigations have been made on other inclusion compounds. Notable among these are the ß-quinol clathrates and the gas hydrates since the relatively simple geometry of their lattice cages allows realistic models of these structures to be proposed and treated theoretically.

Parsonnage and Staveley[82] in their work on the heat capacities of clathrates have found that methane molecules in the approximately spherical cavities of the ß -quinol lattice contribute by virtually free rotation an amount 3/2 R cals deg^{-1} $mole^{-1}$ to the heat capacity from 150°K to room temperature. In these compounds the contribution of the empty ß -quinol lattice could be determined by extrapolation using measured values for clathrates of varied compositions, since the heat capacity is a linear function of the total number of cavities filled. An analysis of the vibrational component of the methane C_p was made, using a theory due to van der Waals[83][84] and a small correction applied for internal vibrational modes. Although the heat capacity could not be accurately calculated at temperatures below 150°K the rotational contribution to C_p differed from that of free gaseous methane showing some restriction to free

rotation. However, this restriction was thought to be small even at 20°K.

Similar investigations[85][86] of the argon and krypton clathrates showed good agreement with the results to be expected from van der Waals treatment of the "rattling" motion of the inert gas molecules in the cavity. Below 60 and 120°K, respectively, discrepancies between theory and experiment arose due to the theory being classical whereas account must be taken of the quantum levels at these temperatures.

Thermodynamic studies of the oxygen, nitrogen and carbon monoxide clathrates by Grey and Steveley[87] however, showed a considerable restriction to rotation, as even at room temperature Crot, the rotational contribution to the heat capacity, is still greater than R the theoretical value for a perfectly free two dimensional rotator. The rotational heat capacity for the oxygen clathrate was consistant with a barrier of 200-250 cal/mole while the barriers for nitrogen and carbon monoxide were estimated at 1000 and 1200 cal/mole respectively. An independent study of the nitrogen clathrate heat capacity by Coulter[41] gave a value of 820 cal/mole, while the pure quadrupole resonance experiments of Meyer and Scott[88] from which the observed nitrogen oscillation frequency of $1{\cdot}55 \times 10^{12}$ c.p.s. corresponds to a barrier of

940 cal/mole in close agreement with the calorimetric estimates.

The low temperature paramagnetic resonance investigation of Foner et al[89]. on the oxygen clathrate between $1{\cdot}5^{\circ}$ - $4{\cdot}2^{\circ}K$ yielded a barrier of 250 cal/mole but in this case to obtain suitable single crystals with only a small fraction of the cavities filled (5%) with oxygen the solid solution was diluted with nitrogen. The nature of the nearest neighbours of the oxygen molecule was therefore unknown although the barrier calculated was for an oxygen molecule for which the two nearest cavities are occupied by nitrogen molecules. Evidence for the free rotation of oxygen in this clathrate at temperatures as low as $2^{\circ}K$ has been provided by Cooke et al.[90] and Meyer et al.[91] from their observations of the temperature dependance of the magnetic susceptibility. However, below $1^{\circ}K$ further susceptibility measurements reported by Meyer et al.[91] have confirmed the presence of a small barrier opposing rotation of the oxygen molecule in the clathrate. The quoted barrier is however only 128 cal/mole.

Hexter and Goldfarb[92] and McKean[41] have studied the infra red spectra of the quinol clathrates of CO_2, SO_2, HCl and H_2S. Here restricted rotation in the case of CO_2 was found while information particularly from the HCl and

H_2S samples was inconclusive due to intense absorption by the quinol lattice. Dielectric measurements by Dryden[93] on the hydroquinone clathrates of H_2S, HCN, C_2H_2, CH_3OH and CH_3CN showed a wide range of barrier heights. A barrier to dipole reorientation of 2·3 K cal/mole was observed for the methanol clathrate which is lower than the activation energy of dipole rotation in a normal polar solid. On the other hand the rotation in the methyl cyanide compound was more highly restricted (18 K cal/mole) attributable to distortion of the lattice cavity along one axis.

Other inclusion complexes studied by dielectric loss experiments include clathrates of Dianins compound (4-p-hydroxylphenyl -2,2,4-trimethyl chroman) and biuret hydrate. In the latter the water molecules form zig-zag chains in channels of the biuret lattice and an observed activation energy for dipole reorientation of $\sim$ 4·5 K cal/mole was considered to be due to the rupture of one hydrogen bond between the water molecules and oxygen atoms of the biuret.

Another class of inclusion complexes on which a considerable literature exists is that of the gas hydrates. Measurements of vapour pressures of the guest species for the ethylene and ethane gas hydrates have been made by van der Waals and Plateeuw[84] and the dissociation pressures

calculated by a statistical mechanical technique from a model analogous to that proposed for ideal localised adsorption. The calculated equilibrium pressures compared with those found experimentally are relatively too low showing that such comparatively large molecules are not capable of free rotation or the central force field assumption used in the model is not suitable for these polyatomic molecules. This model has also been applied to the hydroquinone clathrates of A, Kr, Xe, CH_4, N_2, O_2 and HCl and good agreement for the heats of formation and the equilibrium vapour pressures at $0^{o}C$ obtained [84].

From the wide variety of experimental techniques applied to elucidate the size of energy barriers to rotation of the guest component in inclusion compounds and particularly for the ß -quinol clathrates the agreement is highly satisfactory considering the range of temperature over which the studies have spanned. Indeed, a variation in barrier height with temperature is expected as a change in cavity dimensions arising from thermal expansion of the host lattice will always occur. Furthermore, the increased population of higher vibrational energy levels, bringing more guest molecules into a statistically time averaged closer proximity with the lattice walls, will modify the force field within the cavities.

PART B. EXPERIMENTAL.

CHAPTER II. APPARATUS.

SECTION II. (a). The Adiabatic Calorimeter.

The principle of the adiabatic calorimeter for measuring heat capacity over a wide range of temperatures is simple. However, in practice considerable experimental difficulties have to be overcome. In a typical apparatus a sample container, often called the calorimeter, carrying a suitable thermometer and heater coil are suspended by a non-thermally conducting material from and within an evacuated enclosure (the radiation shield) which can at all times be maintained at the same temperature as the calorimeter. Heat exchange between the calorimeter and its surroundings by conduction, convection and radiation will therefore, under ideal conditions, be negligible.

Heat energy E supplied electrically to the sample container will produce a temperature rise ΔT, usually measured by a platinum resistance thermometer, from which, since no heat has been lost to or gained from the environment, the total heat capacity at constant pressure of the calorimeter plus contents may be calculated directly:

$$Cp_{total} = E/\Delta T$$

Measurements made on the empty calorimeter enable

the heat capacity of the sample to be found by subtraction. However, in practice rigid adiabatic conditions cannot be maintained. Small heat exchanges occur through inadequate equalisation of shield and calorimeter temperature arising from limitations in the methods used for thermal gradient detection and correction. Self heating of the calorimeter, by the small current passing through the resistance thermometer, and conduction of heat along the operative wiring from the calorimeter will also cause a small thermal drift or leak which, when an equilibrium state has been achieved after heat input, is however generally linear with time. Corrections calculated from the rate of drift both before and after heating can be made by extrapolation to the mid point of the energy input period, $\Delta T_{corrected}$ obtained and subsequently Cp evaluated.

The Apparatus for Heat capacity Measurements:

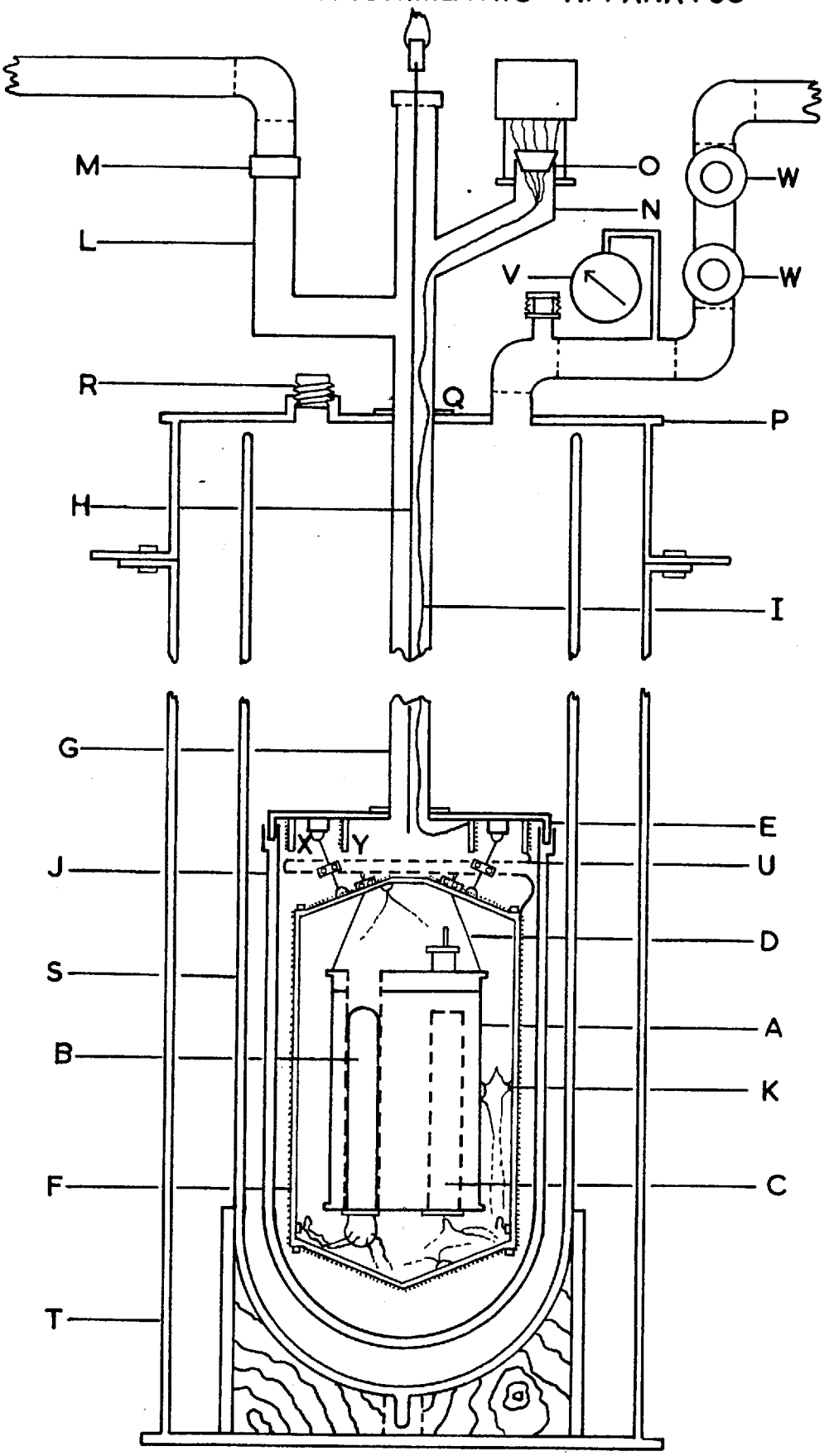
The calorimetric apparatus employed in this research was originally constructed by J.W. Edwards[94] and G.L. Kington[95] based on a design used by the National Bureau of Standards (Washington) and described by Southard and Brickwedde[96]. However, extensive modifications and repairs were found necessary the most important of which, together with a general description of the apparatus are outlined below.

SECTION II.(b). The Cryostat and Calorimeter:

The heat capacity apparatus was of the Nernst adiabatic type and is shown in FIG. 8. The calorimeter (A) with resistance thermometer (B) and heater (C) are shown suspended by three nylon monofilament lines e.g. (D) from the top radiation shield, which in turn is suspended by nylon from the brass top plate (E) - (See PLATE.2.). The whole shield assembly is enclosed by a copper vacuum can (J) soldered to the outer flange of the top plate with low melting-point solder (m.p. 110°C). The wires from the calorimeter and differential copper-constantan thermocouples e.g. (K), used to detect differences in temperature between the various shields and the calorimeter, pass to the bottom of the side shield (F) and out through insulating ebonite plugs around the shield base.

The top plate (E) is carried by the main supporting tube (G) of 1" external diameter monel steel which enclosed the concentric monel steel oxygen vapour pressure inlet tube (H) (0·3 cm. diameter, 0·08 cm. wall thickness) and the cable (I) of wires from the calorimeter-shield measurement and control circuits. Limb (L) of the main supporting tube joins to a glass high vacuum line at (M) and serves to evacuate container (J) and to admit helium for thermal equilibration, while limb (N) carries the electrical leads to the brass plug and picein seal at (O).

FIG. 8. THE CALORIMETRIC APPARATUS. 51



THE CALORIMETER AND RADIATION SHIELD ASSEMBLY.

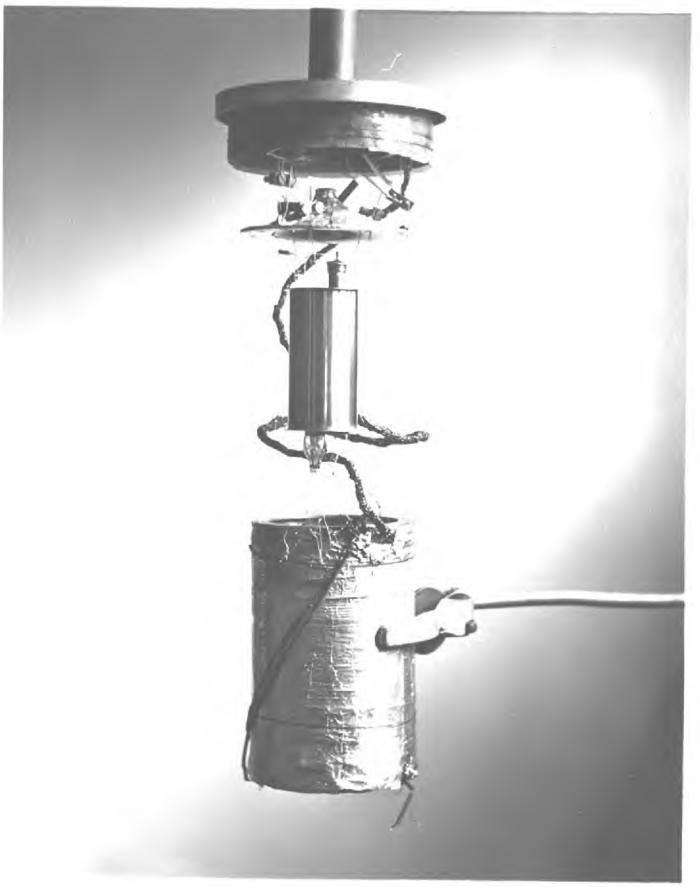


PLATE 2 .

The monel tube (G) was silver-soldered to the steel top plate (P) of the cryostat can at (Q). Two connectors (R) (only one shown in the diagram) on this top plate enabled tubes to be fitted for filling the Dewar (S) with the appropriate refrigerant or blowing out liquid refrigerants by means of an over-pressure of nitrogen gas in the cryostat. The top plate also connected the cryostat to a high capacity (110 cu.ft/min.) Kinney Vacuum pump (W. Edwards and Co.) via a 2" diameter iron pipe and large vacuum valves (W). This pump was situated in a separate pumping-house for reasons of safety when pumping on refrigerants such as liquid hydrogen.

The cryostat was fitted with a vacuum gauge (V), a spring loaded (3 p.s.i.) safety valve and a pipe leading to the roof as an exhaust for gaseous hydrogen. A flexible metal link prevented vibration being transmitted from the Kinney pump to the cryostat.

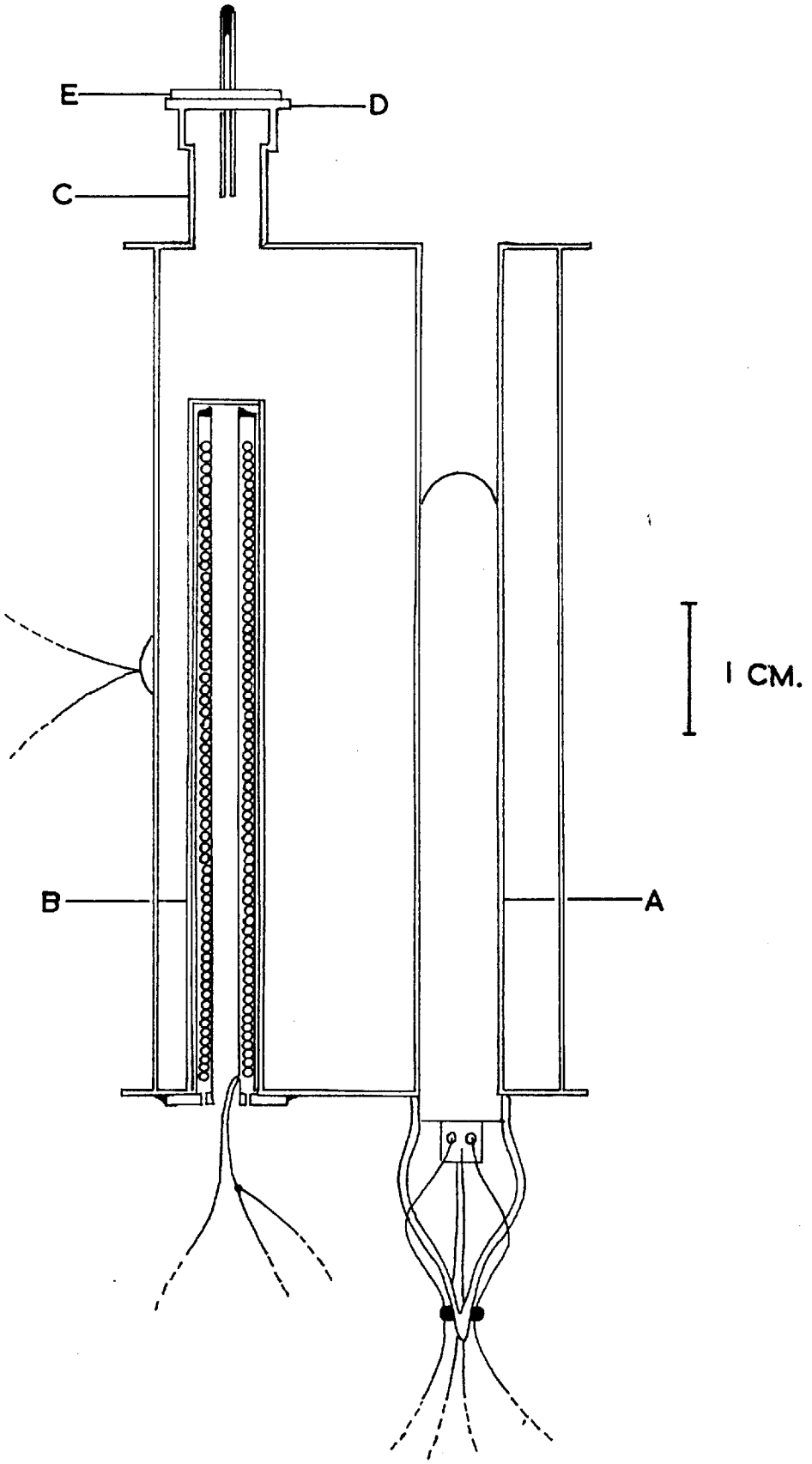
The main cryostat can (T), which held the Dewar on a wooden cradle, could be raised on two guide rails (not shown in the diagram) and bolted to the top plate (P) to give a vacuum-tight seal by means of a rubber gasket. The whole cryostat assembly was supported by a very rigid iron framework bolted to the laboratory floor to prevent relative movement between the cryostat and the glass pumping line.

The calorimeter (sample container) is shown in FIG.9.

and PLATE.3. It was constructed of platinium - 10% iridium by Messrs. Johnson Matthey Ltd., and had a total weight of ca. 109 g. including the heater assembly. The maximum sample volume was 41 c.c.

The cylindrical body of the calorimeter (3·1 cm. diameter, 6·5 cm. long and 0·04 cm. wall thickness) was gold soldered to circular top and bottom plates (3·7 cm. diameter). The bottom plate carried two re-entrant tubes (A) and (B) (See FIG.9.) of 0·8 cm. diameter to hold the thermometer and heater respectively. The calorimeter heater was soldered in one re-entrant well along its whole length with Woods metal (m.p. 78°C) to ensure good thermal contact.with the body of the calorimeter. The rapid attainment of thermal equilibrium between the thermometer and calorimeter was enhanced by coating the former with a thin film of Apiezon T grease; while, by introducing a small sheet of thin aluminium foil around the neck of the thermometer, a firm fit in the well was ensured. In other calorimeters internal vanes have been used to achieve more rapid thermal equilibrium between calorimeter and contents. Fins of this type were not included in the present design. Reliance was placed on a small pressure of dry helium ($\sim$ 1 cm.) for thermal equilibration and this was found to be entirely satisfactory in operation as no additional thermal relaxation time was found to be necessary in the case of the filled calorimeter compared with the empty

FIG.9. THE CALORIMETER ASSEMBLY.



THE CALORIMETER.

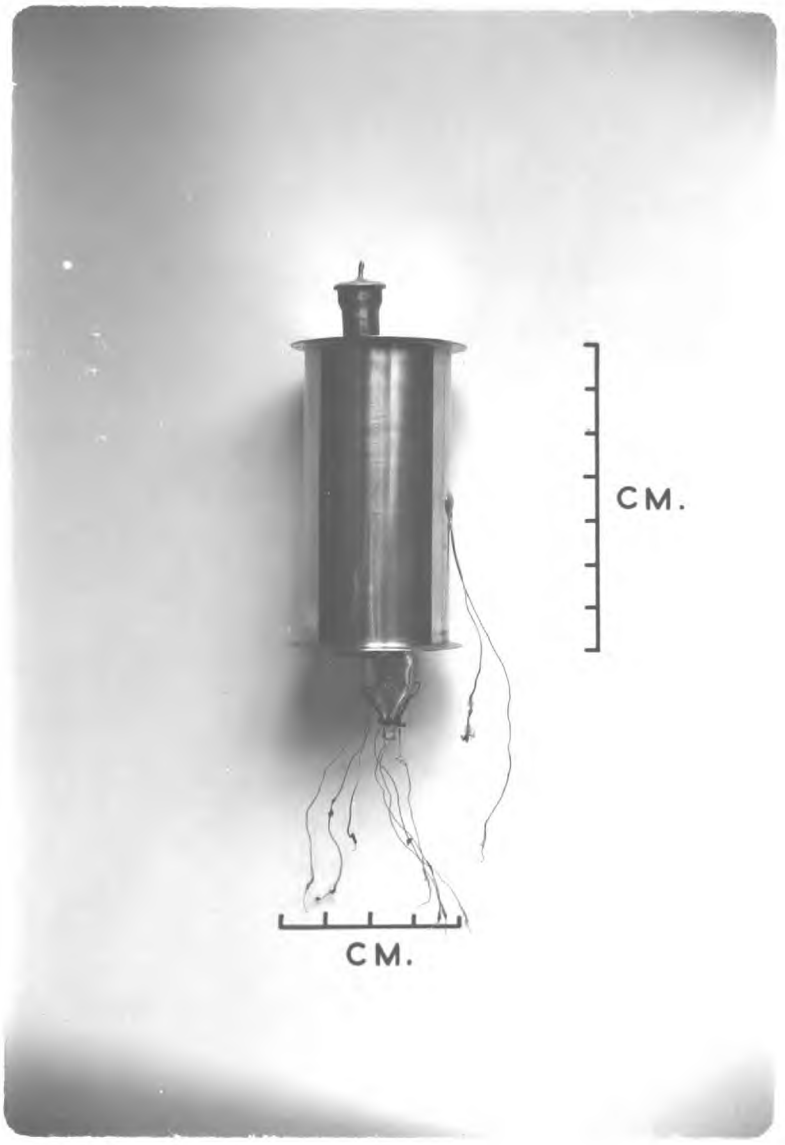


PLATE 3.

calorimeter.

Soldered to the outside of the calorimeter exactly half-way along its length was one junction of a copper-constantan thermocouple, which was used to indicate the difference in temperature between the sample container and the radiation shield.

SECTION II. (c). Filling the Calorimeter.

A short (0·8 cm. diameter, 1 cm. long) German silver tube (C) and brass collar (D) was silver soldered to the calorimeter top plate as is shown in FIG. 9. The substance under investigation was introduced through (C) and a brass cap (E), carrying a length of 1 mm. external diameter silver tube, soldered to the pre-tinned flange (D). A low m.p. solder (110°C) of the following composition (40% Pb, 40% Sn, 20% Bi) was used to prevent decomposition of the sample through excessive heating. In fact only a slight rise of sample temperature occurred owing to the poor thermal conductivity of the German silver and the cooling effect of a stream of air passed over the calorimeter as soon as the soldered joint had been made.

The silver tube was sealed with picein wax to the high vacuum line (see FIG.15.) and the sample container evacuated in stages to better than 2×10^{-5} mm. of mercury. Some helium (1 cm. pressure) was subsequently introduced and the silver tubing was then pinched-off and the exposed end

soldered over[97]. On average a length of 0·6 cm. of the silver tube remained protruding above plate (E) after this operation.

In cases where decomposition of the sample was feared during evacuation the calorimeter was placed within a glass tube cooled in an alcohol-cardice bath. In such instances it was imperative to reduce the free volume of the pumping line between the calorimeter and the first isolating tap on the vacuum line to a minimum to prevent possible condensation of water into the calorimeter.

SECTION II. (d). The Calorimeter heater:

The calorimeter heater consisted of approximately 400 ohms. of 38 s.w.g. double cotton-covered varnished Manganin wire, wound non-inductively in two layers on a brass former over an insulating single thickness of varnished cigarette-paper. A single sheet of thin aluminium foil, to facilitate the flow of heat along the heater coil, separated the two layers of the winding and a further layer ensured good thermal contact with a thin walled brass sleeve (4·8 cm. long) which enclosed the heater coil and was soldered at both ends to the heater former.

The two heater leads came out through an araldite plug at the base of the flange (F) (FIG. 9.), on the heater former and two further holes were made at this point to

permit rapid evacuation of the heater assembly. The heater of weight 11·07 g. slid as a unit into a recess in the calorimeter base and, in the final form of the calorimeter assembly, was soldered in with the minimum weight of Woods metal.

Two 40 s.w.g. copper leads were attached to each end of the heater winding so that both current and potential measurements could be made to determine the amount of heat liberated. The external wiring of these heater leads was so arranged, one "heater potential" lead being attached close to the shield and the other near the calorimeter[98] heater, that only half the heat developed in the current carrying pair was in fact considered as going to the calorimeter. The remaining half of this heat was assumed to be conducted down the leads to the side shield.

SECTION II. (e). The Platinium Resistance Thermometer.

As a preliminary to heat capacity determinations in the range 11° - 300°K suitable thermometers had to be made and a temperature scale, reproducible to ± 0·001°C above 60°K, established (see Section V (b)). To this end two platinium resistance thermometers, hereafter called (B) and (C), of approximately 15 ohms. resistance at 300°K were constructed.

The thermometer (C) used in subsequent heat capacity investigations was of the coiled-coil filament type described by Meyers[99] of the National Bureau of Standards (Washington)

with the glass sheath used by Meyers replaced with a platinium capsule. This has been found by many workers to improve both the thermometer robustness and speed of response.

The 0·1 mm. diameter platinium wire used in the construction of (B) and (C) was of the highest available purity (Johnson Mathey and Co.) and was wound non-inductively as a helix supported on a notched, interlocked, cross-shaped mica former approximately 4·5 cm. long. Two platinium leads 1 cm. long were welded to each end of the winding as current and potential leads for resistance determination. The thermometer was repeatedly annealed for several hours at 600°C in this condition, to minimise any residual strain in the winding, until constant ice point resistance was obtained. The coil was then placed in a thin-walled, round-bottomed platinium capsule ($\sim$ 5 cm. long, diameter 0·8 cm.) fitted with a soft glass seal and the winding leads brought out through the glass head which was sealed off after the thermometer had been evacuated, leak tested and filled with dry helium to a pressure of $\frac{1}{3}$ of an atmosphere. The four emergent leads were separated and tied down to the glass head with cotton, and finally joined to colour coded, varnished 40 s.w.g. double silk covered copper wires $\sim$ 6 cm. in length.

SECTION II. (f). The Radiation Shield Assembly.

The radiation shield assembly (F) is shown in FIG.8. It consisted of three separate copper shields, top, bottom and side of total weight 580 g. The top and bottom shields were conical in shape and attached to the side shield by brass screws sited around their flanged edges. The inner surfaces of all three shields had been rhodium plated on silver to give a highly polished non-tarnishing surface which would reduce radiation exchange to a minimum.

The cylindrical side shield had twenty-two helical grooves cut in its outer surface in which the leads to the calorimeter heater and thermometer and shield-calorimeter control thermocouple wires were embedded to thermally equilibrate them with the shield, and hence, when adiabatic conditions had been established, with the calorimeter itself. These leads were all of 0·010" diameter silk-covered varnished copper wire. The varnish used was Imperial Chemical Industries' air drying insulating varnish type F 268-585 together with thinners type A. At the base of the side shield these leads passed through ebonite insulating plugs to the inner surface of the shield.

Each shield had a separate non-inductively wound heater of 0·010" diameter varnished silk-covered Eureka wire wound uniformly over its outer surface. Both the top and bottom shield windings had a resistance of 25 ohms, whereas

the side shield heater resistance was 400 ohms. Soldered, insulated connections from these heaters to 0·010" diameter varnished silk-covered copper leads were made in all cases. The outer surfaces of the shield heater windings were completely covered with aluminium foil held in place with a thin layer varnish to reduce energy-exchange by radiation with the vacuum jacket (J) - (see FIG.8.).

SECTION II. (g). The Differential thermocouples:

The differential thermocouple system used permitted the temperatures of the top and bottom shields to be independently compared with the side shield, and the temperature of the latter directly compared with the calorimeter or thermometer intercomparison block. During oxygen vapour pressure measurements (see Section VI (b)) the temperature of the lower half of the inlet tube could also be related to that of the side shield.

Single junction copper-constantan couples were used soldered directly to the mid points of the side shield and sloping faces of the top and bottom shields. As heat exchange by conduction can occur along the thermocouple wires between the side shield and calorimeter, this being particularly important at low temperatures, a balance between reduced thermal conductivity and increased resistance and liability to fracture of the thermocouple wires was necessary. The thermal conductivities of copper and constantan have been

reported over a wide range of temperature by Blanpied and Powell[100]. Typical values quoted are shown in TABLE. 5 . below.

TABLE. 5

	Copper	Constantan
$T^{o}K$	Thermal Conductivity (Watts cm^{-1} deg^{-1}.)	
300	4	0·23
80	5	0·18
4C	15	-
20	-	0·088
10	50	0·035

Consequently 40 s.w.g. copper and 34 s.w.g. constantan double cotton covered varnished wires were used, the homogeneity of the latter being checked by constructing and comparing several individual couples made from lengths of wire adjacent to that used for the working thermojunctions. The sample of constantan wire was also tested by connecting the ends of the wire to a potentiometer and slowly passing the wire through liquid nitrogen as suggested by Giauque et al.[101]. The thermoelectric e.m.f. developed in both tests did not exceed 1 μ v. Subsequent checks on the individual top, side, bottom and calorimeter couple e.m.f's with cryostat baths of solid and liquid nitrogen, alcohol-cardice and ice, after thermal equilibration of the shields showed their relative responses to be within $\pm$ 0·5 micro volts.

The side shield - calorimeter differential thermocouple system was simply constructed by joining the constantan wires within the adiabatic enclosure and soldering the copper leads to the incoming copper wires from the measuring circuit at the base of the side shield. The copper leads from the top, bottom and a second side shield thermocouple were similarly joined to a common copper wire at the side shield base and the three corresponding constantan wires taken out through the side shield. These wires were soldered to copper leads and the joints, after being electrically insulated with a single layer of varnished cigarette-paper, securely tied down with cotton to the side shield. They were thus all at the same side shield temperature. This was an essential condition for the maintainance of the top and bottom shields at the side shield temperature by simple balancing of the thermocouple e.m.f's.

During each assembly of the calorimeter care was taken to ensure that the thermocouple leads were not touching the shields or the calorimeter at points other than the thermocouple junctions. Such contact would lead to a variable contribution to the heat capacity of the calorimeter. Satisfactory separation of these leads was achieved by always keeping the relative orientations of the shields and calorimeter constant.

SECTION II. (h). Electrical leads to the measuring circuits.

The copper leads from the side shield and Eureka shield heater wires were soldered to 36 s.w.g. double silk covered copper wires, insulated and bound into a flexible spiral cable (U) FIG. 8. which permitted considerable freedom of movement of the side shield in any direction. To reduce the heat leak to the shields down the wires from the distribution box, which was at ambient room temperature, the cable wires were separated and individually wrapped around, and varnished to, the outer surfaces of the two flanges (X) and (Y). These cooling rings formed part of the top plate (P) which was in contact with the refrigerant in the Dewar. Above this top plate the cable was reformed and passed up the main support tube limb (N). Here again the cable separated into 42 wires which passed out individually through picein filled grooves in the brass plug (O) where they were soldered to stouter P.V.C. covered copper leads from a distribution board. Twin core shielded cables (Henly Ltd.) were soldered to these leads at the distribution board, the shieldings of the cables being earthed to prevent any induced e.m.f's. These cables passed through an iron pipe to the measuring room.

The electrical insulation between earth and all leads in the cryostat and measuring room was tested at intervals throughout the investigations and any wires with resistance below 1 Meg ohm were not used.

CHAPTER III. APPARATUS (Continued)

The Electrical Measuring Circuits:

SECTION III. (a). The Differential Thermocouple Circuit.

The differential-thermocouple e.m.f. measuring circuit is shown in FIG. 10. This circuit was used to detect the difference in e.m.f's from the various shield, calorimeter, intercomparison block or vapour pressure inlet tube thermocouples and thereby to obtain adiabatic conditions by controlling the current supplied to the shield heaters. In principle adiabatic conditions are achieved when the differential thermocouples each give an e.m.f. of zero micro volts.

The signals from the differential thermocouple system were selected by a rotary thermal e.m.f. free switch (A). (Croydon Instrument Co. Ltd.), amplified with a D.C. amplifier of the split photocell type (Pye Instrument Co. Ltd.) and the output read on a micro volt meter (range $\pm$ 10 μv) to $\pm$ 0·1 μv. A range of shunts x 10, x 100, x 1000 incorporated in the amplifier enabled larger differences in temperature between for example the calorimeter and side shield to be detected. The response of the amplifier was however dependent on two extra factors other than the supplied signal:-

(1) The resistance of the thermocouple circuit. To eliminate this effect each circuit was adjusted to have the same resistance (ca. 15 ohms at room temperature) by

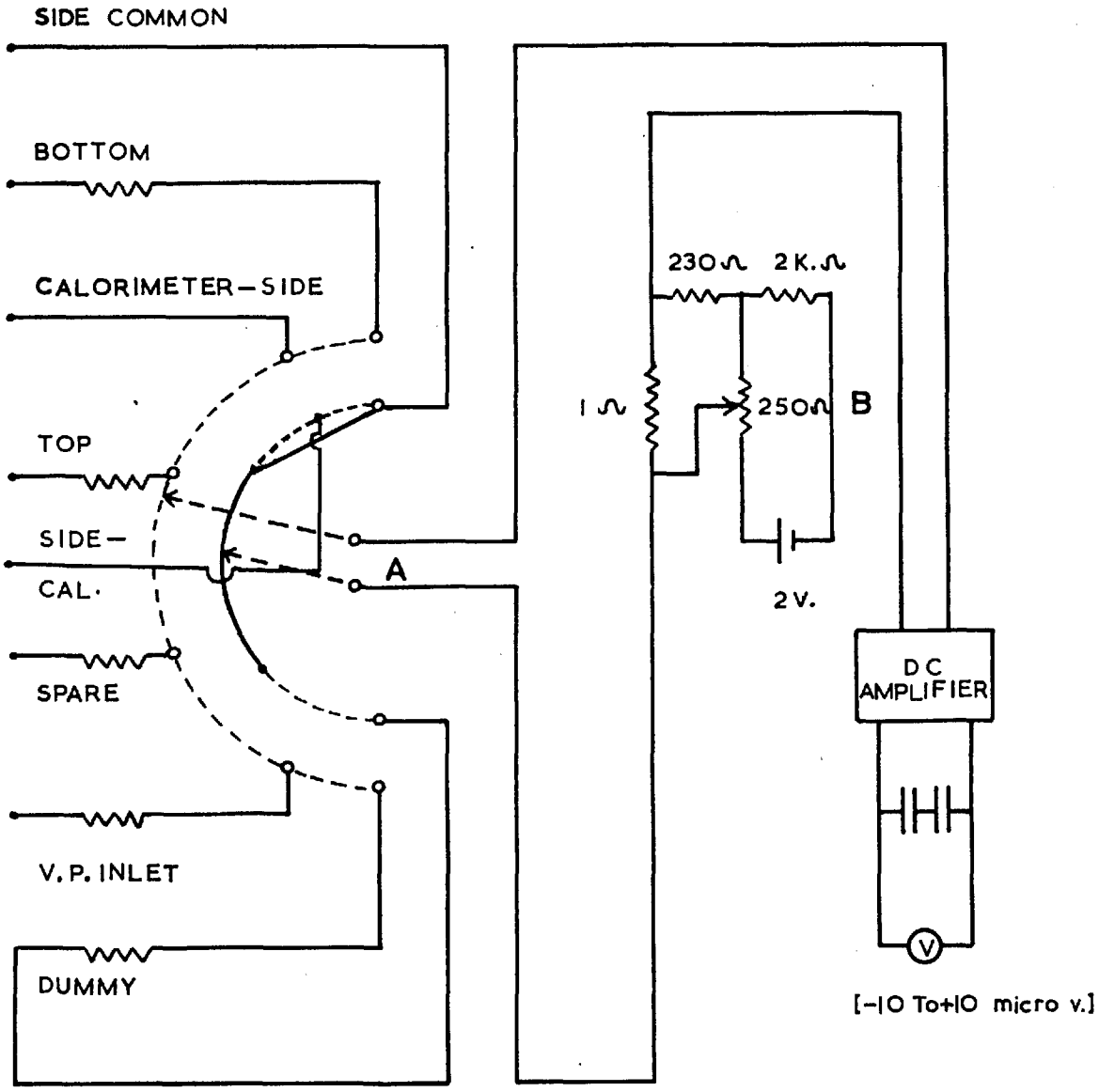


FIG.10 DIFFERENTIAL THERMOCOUPLE CIRCUITS.

introducing in series a non-inductively wound 40 s.w.g. copper coil of the appropriate length. A "dummy resistance" of this copper wire could be selected and applied across the D.C. amplifier input to set the instrument zero. Coarse zeroing adjustments were made via the control of the split photocell unit of the amplifier, and fine corrections by means of a circuit (B) - see FIG. 10. - in series with all e.m.f's from the selection box and supplying up to 10 μ v.

(2) D.C. Amplifier drift with time.

Amplifier drift was dependent on ambient room temperature and was of the order of 5 μ v during any one day's measurements. To correct for this drift the fine zero setting control was continually adjusted throughout all runs with the selector switch set on the "dummy resistance".

SECTION III. (b). Differential thermocouple control during runs:

Throughout "fore" and "after" drift periods of heat capacity runs in the region from 40° to 250° K manual regulation of the shield heater circuit currents enabled the off-balance of the differential thermocouples to be kept within better than $\pm$ 0·2 μv. Above 250°K, where heat exchange by radiation increases rapidly and the sensitivity of the copper-constantan is higher, shield balance was more difficult and limited to $\pm$ 0·3 μ v. During heat input periods of average runs the off-balance e.m.f's were kept below $\pm$ 0·8 μ v over

the temperature range 12° - 300° K.

As the thermoelectric power of copper-constantan is approximately 40 micro volts per degree at 300° K the limit of detection (0·1 μ v) corresponds to a temperature difference of only $0{\cdot}0025^{\circ}$. However, the thermoelectric power decreases with lowering of the temperature[102] and has values of 8 and 4 micro volts per degree at 30°K and 10° respectively. Hence even at these temperatures an overall sensitivity of $\sim 0{\cdot}0125^{\circ}$ and $\sim 0{\cdot}0250^{\circ}$ per 0·1 microvolt was still achieved.

SECTION III. (c). The Thermometer Circuit

The thermometer circuit is shown in FIG. 11. The four colour coded copper leads from the platinium resistance thermometer were soldered to specified leads at the base of the side shield during each assembly of the calorimeter. The thermometer current leads were brought out in series with a 10,000 ohm. stabilising resistance, to limit fluctuations of the circuit current as the thermometer resistance changes with temperature, and a 10 ohm manganin standard resistance (H. Tinsley Type 3504), the absolute value of which was checked in 1963 and found to be 10·0044 absolute ohms at 20°C. A previous calibration of this resistance in 1958 by H.Tinsley and Co. had given a result of 10·0040 absolute ohms. The thermometer current, which was measured across the 10 ohm standard resistance, was supplied by a bank of six volt 50 amp-hour

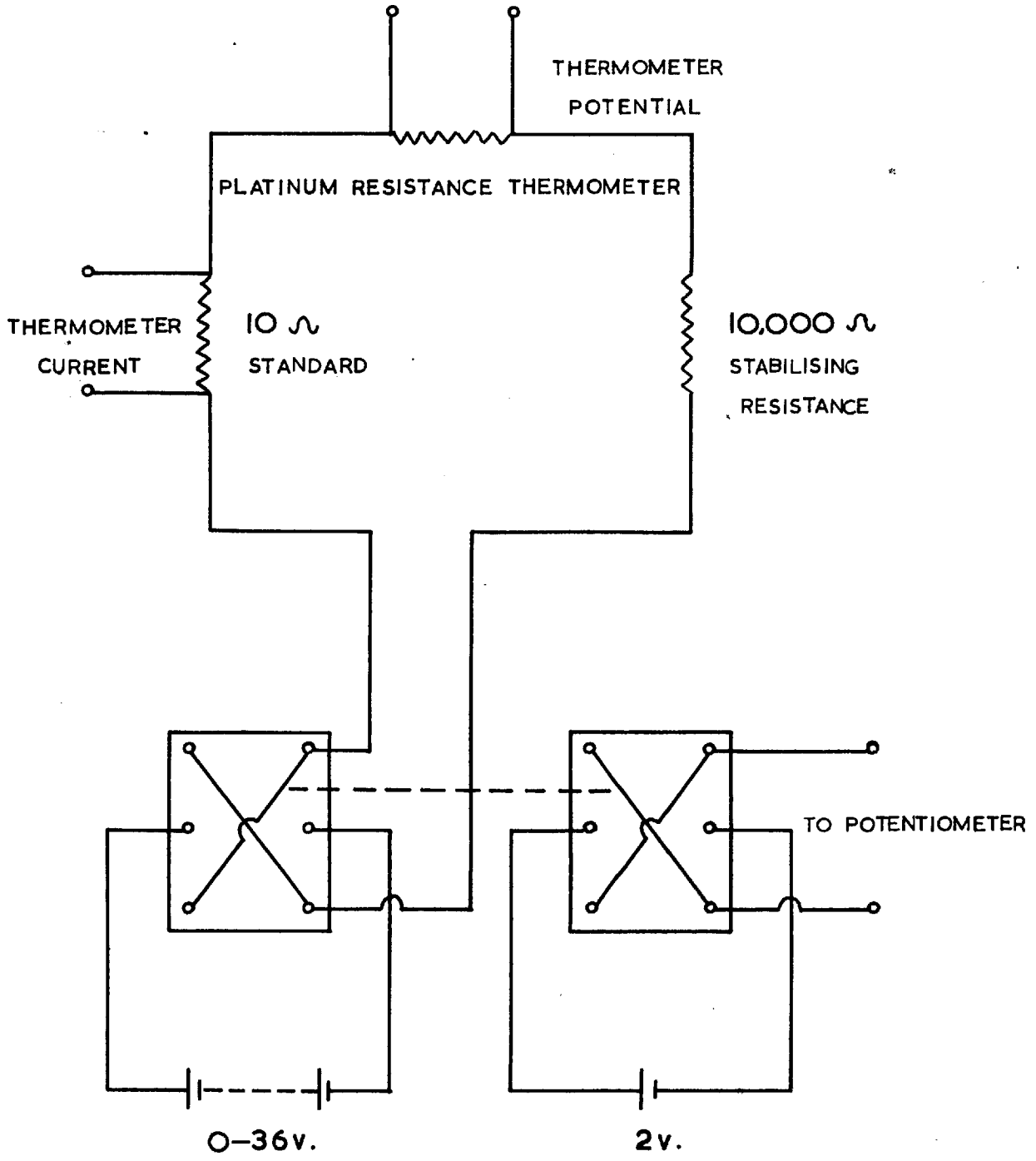


FIG. 11 THERMOMETER CIRCUIT.

lead-acid car accumulators (Silver Exide) housed in a draught-proof cupboard and kept well charged to a specific gravity between 1·215and 1·155. A switch enabled these batteries to be discharged through a dummy resistance, variable to the same value as that of the thermometer at the desired temperature of measurement, for several days prior to heat capacity determinations. Four such accumulators, giving a thermometer current of 2·4 milliamps, were used in the temperature range above 77°K. However below 77°K, due to the decreased sensitivity of the platinium resistance thermometer at lower temperatures, a current of 3·6 milliamps from all six accumulators was employed. Checks on the precision of heat capacities determined in this region showed no discontinuity arose from the change in thermometer current. This was as expected, since during the thermometer calibrations the current had been increased by the same amount below 77°K.

The potential drops across the thermometer and the 10 ohm standard resistance, from which the resistance could be calculated, were measured on a vernier potentiometer (H. Tinsley Type 4363) in conjunction with a Tinsley box galvanometer with an optical path length of 1 meter. The galvanometer deflection was read on a calibrated scale to $\pm$ 0·5 mm.

The sensitivity of the galvanometer circuit for thermometer potential determinations varied with the thermometer

resistance within the range 15 mm. per micro volt at 12°K to 5 mm. per micro volt at 300°K. Thus potentials of ± 0·1 micro volts across the thermometer could be measured by interpolation on the galvanometer scale irrespective of the temperature using the thermometer currents quoted above. The potentiometer galvanometer was critically damped without need for additional resistance in the measuring circuit.

A pair of ganged switches in the potentiometer and thermometer battery circuits enabled the direction of the current flowing in the galvanometer circuit to be reversed. Hence, by taking both normal and reverse readings, it was possible to eliminate parasitic e.m.f's in the galvanometer circuit through averaging the forward and reverse measurements. The reversing switches however, must not introduce any extra resistance into the potentiometer circuit or spurious results are obtained. Consequently the reversing wires of these switches were made of thick 12 S.W.G. copper wire covered with heavy rubber insulation.

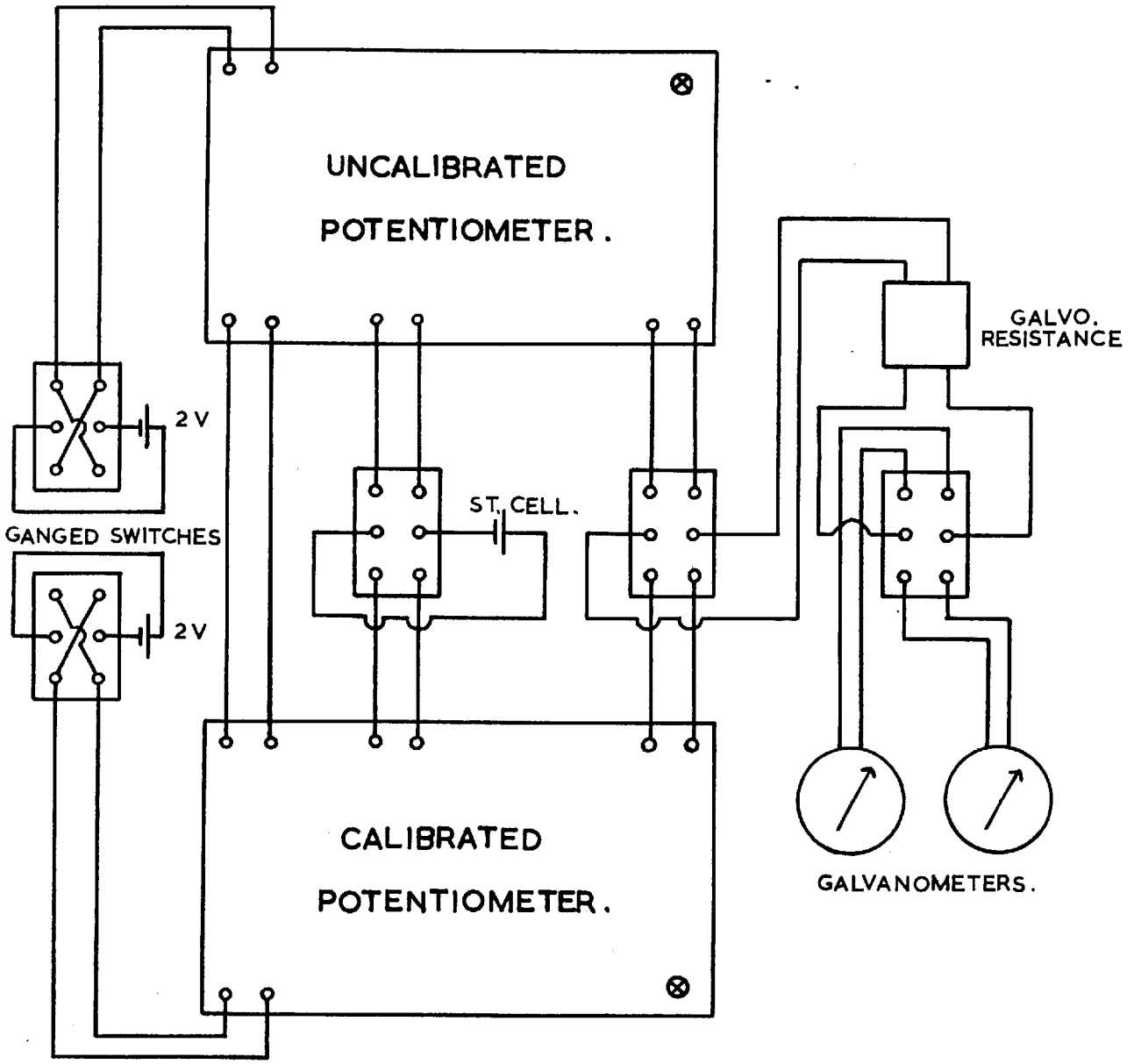
Leeds and Northrup pinch type switches with blades made from a copper-beryllium alloy, which has a very low contact potential against copper, were used throughout. These switches were frequently cleaned with Analar benzene and lubricated with Eulfsil Elvo contact oil (H. Tinsley and Co.). Dust was excluded at all times when the switches were not in use by covering them with plastic sheeting.

As a platinium resistance thermometer of 15 ohms ice point resistance has a temperature co-efficient of approximately 0·06 ohm. per degree from about 50° - 300°K, to obtain a precision of 0·1% in heat capacity measurements with a temperature interval Δ T of 5° requires a determination of thermometer resistance to $\sim 3 \times 10^{-4}$ ohm. This corresponds to a potential change across the thermometer of $\sim$ 1 microvolt using a 3 milliamp thermometer current. Below 50°K, due to both the decrease in thermometer sensitivity and the more rapidly changing heat capacity, smaller temperature intervals Δ T must be used ($\sim 3{\cdot}4^{\circ}$) and consequently even greater precision in resistance measurement to achieve 0·1% in Cp is demanded. Obviously a potentiometer of great reliability was needed and the accuracy of the instrument was therefore checked on all dial settings against a new (1962) vernier potentiometer of the same type using the circuit shown in FIG.12. The divergencies from the dial values are shown below.

Potentiometer dial reading	0 - 100μv	Divergence	0·2-0·6 μv
" " "	10^2 - 10^3	"	0·2
" " "	10^3 - 10^4	"	0·1-1·2

The maximum divergence between the two instruments was 1·2 μv at 7400 μ v which agrees closely with a previous calibration by J.W. Edwards in 1957. Corrections to $\pm$ 0·1 μv for all measured potentials were made from the full calibration table.

FIG. 12 POTENTIOMETER CALIBRATION CIRCUIT.



Two Weston cells (H. Tinsley Type 1268) were used to calibrate the potentiometer in absolute volts, the first giving an approximate off balance reading. These cells were inter-compared from time to time to check their reliability. Variations of the cell e.m.f's never exceeded 5 micro volts. This variation would not affect the accuracy of thermometer resistance measurement since only a ratio of potentiometer readings is involved. However, within the time required for a heat capacity determination, variation of room temperature was accounted for by correcting the cell e.m.f. using a temperature coefficient of $4{\cdot}0 \times 10^{-5}$ abs. volts per degree.

SECTION III. (d). The Calorimeter heater circuit.

The calorimeter heater circuit is shown in FIG. 13. The two heater potential and two heater current leads, arranged as described in Section (II.d.), were taken out via the lead seal (O in FIG.8.) to the 100/1 potential divider (H. Tinsley Type 4281-C) and standard 1 ohm resistance (H. Tinsley Type 3504). Measurements of heater current (i) and potential (v) were made across the 1 ohm and potential divider respectively. The current for the calorimeter heater was supplied from two 50 amp. hr. six volt car accumulators. A decade box (0 - 10,000 ohms in steps of 1 ohm) in series with the accumulators controlled the heater current, as change in heating rate was necessary owing to the large difference in heat capacity between the highest and lowest temperatures at which runs were made.

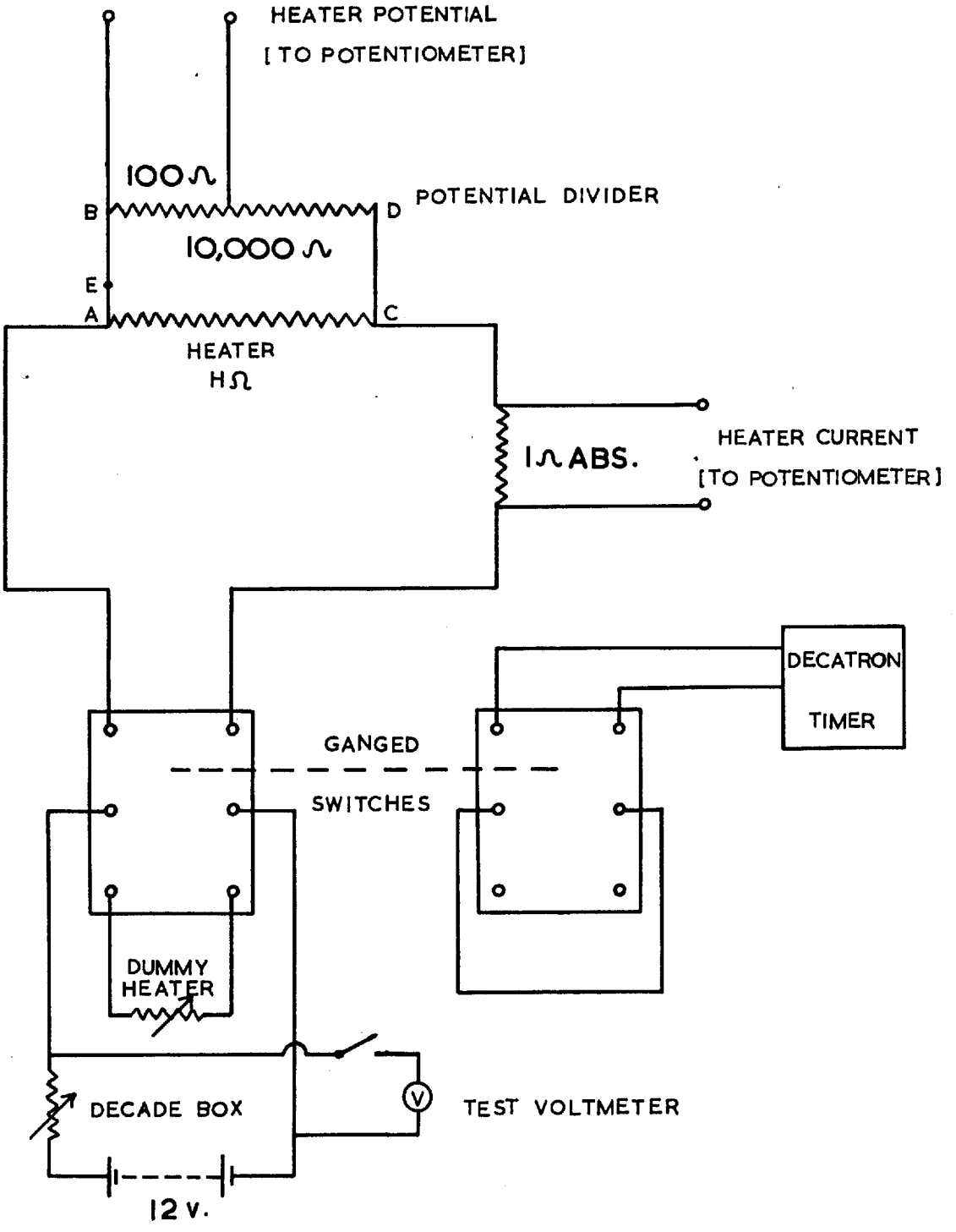


FIG. 13 CALORIMETER HEATER CIRCUIT.

When current was not being passed through the calorimeter heater the accumulators were allowed to discharge through a dummy resistance maintained at the same value as the calorimeter heater resistance. This served to reduce the possibility of unsteadiness in the accumulator voltage during heat input to the calorimeter. By the use of ganged switches throwing the calorimeter heater switch also activated a decatron timer, (Labgear Type D 4108) fitted with a ten second add on register (Type D 4109), simultaneously with the passage of current through the heater. All connections in the calorimeter heater circuit were made with earthed shielded cable, and copper-beryllium switches (Leeds and Northrup) were used throughout to reduce thermo-electric e.m.f's.

The electronic timer could be read in intervals of 0·001 second up to 100,000 seconds. Calibration of the instrument by timing five to nine hour periods, switching the timer on and off at a known time using either the 1 c.p.s. pips from the N.P.L. or the B.B. C. Greenwich Time Signal showed an average error of only 1 in 30,000 too high. Although this is much larger than the personal error involved in the calibration, it would not lead to a significant error (0.003%) in derived heat capacities. A previous calibration (1957) showed the timer then gave readings high by 1 part in 23,000.

However, the add on register occasionally jammed, thus

falsifying the heating period by an integral number of ten second increments. To detect this a stop watch was used as a check in all heat input periods.

SECTION III. (e). The Shield Heater Circuits:

The circuits used to maintain adiabatic conditions within the shield enclosure, by supplying current to the shield heaters, are shown in FIG.14. Direct current (D.C.) was used in all three heater circuits to prevent interference effects with the D.C. amplifier and thermometer circuits or undesirable eddy current heating.

The top shield heater was supplied from two six volt accumulators while the side and bottom shield D.C. came from the 110 volt mains. The D.C. for all the heaters was initially controlled by potential dividers, fine adjustments being made with variable resistances in series with the shield heaters. Each circuit contained two 1 amp fuses and an ammeter, (0 - 50) or (0 - 100) milliamps (see diagram), optionally shunted on a second range to read to approximately 500 milliamps. These shunts were provided as much larger shield currents were necessary during heating periods. However, the shield currents were never allowed to exceed 350 ma. to avoid the possibility of burning out the heater windings. Should one of the shields have become slightly too warm during a run, the relevant heater current

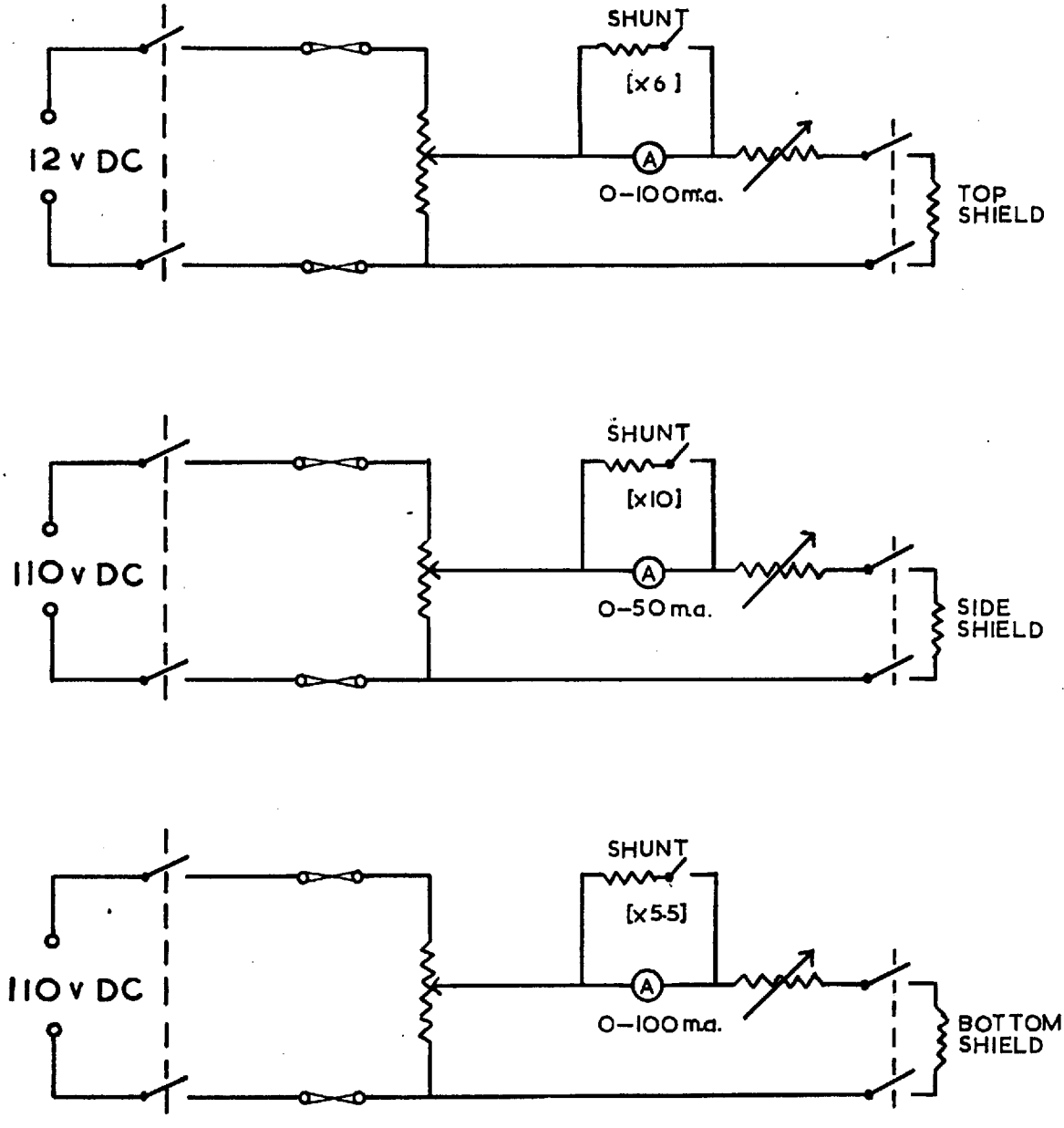


FIG. 14 SHIELD HEATER CIRCUITS.

could be interrupted by means of a toggle switch while still maintaining the original current setting on the potential divider. It was then a simple matter to retain adiabatic conditions, once the shield had cooled to the temperature of the calorimeter, by again completing the shield heater circuit and slightly decreasing the current flowing in it.

CHAPTER IV. APPARATUS (Continued)

SECTION IV.(a). The Vacuum Line and Auxillary Apparatus.

The high-vacuum system shown in FIG.15. constructed of pyrex glass was required for evacuating:

(1) The calorimeter after filling.

(2) The adiabatic shield enclosures.

(3) The relevant gas lines and bulbs, manometers and oxygen vapour pressure bulb during the vapour pressure measurements.

(4)"Dosing" the calorimeter or its enclosing canister with helium as heat exchange gas.

The high pumping rate needed to remove helium exchange gas rapidly from the copper jacket surrounding the shield assembly, at temperatures below the hydrogen boiling point, was achieved by a single stage mercury diffusion pump backed by a 2-stage oil filled rotary pump (Edwards Speedivac). Large 1 cm. bore taps and 2 cm. diameter tubing throughout the main pumping line permitted a vacuum of $\sim 10^{-6}$mm. of mercury to be reached, providing the two cold traps (A) and (B) were filled with liquid nitrogen. The gas pressure in the line was measured by a McLeod gauge or monitored continuously by an Edwards cold cathode Penning gauge reading from 1×10^{-2} to 1×10^{-5} mm. of mercury in two ranges.

Trap (B) was always surrounded by liquid nitrogen when pumping on the calorimeter-shield assembly to prevent

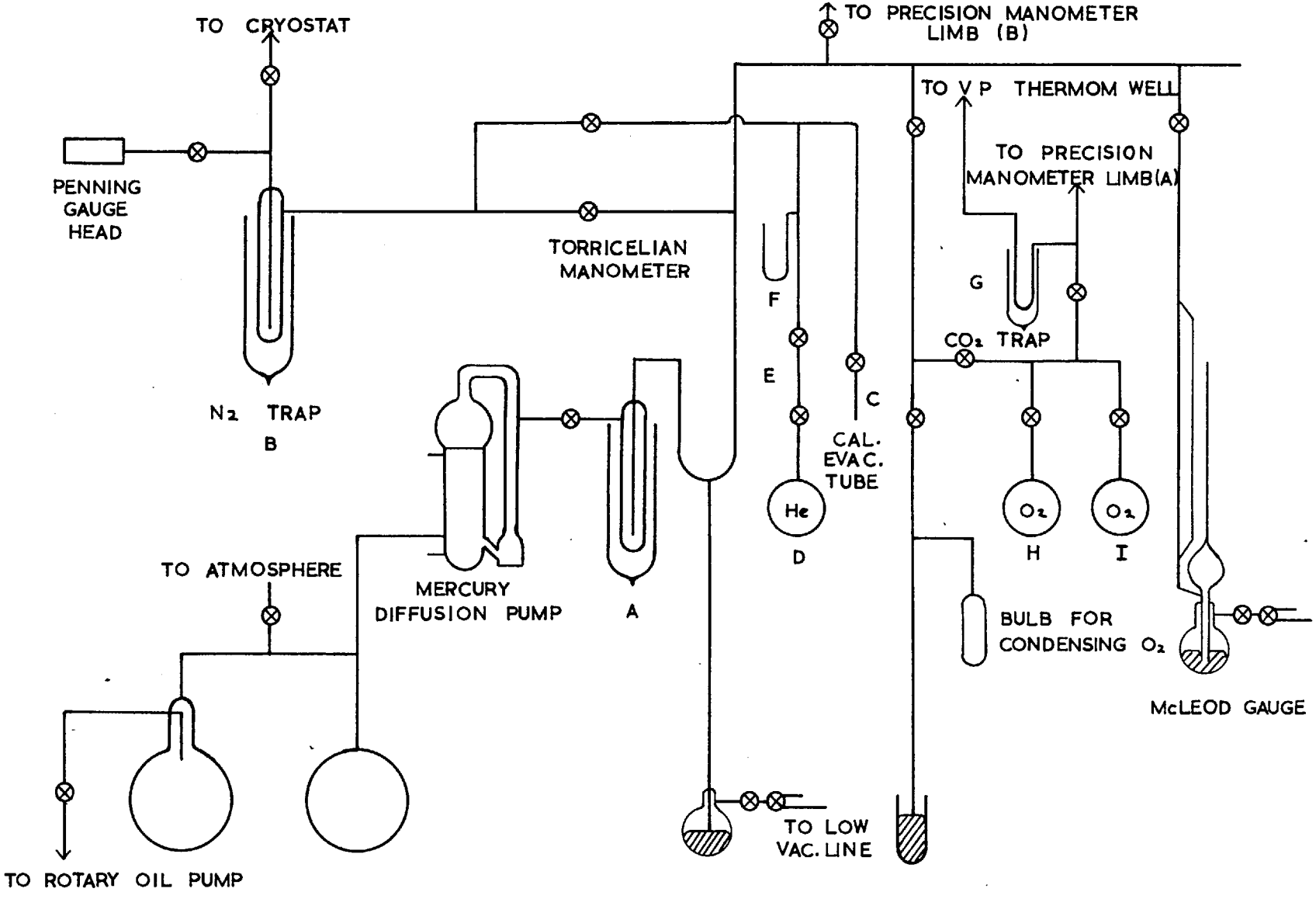


FIG.15. DIAGRAM OF THE VACUUM LINE AND AUXILLARY APPARATUS.

the entry of water or mercury vapour. The presence of mercury at higher temperatures could lead to a breakdown in the electrical insulation of the copper wiring or amalgamation with soldered joints, whereas condensation on the calorimeter at lower temperatures would increase the measured heat capacity above its true value.

The helium "doser", used to introduce a small pressure of spectrally pure gas from globe (D), and calorimeter evacuating tube are shown by (C) and (E) respectively. A small Torricellian manometer (F) indicated the helium pressure after dosing.

The remaining section of the apparatus served to store and admit spectrally pure oxygen (B.O.C.) to the vapour pressure thermometer bulb. To reduce the dead space to a minimum, thick walled capillary tubing was used for the gas line to the vapour pressure thermometer well and the precision manometer. In this case a cardice trap (G) prevented water and mercury vapour from entering the gas thermometer when oxygen was admitted

SECTION IV. (b). The Vibration free Manometer used in oxygen vapour pressure measurements.

This was a U-tube manometer constructed of 16 mm. internal diameter Veridia precision bore tubing joined to a capillary tube on one side (the limb connected to the vapour

pressure bulb) to reduce the "dead space" volume. A glass reservoir containing triple distilled AR mercury enabled, by reduction or increase of the pressure above the mercury, the height of the mercury column in the oxygen containing limb to be adjusted. The same region of the precision bore tube, irrespective of the oxygen vapour pressure could therefore be used for each measurement.

The entire manometer was enclosed in a thick walled wooden draught-proof box fitted with a plate glass window. This permitted the menisci to be observed without distortion or refraction effects. The manometer assembly was firmly bolted to the laboratory wall to prevent vibration. Two mercury in glass thermometers situated at the top and bottom of the manometer case were employed to determine the average temperature to $\pm$ 0·1 C during oxygen vapour pressure determinations. This average temperature was taken to be that of the mercury in the manometer limbs for use in applying the Linder correction (see Section VI (b)).

The height and circumference of the tops of the menisci were measured on an external 1 metre cathetometer (Precision Tool and Instrument Co. Ltd.) mounted on a massive iron table screwed to the floor and carefully aligned to be in the vertical plane. With this arrangement, after making correction for the cathetometer back lash a pressure difference between the two limbs could be measured to $\pm$ 0·004 cm. of mercury.

CHAPTER V. THE PLATINUM RESISTANCE THERMOMETER CALIBRATION

SECTION V.(a). Note on Temperature Scales

Before any useful thermodynamic investigations can be made over a range of temperatures, a reliable thermometric device closely reproducing an internationally recognised temperature scale must be made and tested. Although in theory the thermodynamic scale of temperature can be realised by the absolute ideal gas scale, the associated practical inconveniences and complications make this method prohibitively difficult. As a result several "secondary" temperature scales have been proposed.

The Seventh General Conference on Weights and Measures (1927) adopted the first International Temperature Scale based on two fundamental fixed points - the ice point as $0^{\circ}C$ and the steam point of $100^{\circ}C$ - using the platinum resistance thermometer for its realisation. In the same year Giauque, Buffington and Schulze[101] had established the Temperature Scale of the University of California by comparing copper-constanton thermocouples with the hydrogen gas thermometer in the range of 15° to 283° K giving an overall accuracy of approximately $\pm 0.05^{\circ}$. By 1939 the technical advances of Meyers[99] in the construction of strain free platinum resistance thermometers and Southard and Brickweddes'[96] modification of sealing the thermometer windings in metal capsules instead of glass, enabled the

National Bureau of Standards (Washington) Scale of Temperature from 12° to 90° K, by comparison again with the gas thermometer, to be established. This temperature scale reproduced the thermodynamic scale to ±0.02° but has the weakness of complete dependance on the thermometer stability. This necessitated checking the stability at certain "fixed points" below the oxygen boiling point(103).

Above -183°C and below 0°C the International Temperature scale was defined in terms of the resistance of a platinum resistance thermometer by theCallendar - Van Dusen equation:-

$$t = 100\,\frac{Rt - Ro}{R100 - Ro} + \frac{\delta\, t}{100}\left[\frac{t}{100} - 1\right] + \beta\left[\frac{t}{100}\right]^3\left[\frac{t}{100} - 1\right]$$

and above 0°C by the Callendar equation:

$$t = 100\,\frac{Rt - Ro}{R100 - Ro} + \frac{\delta\, t}{100}\left[\frac{t}{100} - 1\right]$$

where t is the temperature in °C, R the resistance of the thermometer at the appropriate temperature and β and δ constants characteristic of the thermometer. Below 90°K no single relationship has been established for the changing resistance of platinum with temperature due to the increasing importance of impurity conduction at low temperatures.

In 1948 the International Temperature Scale was modified by replacing the ice point by the triple point of water, the latter being lower by 0.0100°C, as the fixed point while the ice point remained at 0°C. Hoge[104] then made his classic investigations of the vapour pressure and triple points of the hydrogens, and oxygen together with the solid-solid transition temperatures for oxygen and nitrogen. Further comparison of the gas and platinum resistance thermometers was made in Germany (1936) - the PTR (Physikalisch-Technische Reichsanstalt Scale) and by Moessen, Aston and Ascah (1954)[105] - the Pennsylvania State University Temperature Scale - which reproduced the thermodynamic scale to ±0.005° K. The temperature scales mentioned above are compared in FIG.16 after Scott(1955)[106].

In 1954, the Conference on Weights and Measures agreed that the thermodynamic scale should be defined by one fixed point, the triple point of water assigned the value of 273.16°K and the absolute temperature. The ice point is thus now 273.15°K. Consequently the N.B.S. have revised their Provisional Temperature Scale -(N.B.S.1955) by correcting for the numerical factor -0.01 degree.

In the present research, platinum resistance thermometers were indirectly related by the intercomparison method to the Provisional Temperature Scale of the N.B.S.

A COMPARISON OF TEMPERATURE SCALES.

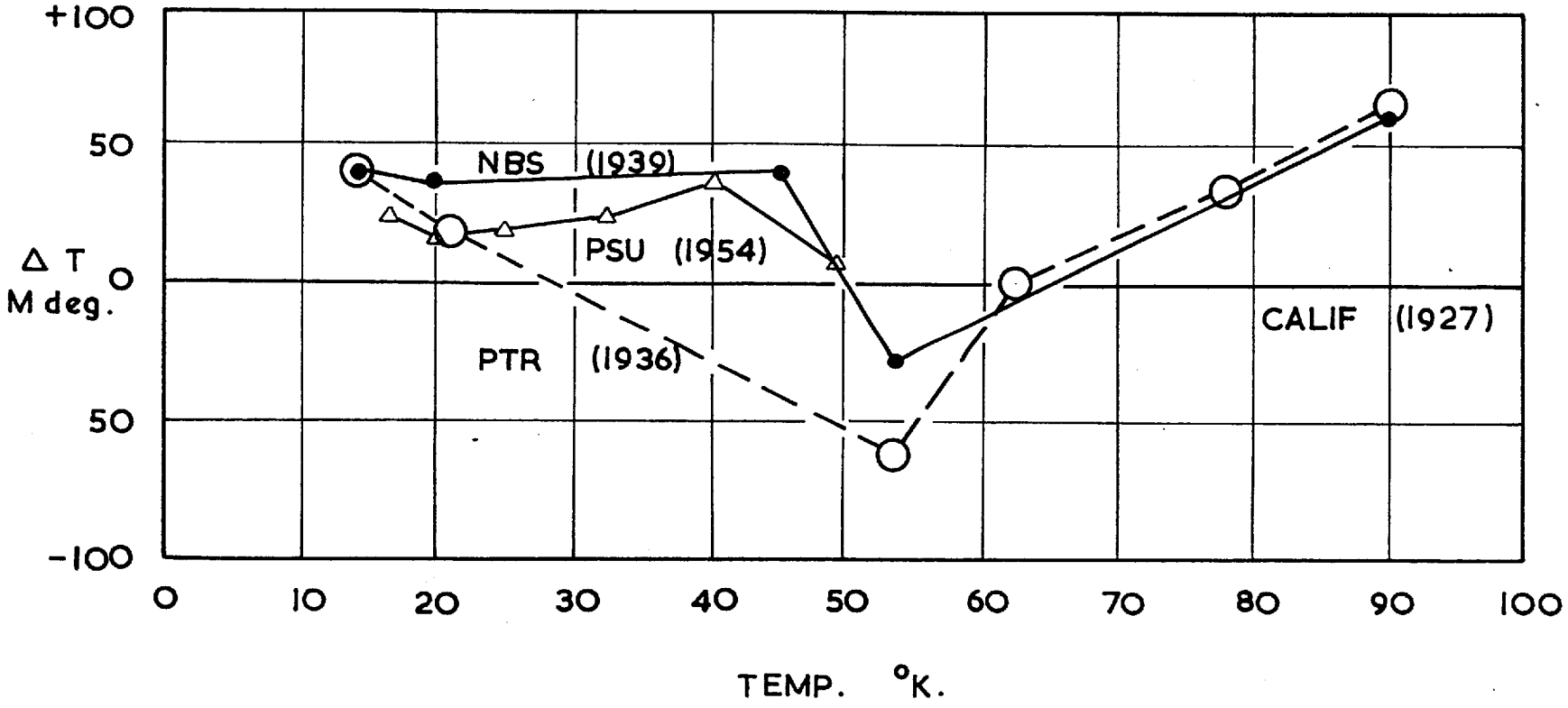


FIG. 16 [AFTER SCOTT 1955].

(1939). The stability of the standard thermometer(A) since its calibration in 1957 was checked by redetermining its ice point and oxygen point resistances and comparing the latter with the oxygen vapour pressure determinations of Hoge(1950).(See sections V(e) and VI(c)). The final calibration of the working thermometer (C) was likewise compared and corrected, by subtraction of 0.01 degree, to the 1955 N.B.S. scale.

SECTION V(b): Calibration of Platinum Resistance Thermometer(B) and (C). Apparatus for the Intercomparison.

The two thermometer(B) and (C) described in Section II(e) were calibrated by the intercomparison method over the entire temperature range 12°-312°K, using as standard, a platinum resistance thermometer(A) made available by Dr.G.L. Kington. This standard thermometer had previously been calibrated in this laboratory by Dr. J.W. Edwards[95] against a similar thermometer obtained from Dr. J.A. Morrison of the National Research Council of Canada. The calibration of this latter thermometer was based on the Provisional Temperature Scale below 90°K (see section V(a)).

The intercomparison circuit was similar to that shown in FIG.11, the thermometer current leads being connected in

series. A massive cylindrical copper block (7 cms.long, 5.5 cms. in diameter) of weight 1,470 g., with a heater of non-inductively wound 36 s.w.g. Minalpha wire (500 Ω at room temperature) insulated from the block by a single layer of varnished cigarette paper was hung by three nylon lines in place of the calorimeter (A) within the radiation shield assembly (see FIG.8). The block held the three platinum resistance thermometers in separate (0.8 cm. diameter, 5 cm.deep) wells in its base, the standard thermometer being retained by Woods metal and thermometers (B) and (C) by a thin film of apiezon T grease. A copper-constanton thermocouple, to enable temperature differences between the block and shield assembly to be detected, was soldered to the mid point of the side of the block. The upper surface of the block had a cavity 1 cm. in diameter and 3 cms. deep which was used subsequently as an oxygen vapour pressure thermometer bulb (see Section VI(b)).

Above 50°K a thermometer current of approximately 2.5 ma. was passed, whereas below 50°K 3.5 ma., to obtain a greater precision in potentiometer readings was used. Larger thermometer currents were not passed since the associated small heating effect, dependent on the square of the current used, would tend to cause the thermometer coils to be at an appreciably higher temperature than the comparison

block. A small temperature difference inevitably results from this effect, the magnitude of which at 273°K is shown in the ice point resistances for two thermometer currents (See Section V(e)).

SECTION V(c): Technique of Calibration

The copper block, previously cooled by addition of the appropriate refrigerant to the cryostat Dewar, was heated to the required temperature by supplying current to the resistance winding and then equilibrated in vacuo ($\sim 1 \times 10^{-5}$ m.m. of mercury) by controlling the shield heater currents.

Before measurements were made a period of 10 minutes was allowed to elapse during which all thermal gradients in the block and shield assembly should have disappeared. Potentiometer forward and reverse measurements, to ± 0.1 microvolt, of i the thermometer current (potential drop across the 10ohm standard resistance) and a,b,c, the "thermometer potentials" were then taken in the sequence:

i, a, b, i, a, c, i, a, b, c, a, i

as a function of time over a period of about 20 minutes.

A total of 103 intercomparisons were made at intervals of 1°- 3° in the region 12°- 20°K and at 5°- 10° intervals in the range 20°- 310° K. The intercomparison

was however extended to approximately 10.5°K, below the lowest temperature (12.380°K) given by the standard thermometer (A) calibration table.

During the initial runs performed at liquid hydrogen temperature (approximately 20°K) a leakage occurred in the apparatus, which disappeared on warming again to room temperature. It was subsequently found that graining in a monel steel alloy oxygen vapour pressure inlet tube (H in FIG.8), due to both age and the large thermal gradient along its length was responsible. As this tube was concentric with the main tube (G in FIG 8) which served to support, evacuate and carry the main wiring for the calorimeter, it was necessary to dismantle and rebuild the apparatus at this stage. The new apparatus was leakproof down to 10.5°K enabling the intercomparisons to be completed and further work to proceed.

SECTION V(d) Treatment of the Intercomparison Results.

By interpolation of current-time and thermometer potential-time plots the resistance of the standard(A) and the corresponding resistances of (B) and (C) at the same time and therefore at the same temperature were obtained. The method employed for the smoothing of this data and the treatment used to enable a table suitable for linear

interpolation to be drawn up is considered below, for thermometer C (chosen as the working thermometer).

(1) From the ice point resistances of (A) (derived from the calibration table) and (C) obtained experimentally, values of the ratios

$$WA = \frac{RA}{RAo} \quad \text{and} \quad WC = \frac{RC}{RCo}$$

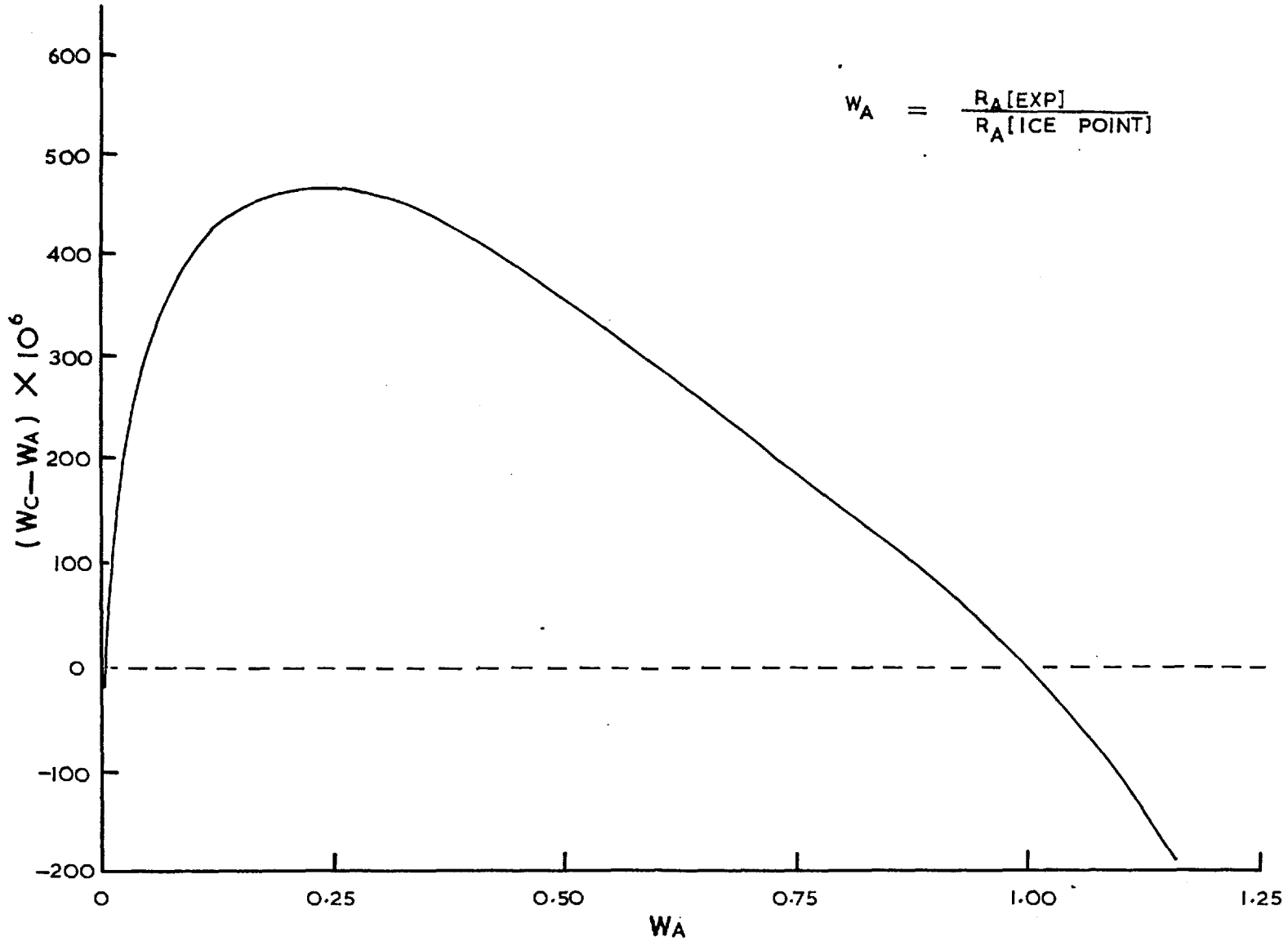
were calculated where RA and RC are resistance values from the intercomparison at temperature T°K and RAo and RCo are the ice point resistances all in absolute ohms.

(2) Values of $(WC - WA)_T$ at temperature T°K were thencalculated and a graph plotted, on a large scale, of $(WC - WA)_T$ vs. $(WA)_T$. The best smooth curve was then drawn through these points. A reduced scale plot of this is shown in FIG.17. If the thermometers had identical characteristics (i.e. purity of the platinum wire and residual strain) then

$$(WC - WA) = f(WA) = 0$$

and the plot would give a straight line through (WC - WA) = 0 parallel to the WA axis. However, the deviation plot was found to be curved.

FIG.17. TREATMENT OF P.R. THERMOMETER INTERCOMPARISON RESULTS.



(3) From the deviation plot values of (WC - WA) were read off for all 598 values of RA in the original standard thermometer calibration table, and a tabulation of (WC - WA), RA and T°K made. Vales of RA were quoted for the following increments $\triangle$ RA to permit a linear interpolation for the appropriate temperature difference between RA and RA + $\triangle$ RA.

$\triangle$RA(ohms)	Temperature Range °K
0.10000	312° - 98°
0.08000	98° - 80°
0.04000	80° - 68°
0.02000	68° - 46°
0.01000	46° - 35°
0.00500	35° - 29°
0.00400	29° - 21°
0.00200	21° - 16°
0.00100	16° - 12°

(4) From the deviation found for each value of WA calculated from the calibration table the corresponding value of WC was found by addition. This was then multiplied by the ice point resistance and the factor 0.999504 to convert from absolute ohms, to international ohms, the unit in which the calibration of (A) was given.

SECTION V(e): Determination of the Ice Point Resistance of the Standard Thermometer(A) and Working Thermometers (B) and (C).

The ice point resistances of the three resistance thermometers were measured for two purposes:

(1) To ensure that the calibration of the standard thermometer (A) had not changed appreciably since 1958[94] and

(2) To test the reliability of the smoothed results from the intercomparison data for thermometers (B) and (C).

The apparatus used in the measurement of ice point resistance consisted of a 3/4" diameter pyrex tube 25 cm. long containing the thermometer held by means of a rubber sleeve to a thin glass rod. At no point did the rod or thermometer touch the sides of the outer tube. This was achieved by the introduction of several cotton wool plugs which also served to reduce convection currents in the tube. A rubber bung, carrying the 38 s.w.g. varnished double cotton covered wires from the thermometer and a silica gel filled drying-tube to remove moisture which could cause conduction between the leads, was sealed by picein wax to the top of the tube housing the thermometer.

This assembly was immersed to a depth of 20cm in a continually stirred ice-water bath contained in a narrow Dewar vessel. The various ice-water bath mixtures used were made from distilled water previously boiled with potassium permanganate to oxidise any organic material present. This distilled water, saturated with air at $0^{o}C$, was mixed with ice, frozen in a sealed plastic tray and crushed in a pestle and mortar. Throughout the preparation and transfer to the Dewar, manual contact with the ice was avoided. The conductivity of the ice bath mixture varied from 1.6 to 4×10^{-6} mho cm^{-1} at $0^{o}C$ for different ice baths. The freezing point depression calculated, sodium chloride being the most probable impurity, amount to only $\sim 3 \times 10^{-4}$ deg. Corrections for the depth of immersion in the ice-water bath given by Stimson[107] were also found to be negligible. Resistance measurements, made by the potentiometric comparison method, were taken over a period of several hours with thermometer currents of 3.6ma and 2.4.ma. The magnitude of the current heating effect on the resistance is shown below together with resistance values from the smoothed intercomparison data for the chosen working thermometer(C).

Table 6

Thermometer	MEAN Resistance ABS.Ω	Current(ma.)	No.of ice baths
(A)	21.6643	3.66	2
(Standard)	21.6639	2.42	2
(B)	17.8445	3.64	4
	17.8439	2.40	4
(C)	15.2935	3.64	2
	15.2932	2.40	2

The smoothed values at $0^{\circ}C$ ($273.15^{\circ}K$) from the inter-comparison data are;

$\frac{B}{17.8430}$ ABS.Ω $\frac{C}{15.2931}$ ABS.Ω

The value of RA at the ice point interpolated from Kington's table (1958) was 21.6632 ABS.Ω. Since the comparison resistance used was calibrated to approximately 1 in 2×10^5 the resistance calibrations should be correct to $\pm$ 0.0002 ohm or $\pm$ 0.003° (for thermometer C). Fluctuations of the order of 0.002° for the ice bath temperature have however been reported by Barber[108]. The overall error establishing the ice point could therefore amount to $\sim$ 0.008° when the variation of the measured thermometer resistance with current is accounted for.

The change in ice point resistance of A over four years corresponds to less than 0.008° and the agreement of the experimental ice point resistance with

the smooth table value for thermometer C (used in the heat capacity determinations)was within ± 0.0002 Ω or $\pm$ 0.0033°C.

CHAPTER VI. OXYGEN VAPOUR PRESSURE MEASUREMENTS

SECTION VI(a). Apparatus

The apparatus for intercomparing the three resistance thermometers with the oxygen vapour pressure was basically similar to the intercomparison block assembly as described in Section V(b) with the addition of a brass plate and tube soldered to cover the oxygen vapour pressure well. This tube was joined by a soft soldered seal to the thin monel-metal oxygen inlet tube, denoted by H. in FIG.8, by means of a brass sleeve passing through but electrically and thermally insulated from the top shield. In turn the inlet tube passed out of the cryostat through a soldered joint and was connected by a glass-metal seal to narrow (1.5 mm diameter), thick-walled, capillary tubing which led to the gas line of the auxillary pumping apparatus (FIG.15).

SECTION VI(b): Procedure for a run

The cryostat was filled with liquid nitrogen and 2 m.m of helium admitted to the insulating vacuum space. This permitted the shields and intercomparison block to cool to 77°K overnight. The oxygen vapour pressure well, inlet tube and gas lines were then evacuated to 1×10^{-6} m.m of mercury and spectrally pure 99.98% oxygen (British

Oxygen Co.) from a one litre globe (e.g. H in FIG.15) was admitted. As the density of liquid oxygen is approximately 1.14 gm per c.c. at the boiling point the oxygen vapour pressure bulb, which could hold in the condensed phase 2.8 litres of oxygen at N.T.P., was only about half full.

The cryostat jacket was then evacuated and the shield assembly controlled to give adiabatic conditions. To prevent "cold spots" on the inlet tube the current through a heater, wound non-inductively along the lower half of its length, was adjusted to ensure that a slight warm thermal head existed with respect to the copper comparison block. This produced a slight warm drift, arising also from the self-heating effect of the current passing through the resistance thermometers in the block temperature. The shield heaters were accurately controlled to reproduce this drift.

Values of "forward" and "reverse" thermometer current and potentials (to correct for parasitic e.m.f's in the galvanometer circuit) for (A),(B) and (C) were recorded as a function of time over a 20 minute period as described in section V(c). A thermometer current of 3.5 mA was used. Simultaneous determinations of the oxygen vapour pressure were made with a vibration free mercury manometer described in section IV(b). Measurements

of the menisci crowns and circumferences in each limb of the manometer were made using a cathetometer and 5 individual determinations of the vapour pressure were made over 20 minutes while the vacuum side of the manometer was continuously evacuated to approximately 10^{-6} m.m of mercury.

Intercomparisons were made in the temperature range of 73° - 91°K, using solid nitrogen as refrigerant below 77°K, for two different samples of oxygen (B.O.C.) denoted by (1) and (2) in TABLE 7. From the resistance-time plots, which in all cases showed a slight positive temperature drift with time, interpolated values at time (S) were obtained.

The individual vapour pressure determination data were corrected for surface tension meniscus depression for mercury using the results of Kistemaker[109] for 16 m.m tubing. Readings were also reduced to standard gravity go = 980.665 cm.sec^{-2} from the local gravitational constant of 981.195 cm sec^{-2} and corrected to give mercury column heights at 0°C using Linder's[110] formula:

$$ho = ht. \frac{981.195}{980.665} \left[\frac{1 + 18 \times 10^{-6}(t - 20)}{1 + 181.6 \times 10^{-6}t} \right]$$

where ho is the corrected height at 0°C and standard g, ht, is the observed height, t the temperature of the

mercury in the manometer, and the factors 18×10^{-6} and 181.6×10^{-6} the linear coefficient of expansion for the brass cathetometer scale and the cubical coefficient of expansion of mercury respectively. The total correction is of the order of -0.35% of ht when t = 21°C.

These corrected vapour pressures were plotted as a function of the time of measurement and interpolated values at time (S) read off. The absolute temperatures corresponding to these vapour pressures were then calculated from Hoge's data[104]. In particular the thermometer resistances corresponding to the oxygen boiling point (90.190°K - according to Hoge) were recorded, together with the smooth calibration table resistances for both (A) and (C). These values are shown below:

TABLE 8

Thermometer	Experimental RO_2 ABS. OHMS.	Calibration Table RO_2 ABS.OHMS
(A)	5.2841(0)	5.2848(5)
(B)	4.3570(6)	-------
(C)	3.7371(7)	3.7379(4)

The difference in these "two" oxygen boiling point resistances for (A) is equivalent to only 0.008°. It was concluded that the calibration of thermometer (A) had not changed appreciably since 1958 at this temperature and any errors arising from it would make a negligible contribution to the heat capacity data.

A more detailed comparison of the temperatures calculated from the smoothed table and oxygen vapour pressure data for the thermometer (C), chosen as the working thermometer for heat capacity measurements, is given in TABLE 7 and FIG.18. This table shows the differences ΔT between the vapour pressure and resistance thermometer temperatures and the increment in vapour pressure in cm. of mercury equivalent to ΔT. The smoothed thermometer(C) calibration table values are in good agreement $\pm 0.005^{\circ}$, over the temperature range $77^{\circ} - 91^{\circ}K$. Also recorded in FIG.18 are the deviations in millidegrees found by Edwards and Kington[95] in their comparison of the calibration table of (T5), the standard platinum resistance thermometer originally employed tc calibrate thermometer (A) of the present research. It is perhaps significant that the general trend of deviations is similar for both thermometers. This may reflect either a slight inconsistency in the temperature scale of (T5) or more probably an inherent error in the experimental technique used, since basically the same apparatus and method was used in both investigations.

SECTION VI(c) The Reliability of the Temperature Scale established for Thermometer(C)

The absolute accuracy of temperatures measured by thermometer (C) using the calibration table from

TABLE 7 . - LIQUID OXYGEN VAPOUR PRESSURE RUNS.
A comparison of temperatures derived from oxygen vapour pressure measurements with those from platinum resistance thermometer C.

Oxygen Sample	O_2 vapour pressure	T°K. (Hoge)	Temp.°K. Thermom.C.	(Tv.p.-Tc.) mdeg.	Error in v.p.=ΔT.
2	8.188cm.	73.234	73.220	+ 14	0.014cm.
2	12.722	76.025	76.016	+ 9	0.018
2	16.593	77.816	77.811	+ 5	0.012
2	21.152	79.571	79.524	+ 47	0.095
1	23.248	80.232	80.228	+ 4	0.012
2	30.579	82.323	82.322	+ 1	0.004
1	35.757	83.572	83.572	0	0.000
1	50.475	86.460	86.461	- 1	0.005
2	61.440	88.210	88.206	+ 4	0.028
1	71.181	89.569	89.570	- 1	0.007
2	72.714	89.769	89.765	+ 4	0.028
1	75.587	90.136	90.137	- 1	0.008
2	76.000	90.190	90.188	+ 2	0.016
2	78.031	90.445	90.439	+ 6	0.048
1	78.750	90.533	90.529	+ 4	0.032
2	80.863	90.786	90.784	+ 2	0.016
1	83.167	90.881	90.876	+ 5	0.040

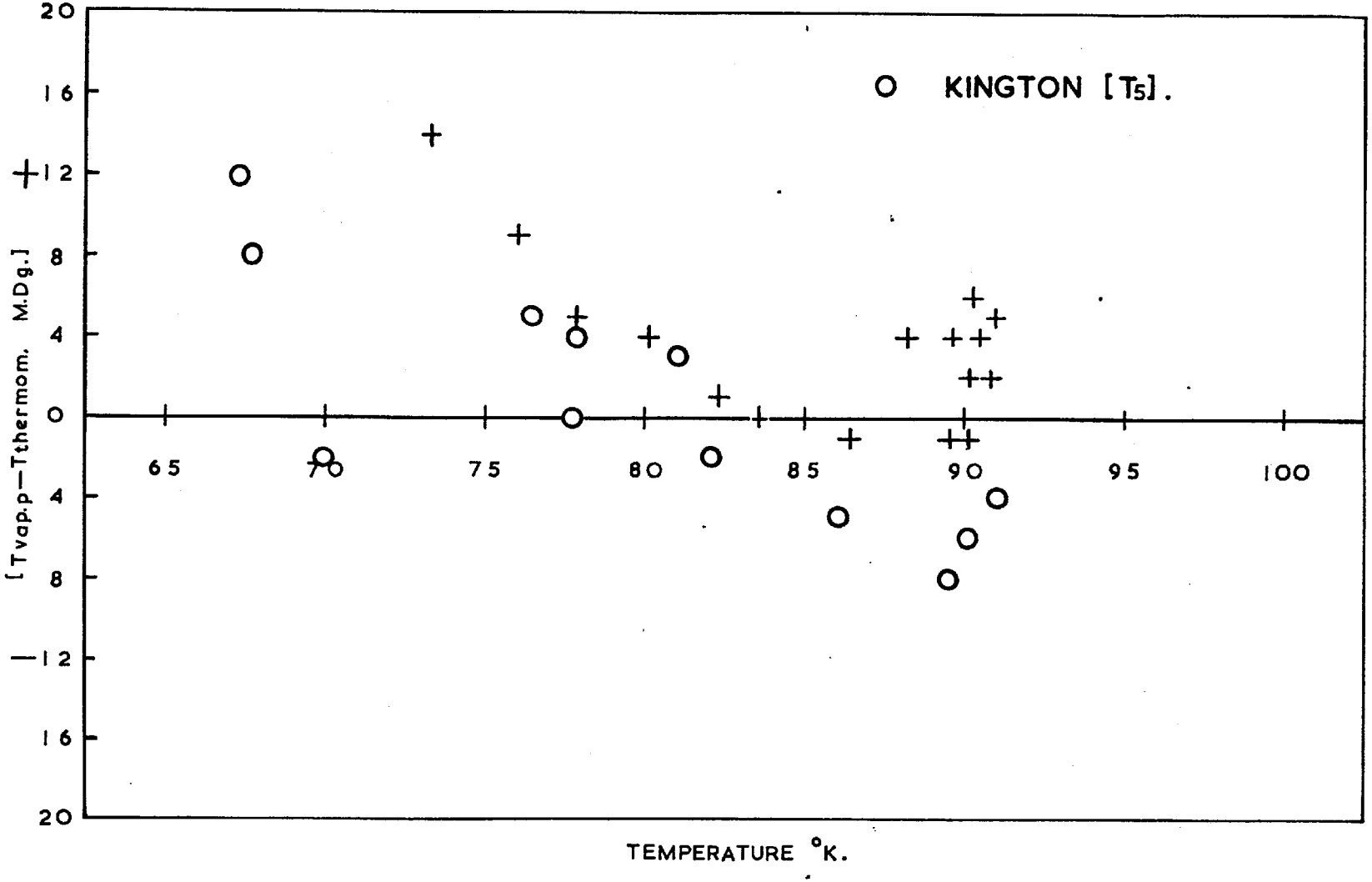


FIG. 18 COMPARISON OF P.R.T. WITH OXYGEN VAPOUR PRESSURE.

results of intercomparison with the standard thermometer (A) (see section V(b)) has been found by determination of ice point and oxygen boiling point resistances to be better than $\pm 0.01^{\circ}$C above 90°K. The precision in temperature measurement on the other hand, using a 3.5ma thermometer current is of the order of $\pm 0.001^{\circ}$ down to about 30°K. Below this temperature, where the coefficient dT/dRc ($\sim$ 34 deg.ohm^{-1}) has already doubled its ice point (273.15°K) value and is rising rapidly (88 deg.ohm^{-1} at 20°K, 127 deg.ohm^{-1} at 17.5°K and 196 deg.ohm^{-1} at 15°K), the precision falls to between $\pm 0.003^{\circ}$and $\pm 0.006^{\circ}$. Since the evaluation of the heat capacity requires the measurement of temperature rise, this should be accurately determined to $\pm 0.003^{\circ}$ above 90°K or approximately 0.010° at the temperatures below the hydrogen boiling point. The increment in temperature of approximately 5° characteristic of heat capacity runs in the temperature range above 45°K could therefore in principle be measured to better than 0.06%.

CHAPTER VII. THE TECHNIQUE OF HEAT CAPACITY MEASUREMENT

SECTION VII(a). Experimental Procedure

The calorimeter once filled with the sample and a pressure of about 1 cm of dry helium gas was sealed off and leak tested as described in section II(c). During the filling and sealing operations careful account was kept of the weight of the calorimeter assembly at various stages. This enabled the sample weight and corrections for weights of low melting point sealing solder, silver tube and Apiezon T grease relative to the corresponding amounts used in sealing and assembling the empty calorimeter to be determined. The calorimeter was then suspended within the experimental volume of the adiabatic shields (see FIG.8) and the electrical connections for the thermometer, calorimeter heater, differential thermocouples and shield heater circuits made.

The orientations of the calorimeter and its electrical connections with respect to the shield assembly and of the latter with reference to the cryostat framework were always maintained the same each time the apparatus was assembled. This ensured an identical environment for the sample holder during each set of measurements.

After testing the electrical circuits for both continuity and insulation, the copper vacuum can (J)(FIG 8) was soldered with low melting point solder (110°C) to the

outer flange of the top plate (E). During this operation vessel (J) was surrounded by an ice-water bath to act as a thermal sink and thereby prevent decomposition of the sample within the calorimeter and deterioration by charing of the wiring wound round flanges on plate (E). It was found, from measurements made with the calorimeter platinum resistance thermometers, that during this operation the sample always remained at a temperature below 20°C. The vacuum can (J) was then evacuated over a period of several days at room temperature to a pressure of $\sim 1 \times 10^{-6}$ mm. of mercury as measured by a cold cathode Penning gauge using a liquid nitrogen trap on the pumping line.

In order to cool the calorimeter a refrigerant gas was admitted to the cryostat Dewar and a small pressure (2 mm) of helium, as heat exchange gas, introduced into the insulating vacuum space within can (J). For measurement of heat capacity at temperatures between 77° and 300°K a liquid nitrogen bath was used. By reducing the pressure above the liquid nitrogen in the cryostat by means of a high capacity Kinney vacuum pump (see section II(b)), the calorimeter could be lowered to a temperature of about 48°K. To achieve temperatures below this an initial cooling bath of liquid nitrogen was used to lower the temperature to 77°K and then the excess liquid nitrogen was blown out of

the Dewar by applying an over pressure of nitrogen gas. Five litres of liquid hydrogen, from a double Dewar, were immediately blown in through an unsilvered evacuated transfer tube over a period of about 20 minutes in such a way that the stream of liquid fell directly onto the top plate (E) (see FIG. 8) and then ran down container (J) to derive the maximum cooling effect for the quantity of hydrogen used. For work between 10°and 20°K (the hydrogen boiling point) the cryostat was sealed and the pressure above the hydrogen reduced by pumping, thereby producing solid hydrogen. Five litres of hydrogen introduced into the cryostat in this way enabled the experimental measurements for about 15 runs between 11°and 48°K to be made over a period of approximately 8 hours.

During transfer and pumping operations involving liquid hydrogen all possible safety precautions were taken to reduce the explosion hazard. The laboratory was kept thoroughly ventilated and all electrical apparatus, apart from the gauge monitoring the pressure within can(J), was switched off during the period of transfer of hydrogen to the cryostat. Once the required measurements had been made the cryostat was isolated from the Kinney vacuum pump and carefully brought up to pressure with gaseous hydrogen. This prevented condensation of atmospheric oxygen in the Dewar when the apparatus was vented to the roof through an iron pipe (see section II(b)) leading

from the cryostat.

After cooling to the desired temperature the insulating vacuum space enclosing the shield and calorimeter was again pumped out to give a vacuum better than 1×10^{-6} mm of mercury. The currents through the three separate shield heaters were then adjusted to give as closely adiabatic conditions as possible and once the calorimeter had equilibrated at this temperature a series of measurements was started. The usual method of determining "fore" and "after" drifts of the calorimeter temperature with time was employed to correct the measured increment ΔT in the calorimeter temperature for the small inevitable heat exchange which occurs when heat Q is generated by passing an electric current through the calorimeter heater. The calorimeter heater and thermometer circuits have been previously discussed in sections III(d) and III(c). The procedure for a run is summarised below.

1) The potentiometer(see section III(c)) was standardised against a Weston standard cell to read in absolute volts.

2) Fore drift. Measurements of both "forward" and "reverse" thermometer current and potential were made to a precision of $\pm$ 0.1 microvolts by reversing the direction of current flow through the thermometer and potentiometer

circuits. By averaging these values it is possible to eliminate parasitic e.m.f's which occur in the galvanometer circuit. Each current "i" and potential "v" reading, taken in the sequence:

i(F-R), v(F-R),i(F-R), v(F-R), i(F-R), v(F-R),
i(F-R), v(F-R), i(F-R),v(F-R).

was recorded together with the time of measurement to ±5 seconds. Separate determinations of i and v occupied about 30 seconds giving a total drift time of approximately 10 minutes.

3) Heat input was then initiated by simultaneously switching from the dummy to the real calorimeter heater and activating the decatron time period counter. A stop watch was also started to check that an integral number of ten second periods of the heat input were not lost by jamming of the add-on register associated with the counter. Alternate measurements of heater current and potential, the former measured across a 1 ohm standard resistance (see section III(d)), with time to ± 1 microvolt, were made throughout the heat input period. The rate of heating was determined by the ease of control of the adiabatic shield temperatures and was usually of the order of 0.5 deg.min^{-1}. The heating current used was varied in conjunction with the duration of heat input to minimise

curvature corrections to the measured value of Cp. Typical temperature rises were as follows: 0.5-2 deg. below 20°K, 3-4 deg. from 30°-50°K and 4-8 deg. from 50°-300°K. Representative heating currents and heating periods together with the average heater resistance over the whole temperature range 11°-300°K are shown in TABLE 9. for the calorimeter filled with approximately 20g. of a urea adduct.

4) When heat input was terminated an equilibration period of length dependent upon the thermal conductivity of the calorimeter and sample and hence on the temperature of the Cp determination was allowed. This varied from 3 minutes at 12°K up to 20 minutes at about 50°K then reduced again to circa 10 minutes at 300°K. During this period the shield heater currents were reduced to typical "drift values", for that temperature, as the rate of rise of the calorimeter temperature fell. For the majority of runs the calorimeter reached its final thermal drift rate within one half of the total equibration period. The potentiometer was then restandardised prior to determining the after drift rate.

5) <u>After Drift</u>. After equilibration, measurements of thermometer current and potential were

TABLE 9 .- HEAT INPUT DATA.

Typical values for calorimeter + approximately 20g. adduct.

T° K	Heating Current (milliamps)	Heating Period (mins)	Heater Resistance (ohms)
300	28	26.0	407
275	28	23.0	407
250	28	21.5	406
225	28	18.5	405
200	28	16.5	403
150	26	14.5	397
125	26	11.5	391
100	24	12.0	385
80	24	9.0	382
70	24	8.5	378
55	24	8.0	374
50	18	11.5	371
45	18	9.5	370
40	14	9.0	369
35	14	8.0	367
30	14	7.0	365
25	9	9.0	363
20	9	4.5	362
18	7	5.5	361
16	5	7.0	360
14	5	5.0	360
13	5	2.5	359
12	5	2.0	359
11	5	1.5	359

again made as described for the fore drift. These after drift data also consituted the fore drift of the subsequent point.

The drift rates (see TABLE 10) were found to vary with the temperature of measurement and generally increase with a greater difference in the thermal head between the cryostat bath and the calorimeter-shield assemblies. This is most probably due to a flow of heat along the operative wiring to the cryostat or shield assembly. At the highest temperatures(above 280°K) a deterioration in the vacuum to about 2×10^{-5}mm of mercury also tended to increase the drift rate. However, the drifts were always linear with time, and, as is shown in the table, were negative above 75°K with solid nitrogen in the cryostat Dewar. Large positive drifts were found at the lowest temperatures(11°K) with solid hydrogen as refrigerant. On pumping away the helium exchange gas from the can(J) thermal conduction to the shield from the incoming wires was often sufficient to maintain the side shield at the same temperature as the calorimeter without passing a current through the shield heater.

To check the effect of the drift rate on the measured heat capacity three sets of runs above 273°K

TABLE 10 .- TYPICAL DRIFT VALUES.

Calorimeter filled with n-paraffin urea adduct.

(11-50)°K solid or liquid hydrogen in cryostat.

(50-300)°K solid or liquid nitrogen

T° K.	Drift rate in °per min.x10⁵	Drift correction as % of heat input for heating period.	Drift correction as % of heat input for eqlib.+heating period.
300	-360	1.41	2.0
275	-205	0.65	0.98
250	-130	0.36	0.56
225	-90	0.22	0.40
200	-55	0.13	0.22
175	-30	0.07	0.14
150	-15	0.03	0.06
125	-8	0.015	0.03
100	-4	0.007	0.014
75	-2	0.003	0.009
50	+2	0.003	0.012
40	+4	0.002	0.010
35	+10	0.005	0.015
30	+40	0.03	0.09
25	+80	0.15	0.55
20	+150	0.35	1.40
18	+190	0.50	1.90
16	+230	0.75	2.10
15	+280	0.95	2.80
14	+340	1.3	3.1
13	+450	2.7	8.2
12	+600	3.3	11.5
11	+4000	5.5	22.0

were made on the same sample of benzoic acid(see section IX(a)). Cryostat baths of ice-water,cardice-alcohol and finally liquid nitrogen were used. However, although the drift rates differed by a factor of up to fifty, the resulting heat capacities were always within $\pm$0.1% of the best line drawn through all the points.

The overall average drift corrections as a percentage of the temperature rise due to heat input for both the heat input period and for the equilibration plus the heat input period for various temperatures are also shown in TABLE 10.

SECTION VII(b) The Energy Input Measurements.

The energy(E) evolved when a constant current i(amps) flows through a constant resistance R(ohms) for t seconds is given by

$$E = i^2Rt = vit \text{ joules}$$

where v is the potential drop(volts) across the resistance. In practice however, the resistance R increases with the subsequent temperature rise and consequently i or both i and v(due to polarisation of the accumulator supplying the current) may vary with time.

Now the total energy liberated is given by:

$$E = V_{Av}.I_{Av}.t \text{ joules}$$

where VAv and IAv are the average potential and currents across and through the resistance respectively. These average values may be obtained by integrating under the i and v vs. time plots and dividing by the total time of heat input. The mean values IAv and VAv correspond closely to V½ and i½, the values at the half-time of heating, when the increase in R is approximately linear with time, as is usually found experimentally. The largest deviations from this linear dependence occur at the start of heat input, when a small thermal head is inevitably built up between the heater windings and the body of the calorimeter.

The practical circuit for heat input measurement (see FIG 13) is complicated by the introduction of a 100:1 potential divider to reduce the potential drop across the heater to the same order of magnitude, for convenience of measurement, as that across the 1 ohm standard used for current determination. Furthermore, account must be taken of the heat developed in the two current carrying leads to the heater. One half of the total heat produced was considered to flow to the calorimeter, the other half going to the side shield. Additional small corrections have also to be made for the potential drop along the relevant operative wiring

to the potentiometer. The detailed calculation for the energy input is presented below.

SECTION VII(c) The Calculation of Energy Input

Let i be the current through the 1 ohm standard resistance and i_1 and i_2 the currents through the potential divider and heater respectively (see FIG 13). Then from Kirchoff's law:

$$i = i_1 + i_2 \quad \text{.....(1)}$$

If the resistance of the potential divider leads (AB) and (CD) is RL then

$$Hi_2 = (10{,}000 + RL)\, i_1 \quad \text{.....(2)}$$

where H is the heater resistance and

$$V = 100\, i_1 \quad \text{.....(3)}$$

$$I = ls.i \quad \text{.....(4)}$$

where ls is the resistance of the 1 ohm standard, V is the potential drop across the potential divider 100 ohm tapping and I is the potential across the 1 ohm standard.

Consequently the energy E^1 liberated per second in the heater is given by

$$E^1 = i_2^2\, H \text{ joules} \quad \text{.....(5)}$$

$$= i_1 i_2 (10{,}000 + RL) \text{ joules} \quad \text{.....(6)}$$

and since

$$i_2 = i - i_1 = (I/1s - V/100) \quad \ldots\ldots\ldots(7)$$

therefore:

$$E^1 = (10,000 + RL)(V/100)(I/1s - V/100) \ldots(8)$$

$$= V(^{10,000}/_{100})(I/1s - V/100) + {}^{VRL}/_{100}(I/1s - V/100) \quad \ldots\ldots(9)$$

However, since a current i_1 flows in the potential leads AB and CD, heat will be developed in these leads, half of which is involved in raising the calorimeter temperature. This is given by:

$$(V/100)^2 \, RCL \quad \ldots\ldots\ldots\ldots\ldots\ldots(10)$$

where RCL is the resistance of the copper lead AE. Therefore the total energy reaching the calorimeter per second is given by:

$$E^1 = V(^{10,000}/_{100})(I/1s - V/100) + {}^{VRL}/_{100}(I/1s - V/100) + (V/100)^2 RCL \quad \ldots\ldots\ldots(11)$$

Besides the potentiometer measurement of I and V during the heat input this equation is dependent upon the absolute values of:

(a) The 1 ohm standard

(b) The potential divider ratio $^{10,000}/_{100}$

(c) The 100 ohm tapping of the potential divider

(d) The resistances of RL and RCL

These values have all been measured experimentally and are recorded below together with values of a previous calibration.

(a) 1s = 1.0001(3) abs.ohm at 20°C

Previous calibration(1958) gave 1.0000(4) abs. ohm.

(b) $(^{10,000}/_{100})$ ratio = 100.015:1 at 20°C

Previous calibration(1959) 99.987:1

(c) 100 ohm tapping of potential divided = 100.015 abs.ohm at 20°C

Previous calibration(1958) 100.030 abs.ohm.

(d) The magnitudes of RL and RCL were approximately 4 ohms and 1 ohm respectively.

Consideration of the three terms contributing to the heat input per second, once the average values of IAV and VAv have been substituted for I and V, shows the last to be negligible (maximum contribution is 0.0001 %).

$$E^1 = VAv(10,000/100)(IAv/1s - VAv/100) + \frac{VAvRL}{100}\left(IAv/1s - VAv/100\right) + \left(\frac{VAv}{100}\right)^2 RCL \quad \ldots\ldots(12)$$

The second term, involving the heat developed in the heater leads (RL), contributes 0.04% of the total E^1. In order to ensure that the measured heat input was correct to better than 0.1% the equation:

$$E_{TOTAL} = T^1\left[V_{Av}(^{10,000}/_{100}).(^{I_{Av}}/_{1s} - {}^{V_{Av}}/_{100}) + \frac{V_{Av}R_L}{100}\,(^{I_{Av}}/_{1s} - {}^{V_{Av}}/_{100})\right] \quad \ldots\ldots\ldots(13)$$

was used where T^1 is the absolute heat input period in seconds and the calibrated values substitued for the standard resistances and the potential divider ratios.

The energy inputs from this equation were correct to $\pm 0.01\%$ since RL was measured to ± 0.2 ohm and the calibration of resistances could be in error by 1 in 2×10^{-4}.

SECTION VII(d). Evaluation of Heat Capacity from Experimental Data for a Specimen Point.

Run(68) n-Eicosane Adduct (Solid hydrogen in the cryostat). The experimental values for both "forward" and "reverse" measurements of the thermometer current(i) and potential (v), the former deterrined from the potential drop across a standard 10 ohm resistance (see FIG.11.), for the fore-drift of run 68 are recorded below. This series of results also formed the after-drift of the previous run.

TABLE 11

(1)	(2) "Forward"	(3) "Reverse"	(4)	(5) Average	(6) Average	(7) Thermom.
Thermom.C	(volts x10^{-2})		Time	F-R	Time	Resistance
i.	3.12565		48:40	3.12557	48:55	
	(3.12554)	3.12570	49:10			
v.	0.02043	(3.12559)	50:10	0.02035	50:30	0.06511
	(0.02036)	0.02042	50:45			
i.	3.12564	(0.02035)	51:45	3.12555	51:55	
	(3.12553)	3.12569	52:00			
v.	0.02043	(3.12558)	52:45	0.02036	53:05	0.06514
	(0.02036)	0.02043	53:20			
i.	3.12564	(0.02036)	53:45	3.12555	53:55	
	(3.12553)	3.12567	54:05			
v.	0.02045	(3.12556)	54:45	0.02037	55:00	0.06517
	(0.02038)	0.02043	55:10			
i.	3.12562	(0.02036)	55:40	3.12552	55:55	
	(3.12551)	3.12563	56:05			
v.	0.02046	(3.12552)	56:50	0.02038	57:05	0.06520
	(0.02039)	0.02044	57:20			
i.	3.12565	(0.02037)	57:55	3.12555	58:05	
	(3.12554)	3.12567	58:15			
v.	0.02047	(3.12556)	58:55	0.02039	59:10	0.06524
	(0.02040)	0.02045	59:20			
i.	3.12566	(0.02038)	59:50	3.12556	0:05	
	(3.12555)	3.12568	0:15			
v.	0.02048	(3.12557)	0:55	0.02040	1:10	0.06527
	(0.02041)	0.02038	1:20			
		(0.02038)				

The potentials in brackets are values corrected for the potentiometer calibration and those in the fifth column the average of these corrected forward and reverse readings. The time of measurement within ± 5 seconds and the average time for both the forward and reverse pair i and v are shown in columns (4) and (6).

The notation for representing times of readings is as follows - minutes:seconds.

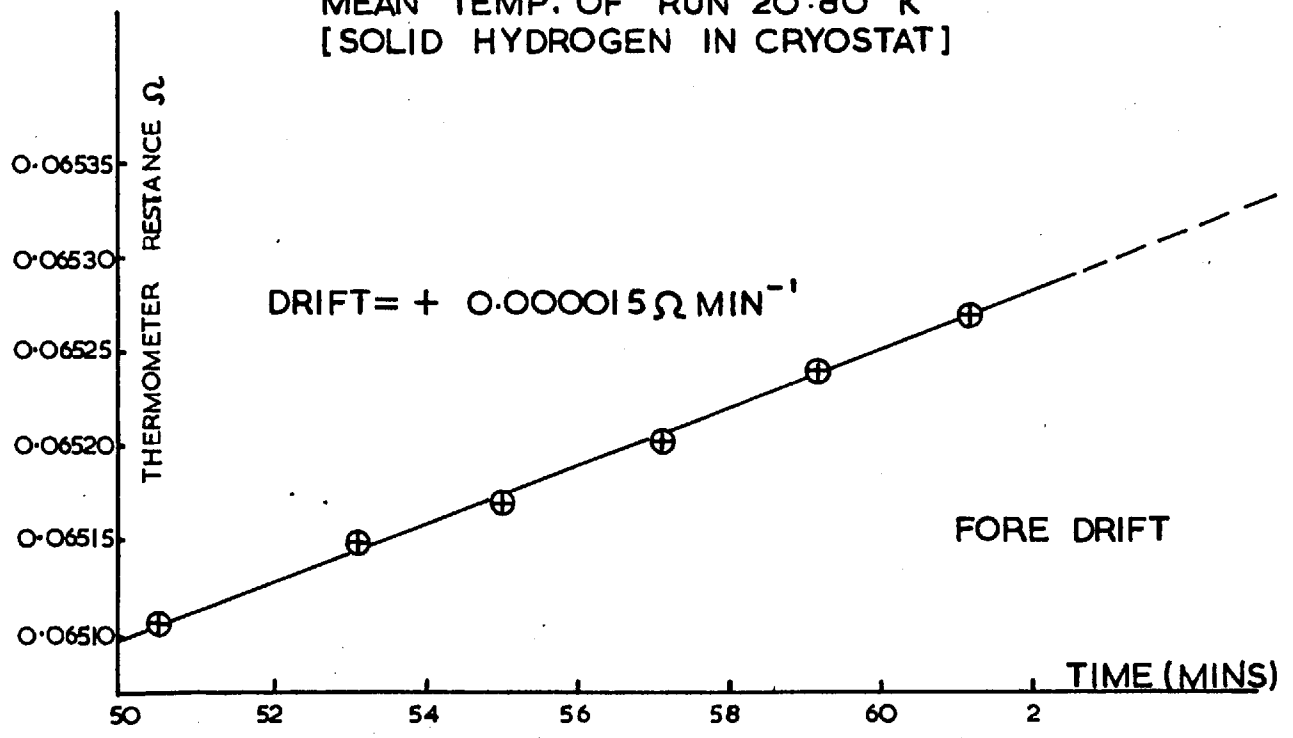
The thermometer resistance, given in column (7), was calculated from the interpolated value of the thermometer current at the average F-R time for each potential measurement in turn. A plot of the variation of thermometer resistance with time was then made (see FIG 19) and the fore-drift rate of +0.000015 ohms min^{-1} obtained.

By extrapolation to time 4:08, corresponding to the midpoint of the heat input period, the thermometer resistance (Initial Resistance) corrected for the linear temperature rise was determined.

The variation of thermometer resistance as a function of time during the after-drift was found by a similar procedure and the drift rate (+0.000014 ohms min^{-1}) derived from the drift plot (FIG.19). The value of the thermometer resistance (Final Resistance), again at the time of 4:08, was calculated by extrapolating back through the 14 minute long equilibration period.

The data for this after-drift, which in this instance also formed the fore-drift of the subsequent run is shown below.

FIG. 19 . GRAPHS OF FORE AND AFTER DRIFTS FOR Cp RUN (68) WITH 26·2953 g. OF N EICOSANE ADDUCT IN THE CALORIMETER.
MEAN TEMP. OF RUN 20·80°K
[SOLID HYDROGEN IN CRYOSTAT]



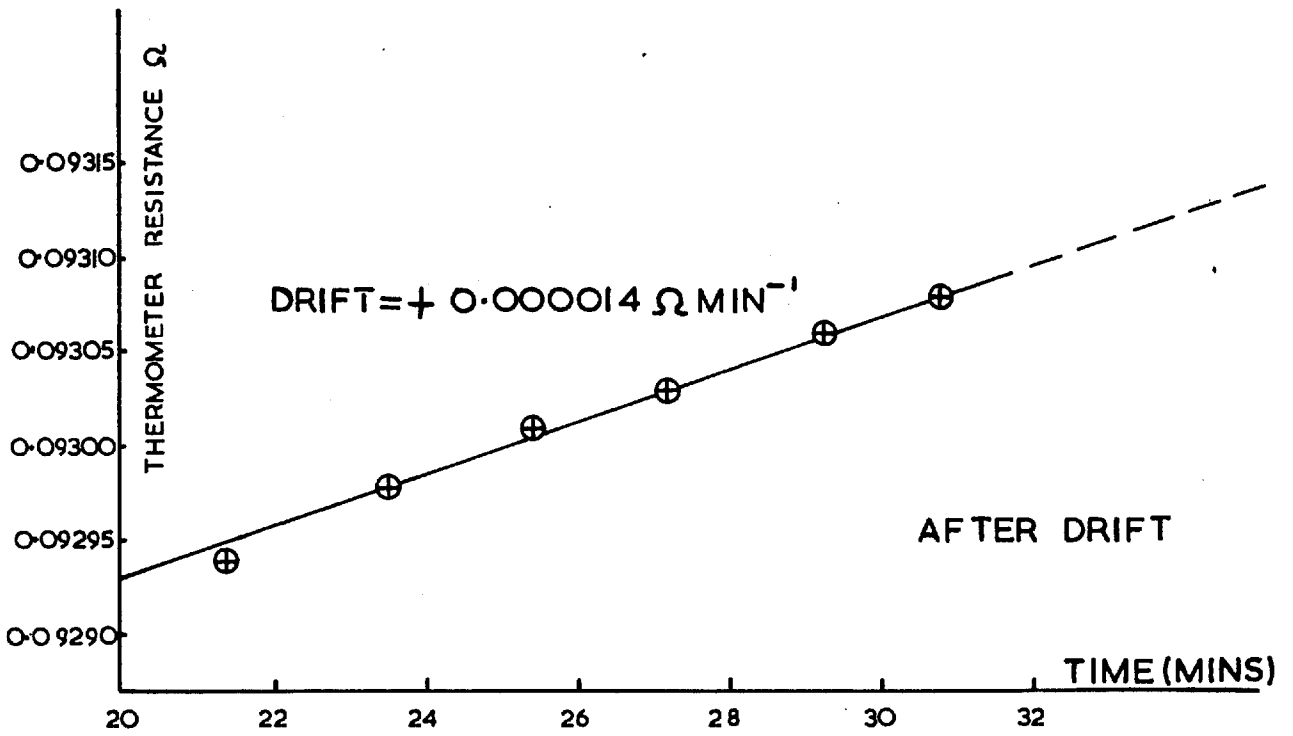


TABLE 12

(1)	(2) "Forward"	(3) "Reverse"	(4)	(5) Average	(6) Average	(7) Thermom.
Thermom.C	(volts x10^{-2})		Time	F-R	Time	Resistance
i.	3.12561		19:30	3.12554	19:50	
	(3.12550)	3.12570	20:05			
v.	0.02915	(3.12559	21:10	0.02905	21:25	0.09294
	(0.02907)	0.02911	21:35			
i.	3.12565	(0.02903)	22:20	3.12557	22:25	
	(3.12554)	3.12571	22:35			
v.	0.02916	(3.12560)	23:20	0.02906	23:30	0.09298
	(0.02908)	0.02912	23:40			
i.	3.12564	(0.02904)	24:15	3.12556	24:20	
	(3.12553)	3.12569	24:30			
v.	0.02917	(3.12558)	25:15	0.02907	25:25	0.09301
	(0.02909)	0.02913	25:35			
i.	3.12564	(0.02905)	26:10	3.12556	26:20	
	(3.12553)	3.12570	26:25			
v.	0.02917	(3.12559)	27:00	0.02908	27:10	0.09303
	(0.02909)	0.02915	27:20			
i.	3.12564	(0.02907)	28:05	3.12555	28:20	
	(3.12553)	3.12567	28:30			
v.	0.02917	(3.12556)	29:00	0.02907	29:15	0.09306
	(0.02917)	0.02913	29:30			
i.	3.12561	(0.02905)	29:55	3.12552	30:05	
	(3.12550)	3.12565	30:15			
v.	0.02919	(3.12554)	30:40	0.02909	30:50	0.09308
	(0.02911)	0.02914	31:00			
		(0.02906)				

Heat input Data:

Starting time of heat input = 2:00.

Total heat input period = 255.7001 seconds (from decatron timer).

Heat input period corrected for timer calibration = 255.69157 seconds.

Initial Resistance = 0.06532 ohms.

Final Resistance = 0.09270 ohms.

Both initial and final resistance values were then corrected for the true value of the 10 ohm standard

resistance (10.0044 ABS.ohms) and the resulting values in absolute ohms converted to International ohms.

(1 Absolute ohm = 0.999504 International ohms).

The corrected resistances are shown below:

Initial R(corrected) = 0.06528 INT.ohms.

Final R (corrected) = 0.09265 INT.ohms.

From the thermometer calibration table, which gives the thermometer resistance Rc at intervals of Rc = 0.002 INT. ohms for the temperature range 23.0°-18.13°K, the listed resistances lower than but closest to the experimental values were read off together with the coefficients $\Delta T/\Delta R$. These were as follows:-

0.064 ohm. = 19.589°K. $\Delta T/\Delta R = 93.50 \frac{\text{deg}}{\text{ohm}}$

0.09200 ohm = 21.846°K $\Delta T/\Delta R = 70.00 \frac{\text{deg}}{\text{ohm}}$.

Thus a resistance of 0.06528 INT.ohms corresponds to a temperature given by:-

$$19.589 + (0.00128 \times 93.50)$$

$$= 19.589 + 0.120 = 19.709^{\circ}K.$$

Similarly 0.09265 INT.ohms represents a temperature of 21.892°K.

The mean temperature was therefore 20.801°K and the change in temperature $\Delta T = 2.183^{\circ}$.

The energy produced per second in the calorimeter heater was calculated from equation (13) developed in section VII(c). For this computation the average values of heater current and potential were required. These were obtained from the experimental readings of heater current (I) and potential (V) by graphical integration under plots of (I) and (V) against time over the entire heating period.

The data and derived average heater current and potential, the former being measured as the potential drop across a 1 ohm standard resistance, are recorded below.

TABLE 13

Start of heat input at time = 2:00

Stop heat input at time = 6:15

Heater	Measured Potential in (volts)	Time
I	0.009310	2:30
V	0.033668	3.20
I	0.009307	3:45
V	0.033677	4:10
I	0.009306	4:30
V	0.033686	5:05
I	0.009305	5:30
V	0.033694	6:05

(I)Av. = 0.009307 volts.

(V)Av. = 0.033681 volts.

The average heat input per second was thus 0.030228 ABS.joules from equation(13) in section VII(c), when correctionsfor the true calibrated values of the standard 1 ohm resistance and potential divider had been applied. The total heat input (Q) is thus given by:-

$$0.030228 \times 255.69157 = 7.7290 \text{ ABS.JOULES}$$

and the net heat capacity at 20.80(1)^{o}K by

$$Cp = \frac{Q}{T} = \frac{7.729}{2.183} = 3.541 \text{ ABS.JOULES DEG.}^{-1}$$

Interpolation from TABLE 15 gives the empty calorimeter heat capacity at 20.801^{o} as 1.215 ABS.JOULES DEG^{-1} and calculated corrections for the different amounts of low melting point sealing solder, silver tube and Apiezon grease used relative to the empty calorimeter total - 0.010 ABS.J.DEG^{-1}. The heat capacity of the eicosane adduct(26.2953g. in vacuo) was therefore 2.316 ABS.J.DEG.$^{-1}$. From the analysis of the adduct it was shown that this weight of adduct contained 19.9844g. of urea. Consequently the weight of adduct containing 1 mole (60.058g.) is given by

$$\frac{60.058 \times 26.2953}{19.9844} = 79.024\text{g.}$$

Thus to convert the experimental heat capacities to calories per degree per weight of adduct containing 1 mole of urea a multiplying factor of

$$\frac{79.024}{26.2953 \times 4.1840} = 0.7183$$

must be used.

At 20.801°K the adduct heat capacity was therefore 1.663 cals.deg^{-1} wt. adduct containing 1 mole of urea.

Owing to the time-consuming nature of these calculations and the large number of "runs" carried out on each sample, a computer programme was written to evaluate heat capacity from the experimental data. This programme was in Mercury Autocode and was used on both the Mercury and Atlas computers in London.

CHAPTER VIII. THE HEAT CAPACITY OF THE EMPTY CALORIMETER

SECTION VIII(a). Determination and Results of the empty Calorimeter Heat Capacity

The heat capacity of the empty calorimeter (after the modifications described in section IX(a)) used in the work on benzoic acid and the urea adducts was determined at 75 points between 12° and 300°K. The experimental curvature corrected results in absolute joules degree^{-1} are shown in TABLE 14. Also recorded are the mean temperatures and the temperature increments of the individual runs Δ T. In order to reduce the curvature correction in the Cp. vs. temperature curve, the value of Δ T was varied according to the temperature range in which measurements were being made.(e.g.1-3 degrees in the range 12°-20°K rising to 3°-5° from 20°-100°K and 5°-7° above 100°K. These increments gave a maximum curvature correction of only 0.2%.

From a large scale plot of the experimental heat capacities vs temperature a smooth curve was drawn and Cp values at 1° intervals, from 13°to 300°K, suitable for linear interpolation (see TABLE 15) were read off. Values of Cp at 11°and 12°K were also found by extrapolation. The precision of the heat capacity determinations

TABLE 14.- EXPERIMENTAL VALUES OF THE EMPTY CALORIMETER HEAT CAPACITY IN ABS. J. DEG^{-1}.

Run No.	Temp. °K.	ΔT°	Cp.
1	199.77	5.594	18.821
2	205.35	5.609	18.939
3	210.97	5.654	19.103
4	216.60	5.623	19.210
5	222.40	6.174	19.310
6	228.66	6.427	19.434
7	235.17	6.685	19.536
8	241.89	6.920	19.678
9	248.84	7.174	19.770
10	256.00	7.410	19.903
11	263.37	7.642	20.011
12	270.89	7.736	20.146
13	80.66	4.936	12.558
14	85.49	4.710	13.155
15	90.23	4.786	13.648
16	95.30	5.358	14.122
17	100.57	5.190	14.566
18	105.74	5.161	14.973
19	110.99	5.368	15.348
20	116.40	5.459	15.718
21	121.85	5.449	16.047
22	127.34	5.554	16.358
23	132.88	5.551	16.666
24	139.34	5.246	16.960
25	144.60	5.306	17.193
26	150.00	5.514	17.407
27	155.51	5.588	17.594
28	161.11	5.647	17.806
29	166.70	5.583	17.987

TABLE 14(Continued).

Run No.	Temp. °K.	ΔT°	Cp.
30	172.30	5.666	18.148
32	178.06	5.750	18.324
33	183.51	5.220	18.444
34	188.87	5.567	18.600
35	194.37	5.523	18.729
36	50.26	4.281	7.510
37	54.51	4.163	8.376
38	58.65	4.092	9.168
39	62.81	4.184	9.930
40	66.92	4.037	10.620
41	70.91	3.942	11.226
42	74.82	3.872	11.767
43	78.51	3.495	12.266
44	276.59	6.340	20.252
45	282.98	6.532	20.351
46	289.46	6.510	20.417
47	295.64	6.003	20.439
48	199.81	6.042	18.818
49	205.89	6.294	18.953
50	212.14	6.396	19.089
51	218.38	6.500	19.216
52	224.82	6.601	19.326
53	231.35	6.693	19.484
54	237.92	6.151	19.581
55	242.05	6.405	19.712
56	250.51	6.809	19.822
57	257.26	7.069	19.913
58	263.71	7.033	20.012
59	270.49	6.985	20.143
62	19.57	2.806	1.061
63	22.72	2.728	1.510

TABLE 14(Continued).

Run No.	Temp. °K.	ΔT°	Cp.
64	25.47	2.303	2.024
65	27.96	2.396	2.476
66	30.85	3.194	3.106
67	34.39	3.813	3.900
68	38.27	3.837	4.813
69	42.26	4.068	5.723
70	46.51	4.377	6.677
71	12.66	0.866	0.345
72	14.56	1.577	0.459
73	17.22	3.052	0.740
74	20.51	2.982	1.171
75	23.97	3.565	1.726

TABLE 15.- SMOOTHED VALUES OF THE HEAT CAPACITY OF THE EMPTY CALORIMETER FROM 11 - 310°K IN ABS. J. DEG^{-1}. Suitable for linear interpolation.

Temp. °K.	Cp.	Temp. °K.	Cp.	Temp. °K.	Cp.
11	0.269	40	5.189	69	10.936
12	0.312	41	5.422	70	11.082
13	0.358	42	5.661	71	11.229
14	0.417	43	5.888	72	11.371
15	0.494	44	6.119	73	11.509
16	0.589	45	6.341	74	11.648
17	0.704	46	6.569	75	11.789
18	0.833	47	6.792	76	11.928
19	0.962	48	7.016	77	12.066
20	1.099	49	7.235	78	12.201
21	1.243	50	7.453	79	12.332
22	1.398	51	7.664	80	12.462
23	1.557	52	7.871	81	12.594
24	1.733	53	8.077	82	12.725
25	1.912	54	8.277	83	12.849
26	2.103	55	8.468	84	12.972
27	2.299	56	8.664	85	13.096
28	2.505	57	8.858	86	13.213
29	2.711	58	9.047	87	13.317
30	2.922	59	9.231	88	13.423
31	3.141	60	9.417	89	13.528
32	3.359	61	9.603	90	13.628
33	3.581	62	9.778	91	13.726
34	3.816	63	9.960	92	13.819
35	4.042	64	10.132	93	13.914
36	4.277	65	10.300	94	14.007
37	4.501	66	10.467	95	14.097
38	4.733	67	10.628	96	14.184
39	4.955	68	10.784	97	14.267

TABLE 15 (Continued).

Temp. °K.	Cp.	Temp. °K.	Cp.	Temp. °K.	Cp.
98	14.352	129	16.449	160	17.773
99	14.436	130	16.500	161	17.808
100	14.517	131	16.553	162	17.842
101	14.600	132	16.601	163	17.878
102	14.680	133	16.653	164	17.909
103	14.757	134	16.703	165	17.941
104	14.836	135	16.752	166	17.971
105	14.912	136	16.802	167	18.003
106	14.991	137	16.851	168	18.034
107	15.064	138	16.900	169	18.064
108	15.137	139	16.948	170	18.097
109	15.208	140	16.994	171	18.128
110	15.280	141	17.038	172	18.156
111	15.351	142	17.082	173	18.186
112	15.421	143	17.128	174	18.213
113	15.489	144	17.171	175	18.241
114	15.558	145	17.213	176	18.269
115	15.627	146	17.254	177	18.294
116	15.693	147	17.292	178	18.320
117	15.757	148	17.332	179	18.348
118	15.820	149	17.369	180	18.372
119	15.881	150	17.407	181	18.398
120	15.940	151	17.443	182	18.424
121	16.000	152	17.481	183	18.450
122	16.058	153	17.518	184	18.474
123	16.118	154	17.556	185	18.500
124	16.175	155	17.592	186	18.526
125	16.232	156	17.631	187	18.550
126	16.287	157	17.668	188	18.572
127	16.339	158	17.703	189	18.597
128	16.393	159	17.740	190	18.619

TABLE 15 (Continued).

Temp. °K.	Cp.	Temp. °K.	Cp.	Temp. °K.	Cp.
191	18.642	222	19.301	253	19.869
192	18.663	223	19.322	254	19.885
193	18.684	224	19.344	255	19.900
194	18.703	225	19.366	256	19.918
195	18.723	226	19.388	257	19.934
196	18.743	227	19.406	258	19.950
197	18.763	228	19.427	259	19.966
198	18.785	229	19.442	260	19.982
199	18.807	230	19.461	261	19.998
200	18.828	231	19.479	262	20.012
201	18.849	232	19.499	263	20.028
202	18.868	233	19.518	264	20.045
203	18.891	234	19.537	265	20.061
204	18.912	235	19.557	266	20.078
205	18.934	236	19.576	267	20.094
206	18.953	237	19.593	268	20.110
207	18.977	238	19.611	269	20.128
208	19.000	239	19.630	270	20.142
209	19.020	240	19.648	271	20.159
210	19.042	241	19.663	272	20.177
211	19.063	242	19.682	273	20.191
212	19.084	243	19.699	274	20.208
213	19.105	244	19.714	275	20.225
214	19.127	245	19.732	276	20.242
215	19.148	246	19.750	277	20.258
216	19.170	247	19.768	278	20.277
217	19.193	248	19.783	279	20.293
218	19.214	249	19.800	280	20.309
219	19.237	250	19.818	281	20.323
220	19.258	251	19.836	282	20.338
221	19.280	252	19.852	283	20.352

TABLE 15 (Continued).

Temp. °K.	Cp.	Temp. °K.	Cp.	Temp. °K.	Cp.
284	20.364	293	20.452	302	20.509
285	20.378	294	20.458	303	20.514
286	20.389	295	20.466	304	20.520
287	20.400	296	20.472	305	20.525
288	20.410	297	20.479	306	20.529
289	20.419	298	20.486	307	20.532
290	20.426	299	20.491	308	20.538
291	20.435	300	20.498	309	20.541
292	20.443	301	20.503	310	20.546

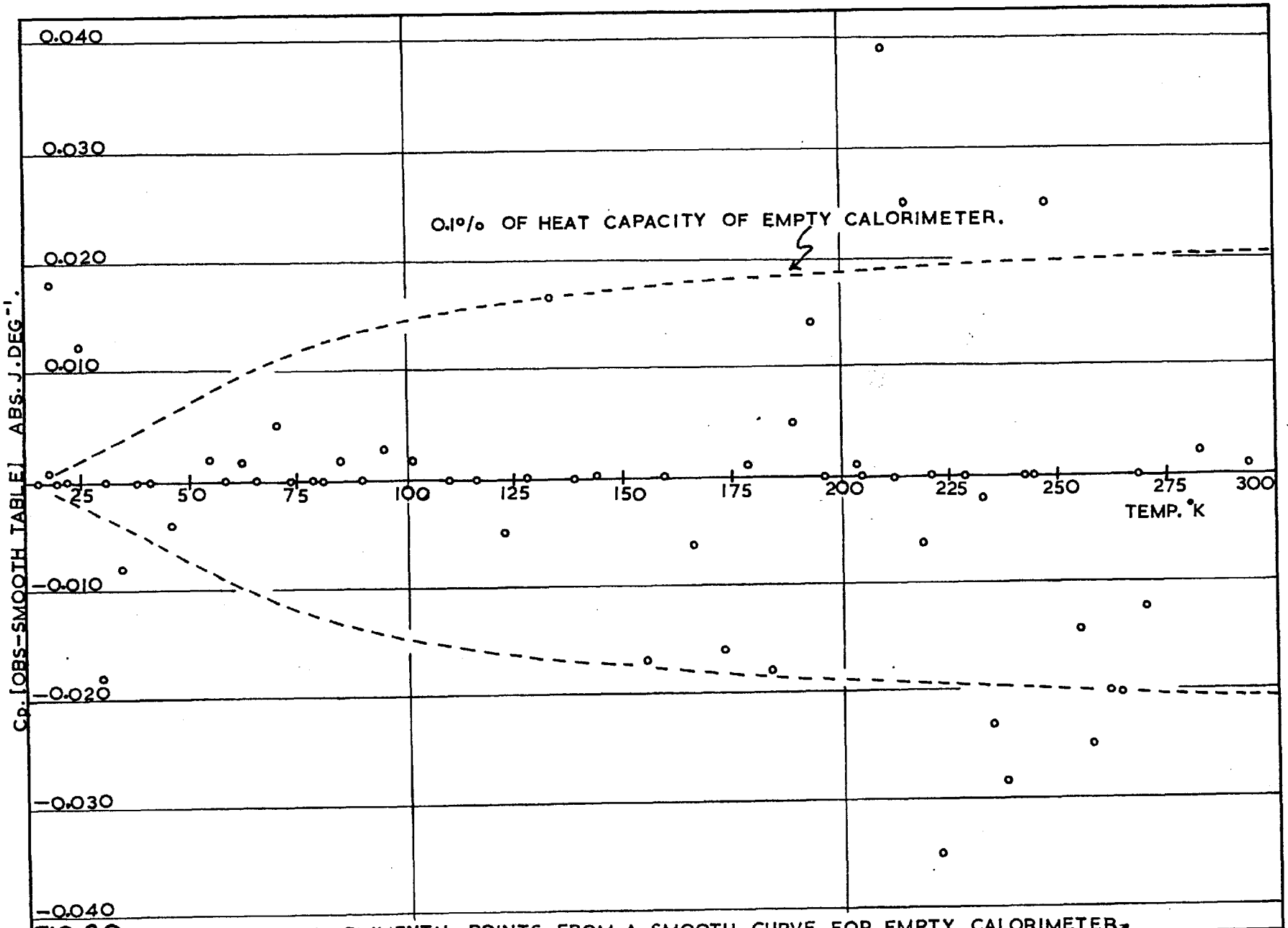


FIG. 20 DEVIATIONS OF EXPERIMENTAL POINTS FROM A SMOOTH CURVE FOR EMPTY CALORIMETER.

is shown in FIG 20. where deviations of the experimental points from the smooth curve are plotted and also as the root mean square % deviation in TABLE 29. Above 70°K the r.m.s. standard deviations are less than 0.1% of the total heat capacity of the empty calorimeter which would give an error of only approximately 0.08% in Cp for a typical sample ofaurea adduct. Below 25°K the r.m.s. deviation rises to 0.64% owing to the rapid decrease in both the calorimeter heat capacity and thermometer sensitivity.

CHAPTER IX. HEAT CAPACITY MEASUREMENTS ON A STANDARD THERMODYNAMIC SUBSTANCE

SECTION IX(a) The Heat Capacity of Benzoic Acid

To check the reliability of the low temperature calorimetricapparatus and technique of heat capacity determination with respect to both systematic and absolute errors, control measurements were conducted on a standard thermodynamic substance. The National Bureau of Standards (Washington) has proposed several such substances (e.g. diphenyl ether,n-heptane and benzoic acid) and has published tables of their heat capacities and enthalpies[111]. Benzoic acid was selected as the standard in this research primarily because of its ready commercial availability in extremely pure form.

The sample used was B.D.H. thermochemical standard benzoic acid supplied as tablets having a moisture content not exceeding 0.001%. A representative fraction of the batch of benzoic acid supplied had been submitted by the manufacturers to the National Physical Laboratory for certification of purity as determined by its heat of combustion (6320.8 $\pm$ 0.4 cals. 15°C per gm.) under standard conditions[112]. The tablets were crushed in a pestle and mortar and desicated for two weeks over anhydrous silica gel prior to filling the calorimeter.

The sample weighing 26.4169 gm. in vacuo was then thoroughly evacuated to remove any remaining surface moisture at $1x10^{-5}$ mm. of mercury for 30 minutes using a liquid nitrogen trap on the pumping line. After leak testing the calorimeter was filled with a pressure of 1cm of dry helium and sealed off as described in section II(c).

Heat capacities were measured at 18 points in the temperature range 50°-286°K and for 10 points between 12° and 48°K. The values of Cp obtained were corrected for curvature, the smoothed heat capacity of the empty calorimeter and differences in the weights of solder, silver tube and Apeizon T grease used in the empty and filled calorimeter runs to give the heat capacity of the benzoic acid sample alone. The contribution of the empty calorimeter heat capacity to the total filled Cp values was 28% at 12°K, 51% at 90°K and 40% at 280°K. The experimental Cp values for the weight of benzoic acid in the calorimeter and the molar heat capacity derived from these results are shown in TABLE 16.

Values obtained by interpolation in the table of smoothed results reported by Furukawa and Ginnings[111] were compared with the present data and the difference expressed as a percentage deviation. Percentage deviation plots from the N.B.S. values (FIGS.21 and 22) were made and

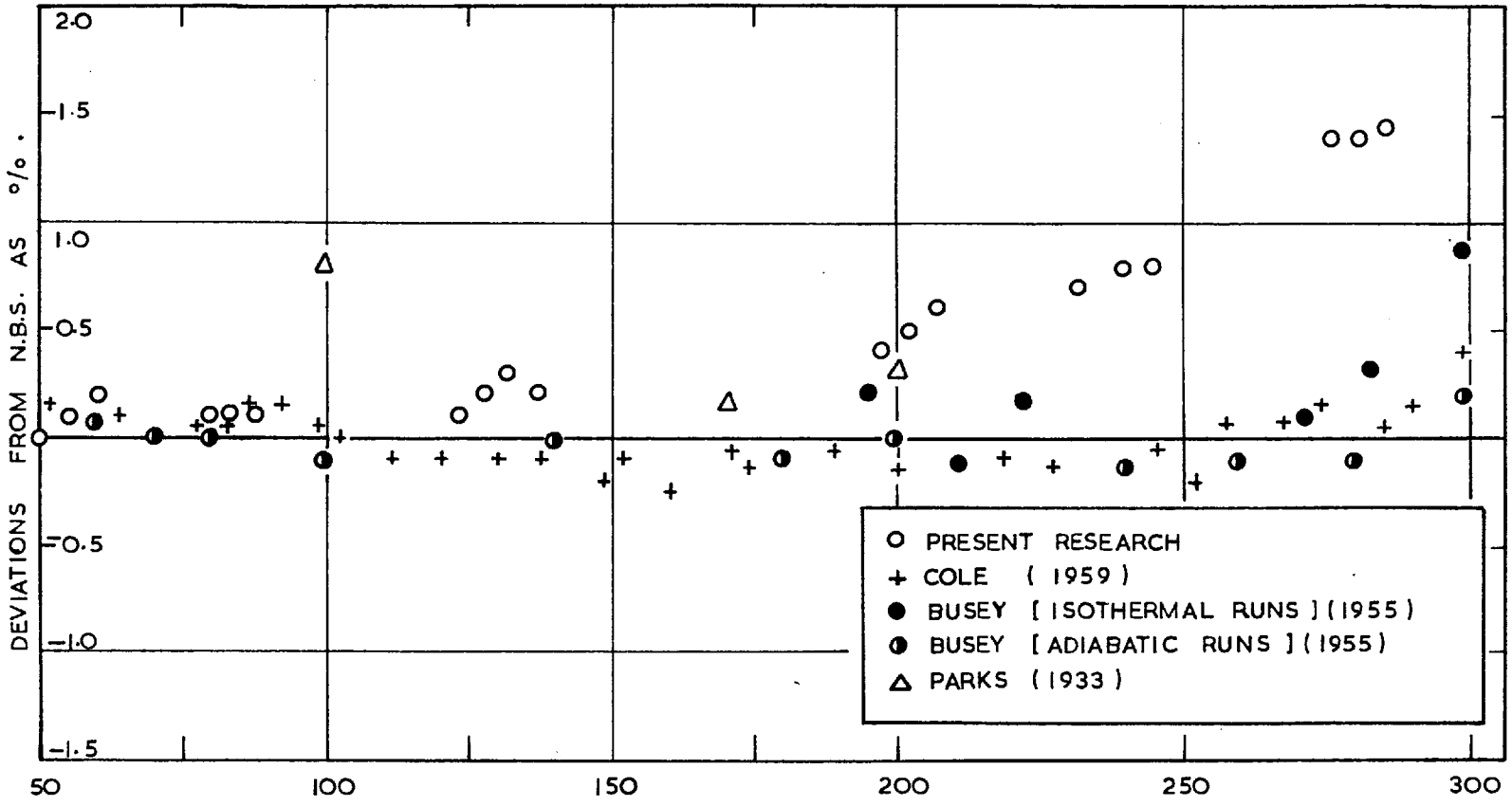
TABLE 16 .- HEAT CAPACITY OF BENZOIC ACID.

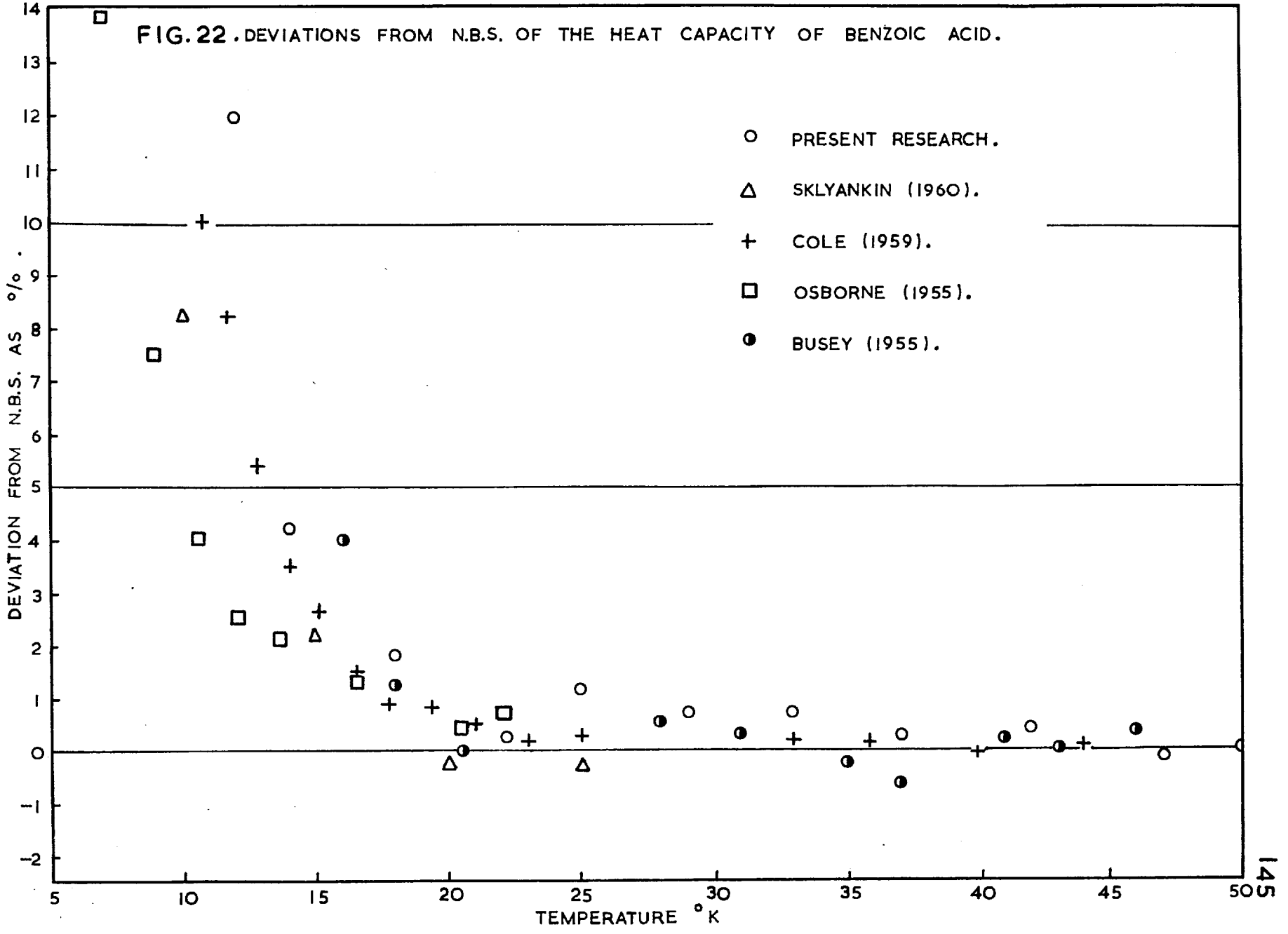
Wt. in calorimeter = 26.4169g. (in vacuo) = 0.23561 moles.

Molecular weight = 112.118 0°C. = 273.15°K.

Run No.	Temp.°K.	ΔT°	Cp. (abs.j.deg^{-1})	Cp. (abs.j.deg^{-1} mole^{-1})
1	275.78	5.138	29.949	138.45
2	280.88	5.072	30.494	140.91
3	286.02	5.258	31.059	143.58
4	198.18	4.083	22.210	102.67
5	202.23	4.033	22.605	104.50
6	206.39	4.294	22.979	106.23
7	233.33	5.471	25.553	118.13
8	238.95	5.845	26.142	120.85
9	244.51	5.380	26.683	123.35
10	127.96	4.390	16.142	74.62
11	132.32	4.330	16.520	76.37
12	136.77	4.581	16.857	77.93
13	50.49	5.394	8.632	39.90
14	55.69	5.006	9.366	43.30
15	60.56	4.734	10.009	46.27
16	80.16	4.394	12.101	55.94
17	84.67	4.629	12.555	58.04
18	89.31	4.661	12.977	59.99
19	12.11	1.126	0.816	3.792
20	14.48	3.076	1.209	5.589
21	18.09	3.755	1.954	9.033
22	21.78	3.493	2.811	13.00
23	25.28	3.454	3.677	17.00
24	29.05	4.018	4.556	21.06
25	33.22	4.266	5.510	25.47
26	37.53	4.321	6.395	29.56
27	42.31	5.216	7.314	33.81
28	47.63	5.398	8.182	37.82

FIG.21 . DEVIATIONS FROM N.B.S. OF THE HEAT CAPACITY OF BENZOIC ACID.




FIG. 22. DEVIATIONS FROM N.B.S. OF THE HEAT CAPACITY OF BENZOIC ACID.
PRESENT RESEARCH.
SKLYANKIN (1960).
COLE (1959).
OSBORNE (1955).
BUSEY (1955).
DEVIATION FROM N.B.S. AS °/o .
TEMPERATURE °K
14
13
12
11
10
9
8
7
6
5
4
3
2
1
0
-1
-2
5
10
15
20
25
30
35
40
45
50

include the results of Busey[113], Cole et al.[114], Osborne[115], Parks et al.[116] and Sklyankin et al.[117].

The present determinations show deviations from the N.B.S. benzoic acid heat capacity of +12% at 12°K, +1.8% at 18°K, +0.3% at 37°K, between 0.0 and +0.3% from 40 - 200°K then rising to +0.8% at 250°K and +1.4% at 290°K.

In fact the quoted results are for the third of three independent investigations made with the benzoic acid standard. Initially discrepancies from the N.B.S. results over the temperature range 50-280°K were found to be unacceptably high. Modifications to either or both the radiation shield or calorimeter assemblies were made between each set of experiments. These modifications are discussed below, together with the % deviations from the N.B.S. results found with the various experimental arrangements.

(1) Cp determinations were first made with the calorimeter heater retained within the re-entrant well in the calorimeter base (see section II(b)) with a thin film of Apeizon T grease. This arrangement gave deviations of +0.5% at 90°K, +1.0% at 200°K and +2.2% at 270°K.

(2) Further measurements with the heater soldered along its entire length to the walls of the calorimeter heater cavity with Wood's metal, to reduce any thermal lag between them which might give rise to an excessive heat loss by radiation from the outer end of the heater shell or conduction along the heater leads, were then carried out. This arrangement gave results not significantly different in either the time required for the calorimeter to come to equilibrium after the heat input or the final deviation from the N.B.S. heat capacities from those found in the first set of experiments above. Indeed, measurements by Martin et al.[118] at the National Chemical Laboratory on the heat capacity of n-heptane employing a calorimeter with a heater greased in a retaining well have proved entirely satisfactory in their agreement with the accepted standard values.

(3) Arrangement (2) was then further modified by replacing the 6 cm. long current carrying heater leads, initially of 38 s.w.g. Manganin wire (diameter 0.152 mm, 0.590 ohms per cm.), with the same length of 40 s.w.g. copper wire (diameter 0.122 mm, 0.034 ohms per cm.) to reduce the amount of heat generated in them. Additionally, an aperture in the top member of the adiabatic shield, which served to admit the oxygen vapour pressure inlet tube when required was sealed off with a brass plate. This

aperture was originally covered with aluminium foil which had however been displaced and had passed unnoticed subsequent to the reassembly of the apparatus after oxygen vapour pressure measurements. Energy loss from the calorimeter by radiation exchange with the inner surface of the cryostat can, which was always at a lower temperature than the calorimeter, through this opening is roughly quantitatively consistent with the positive deviations from the standard heat capacities observed for arrangement (2) above.

The agreement of the measured Cp of benzoic acid with the N.B.S. values after these modifications had been made and a recalibration of the empty calorimeter over the entire temperature range of 12°-300°K had been undertaken, showed a marked improvement (±0.3% from 40°-200°K). However, above 200°K deviations rise noticeably to +1.4% at 290°K and are always positive. As can be seen from FIG.21, the literature values of the heat capacity above 270°K tend to be higher than the N.B.S. results by up to 0.9% at 300°K. It is therefore possible that the National Bureau of Standards determinations are too low in this region. The precision of the present measurements in this temperature range expressed as a root mean square percentage deviation was nevertheless within 0.1%.

Below 25°K the deviations of the present data from the tables of Furukawa and Ginnings[111] again become increasingly large (see FIG.22) and reach a maximum deviation of +12% for our lowest point. Positive deviations of similar magnitude have been reported by Cole et al.[114], Busey[113], Osborne[115] and Sklyankin[117] and again the heat capacity quoted by the N.B.S. appears to be too low by more than the estimated uncertainties of the experiments. Despite the sharp fall in the sensitivities of both the platinum resistance thermometer and the copper-constantan difference thermocouples used to control the adiabatic shield temperatures, the root mean square deviations of experimental points from a smooth curve is still less than 0.7% in this temperature range (see FIG.20), for the empty calorimeter. Analysis of subsequent results with the calorimeter filled with the various adducts of urea showed a r.m.s. deviation of below 0.5% in the temperature range (12°-25°K) (see TABLE 29).

Sklyankin et al.[117] have noted that the smoothed N.B.S. values below 14°K were obtained by extrapolation of the experimental data using the Debye function with a constant Debye temperature Θ_D. They point out that Θ_D is not constant between 14°K and 4°K, as shown by experiment and consequently the N.B.S. data below 14°K is ill-founded. It was concluded that the agreement of the present data

with that of Osborne et al., Busey, Cole et al. and Skvankin below 25°K was quite satisfactory.

A consideration of the factors affecting the accuracy of the adiabatic low temperature calorimeter with special reference to the magnitudes of the differences between the present results and those of Furukawa and Ginnings[111], are discussed below.

SECTION IX(b) The Factors affecting the Accuracy of the Calorimeter Measurements

The problems of attaining measurements of heat capacity to an accuracy of better than 0.1% are chiefly those of reducing, measuring and accounting for any heat exchange between the calorimeter and its surroundings throughout the three phases (fore drift, energy input and after drift) of the experimental determination. The factors determining the absolute errors in a calorimeter are listed below and discussed with reference to the present apparatus.

(1) Adequate control of the adiabatic shield assembly during drift and heating periods.

(2) The absence of thermal gradients in the radiating surfaces of both adiabatic shield and calorimeter.

(3) The absence of holes or other apertures in the shield through which radiation exchange with the calorimeter may occur.

(4) Adequate thermal contact of both heater and platinum resistance thermometer with the calorimeter to reduce equilibration times and prevent "hot spots" which would give a radiation loss from the calorimeter to the shields.

(5) The use of a calorimetric heater with a "high" electrical resistance (400 ohms) and by employing current leads to the calorimeter with as small a resistance as is consistent with tolerable thermal conductivity.

The degree of temperature control of the inner shield surfaces relative to the outer surface of the calorimeter as indicated by the differential thermocouple system has been discussed in section III(b). Additional tests were made with helium in the vacuum can(J)(FIG.8) and a surrounding refrigerant bath of liquid nitrogen, when after standing overnight, all three shields and the calorimeter would be at the same temperature($77^{\circ}K$). Observation of any spurious e.m.f.'s arising from the difference in construction of the copper-constantan junctions or the presence of such effects in the thermocouple lead-switch circuit was then possible. Such thermoelectric e.m.f.'s were found to be always within ± 0.2 microvolts which at this temperature would correspond to a temperature difference of only $0.01^{\circ}C$ at $77^{\circ}K$. However, during the

heating period the heat flow from the shield heaters may set up thermal gradients and "cold spots" on the shields relative to the sensing thermocouple junction. A similar effect may be found in the calorimeter arising from poor thermal contact of the heater with the remainder of the assembly. Under these conditions a non-isothermal surface results and the shield or the calorimeter may be considered to be overheated by an amount δT producing a net energy exchange by radiation and conduction to or from the calorimeter.

The total drift, the rate of which had previously been determined when transients were absent will therefore be in error during heat input by an amount given by:

$$\delta T \times \frac{d(\text{Drift})}{dT} \times \text{heating period}$$

In this equation $\frac{d(\text{Drift})}{dT}$ depends on the absolute temperature of the system and on the position and degree of thermal contact between the thermocouples and the surface the temperature of which is being indicated. Furthermore it can be deduced that δT will depend on the bulk thermal conductivity of the shield, calorimeter or sample, the geometry of the calorimeter, the method of mounting the calorimeter heater and the pressure of heat exchange gas within the calorimeter. This pressure, in general, should be sufficiently high for the gas molecules

to have a mean free path smaller than the distance separating adjacent crystals in the sample.

Changes in the surface temperature distribution and also the degree of thermal contact of the control thermocouple mounted on the calorimeter, for a fixed heating current, may occur when a sample is introduced thereby producing a relative error between determinations of Cp(calorimeter) in the case of the empty and filled calorimeter. This effect will vary from one sample, depending on packing and particle size, or substance to another and there is no easy method available to demonstrate its presence.

Many workers[95],[96],[119], have used the variation of the heating rate to investigate possible non-isothermal conditions of the calorimeter or radiation shield surfaces. This has been found to be physically unsound by West[120]. He has shown that providing the calorimeter drift rates are measured in the steady state, the sum of the time integrals of the heat flow due to the transient states of the heating period are negligible. West concludes that heat exchange between calorimeter and shield is due to the quasi-steady state gradients established in both during the heating period and that those will be proportional to the rate of heating. However, the total energy exchanged, which is reflected in the value of the heat capacity is also proportional to the heating period,

and the heating period is likewise determined in the same proportion by the rate of heating if the same temperature increase occurs. Thus rate of heating experiments can not be useful as tests for non-isothermal surface conditions on the calorimeter or radiation shields.

In the case where a temperature difference ΔT is known to exist between two surfaces at T and To respectively and the radiating area may be considered as a black body, the radiation exchange between two unit surface areas is given by Stefan's radiation law as:

$$H = \sigma(T^4 - To^4)$$

where σ is Stefans constant (5.67×10^{-12} joules cm^{-2} sec^{-1} deg^{-4}). If $To \ll T$, this reduces to,

$$H \simeq \sigma T^4$$

therefore, by differentiating, the rate of energy lost by radiation is given by

$$\sigma 4T^3 . \Delta T . A . t$$

where A is the surface area of the radiator in cm^2 and t the period of emission in seconds.

Although the heater in the present case was in excellent thermal contact with the calorimeter once it had been soldered in the re-entrant well, an estimate of the thermal head between the heater and shield necessary to

give the observed discrepancy at 300°K from the N.B.S. data for benzoic acid was made.

It was assumed that only the end of the heater of area $\sim$ 0.5 cm^2 facing the shield radiated as a black body to the shield over the heating period of approximately 1,200 seconds. The radiant energy H will be given by:

$$H = 4 \times 5.67 \times 10^{-12} \times (300)^3 \times \Delta T \times 0.5 \times 1200$$

As the heat capacity is approximately 1.5% higher than the N.B.S. value at this temperature the "extra heat loss" once drift corrections had been applied amounted to 2 joules. On this basis ΔT would have to be 5.5°C. It is inconceivable that such a large thermal gradient would occur as an excellent thermal path existed between the heater and the calorimeter. An identical loss of heat by radiation could occur with a smaller value of ΔT if the radiating area was increased in the same proportion. Thus if the entire base of the calorimeter were radiating (an area of 10.8 cm^2) ΔT would only have to be 0.25°C to produce the observed discrepancy in Cp.

Although thermal gradients of this order on the calorimeter are possible during the transient state of heat input they undoubtedly exist between the winding inside the heater capsule and the calorimeter (mean temperature). During heat input heat loss from this source

would have to take place by conduction down the heater leads to the side shield and not by radiation direct from the heater coil as this was completely enclosed. However, to reduce such a conductive heat loss the winding was in as good a thermal contact as possible with the heater core (a single layer of varnished cigarette paper) while maintaining electrical insulation.

The rate of flow of heat down a wire of radius R and thermal conductivity K is given by:

$$Q = \frac{K . \pi R^2 \Delta T}{l}$$

where l is the length of the wire and ΔT the thermal gradient between the ends.

At 300°K the thermal conductivity of copper is appoximately 4 watts cm^{-1}, deg^{-1} and the cross-sectional area of 40 s.w.g. wire 0.0001167 cm^2. As two current carrying leads go to the heater and one potential lead is connected approximately at the shield end of its current carrying lead (see section II(d)) three leads may be considered as carrying heat by conduction to the adiabatic shield. Thus the necessary heat loss of 2 joules would give rise to a value of $\Delta T = 7.2°C$. This value again seems large considering the good thermal path available for heat to flow from the winding into the calorimeter.

In addition the "heater lead problem" or position of attachment of the "potential leads" to the heater current carrying wires between shield and calorimeter to include the correct quantity of liberated heat flowing to the calorimeter must be considered (see section II(d)). A mathematical analysis of this problem has been made by Ginning and West[121] who conclude that the assumption of equipartition of the heat developed in the calorimeter heater leads measured by midpoint attachment of the potential leads[122] may not be valid due to unequal thermal contact of a current lead with the calorimeter and the surrounding shield. However, calculation showed these errors are likely to be less than 0.1%. The technique employed in the present apparatus with the potential leads attached at the calorimeter and shield ends of the heater current leads respectively avoids this problem, but demands that the current leads are identical and a relatively good thermal connection exists between a current lead and the calorimeter or shield.

It may be concluded that the problem of heat exchange is complex and particularly so when thermal transients are introduced. Therefore the reasons for the discrepancies in the heat capacity of benzoic acid compared with the N.B.S. values above 200°K are not well understood.

CHAPTER X: THE UREA ADDUCT SAMPLES

SECTION X(a) Preparation

Methods for the preparation of the n-hydrocarbon adducts of urea reported in the literature are numerous but all involve the direct reaction between urea and the hydrocarbon either or both being in solution. Schlenk[62] used benzene as solvent for the paraffin to which finely powdered urea was added, whereas Zimmerschied et al.[60][63] employed methanol and decalin as solvents for the urea and hydrocarbon respectively. Other workers have employed urea solutions in water, methyl or isopropyl alcohol. From the rate of adduct formation in these and other studies[63] it has been found that methanol and other alcohols, together with some ketones (e.g. methyl isobutyl ketone) acts as an activator to adduct precipitation. In systems involving solutions of n-paraffin in inert solvents it has been shown that a negligible amount of urea dissolves in the hydrocarbon layer for appreciable reaction in that phase, and at the hydrocarbon-urea solution interface forces orientate the urea molecules unfavourably for adduct formation[46]. The efficiency of these accelerators is therefore thought to result from a disruption, through hydrogen bonding, of the interphase surface tension arising from tenaciously held surface water. Adduct formation is inhibited by

sulphur compound [63] and also in cases where the maximum cross-sectional dimensions of the guest molecule are comparable with the urea channel size.

In the present study the adducts of n-decane, n-dodecane, n-pentadecane, n-hecadecane, n-eicosane and 2-methyl-pentadecane were made by the slow addition of slight excess of the appropriate n-paraffin to a saturated methanolic solution of urea at room temperature (22g per 100g. methanol at 20°C). The complex formed as a bulky white crystaline precipitate which separated leaving the excess hydrocarbon as a supernatant layer. In the case of eicosane, which is a solid at room temperature(m.p. 36.4°C) it was necessary to warm the methanolic urea solution to 40°C and add iso-propyl alcohol to dissolve the hydrocarbon as has been reported by McAide[64]. On slowly cooling in a water bath long needles of the adduct free from the plate—shaped hydrocarbon crystals were formed. In all cases the precipitates were allowed to digest for a minimum of two days, when the excess hydrocarbon was decanted off and the mixture filtered on a Buchner funnel. Excess hydrocarbon was used in the preparation to prevent tetragonal urea from separating out on the surface of the adduct crystals at this stage. After draining the complex was thoroughly washed with n-pentane to remove any excess

hydrocarbon present on the surface, and allowed to dry in the air for 24 hours. However, in the case of the decane adduct the drying period was reduced to 3 hours as this complex decomposes slowly at room temperature.

The yield of adduct increased with the guest hydrocarbon chain length up to the cetane compound for which Zimmerschied[63] has reported a 97% inclusion of the hydrocarbon. Further adduct crystals could however be separated from the filtrate on cooling but these were not used in the heat capacity investigations.

The chemicals used were obtained from the following sources:-

Compound	Source	Purity
Urea	British Drug Houses (B.D.H.)	Analar(recrystalised) 99%
Methanol	"	Analar
Iso-propyl alcohol	"	Analar
n-pentane	"	(Boiling range 1°C) -Redistilled-
Hydrocarbons		
n-decane	B.D.H.	Reagent quality
n-dodecane	B.D.H.	Reagent quality
n-pentadecane	British Petroleum(B.P.)	99.8%
n-hexadecane	B.D.H.	gas chromatography quality

n-eicosane	B.P.	99.8%
2-methyl-pentadecane	B.P.	$\sim$ 98%

The purity of all the hydrocarbons was investigated by gas chromatography. A celite column of 600 theoretical plates using a polyester as the liquid phase specifically designed for hydrocarbon separation was employed in conjunction with a Pye(ionisation-detector) gas chromatographic apparatus. Argon at 5 lbs. per sq.inch was used as carrier gas and the column was operated at temperatures ranging from $100^{\circ} \pm 2^{\circ}C$ to $210^{\circ} \pm 2^{\circ}C$ for the most and least volatile hydrocarbons (decane and eicosane) respectively. The traces obtained from the dodecane and 2-methyl-pentadecane hydrocarbon samples exhibited "tailing", indicative of impurities. In dodecane the impurities were most probably unsaturated hydrocarbons produced during commercial distillation under atmospheric pressure. Consequently the impure bulk sample (300 ml) was distilled under a reduced pressure of 100 m.m of mercury, controlled by a vacuostat to $\pm$ 0.1 mm, in a three stage Stedman column each stage of which was independently controlled in successive intervals of $5^{\circ}C$ to give a negative temperature gradient up the column. To prevent grease entering the distillate all taps and sockets were covered with polythene

sleeving. The distillate was collected in 30 ml. fractions all of which were analysed by gas chromatography. All the impurities were found in the first two fractions, successive fractions having sharp traces without satelite peaks. The middle three fractions (b.p.145.3°C) were used in the preparation of the adduct. The decane sample was distilled in the same apparatus under atmospheric pressure(b.p.174°C).[124][125].

Owing to the small quantity of 2-methylpentadecane available it was decided not to attempt further purification. It is important to note however that adduct formation is in itself a means of separating branched from straight chained hydrocarbons where the main chain is short and thus the preparative process will eliminate such impurities.

SECTION X(b). Analysis of the Adducts

Many of the methods[63] for determining adduct composition reported in the literature involve analysis of the unwashed precipitate or estimation of concentration change in the urea solution during preparation for a known quantity of added hydrocarbon. These methods, which give the most reproducible results, are not applicable where the washed and dried solid, prepared from a solution

containing excess hydrocarbon, must be analysed. Two separate techniques:- volumetric and elemental analysis were therefore employed to analyse the solid complexes. The adduct compositions were found both at the time of filling the calorimeter (immediately the adduct had been dried in air) and on its removal after the heat capacity measurements had been made.

1) Volumetric Method: (Analysis for urea by the urease method.

Urea may be conveniently estimated quantitatively by hydrolysis to ammonium carbonate using the enzyme urease and subsequent titration with hydrochloric acid employing methyl red or screened methyl orange as indicator. This method was suitable for the analysis of the urea-n-hydrocarbon adducts as in several control experiments on solutions of known urea content, both with and without added hydrocarbons, errors of less than 0.6% of the total urea present were found.

The procedure for adduct analysis was as follows: Four 25ml. aliquots of an aqueous solution, containing approximately 2.5g per litre of the adduct weighed out to ±0.1 mg., were pipetted into 250ml conical flasks fitted with ground glass stoppers and to each ten drops of phenolphthalein indicator (0.5g in 50% water/alcohol solution)

added. To the first, hereafter called the control, 2ml. of 0.5% mercuric chloride were added to prevent enzymic activity. Ten ml. of a freshly prepared suspension of twenty finely ground urease tablets(B.D.H.), each tablet being capable of hydrolising 80 mg. of urea in 3 hours at 15°C, in 100 ml. of distilled water served to hydrolise the urea in each flask, except the control, over a period of about 18 hours. The formation of ammonium carbonate was shown by the change in colour of the indicator to the pink form. Before titration, in order to make the solutions ionically similar 1ml. of 10% ammonium chloride and 15 drops of methyl red (0.08g/ 100ml water) (or screened methyl orange) were added to the control and 2 ml. of mercuric chloride and the same amount of the indicator introduced into the remaining three flasks.

The control was first titrated with N/10 hydrochloric acid to give a pale pink end point (in general approximately 0.3 ml. N/10 HCl necessary), then the remaining flasks in turn. Throughout the latter titrations the indicator colour was compared with the control. Once the "end point" had been reached, the solution was sparged with a stream of nitrogen to remove

dissolved carbon dioxide. Extensive frothing occured during this process; this could be minimised by the addition of 2 ml. of alcohol. Removal of CO_2 caused the indicator to revert to the basic yellow/green form and the careful addition of further acid then gave the true end point. This was in general reproducible to $\pm$0.05ml, which represents approximately 0.2% of the total titre. Subtraction of the control titre gave the volume of N/10 HCl equivalent to the ammonium carbonate formed by hydrolysis.

1 ml. of the N/10 hydrochloric acid was therefore equivalent to 3.00 mg. of urea in the original solution. Once the weight of urea in the adduct sample was established the associated quantity of hydrocarbon was found by difference. The average value of six determinations, three on each of two independent adduct solutions, were taken both before and after Cp measurements. Agreement for the urea content was always within $\pm$0.6% showing that negligible decomposition of the adduct occurred on evacuation of the calorimeter. The results of the analysis are given in the table below:

TABLE 17

Hydrocarbon as % of Adduct	C_{10}	C_{12}	C_{16}	C_{20}	C_{15}	2-methyl pentadecane
Before Cp measurements	21.55	21.80	23.70	24.05	23.65	25.65
After Cp measurements	21.40	21.60	23.30	24.00	23.50	25.60

2) Elemental analysis for carbon, oxygen and nitrogen

Elemental analysis was made through a service organised by the Organic Chemistry Department at Imperial College and involved the standard techniques of micro organic analysis. In general fair agreement with the volumetric results was obtained for adduct composition calculated from the analysis for nitrogen and oxygen. However, this method did not give results as consistent as those from volumetric analysis.

In addition a gravimetric method for estimating urea using 9-xanthenol was attempted. The use of methanolic 9-xanthenol solution to precipitate urea as the di-xanthydryl compound in acetic acid has been described by Kiser et al.(126) with special reference to the urea-hydrocarbon complexes. Their results indicate that the reaction is quantitative to ±0.2% for test samples of urea and good agreement with both Redich's and

Zimmerscheid's data for adduct composition was found. However, similar determinations in this laboratory were not found to be quantitative due to decomposition of di-xanthydryl-urea at 100°C during drying although the precipitate had been thoroughly washed with a saturated solution of di-xanthydryl urea. Furthermore, the wash solution tended to leave a considerable deposit of the precipitate on the under side of the filter crucible through evaporation of the solvent methanol. This procedure was considered inferior to the volumetric method described above. The adduct compositions found by Schlenk[51], Redich et al.[61] and Zimmerschied et al.[60] are shown in FIG.3.

To confirm that the adducts did not contain any free unadducted tetragonal urea X-ray powder diagrams for pure urea and the various adducts, both before and after Cp measurements, were taken and compared. The adducts had powder diagrams distinct from those of urea in all cases and no lines characteristic of the tetragonal form were observed. From the line spacings (d) and the camera constants the Miller index (h,k,l,) for each reflecting plane was found. The results for urea (tetragonal) and the hexadecane adducts are shown in TABLES 18 and 19 below.

TABLE 18 .- X-RAY POWDER DIAGRAM RESULTS FOR TETRAGONAL UREA.

"d"	Nature of line.	Miller index	"d"	Nature of line.	Miller index
4.70	W	001	1.74	W	301
4.00	VVS	110	1.71	W	212
3.62	VS	101	1.66	M	311
3.05	VS	111	1.56	VVW	
2.82	MS	200	1.51	VW	222
2.52	S	210	1.50	M	103
2.42	MS	201	1.46	VVW	302
2.35	MW	002	1.45	VVW	113
2.22	MW	211	1.415	VVW	
2.16	MS	102	1.363	W	410
2.02	W	112	1.340	W	401
1.98	MW	220	1.322	M	213
1.83	MS	221	1.295	VVW	322
1.80	VVW	202	1.255	VW	420
1.78	VVW	310	1.225	W	223

S=strong. M=medium. W=weak. V=very.
(e.g. VS means the line is very strong.)

TABLE 19 .- X-RAY POWDER DIAGRAM RESULTS FOR THE UREA-HEXADECANE ADDUCT.

"d"	Nature of line.	Miller index	"d"	Nature of line.	Miller index
7.2	M	100	2.05	MW	220
6.0	VW	101	2.02	MW	221
4.37	M	102	1.97	W	310
4.12	VS	110	1.94	W	
3.85	M	111	1.92	W	
3.56	S	200	1.87	VVW	
3.40	S	201	1.86	VVW	
3.26	S	103	1.79	VW	
2.97	VW		1.73	VW	
2.76	VW	004	1.67	W	
2.68	W	210	1.62	W	
2.62	MW	211	1.55	VVW	
2.56	M		1.53	VVW	
2.55	M		1.463	VW	
2.41	VW	212	1.443	VW	
2.36	VW	300	1.380	VVW	
2.28	MW	114	1.365	VVW	
2.16	M	213			

S=strong. M=medium. W=weak. V=very.
The presence of a blank in the Miller index column indicates that an assignment was not made for thatline.

Calculation of the hexagonal urea lattice parameters "a" and "c" from the formula:

$$\frac{1}{d2} = \frac{4}{3}\,\frac{h^2+hk+k^2}{a^2} + \frac{l^2}{c^2}$$

gave average values of

$$a = 8.22\ \text{Å}\ ,\ c = 11.10\ \text{Å}$$

compared with Smith's results[49]

$$a = b = 8.230 \pm 0.004\ \text{A}$$

$$c = 11.005 \pm 0.005\ \text{A}$$

PART C : RESULTS

CHAPTER XI. RESULTS OF THE HEAT CAPACITY DETERMINATIONS

SECTION XI(a) Results for six urea-hydrocarbon adducts

The experimental curvature corrected heat capacity results, from the measurements on the n-decane, n-dodecane, n-pentadecane, n-hexadecane, eicosane and 2-methyl-pentadecane -urea adducts, are recorded in TABLES 20 to 25. Also listed in these tables are the run numbers which represent the chronological order in which the Cp determinations were made and ΔT the temperature interval in ^{o}K for each point. The presence of an asterisk after a run number indicates that the point falls in an anomalous region of the heat capacity vs temperature curve. However, only runs for the "high temperature" anomaly which exceed the smooth curve heat capacity by more than 3% are thus indicated. Anomalies in the temperature range 110^{o}-$190^{o}K$ were observed in all but the 2-methyl-pentadecane adduct.

For each adduct the experimental Cp.values were multiplied by a factor determined by the compound analysis, the weight of adduct in the calorimeter and the relationship between the joule and the calorie(1 calorie = 4.1840 joules), to convert to a heat capacity in calories $degree^{-1}$ per weight of adduct containing one mole of urea (60.058 g). These values were plotted against temperature on a large scale and from the best smooth curve drawn through the

points the heat capacity at 5° intervals was read off. This data is recorded in TABLES 26 and 27. TABLES 26(a) and 27(a) contain the adduct entropies obtained by graphical integration under large scale plots of CP/T against T.

The "calculated" Cp. values for the n-decane, n-dodecane and n-hexadecane adducts obtained by summing contributions from the measured heat capacity of tetragonal urea[127] and the appropriate weight of hydrocarbon[128] as determined from analysis of the adducts are shown in TABLE 28. Comparison of these values with the smooth curve experimental heat capacities in temperature regions which do not include the co-operative transitions and which are below the melting point of the hydrocarbon, shows a close correspondence of Cp values. In general the adduct heat capacities are lower than the "calculated" values by approximately 2% at 70°K, 0.5% at 90°K and 0.5% between 200° and 250°K.

TABLE 20.- EXPERIMENTAL VALUES OF THE HEAT CAPACITY OF UREA–DECANE ADDUCT IN ABS. J. DEG^{-1}.

Wt. of adduct in calorimeter = 15.4143g. (in vacuo)
(12.1156g. urea + 3.2987g. decane.)

Run No.		Temp. °K.	ΔT°	Cp.
1		80.21	4.842	9.452
2		84.94	4.612	9.897
3		89.57	4.646	10.320
4		94.13	4.485	10.739
5		98.75	4.748	11.145
6	*	103.51	4.791	11.611
7	*	108.22	4.630	12.703
8	*	112.75	4.430	14.191
9	*	117.38	4.856	12.340
10	*	106.17	2.329	11.890
11	*	108.05	1.435	12.124
12	*	109.45	1.382	13.068
13	*	110.40	0.518	15.328
14	*	110.85	0.383	15.829
15	*	111.24	0.414	15.786
16	*	111.66	0.447	15.689
17	*	112.14	0.515	15.476
18	*	112.66	0.534	14.307
19	*	113.20	0.558	12.988
20	*	113.84	0.708	12.522
21	*	114.65	0.925	12.302
22		121.92	4.173	12.593
23		126.45	4.906	12.882
24		131.39	4.997	13.227
25		136.87	5.974	13.537
26		142.37	5.078	13.923
27		147.64	5.479	14.324
28		153.05	5.373	14.695

TABLE 20(Continued).

Run No.	Temp. °K	ΔT°	Cp.
29	158.37	5.283	14.998
30	163.80	5.169	15.378
31	169.37	6.000	15.746
32	175.52	6.341	16.166
33	181.89	6.448	16.583
34	188.29	6.424	17.063
35	194.74	6.540	17.533
36	201.30	6.660	17.975
37	208.03	6.878	18.446
38	214.84	6.859	18.966
39	221.64	6.852	19.447
40	221.88	7.253	19.490
41	229.77	8.668	20.052
42	237.73	7.408	20.668
43	245.19	7.699	21.263
44	252.82	7.766	21.867
45	260.50	7.836	22.470
46	268.27	7.979	23.208
47	276.10	7.939	23.820
48	283.82	7.828	24.306
49	290.65	6.188	24.741
50	296.45	5.746	25.143
51	51.56	6.096	6.225
52	57.28	5.361	6.983
53	62.55	5.158	7.627
54	67.65	5.043	8.209
55	72.66	4.981	8.723
56	77.62	4.946	9.230
57	11.17	0.840	0.362
58	12.07	0.894	0.485
59	13.84	2.424	0.658
60	16.13	2.295	0.941

TABLE 20 (Continued).

Run No.	Temp. °K	ΔT°	Cp.
61	18.27	2.027	1.167
62	20.67	2.675	1.506
63	23.40	2.743	1.903
64	26.21	2.817	2.349
65	29.21	3.092	2.788
66	32.39	3.242	3.307
67	35.86	3.665	3.852
68	39.66	3.904	4.478
69	44.05	4.857	5.148
70	48.54	4.111	5.801

TABLE20.- EXPERIMENTAL VALUES OF THE HEAT CAPACITY OF UREA-DODECANE ADDUCT IN ABS. J. DEG^{-1}.
Wt. of adduct in calorimeter = 17.3226g. (in vacuo)
(13.5809g. urea + 3.7417g. dodecane.)

Run No.	Temp. °K.	ΔT°	Cp.
1	106.55	3.869	13.070
2	110.93	4.897	13.492
3 *	115.75	4.748	14.015
4 *	120.40	4.551	15.408
5 *	124.84	4.342	16.291
6	129.38	4.741	14.611
7	134.12	4.751	14.905
8	138.91	4.850	15.261
9	143.80	4.942	15.671
10	148.75	4.949	16.016
11	153.70	4.956	16.379
12	158.65	4.976	16.643
14	164.45	4.831	17.111
15	169.42	5.126	17.489
16	174.50	5.074	17.847
17	179.76	5.484	18.238
18	185.36	5.775	18.688
19	191.16	5.862	19.168
20	197.04	5.957	19.618
21	202.34	6.216	20.111
22	208.57	6.313	20.619
23	215.19	7.007	21.093
24	222.18	7.078	21.651
25	229.17	7.037	22.273
26	236.42	7.576	22.884
27	244.02	7.806	23.506
28	251.72	7.773	24.174
29	258.63	6.270	24.777

TABLE 21(Continued).

Run No.		Temp. °K.	ΔT°	Cp.
30		265.14	6.950	25.322
31		271.67	6.473	25.834
32		104.11	5.335	12.839
33		109.35	5.160	13.327
34	*	114.43	4.999	13.847
35	*	117.96	2.070	14.242
36	*	120.01	2.035	14.591
37	*	121.75	1.440	15.315
38	*	123.19	1.439	19.135
39	*	124.46	1.101	17.095
40	*	125.33	0.654	15.764
41	*	125.99	0.687	14.287
42	*	126.68	0.681	14.425
43		127.66	1.283	14.365
44		129.20	1.814	14.523
45		51.97	6.028	7.001
46		57.68	5.364	7.826
47		62.77	4.824	8.537
48		67.61	4.862	9.149
49		72.50	4.929	9.702
50		77.40	4.873	10.247
51		82.36	5.054	10.778
52		87.39	5.020	11.304
53		92.40	5.020	11.744
54		98.26	6.719	12.284
55		11.29	0.690	0.479
56		12.14	0.575	0.570
57		13.70	2.233	0.774
58		15.94	2.204	1.067
59		18.05	1.916	1.302
60		20.41	2.782	1.610

TABLE 21 (Continued).

Run No.	Temp. °K.	ΔT°	Cp.
61	23.14	2.729	2.074
62	25.94	2.808	2.540
63	28.91	3.064	3.050
64	32.08	3.231	3.614
65	35.53	3.635	4.214
66	39.36	4.012	4.914
67	43.73	4.722	5.644
68	48.09	3.972	6.349
69	277.35	8.217	26.343
70	286.01	9.175	27.181
71	295.25	9.409	28.074

TABLE 22.- EXPERIMENTAL VALUES OF THE HEAT CAPACITY OF UREA-PENTADECANE ADDUCT IN ABS. J. DEG^{-1}.
Wt. of adduct in calorimeter = 18.6496g. (in vacuo)
(14.2669g. urea + 4.3827g. pentadecane.)

Run No.		Temp. °K	ΔT°	Cp.
1		86.24	4.982	11.751
2		91.12	4.783	12.244
3		95.93	4.850	12.684
4		100.76	4.801	13.123
5		105.54	4.766	13.569
6		110.34	4.837	14.010
7		115.20	4.911	14.446
8		120.15	4.981	14.921
9		125.16	5.054	15.238
10		130.19	4.863	15.778
11		135.08	4.954	16.250
12		140.07	5.037	16.789
13	*	145.14	5.103	17.399
14	*	150.25	5.136	18.253
15	*	155.37	5.132	19.379
16	*	160.55	5.223	19.798
17		166.05	5.797	18.729
18		170.39	2.914	18.995
19	*	148.21	2.690	17.909
20	*	151.15	3.205	18.417
21	*	154.22	2.951	19.085
22	*	156.42	1.458	19.433
23	*	157.61	0.921	20.125
24	*	158.38	0.623	20.595
25	*	159.00	0.630	20.012
26	*	159.62	0.631	20.014
27	*	160.31	0.776	20.040
28	*	161.09	0.781	19.719

TABLE 22(Continued).

Run No.	Temp. °K	ΔT°	Cp.
29 *	161.87	0.791	19.242
30 *	162.85	1.201	18.772
31	164.05	1.205	18.596
32	174.54	5.464	19.262
33	179.97	5.443	19.651
34	185.80	6.244	20.109
35	192.08	6.350	20.633
36	198.41	6.342	21.170
37	204.72	6.340	21.686
38	211.10	6.507	22.262
39	217.76	6.894	22.840
40	224.55	6.764	23.463
41	231.52	7.260	24.115
42	238.84	7.530	24.697
43	246.30	7.578	25.395
44	253.80	7.609	26.220
45	261.33	7.638	27.031
46	268.88	7.681	27.767
47	276.45	7.703	28.593
48	283.63	5.452	29.217
49	289.45	6.467	29.876
50	295.45	5.844	30.673
51	51.41	5.869	7.231
52	57.10	5.500	8.135
53	62.42	5.131	8.927
54	67.43	4.889	9.568
55	72.29	4.851	10.176
56	77.12	4.796	10.752
57	81.91	4.795	11.255
58	11.16	0.630	0.521
59	12.07	0.752	0.576
60	13.20	1.330	0.756

TABLE 22(Continued).

Run No.	Temp. °K.	ΔT°	Cp.
61	14.67	1.381	0.920
62	16.13	1.348	1.125
63	17.82	1.869	1.267
64	19.90	2.195	1.563
65	22.43	2.827	2.023
66	25.38	2.999	2.546
67	28.60	3.389	3.097
68	32.03	3.486	3.731
69	35.70	3.850	4.446
70	39.62	3.987	5.186
71	43.98	4.718	5.961
72	48.23	3.784	6.707

TABLE23.- EXPERIMENTAL VALUES OF THE HEAT CAPACITY OF UREA-HEXADECANE ADDUCT IN ABS. J. DEG^{-1}.
Wt. of adduct in calorimeter = 22.0044g. (in vacuo)
(16.8774g. urea + 5.1270g. hexadecane.)

Run No.		Temp. °K.	ΔT°	Cp.
1		79.78	1.805	13.020
2		81.93	2.500	13.310
3		84.47	2.579	13.662
4		87.23	2.936	13.982
5		90.65	3.895	14.397
6		94.58	3.969	14.821
7		98.77	4.410	15.284
8		103.38	4.808	15.798
9		108.21	4.846	16.287
10		112.19	4.685	16.706
11		117.10	5.126	17.235
12		122.24	5.170	17.791
13		127.43	5.216	18.345
14	*	132.62	5.197	19.338
15	*	137.80	5.194	20.248
16	*	143.07	5.346	20.072
17	*	148.41	5.356	20.921
18	*	153.54	4.926	25.231
19		155.15	2.548	20.972
20		159.73	6.617	21.262
21		166.34	6.640	21.851
22		173.09	6.858	22.461
23		179.85	6.652	22.960
24		186.64	6.894	23.609
25		193.55	6.931	24.354
26		198.06	6.822	24.907
27		204.99	7.080	25.576
28		212.17	7.330	26.231

TABLE 23(Continued).

Run No.		Temp. °K.	ΔT°	Cp.
29		219.56	7.561	26.956
30		226.96	7.353	27.765
31		234.38	7.592	28.492
32		241.90	7.623	29.309
33		249.45	7.650	30.168
34		257.00	7.649	31.098
35		264.43	7.702	31.940
36		272.03	7.742	32.757
37	*	150.12	1.950	21.433
38	*	151.68	1.163	34.634
39	*	153.02	1.520	24.356
40		49.97	3.346	8.227
41		54.16	5.024	9.008
42		59.20	5.029	9.918
43		64.19	4.955	10.776
44		69.35	5.357	11.558
45		75.09	6.137	12.339
46		80.54	4.768	13.077
47		10.96	0.730	0.422
48		13.10	1.823	0.739
50		16.19	1.555	1.231
51		18.91	3.197	1.644
52		21.93	2.528	2.219
53		24.76	2.841	2.807
54		27.84	3.097	3.435
55		31.05	3.187	4.148
56		34.48	3.572	4.910
57		38.28	3.944	5.746
58		42.46	4.373	6.650
59		46.84	4.327	7.566
60		278.16	9.967	33.618

TABLE 23(Continued).

Run No.		Temp. °K.	ΔT°	Cp.
61		287.69	9.177	35.062
62		296.16	7.948	35.685
63		302.40	4.703	36.472
64		130.23	2.095	18.686
65	*	132.09	1.630	19.151
66	*	133.72	1.612	19.459
67	*	135.30	1.552	20.135
68	*	136.86	1.588	19.848
69	*	138.42	1.516	19.476
70	*	139.84	1.353	19.553
71	*	141.34	2.471	19.846
72	*	143.63	2.113	20.165
73	*	145.81	2.251	20.454
74	*	147.64	1.414	20.799
75	*	148.85	1.017	21.129
76	*	149.73	0.745	21.321
77	*	150.48	0.741	21.506
78	*	151.19	0.714	22.887
79	*	151.77	0.430	57.065
80	*	152.30	0.635	27.893
81	*	153.04	0.819	21.562
82	*	153.94	0.998	20.916
83		155.23	1.577	20.895

TABLE 24.- EXPERIMENTAL VALUES OF THE HEAT CAPACITY OF UREA-EICOSANE ADDUCT IN ABS. J. DEG^{-1}.
Wt. of adduct in calorimeter = 26.2953g. (in vacuo)
(19.9844g. urea + 6.3109g. eicosane.)

Run No.	Temp. °K.	ΔT°	Cp.
1	82.95	4.477	15.785
2	87.44	4.497	16.508
3	91.97	4.547	17.074
4	96.54	4.605	17.603
5	101.26	4.846	18.192
6	106.12	4.880	18.838
7	111.02	4.925	19.415
8	115.96	4.963	20.019
9	120.86	4.836	20.578
10	125.80	5.052	21.208
11	131.02	4.994	21.847
12	136.07	5.104	22.399
13	141.21	5.194	23.060
14	146.34	5.073	23.727
15	151.49	5.235	24.456
16	156.73	5.256	25.057
17	162.01	5.332	25.798
18	167.36	5.406	26.565
19	172.78	5.467	27.403
20 *	178.26	5.514	28.378
21 *	183.47	5.505	29.697
22 *	188.83	5.242	33.556
23 *	194.24	5.629	31.340
24	200.00	5.935	29.990
25	205.95	6.008	30.623
26	211.96	6.073	31.316
27	218.03	6.142	31.971
28	224.16	6.204	32.649

TABLE 24(Continued).

Run No.		Temp. °K.	ΔT°	Cp.
29	*	182.26	3.038	29.261
30	*	184.73	1.916	30.461
31	*	186.16	0.960	31.072
32	*	186.95	0.649	31.591
33	*	187.49	0.466	32.601
34	*	187.95	0.459	33.334
35	*	188.39	0.455	33.827
36	*	188.83	0.457	33.563
37	*	189.27	0.447	34.605
38	*	189.71	0.455	33.898
39	*	190.15	0.461	33.129
40	*	190.62	0.520	33.788
41	*	191.17	0.605	32.950
42	*	191.78	0.665	32.544
43	*	192.50	0.797	32.506
44	*	193.56	1.350	31.691
45	*	195.33	2.230	30.792
46		230.48	6.323	33.487
47		236.77	6.387	34.191
48		243.10	6.436	34.984
49		249.54	6.641	35.809
50		256.19	6.831	36.689
51		263.02	7.037	37.501
52		269.80	7.181	38.521
53		276.96	7.346	39.559
54		284.00	6.961	40.089
55		290.74	6.854	40.937
56		296.34	4.672	41.853
57		51.11	5.883	9.901
58		56.79	5.484	11.163
59		62.22	5.377	12.305
60		67.58	5.335	13.314

TABLE 24(Continued).

Run No.	Temp. °K.	ΔT°	Cp.
61	72.92	5.348	14.200
62	78.28	5.377	15.036
63	11.20	0.720	0.713
64	12.11	0.875	0.771
65	13.72	2.244	0.970
66	15.95	2.164	1.426
67	18.38	2.560	1.786
68	20.80	2.183	2.316
69	23.05	2.266	2.834
70	25.52	2.658	3.438
71	28.89	4.050	4.278
72	32.75	3.659	5.328
73	36.26	3.355	6.265
74	39.54	3.175	7.107
75	43.49	4.718	8.122
76	48.31	4.906	9.273

TABLE 25.- EXPERIMENTAL VALUES OF THE HEAT CAPACITY OF UREA- 2-METHYLPENTADECANE ADDUCT IN ABS. J. DEG^{-1}.
Wt. of adduct in calorimeter = 25.1588g. (in vacuo)
(18.7181g. urea + 6.4407g. 2-methylpentadecane.)

Run No.	Temp. °K.	ΔT°	Cp.
1	79.82	4.272	14.754
2	84.22	4.522	15.455
3	88.82	4.670	16.070
4	93.55	4.804	16.732
5	98.37	4.843	17.231
6	103.22	4.866	18.030
7	108.10	4.903	18.674
8	113.03	4.946	19.263
9	118.04	5.082	19.825
10	122.70	4.655	20.522
11	127.41	4.748	21.019
12	132.30	5.035	21.698
13	137.38	5.116	22.281
14	142.53	5.182	22.947
15	147.73	5.242	23.682
16	152.98	5.264	24.711
17	158.28	5.380	24.955
18	163.68	5.441	25.627
19	169.14	5.509	26.247
20	174.66	5.569	26.924
21	180.28	5.641	27.488
22	186.24	5.610	28.131
23	191.86	5.669	29.041
24	197.68	5.996	29.251
25	203.71	6.091	29.796
26	209.89	6.342	30.514
27	216.22	6.386	31.384
28	222.60	6.791	32.209
29	229.11	6.655	33.020

TABLE 25 (Continued).

Run No.	Temp. °K.	ΔT°	Cp.
30	235.70	6.689	33.911
31	243.36	6.870	34.729
32	250.14	6.803	35.922
33	257.07	7.097	36.199
34	264.10	7.169	36.977
35	271.25	7.339	37.937
36	278.39	7.217	38.775
37	285.37	7.084	39.762
38	292.26	6.975	40.612
39	298.18	5.161	41.392
40	50.89	5.622	9.317
41	56.42	5.435	10.506
42	61.79	5.319	11.662
43	67.16	5.413	12.670
44	72.70	5.653	13.587
45	77.89	4.720	14.427
46	11.39	0.860	0.628
47	12.56	0.970	0.736
48	14.08	1.912	0.933
49	16.07	1.929	1.288
50	18.20	2.203	1.770
51	20.51	2.121	2.121
52	22.79	2.308	2.569
53	25.37	2.795	3.166
54	28.92	4.267	4.020
55	32.84	3.579	5.028
56	36.25	3.212	5.855
57	39.44	3.145	6.653
58	43.47	4.930	7.619
59	48.38	4.880	8.760

TABLE 26 .- SMOOTHED HEAT CAPACITIES OF SOME UREA-HYDROCARBON ADDUCTS IN CAL. DEG^{-1} WT. CONTAINING 1 MOLE (60.058g.) OF $UREA^{-1}$.

1 Cal. = 4.1840 Joules. 0°C = 273.15°K.

Temp. °K.	Decane Adduct	Dodecane Adduct	Hexadecane Adduct
0	0.000	0.000	0.000
5	0.040	0.044	0.036
10	0.321	0.348	0.279
11	0.426	0.462	0.359
12	0.550	0.566	0.480
13	0.677	0.719	0.611
14	0.803	0.858	0.749
15	0.942	1.003	0.897
16	1.092	1.141	1.056
17	1.212	1.253	1.150
18	1.342	1.371	1.266
19	1.497	1.497	1.411
20	1.668	1.639	1.577
25	2.553	2.517	2.431
30	3.460	3.427	3.328
35	4.403	4.367	4.273
40	5.366	5.308	5.204
45	6.267	6.188	6.108
50	7.122	7.060	7.002
55	7.936	7.883	7.800
60	8.674	8.632	8.562
65	9.376	9.331	9.272
70	10.02	9.964	9.910
75	10.62	10.56	10.52
80	11.18	11.12	11.10
85	11.73	11.69	11.66
90	12.28	12.19	12.18
95	12.81	12.67	12.65

TABLE 26 (Continued).

Temp. °K.	Decane Adduct	Dodecane Adduct	Hexadecane Adduct
100	13.35	13.15	13.11
105	13.93	13.66	13.58
110	17.03	14.15	14.01
115	14.55	14.70	14.46
120	14.78	15.42	14.93
125	15.15	17.20	15.38
130	15.56	15.42	15.86
135	15.92	15.82	16.95
140	16.31	16.22	16.65
145	16.74	16.63	17.29
150	17.15	17.03	18.19
155	17.55	17.40	17.76
160	17.93	17.71	18.10
165	18.31	18.13	18.48
170	18.71	18.52	18.88
175	18.11	18.90	19.25
180	19.50	19.30	19.54
185	19.91	19.73	19.94
190	20.36	20.16	20.39
195	20.80	20.59	20.84
200	21.22	21.02	21.29
205	21.64	21.45	21.73
210	22.06	21.88	22.16
215	22.48	22.31	22.59
220	22.91	22.74	23.02
225	23.34	23.18	23.45
230	23.78	23.61	23.88
235	24.23	24.05	24.33
240	24.68	24.50	24.79
245	25.17	24.94	25.25
250	25.64	25.39	25.72

TABLE 26 (Continued).

Temp. °K.	Decane Adduct	Dodecane Adduct	Hexadecane Adduct
255	26.12	25.85	26.23
260	26.61	26.30	26.74
265	27.11	26.76	27.25
270	27.61	27.23	27.76
273.15	27.922	27.520	28.081
275	28.11	27.69	28.26
280	28.60	28.16	28.77
285	29.06	28.63	29.28
290	29.51	29.10	29.79
295	29.95	29.58	30.29
298.15	30.227	29.879	30.611
300	30.39	30.06	30.80

TABLE 26a.- ENTROPY (S_T - So) OF SOME UREA-HYDROCARBON ADDUCTS IN CAL. DEG^{-1} WT. CONTAINING 1 MOLE (60.058g.) OF $UREA^{-1}$.

1 Cal. = 4.1840 Joules. 0°C = 273.15°K.

Temp. °K.	Decane Adduct	Dodecane Adduct	Hexadecane Adduct
0	0.000	0.000	0.000
10	0.107	0.116	0.093
20	0.714	0.747	0.656
30	1.720	1.741	1.611
40	2.973	2.981	2.824
50	4.361	4.351	4.178
60	5.800	5.780	5.594
70	7.242	7.214	7.018
80	8.656	8.621	8.420
90	10.04	9.995	9.790
100	11.38	11.33	11.12
110	12.72	12.63	12.41
120	14.09	13.91	13.67
130	15.31	15.22	14.90
140	16.49	16.39	16.13
150	17.64	17.54	17.33
160	18.77	18.66	18.60
170	19.88	19.76	19.72
180	20.98	20.84	20.82
190	22.05	21.90	21.90
200	23.12	22.96	22.97
210	24.17	24.01	24.03
220	25.22	25.04	25.08
230	26.26	26.07	26.12
240	27.29	27.10	27.16
250	28.31	28.12	28.19
260	29.34	29.13	29.21
270	30.36	30.14	30.24

TABLE 26a(Continued).

Temp. °K.	Decane Adduct	Dodecane Adduct	Hexadecane Adduct
273.15	30.68	30.46	30.57
280	31.38	31.15	31.27
290	32.40	32.15	32.30
298.15	33.21	32.97	33.13
300	33.42	33.15	33.33

TABLE 27a .- SMOOTHED HEAT CAPACITIES OF SOME UREA-HYDROCARBON ADDUCTS IN CAL. DEG^{-1} WT. CONTAINING 1 MOLE (60.058g.) OF $UREA^{-1}$.

1 Cal. = 4.1840 Joules. 0°C = 273.15°K.

Temp. °K.	Eicosane Adduct	Pentadecane Adduct	2-methylpentadecane Adduct
0	0.000	0.000	0.000
5	0.035	0.042	0.038
10	0.281	0.345	0.304
11	0.510	0.450	0.455
12	0.543	0.572	0.523
13	0.616	0.703	0.604
14	0.733	0.837	0.706
15	0.879	0.977	0.831
16	1.031	1.117	0.978
17	1.131	1.194	1.152
18	1.238	1.296	1.337
19	1.375	1.433	1.435
20	1.533	1.592	1.557
25	2.380	2.456	2.359
30	3.289	3.377	3.296
35	4.259	4.336	4.266
40	5.192	5.287	5.205
45	6.097	6.182	6.123
50	6.937	7.042	7.000
55	7.734	7.862	7.818
60	8.505	8.531	8.658
65	9.222	9.327	9.423
70	9.862	9.963	10.09
75	10.45	10.56	10.71
80	11.02	11.14	11.32
85	11.55	11.69	11.91
90	12.06	12.21	12.46
95	12.53	12.68	12.98

TABLE 27 (Continued).

Temp. °K.	Eicosane Adduct	Pentadecane Adduct	2-methylpentadecane Adduct
100	12.98	13.14	13.50
105	13.43	13.60	14.00
110	13.86	14.07	14.49
115	14.29	14.52	14.96
120	14.72	14.96	15.42
125	15.16	15.41	15.89
130	15.60	15.86	16.36
135	16.03	16.34	16.85
140	16.47	16.88	17.35
145	16.91	17.52	17.84
150	17.37	18.32	18.34
155	17.84	19.36	18.83
160	18.32	20.15	19.30
165	18.84	18.76	19.76
170	19.37	19.09	20.20
175	19.94	19.41	20.63
180	20.59	19.77	21.04
185	21.98	20.16	21.44
190	24.03	20.58	21.83
195	22.22	21.01	22.22
200	21.54	21.44	22.60
205	21.92	21.86	23.01
210	22.33	22.30	23.45
215	22.74	22.74	23.95
220	23.12	23.19	24.46
225	23.52	23.65	24.94
230	23.95	24.10	25.41
235	24.39	24.56	25.86
240	24.85	25.04	26.32
245	24.30	25.52	26.78
250	25.77	26.00	27.23

TABLE 27 (Continued).

Temp. °K.	Eicosane Adduct	Pentadecane Adduct	2-methylpentadecane Adduct
255	26.25	26.50	27.66
260	26.73	27.07	28.09
265	27.21	27.55	28.54
270	27.69	28.06	28.98
273.15	27.989	28.380	29.270
275	28.16	28.56	29.44
280	28.63	29.08	29.92
285	29.10	29.59	30.42
290	29.56	30.12	30.91
295	30.03	30.66	31.42
298.15	30.322	31.007	31.740
300	30.49	31.21	31.92

TABLE 27a .- ENTROPY (S_T - So) OF SOME UREA-HYDROCARBON ADDUCTS IN CAL. DEG^{-1} WT. CONTAINING 1 MOLE (60.058g.) OF $UREA^{-1}$.

1 Cal. = 4.1840 Joules. 0°C = 273.15°K.

Temp. °K.	Eicosane Adduct	Pentadecane Adduct	2-methylpentadecane Adduct
0	0.000	0.000	0.000
10	0.094	0.113	0.101
20	0.650	0.724	0.662
30	1.589	1.695	1.600
40	2.796	2.923	2.808
50	4.145	4.293	4.165
60	5.550	5.721	5.590
70	6.967	7.155	7.033
80	8.359	8.563	8.461
90	9.718	9.938	9.861
100	11.04	11.27	11.23
110	12.32	12.57	12.56
120	13.56	13.83	13.86
130	14.77	15.06	15.13
140	15.96	16.27	16.38
150	17.12	17.48	17.61
160	18.27	18.73	18.83
170	19.42	19.88	20.02
180	20.56	20.99	21.20
190	21.76	22.08	22.36
200	22.91	23.16	23.50
210	23.98	24.23	24.62
220	25.04	25.28	25.74
230	26.08	26.33	26.84
240	27.12	27.38	27.94
250	28.15	28.42	29.04
260	29.18	29.46	30.12
270	30.21	30.50	31.20

TABLE 27a(Continued).

Temp. °K.	Eicosane Adduct	Pentadecane Adduct	2-methylpentadecane Adduct
273.15	30.53	30.83	31.54
280	31.23	31.54	32.27
290	32.26	32.58	33.33
298.15	33.09	33.42	34.20
300	33.27	33.62	34.40

TABLE 28 .- CALCULATED HEAT CAPACITIES FOR 1 MOLE OF TETRAGONAL UREA + THE ASSOCIATED WEIGHT OF HYDROCARBON FOUND FROM ANALYSIS AFTER Cp MEASUREMENTS. Cp IN CALS.DEG^{-1}.

Temp. °K.	Decane Adduct	Dodecane Adduct	Hexadecane Adduct
20	1.57	1.55	1.54
30	3.61	3.56	3.56
40	5.61	5.54	5.56
50	7.37	7.30	7.35
60	8.90	8.84	8.92
70	10.19	10.12	10.23
80	11.31	11.25	11.39
90	12.29	12.24	12.40
100	13.16	13.09	13.28
110	13.97	13.91	14.11
120	14.80	14.72	14.94
130	15.60	15.52	15.75
140	16.40	16.32	16.56
150	17.19	17.10	17.35
160	18.00	17.91	18.17
170	18.80	18.71	18.98
180	19.62	19.53	19.81
190	20.45	20.34	20.64
200	21.29	21.17	21.47
210	22.14	22.00	22.31
220	23.01	22.84	23.15
230	23.91	23.70	24.00
240	24.85	24.60	24.87
250	27.31	25.57	25.80
260	28.03	26.59	26.76
270	28.76	28.91	27.75
280	29.51	29.63	28.80
290	30.26	30.36	29.85
300	31.04	31.13	32.06

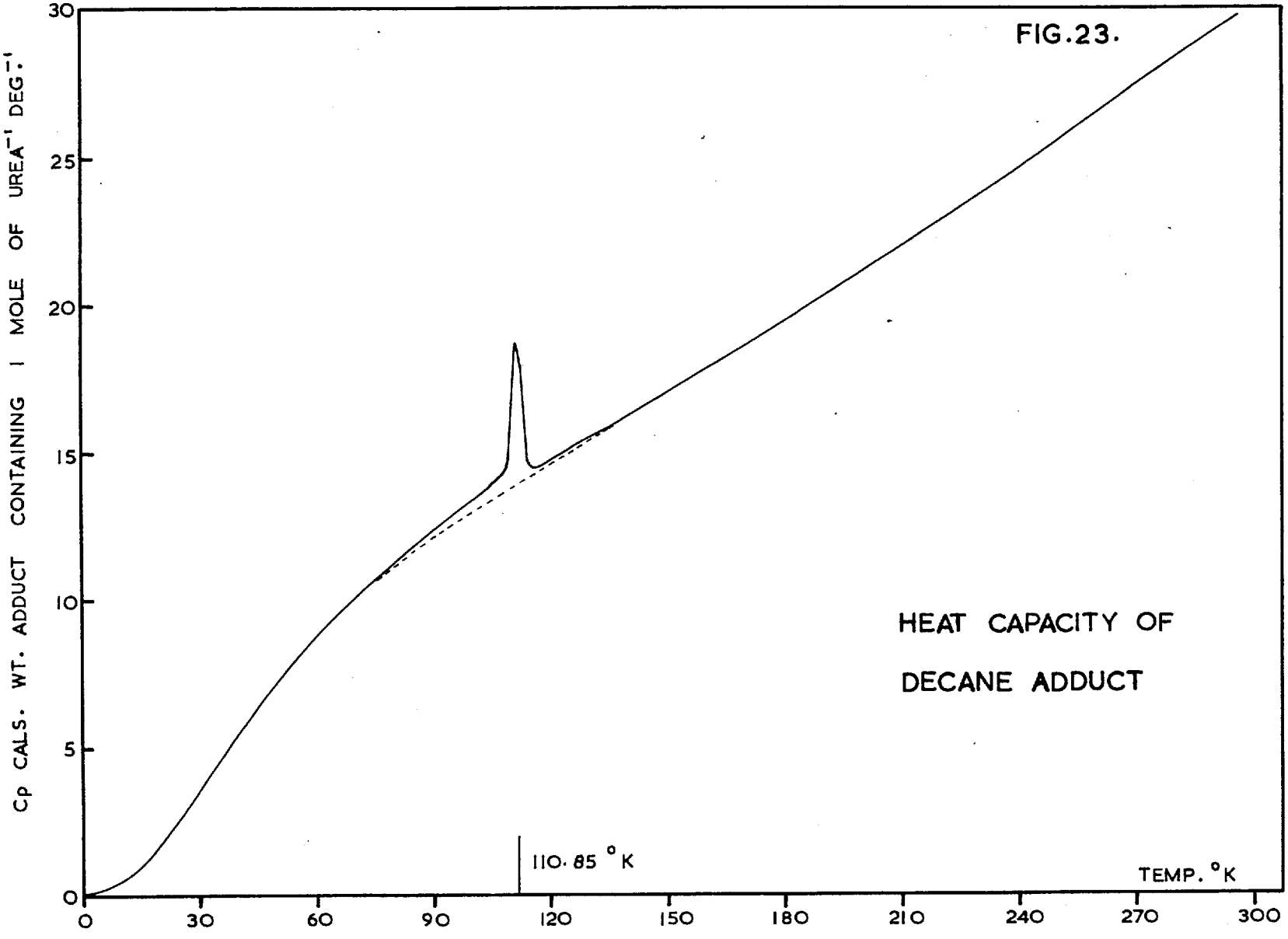
The solid horizontal lines represent the region in which the hydrocarbons have a latent heat of fusion.

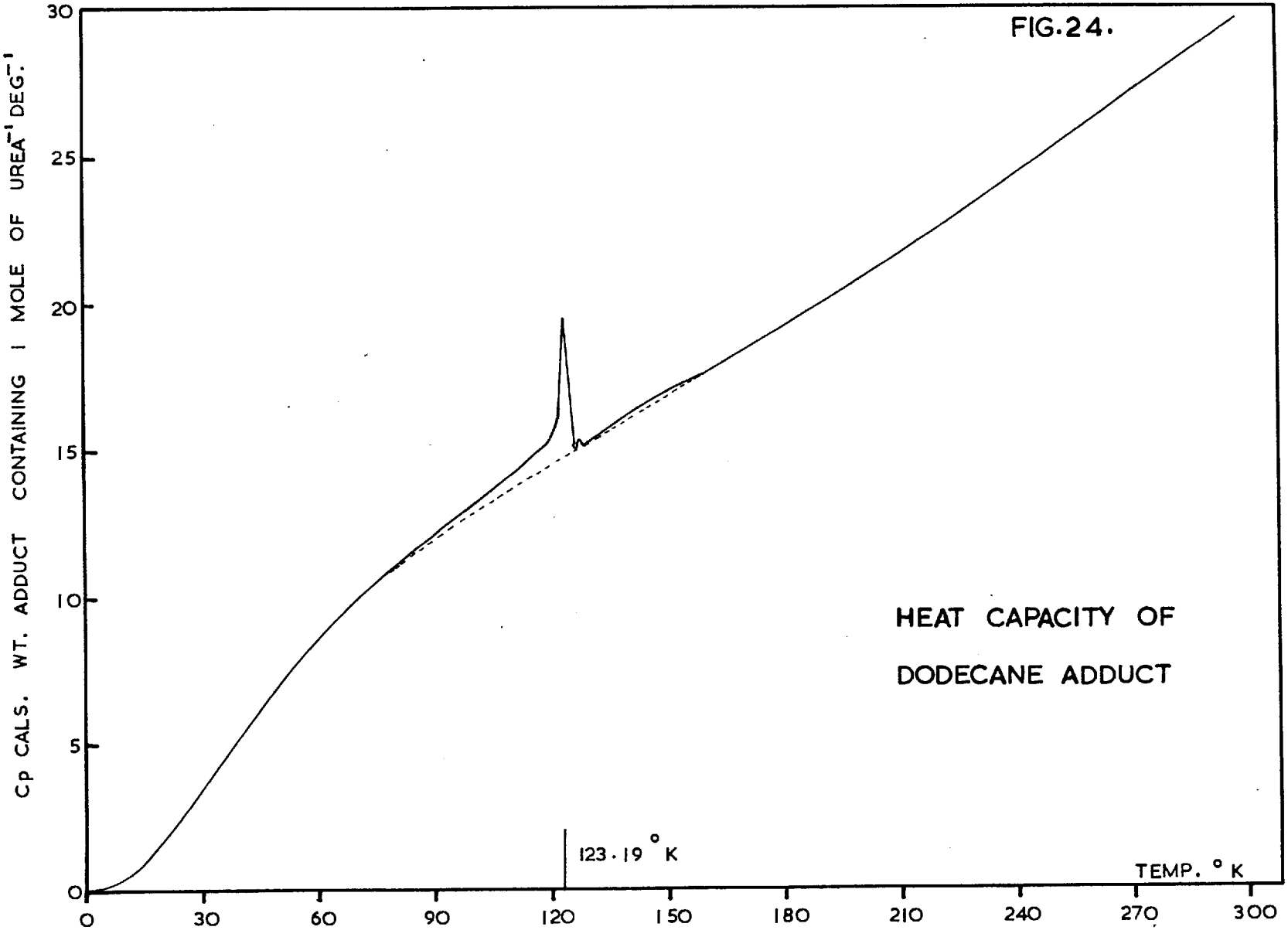
PART D. DISCUSSION

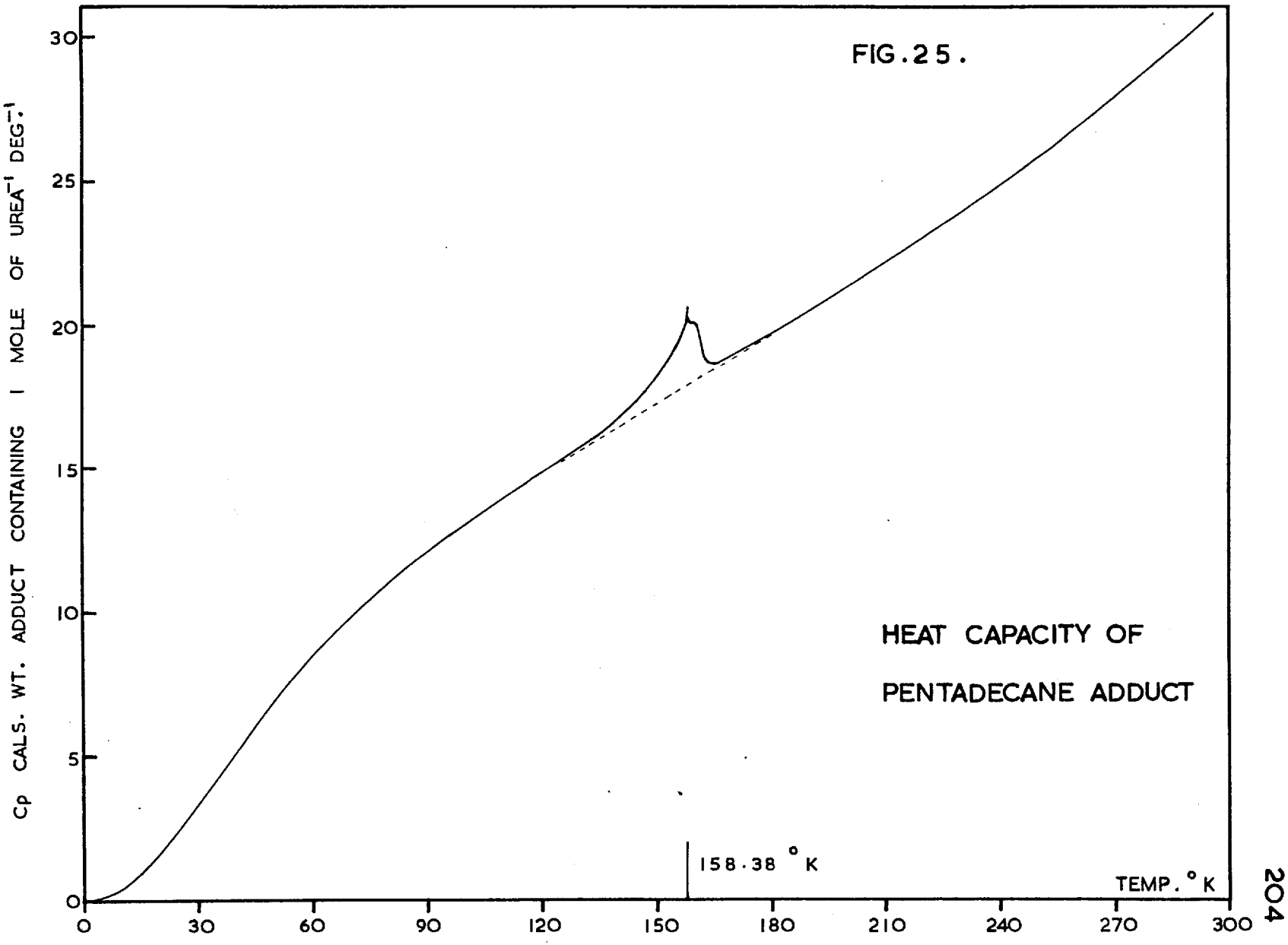
CHAPTER XII

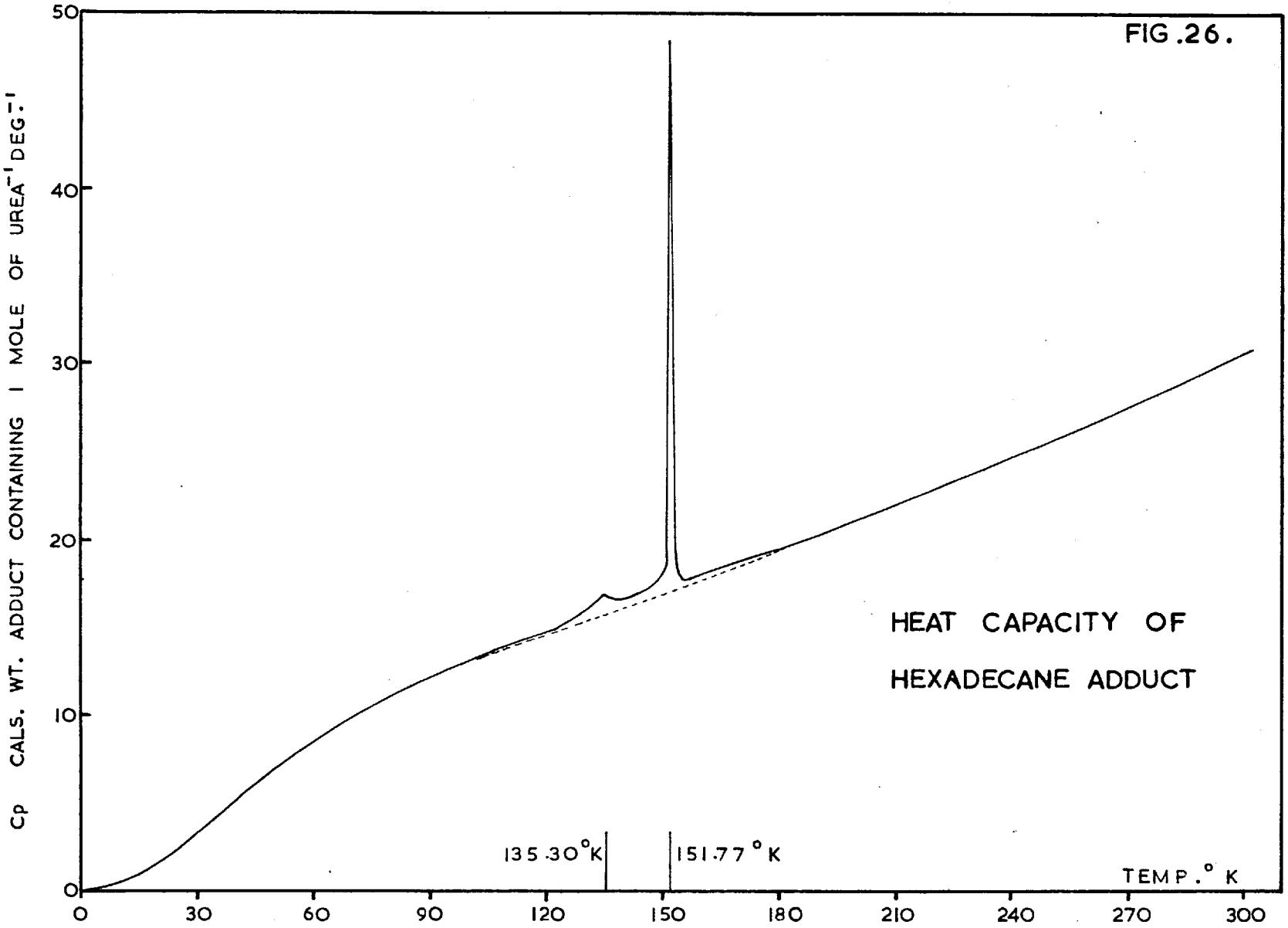
SECTION XII(a). General description of the experimental heat capacity curves.

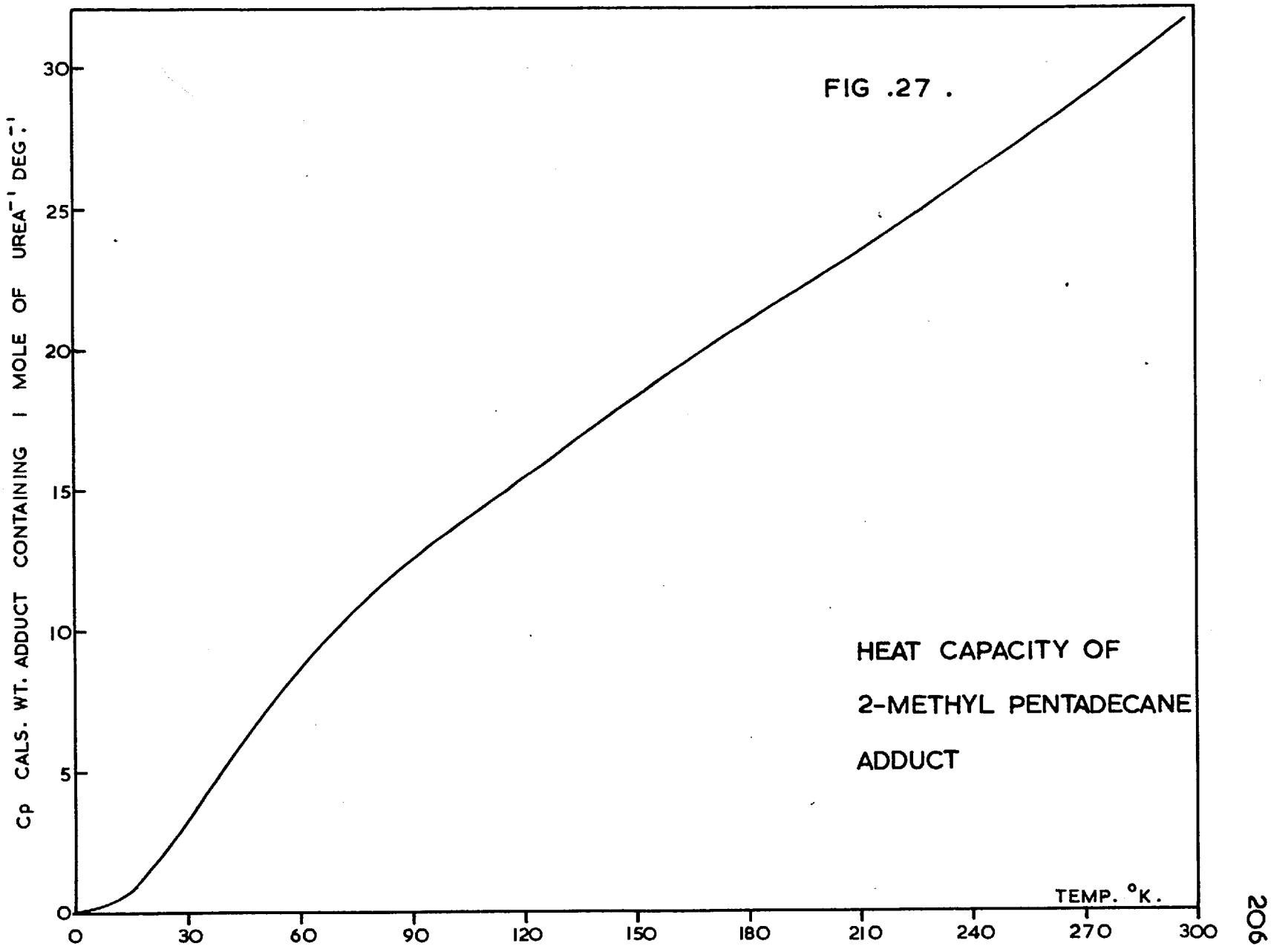
The variation of heat capacity with temperature for the six urea-paraffin adducts studied is shown in FIGS.23 to 28. The plots are all of similar overall shape but at least one anomalous region occurs in each. In the case of the 2-methyl-pentadecane compound the only significant transition was that found at approximately 16.2°K which is common to the other adducts and hereafter called "the low temperature anomaly". The remaining five adducts in addition exhibit a second transition region, the co-operative anomaly, which has a peak heat capacity at a temperature increasing with the guest paraffin chain length. The adduct of n-pentadecane, with an odd number of carbon atoms in the hydrocarbon chain proves somewhat of an exception to this rule. In addition to these major anomalies a small excess heat absorption in the temperature range 220° - 250°K amounting to only 0.2-0.5% of the total heat capacity at that temperature was observed for each substance. An energy absorption of this magnitude is however significant when compared with the root mean square % deviation of the experimental Cp points from a smooth curve. Such deviations for the empty calorimeter

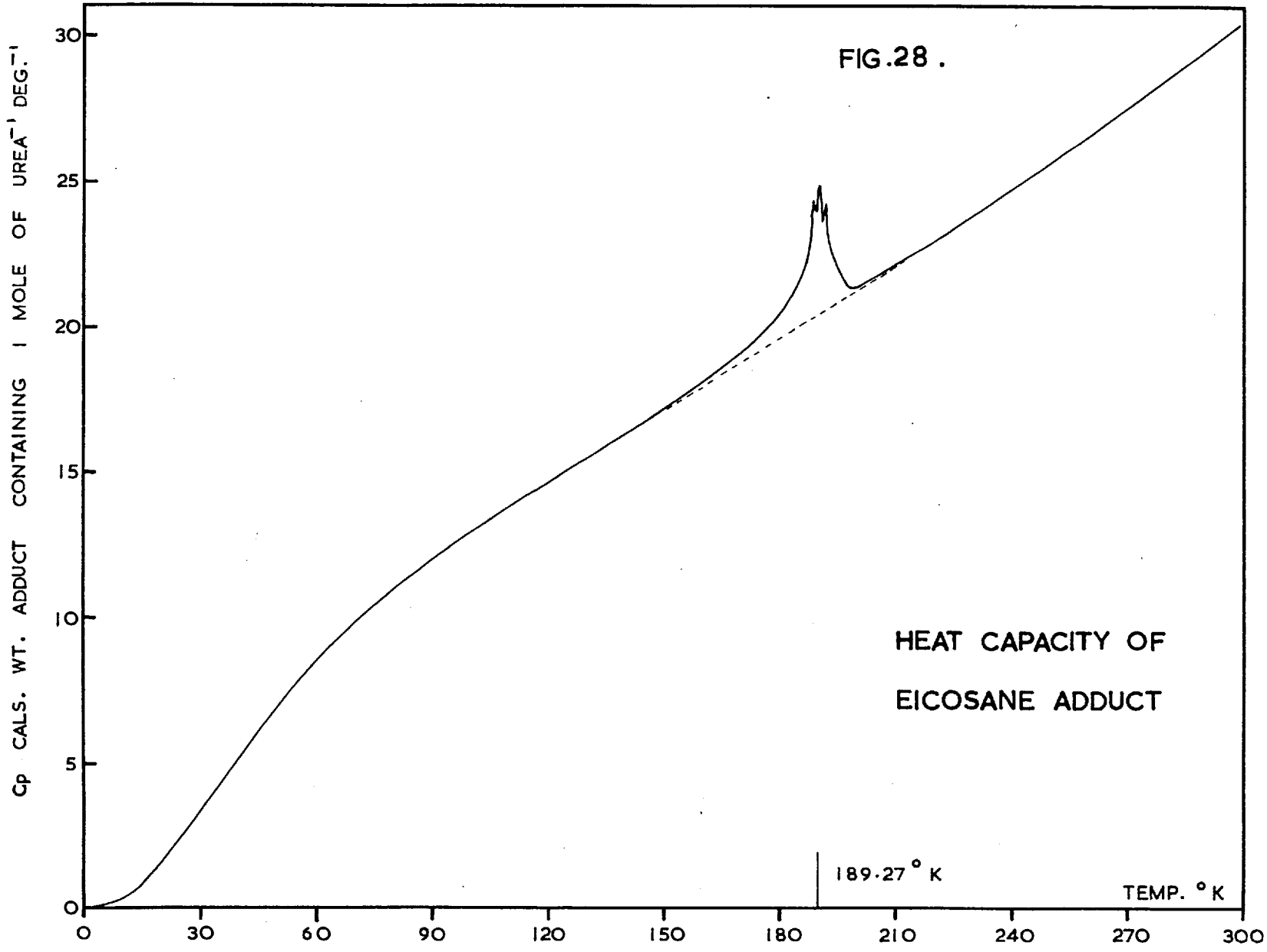

FIG.23.
HEAT CAPACITY OF
DECANE ADDUCT
Cp CALS. WT. ADDUCT CONTAINING 1 MOLE OF UREA^{-1} DEG.$^{-1}$
30
25
20
15
10
5
0
0
30
60
90
120
150
180
210
240
270
300
110.85 °K
TEMP. °K


FIG.24.
HEAT CAPACITY OF
DODECANE ADDUCT
Cp CALS. WT. ADDUCT CONTAINING 1 MOLE OF UREA^{-1} DEG.$^{-1}$
TEMP. ° K
123·19 ° K
0
5
10
15
20
25
30
0
30
60
90
120
150
180
210
240
270
300


FIG. 25.
HEAT CAPACITY OF
PENTADECANE ADDUCT
Cp CALS. WT. ADDUCT CONTAINING 1 MOLE OF UREA^{-1} DEG^{-1}.
0
5
10
15
20
25
30
158.38 °K
TEMP. °K
0
30
60
90
120
150
180
210
240
270
300


FIG.26.
Cp CALS. WT. ADDUCT CONTAINING 1 MOLE OF UREA^{-1} DEG.$^{-1}$
50
40
30
20
10
0
0
30
60
90
120
150
180
210
240
270
300
HEAT CAPACITY OF
HEXADECANE ADDUCT
135.30°K
151.77°K
TEMP.° K


FIG .27 .
HEAT CAPACITY OF
2-METHYL PENTADECANE
ADDUCT
Cp CALS. WT. ADDUCT CONTAINING 1 MOLE OF UREA^{-1} DEG^{-1}.
TEMP. °K.
0
5
10
15
20
25
30
0
30
60
90
120
150
180
210
240
270
300


FIG.28.
HEAT CAPACITY OF
EICOSANE ADDUCT
Cp CALS. WT. ADDUCT CONTAINING 1 MOLE OF UREA^{-1} DEG.$^{-1}$
TEMP. °K
189.27 °K
0
5
10
15
20
25
30
0
30
60
90
120
150
180
210
240
270
300

and also for the calorimeter filled with the various adducts are recorded in TABLE 29 for the temperature ranges (12-25)°K, (25-70)°K and (70-300)°K.

These anomalous regions of the Cp vs temperature plots are discussed in the following sections together with possible explanations for their presence.

SECTION XII(b). The low temperature anomaly.

The low temperature anomaly in Cp was observed for all six adducts investigated, with a maximum excess absorption occurring at approximately 16.2°K ±0.2°K (FIGS 29 to 31). The shape of the anomalous region is best seen from the urea-pentadecane results (FIG.31) where a greater number of Cp determinations were conducted in this region. In the 2-methyl-pentadecane adduct (FIG.31) the peak of the anomaly appears at the slightly higher temperature of 16.7°K but this difference may be attributed to the increment ΔT of the run crossing the anomaly (1.9°) being longer than usual (1.3°) at this temperature. The shallow nature of the anomaly peak and the change in slope of the curve through the maxima in Cp are characteristic for all six adducts. The extent of the anomaly estimated on the basis of the maximum observed excess Cp over a smooth curve drawn through the high and low temperature limbs is approximately 7%

TABLE 29 .- SUMMARY OF THE ROOT MEAN SQUARE % DEVIATIONS OF EXPERIMENTAL HEAT CAPACITY DETERMINATIONS FROM A SMOOTH CURVE.

System	Temperature Range. (12-25)°K.	(25-70)°K.	(70-300)°K.
Empty Calorimeter	0.64	0.24	0.08
Decane Adduct	0.45	0.10	0.07
Dodecane Adduct	0.26	0.08	0.08
Hexadecane Adduct	0.34	0.21	0.08
Eicosane Adduct	0.25	0.10	0.09
Pentadecane Adduct	0.30	0.20	0.09
2-methyl-pentadecane Adduct	0.39	0.09	0.10

FIG.29. LOW TEMP. ANOMALY IN DECANE–UREA AND DODECANE–UREA ADDUCTS.

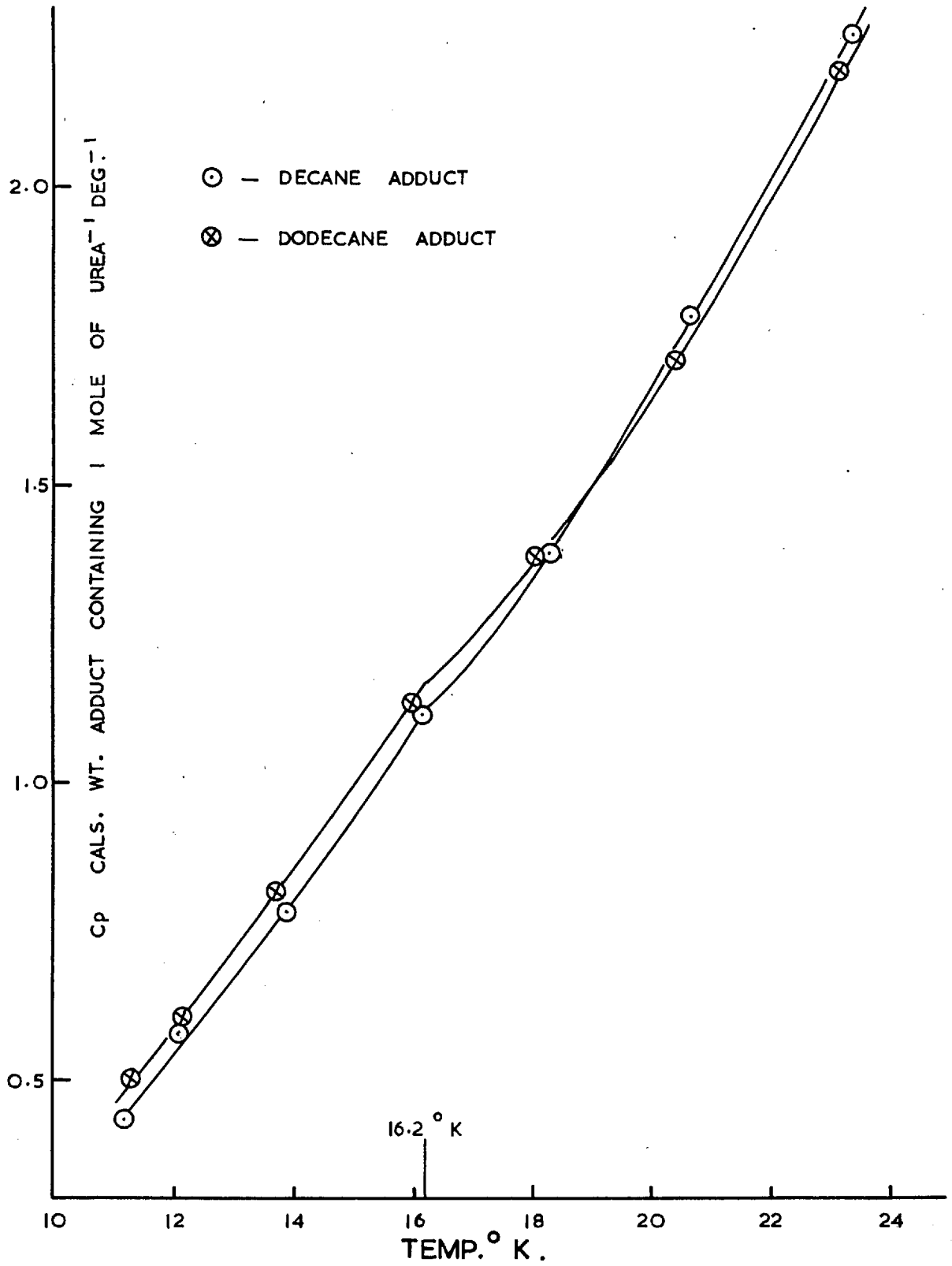


FIG.30. LOW TEMP. ANOMALY IN HEXADECANE–UREA AND EICOSANE–UREA ADDUCTS.

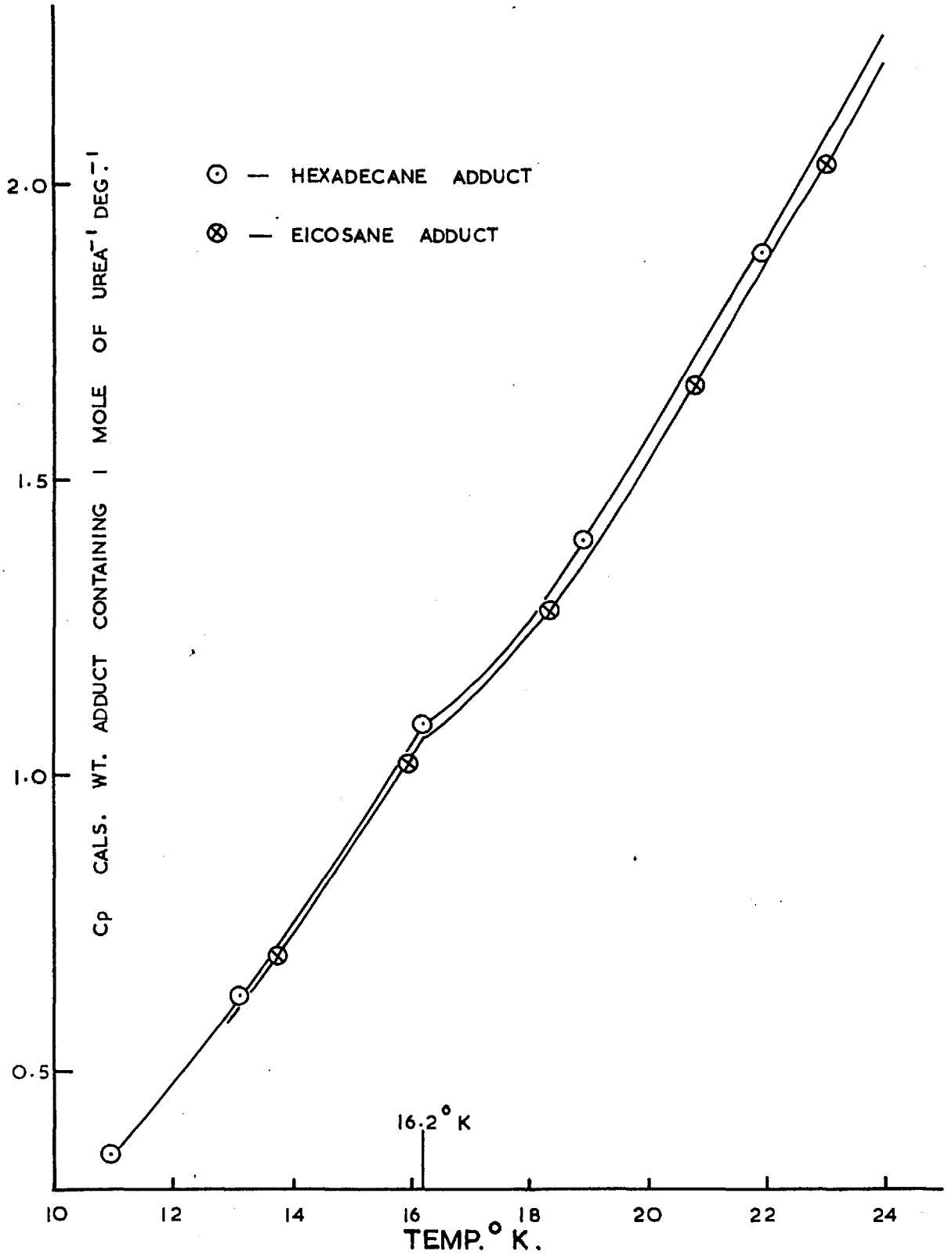
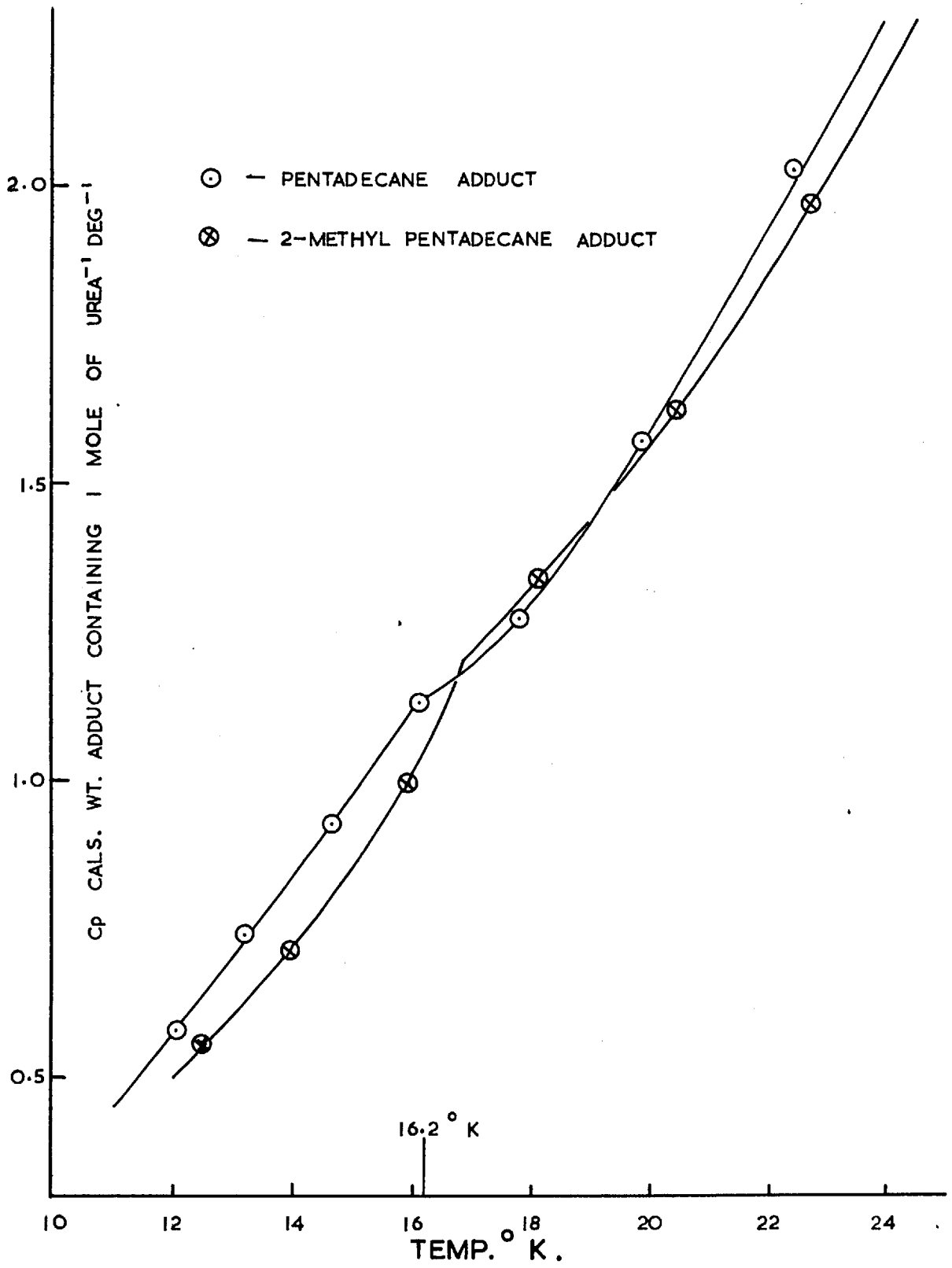


FIG.31 . LOW TEMP. ANOMALY IN PENTADECANE–UREA AND 2–METHYL PENTADECANE–UREA ADDUCTS.



although this varied by $\pm 0.5\%$, an amount attributable to experimental error at this temperature.

The presence of an excess heat capacity over the smooth curve value in this temperature range, which is evidently independent of the molecular species occupying the lattice channels, may be attributed to the hexagonal urea lattice. It appears unlikely that a basic change of crystal structure can be responsible as the anomaly is small, and in general thermal contraction would be expected to have finished above $16^{\circ}K$.

The onset of low frequency librational twisting parallel to the lattice channels through flexing of the hydrogen bonds may be postulated as a possible mechanism. However, an adequate theoretical treatment of such motion would be difficult owing to the complexity of the model required and the small magnitude of the effect to be explained.

The presence of the low temperature anomaly also complicates the Debye extrapolation of the heat capacity to temperatures below those covered by experimental measurements. Calculation of the Debye constant Θ was finally based on heat capacity values interpolated from the smoothed experimental data on the low temperature limb of the anomaly (12°-15° K) using the tabulation of

the specific heat function given by Beattie[129]. The values of θ obtained and subsequently used for the extrapolation below 11°K at intervals of one degree, are shown in the table below:

TABLE 30

Adduct	Debye θ
n-decane	142.5
n-dodecane	138.6
n-pentadecane	139.9
n-hexadecane	149.3
2-methyl-pentadecane	145.0
n-eicosane	149.0

SECTION XII(c) The co-operative "high temperature" anomalies

The presence of a fairly narrow (10°-15°) co-operative anomaly in the n-paraffin urea adduct heat capacities over the temperature range 100°-200°K, for the C_{10} - C_{20} compounds, was unexpected in view of the weak van der Waals forces operating between molecules in neighbouring channels over distances of 8.23 Å[49]. It might have been predicted that such transitions if they occurred at all, would be found at much lower temperatures and be less strongly co-operative.

X-ray diffraction[130][131][132][133] studies and electron diffraction experiments[134] on pure odd and even linear paraffin hydrocarbons, from $C_{18}H_{38}$ to $C_{30}H_{62}$, have shown that packing in layers as parallel chains in an orthorhombic subcell occurs with spacings of a = 7.46Å and b = 4.96Å. The pure hydrocarbons with between 20 and 43 carbon atoms also show a transition[135][136] about 5°- 10°C below their melting points[125] ($\sim$300°K) which has been attributed by Müller[130] (1930) to acquisition of rotational energy about the long molecular axis together with some chain twisting resulting in a change to hexagonal packing. Lonsdale[137] has confirmed this explanation as diffuse X-ray reflections from a single crystal of a hydrocarbon show a maximum in the a-b plane. Since the distance of separation 4.91Å is approximately half that observed in the urea adducts, where a similar parallel packing of hydrocarbon molecules is found, the intereaction energy assuming a London inverse sixth power law would amount to 1/64th of that in the pure hydrocarbons. Consequently this should, to a rough approximation, produce a transition in the region of 5°K for similar molecular motion in the adducts. The adducts investigated however, apart from the 2-methyl-pentadecane compound, all showed a sharp transition as presented in

the detailed graphs for these anomalies (FIGS.32 to 36). In these graphs the adduct heat capacity is given in calories per degree for the weight of adduct containing one mole (60.058g) of urea. The experimental points are shown for the various series of runs made crossing the transition region. Additional series of runs were made once an anomalous region had been detected in order to sharpen the transition by using smaller temperature increments(approximately 0.5°). As a result some of the preliminary runs, shown as the "first set" in the graphs, with an interval ΔT of approximately 5° lie off the final heat capacity curve by several times the calculated root mean square % deviation. This arises primarily from the fact that a curvature correction was not applied to points in the anomaly region.

The low temperature limb of the anomalous section of the Cp curve is observed to diverge above the "normal smooth curve" at temperatures well below the peak of the transition (Tc)(FIGS.32 to 36). This increase in Cp appears at approximately 78°K for the decane and 107°K for the hexadecane adducts respectively some (35°-45°)K below Tc. A small "tail" on the high temperature side of the anomaly is also characteristic of these transitions. For decane and hexadecane this tailing

FIG.32. HIGH TEMP. ANOMALY IN DECANE–UREA ADDUCT.

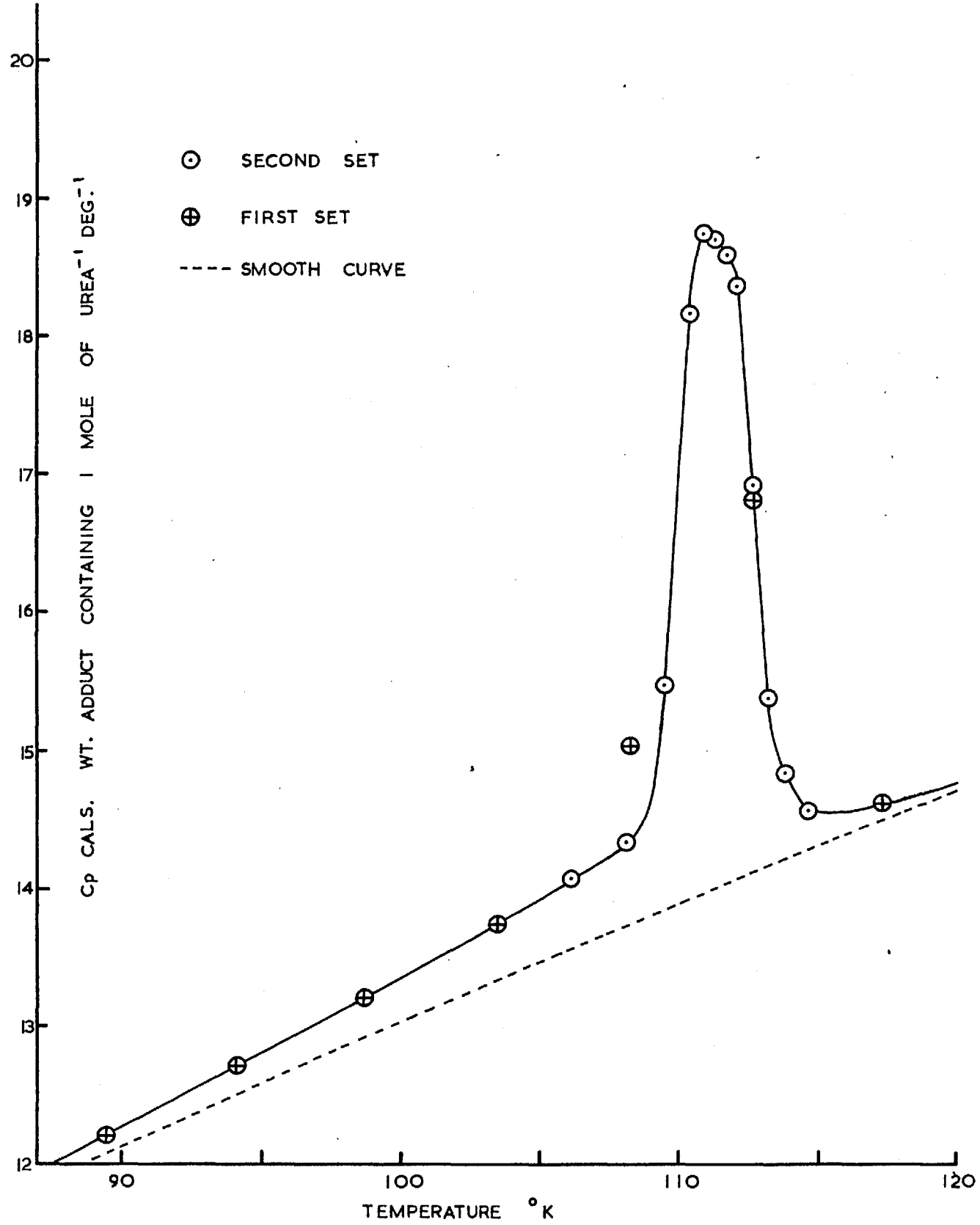


FIG.33. HIGH TEMP. ANOMALY IN DODECANE-UREA ADDUCT.

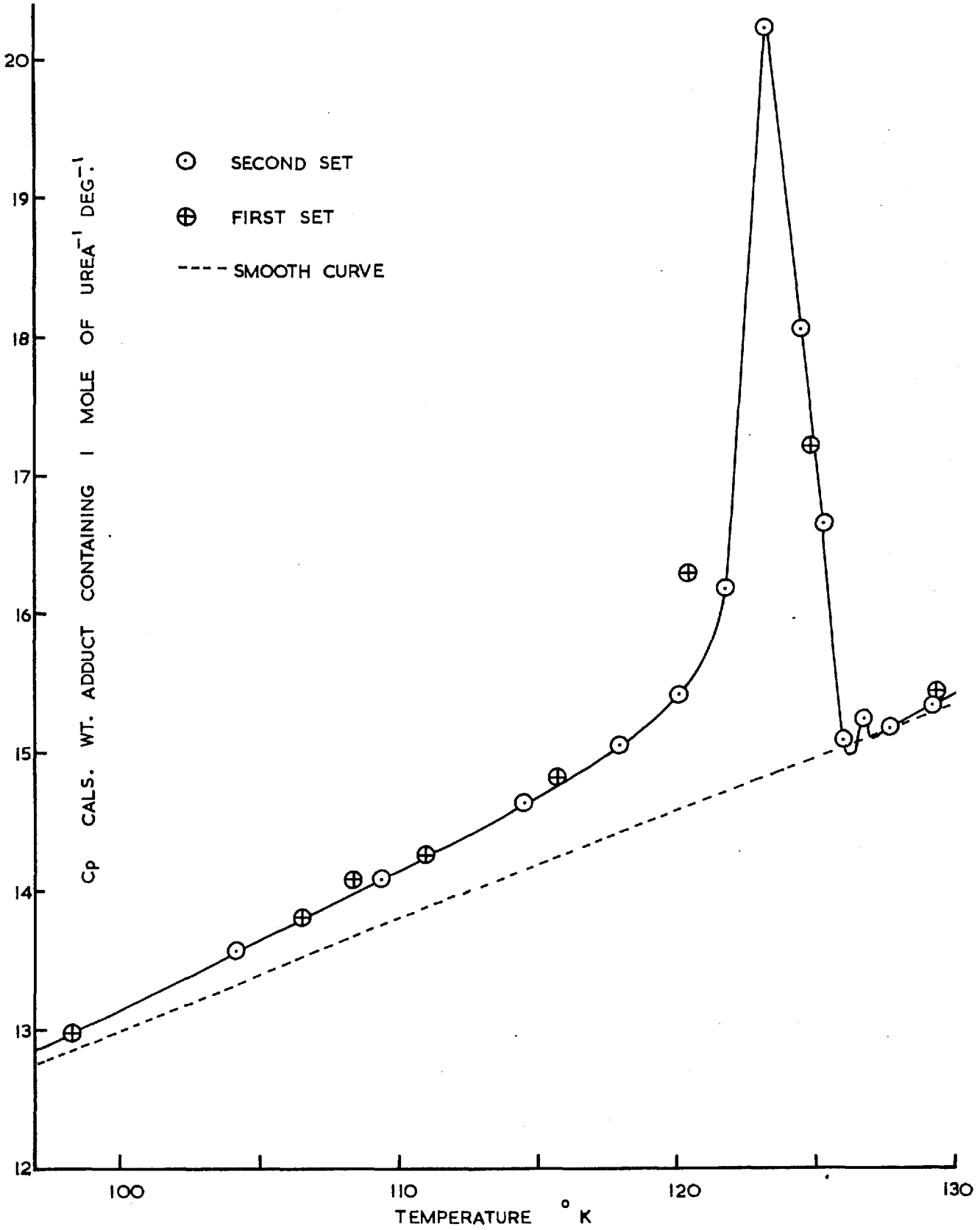


FIG.34. HIGH TEMP. ANOMALY IN PENTADECANE–UREA ADDUCT.

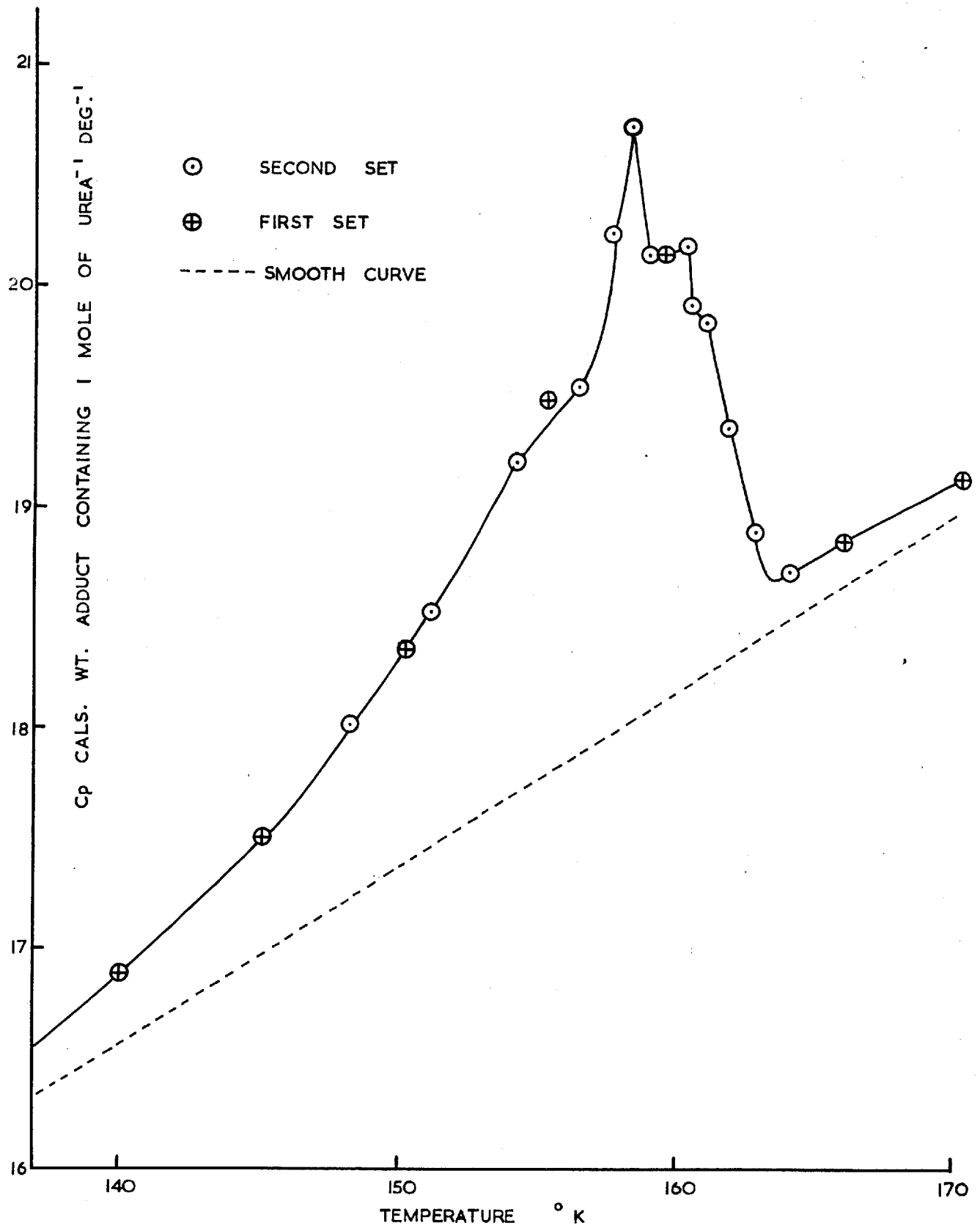


FIG. 35. HIGH TEMP. ANOMALY IN HEXADECANE–UREA ADDUCT.

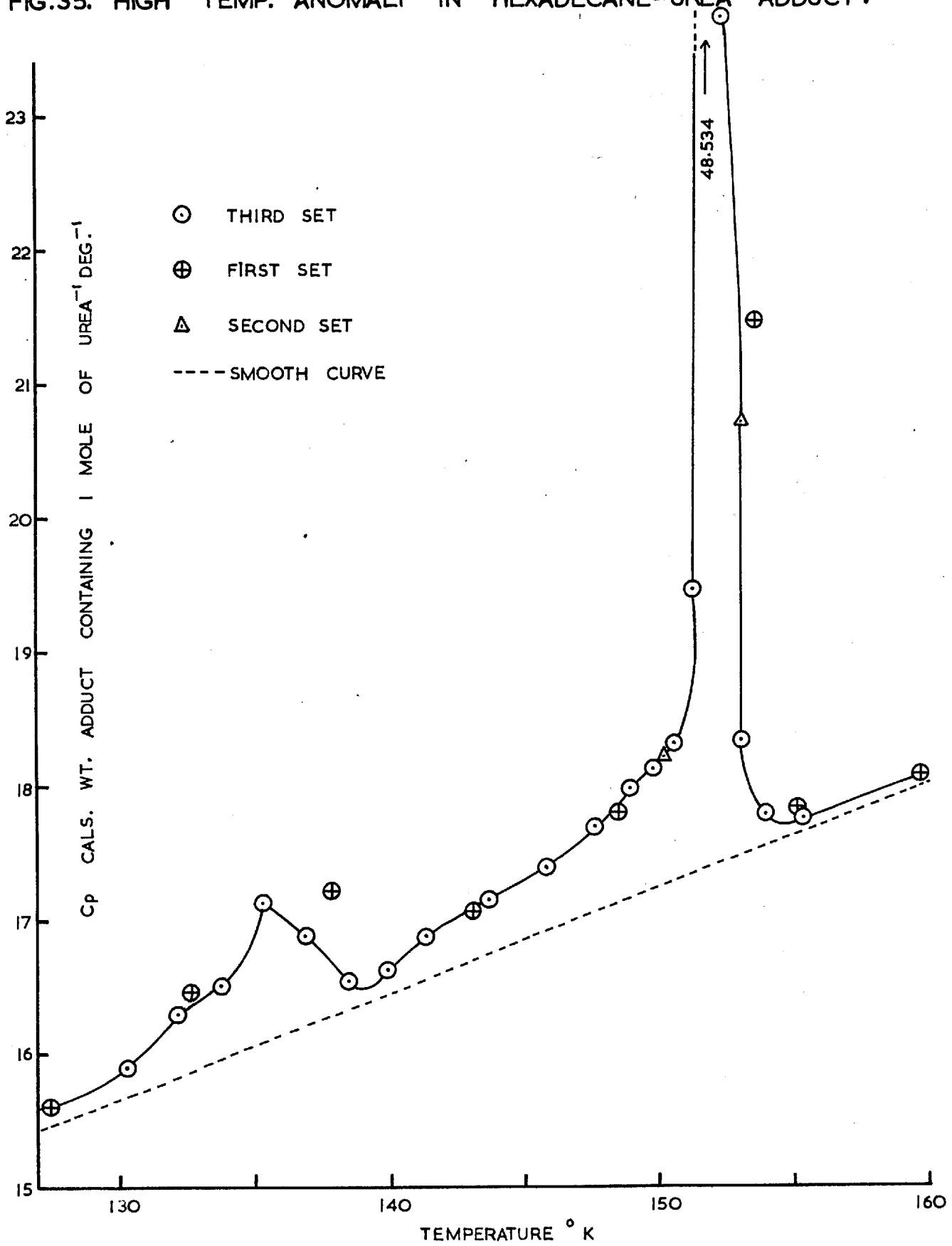
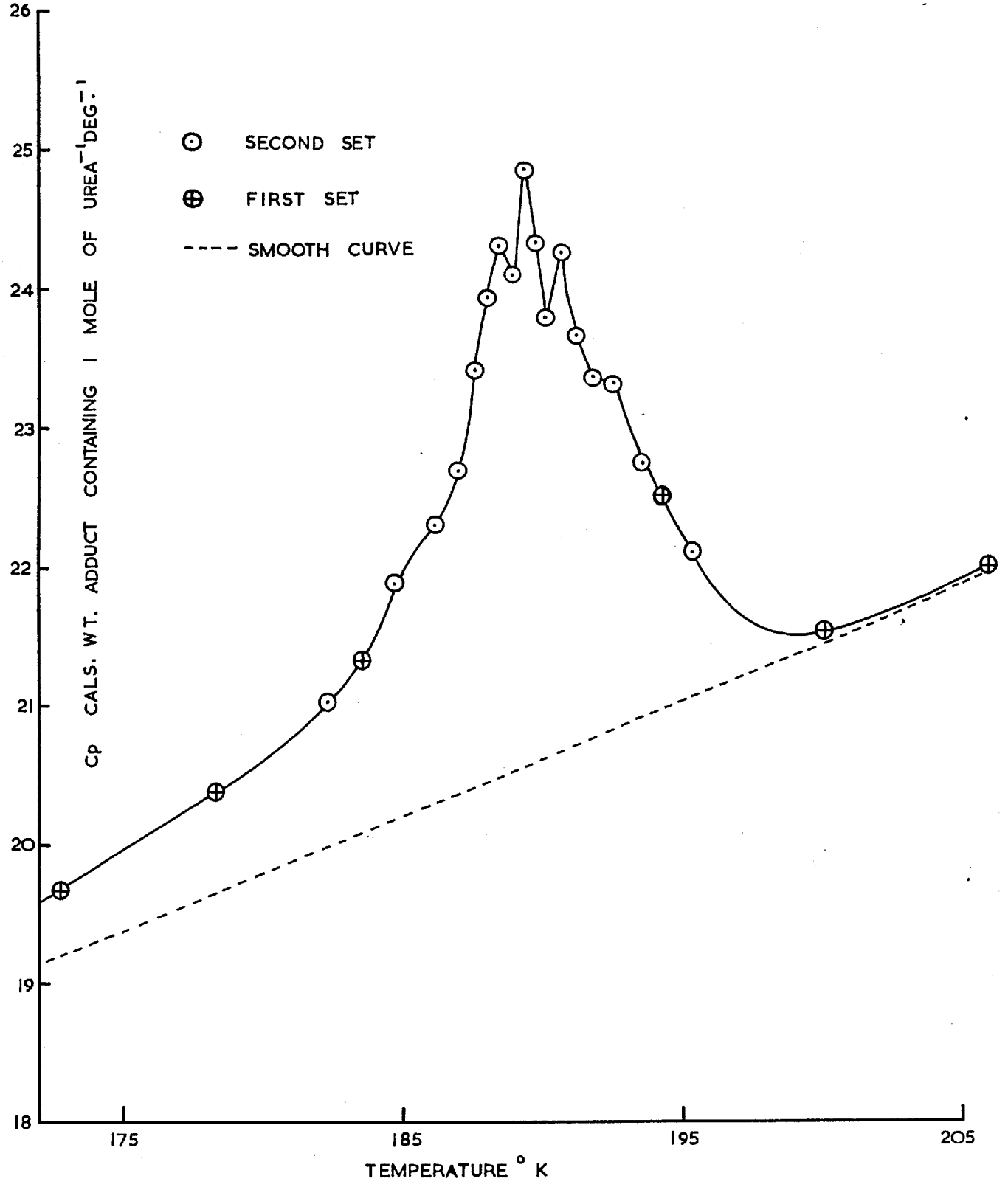


FIG. 36. HIGH TEMP. ANOMALY IN EICOSANE–UREA ADDUCT.



extends over 24° and 28°K respectively where the normal Cp curve is joined again.

The construction of the "smooth curve" under an anomaly region (represented by dotted lines in FIGS. 32 to 36) is somewhat arbitrary, since the empty hexagonal urea lattice is too unstable to permit heat capacity measurement. The method of extrapolation of Cp data to the case of the empty host lattice for various degrees of cavity occupation which has been successfully employed by Parsonage and Staveley[85][138][139] to determine the lattice heat capacity contribution from ß -quinol in the clathrates of the rare gases and methane, cannot be applied since it is impossible to prepare urea adducts having partially filled cavities. Although the sum of Cp values for the appropriate weights of tetragonal urea and of the hydrocarbon were shown to be close (±1%) to the observed adduct heat capacities in non-anomalous temperature regions above 100°K (see TABLE 28), it was not felt justifiable to construct the "normal curve" on this data. Consequently the best smooth curve was drawn by eye.

The presence of a subsidiary transition and the observed overall increase in the sharpness of the

main transition in the n-$C_{16}H_{34}$ compound (FIG.35) probably reflects the slight difference in the structure of this adduct. This arises from a longitudinal contraction of approximately 0.82Å through slight rotation of a terminal methyl group in order to enable the hexadecane molecule to occupy exactly twice the "c" spiral repeat distance of the hexagonal urea lattice (22.02Å). This shortening is illustrated in (a) and (b) of PLATE 4 by means of a Lebold model. Confirmation of this effect may be provided at some later date by a study of the n-C_7H_{16} and n-$C_{24}H_{50}$ adducts where a similar contraction from the planar zig-zag configuration has also been reported.(46)

As the major transition of the cetane adduct (Tc = 152°K) lies in the temperature region in which methanol, the solvent used in preparation of the adduct, has been shown, at least for samples of purity below 99.88%(140), to exhibit a co-operative transition (Tc = 157°K) (141)(142)(143) an attempt was made to detect traces of this substance in the adduct sample taken from the calorimeter. Thermal decomposition of the adduct at 150°C in a small scale distillation apparatus, followed by gas chromatography on the initial distillate failed to detect the presence of even trace amounts of methanol.

(c) (b) (d)

PLATE 4 .

In addition no evidence for occluded solvent methanol was found during the infra-red investigations of Fisher and McDowell[76]. The quantity of methyl alcohol required to produce the observed excess heat absorption, for the entire transition, calculated from Kelley's results (ΔH = 154 cals mole^{-1}) represents 9% of the total adduct weight. This would have been easily detected. Furthermore the other adducts studied did not show a corresponding anomaly at 157°K.

All of the co-operative transitions observed were in a temperature range (110° - 190°K) shown by the investigation of the benzoic acid heat capacity to give results reliable to an accuracy of ±0.3%. The precision of measurement in the anomaly regions was undoubtedly inferior to the ±0.1% deviation normally found due to the smaller temperature interval to be measured and the rapidly changing curvature of the heat capacity vs. temperature plot.

The period necessary to establish thermal equilibrium after heat input during a run did not change in the anomalous regions from the usual value of approximately 15 minutes, as determined by the magnitude of the final drift rate. This was of the order of 0.0003° min^{-1} at temperatures below 150°-200°K. Allowance of

longer periods for equilibration(up to 45 minutes) always gave Cp values lying on the same curve.

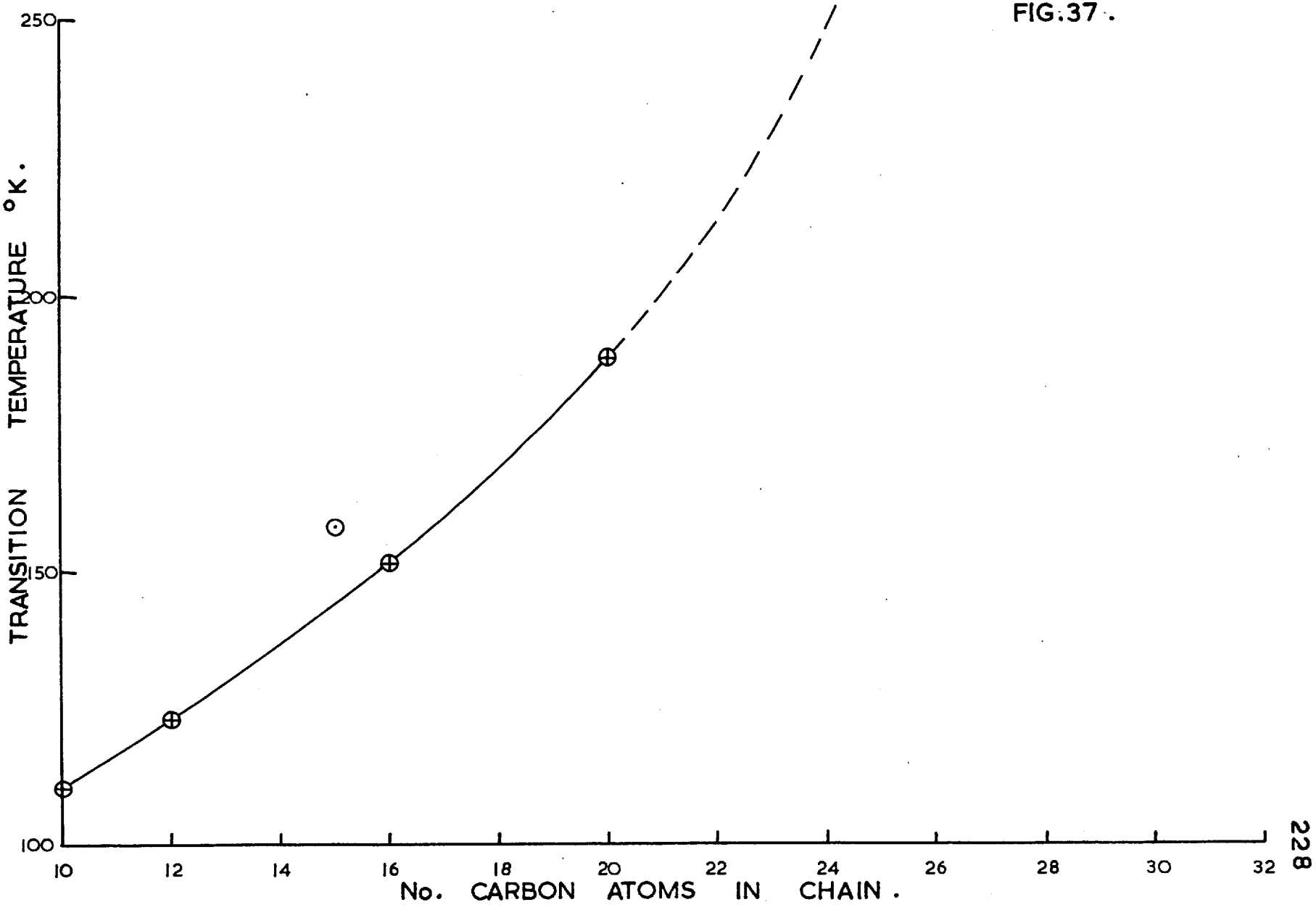
The thermal history of the adduct samples (i.e. the order in which Cp determinations for the various temperature ranges were made) appeared to have negligible effect on the form of the anomalies. Different rates of cooling of the hexadecane adduct sample, ranging from $0.005^{\circ}min^{-1}$ to 0.100° min^{-1}, to temperatures well below the transition region produced only the expected r.m.s. deviations in Cp. This would suggest that the appearance of the subsidiary transition for this adduct is not associated with the sharper main transition due to non-equilibration in crossing the latter during cooling. However, to ensure that "freezing in" of any disorder was minimised, all the adduct samples were cooled slowly ($0.01^{\circ}min^{-1}$) over a wide temperature range(50°) on either side of the major anomalies.

TABLE 31 below shows the transition temperatures (Tc), enthalpies (ΔH cals.mole hydrocarbon^{-1}) and entropies (ΔS cals. deg^{-1} mole hydrocarbon^{-1}) of transition and FIGS.37 to 39 the variation of these quantities with the number of carbon atoms in the guest molecule chain for the n-pentadecane and four even n-paraffins. An approximately linear relationship of chain length(l),

TABLE 31 .- SUMMARY OF THERMODYNAMIC DATA FOR THE TRANSITIONS OBSERVED IN SOME N-PARAFFIN - UREA ADDUCTS.

Adduct	Transition Temp.°K.	ΔH cals.mole Hydrocarbon^{-1}.	ΔS cals. deg^{-1} mole Hydrocarbon^{-1}.
Decane	110.85	203.2	1.94
Dodecane	123.19	264.5	2.26
Hexadecane	(135.30, 151.77)	422.3	2.91
Eicosane	189.27	667.2	3.61
Pentadecane	158.38	343.9	2.26

FIG. 37.


250
200
150
100
TRANSITION TEMPERATURE °K.
10
12
14
16
18
20
22
24
26
28
30
32
No. CARBON ATOMS IN CHAIN.

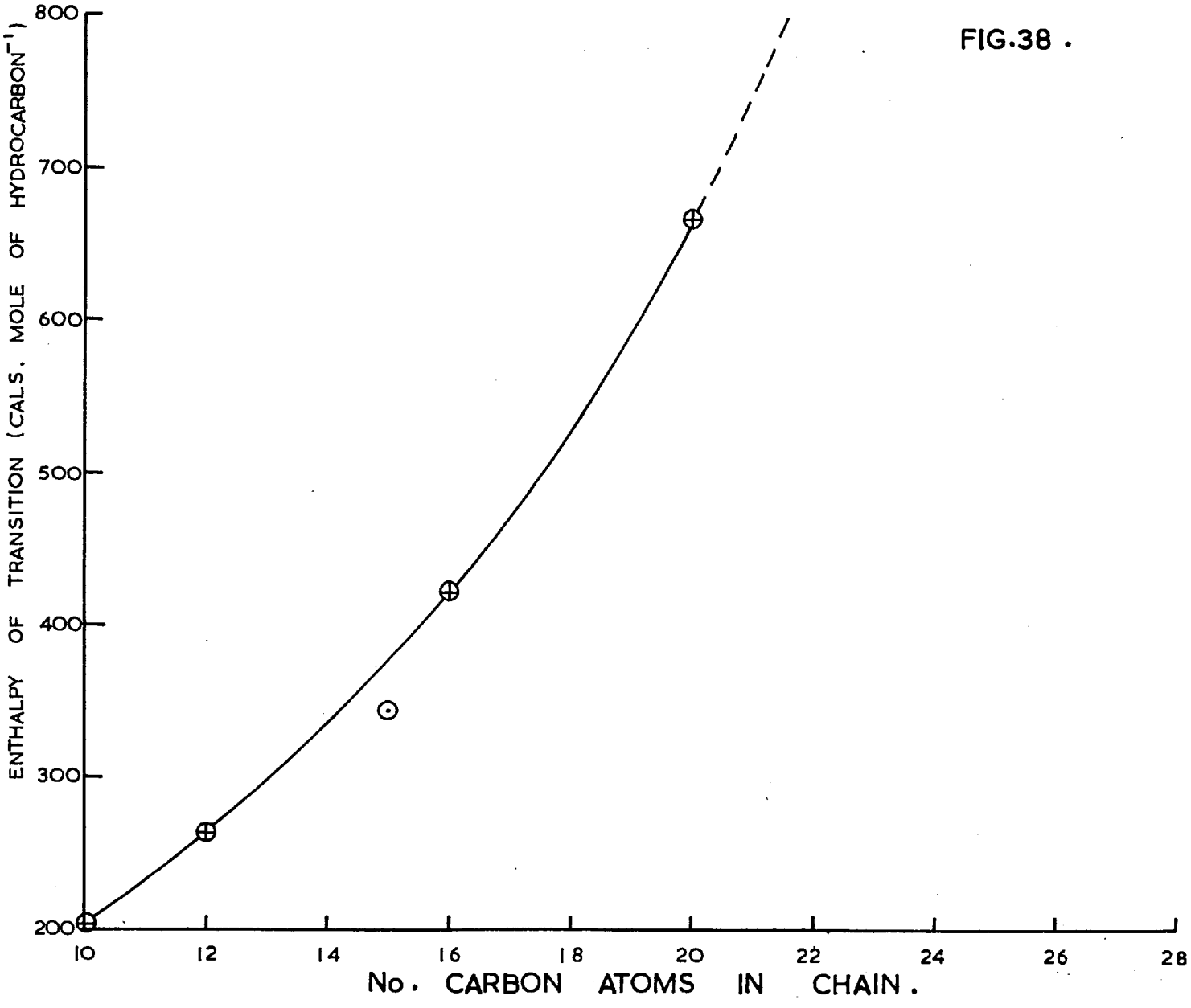

ENTHALPY OF TRANSITION (CALS. MOLE OF HYDROCARBON^{-1})
800
700
600
500
400
300
200
10
12
14
16
18
20
22
24
26
28
No. CARBON ATOMS IN CHAIN.

FIG.38.

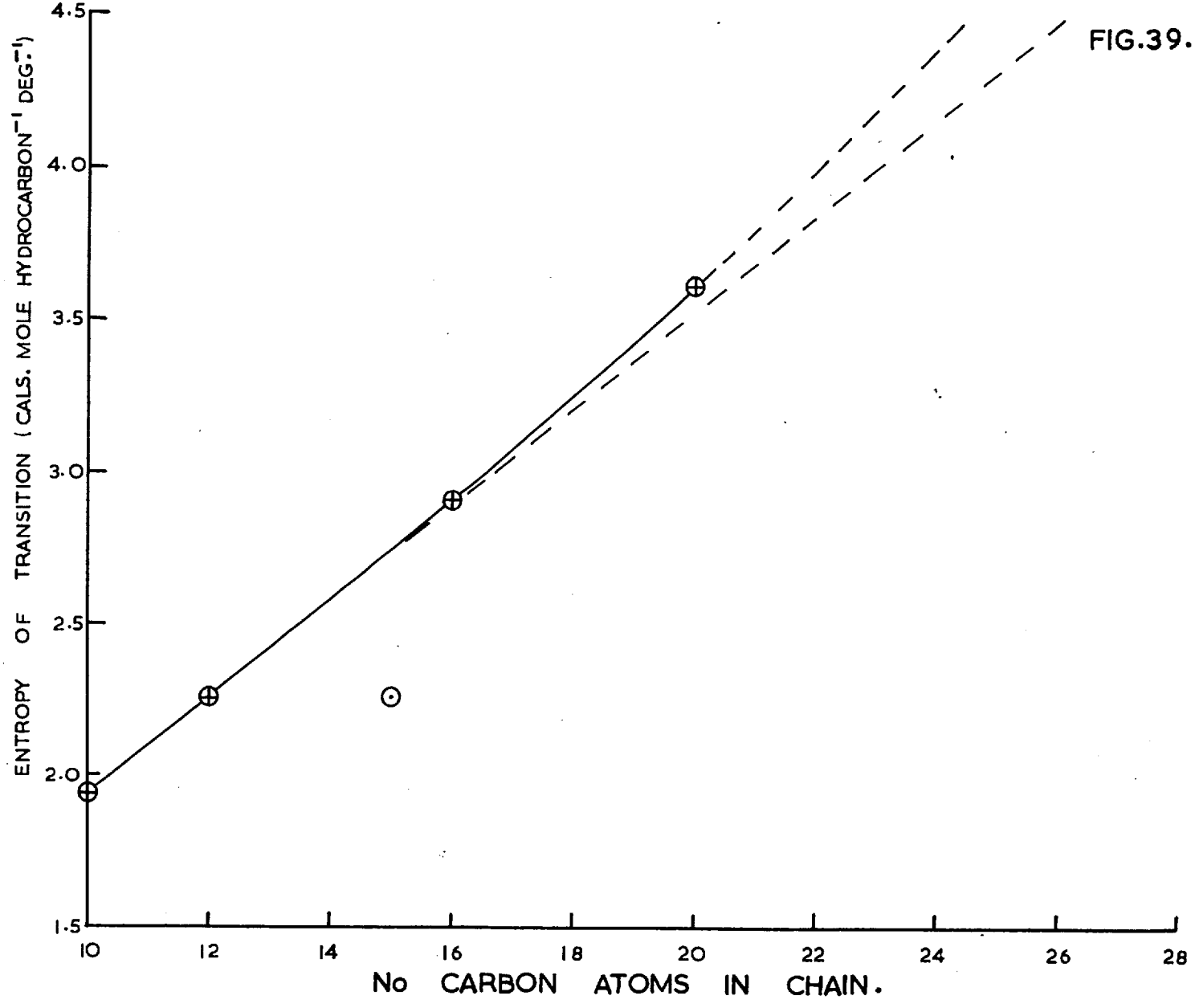
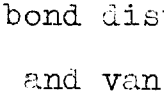

ENTROPY OF TRANSITION (CALS. MOLE HYDROCARBON^{-1} DEG.$^{-1}$)
4.5
4.0
3.5
3.0
2.5
2.0
1.5
10
12
14
16
18
20
22
24
26
28
No CARBON ATOMS IN CHAIN.

FIG.39.

to ΔH and ΔS exists for the n-paraffin adducts studied since, assuming a C-C bond distance of 1.54A,  bond angle of $109^{\circ}28'$ and van der Waals radius of 2.0A for the CH_3-group, the chain length is related to the number of carbon atoms(n) by

$$(l) = 1.256(n-1) + 4.0\text{Å}$$

Despite the appearance of the subsidiary anomaly in the C_{16} compound, when both sections of the anomaly are considered ΔH and ΔS both fall on their respective curves.

The transition temperature of the n-pentadecane adduct is however, higher by 15° than expected from interpolation from the curve formed by the even n-paraffin series while the enthalpy and entropy of transition are 9% and 21% lower respectively. It might be anticipated that the odd hydrocarbon adducts form a second series with constants of transition lying on a separate curve to those of the even homologues. Assuming that this curve is of similar shape to the even series the C_{11} adduct may be tentatively predicted to have Tc = $125^{\circ}K$, ΔH = 200 cals $mole^{-1}$, ΔS = 1.65 cals deg^{-1} $mole^{-1}$. Extrapolation of Fig.37 permits the approximate values of further transition temperatures for the even n-hydrocarbon adducts as shown below:-

TABLE 32

Number of Carbon Atoms	Tc °K Estimated
C_8	99
C_{24}	250
C_{26} or C_{28}	300

Although a major "high temperature" anomaly is absent in the 2-methyl-pentadecane adduct heat capacity, three regions at 153°K, 192°K and 250°K having a small excess heat absorption were found. These temperatures correspond to Tc as found for the C_{16} and C_{20} adducts and the extrapolated value for the C_{24} compound. In view of this and the magnitude of these excess Cp values compared with the transitions of the other adducts studied, the largest represnting only 0.8% of the heat capacity at 250°K, these "blips" may be attributed to the presence of the hydrocarbons mentioned above as impurities. From observed and extrapolated enthalpies of transition a total impurity of 2.9% (0.8% C_{16}, 0.9% C_{20} and 1.2% C_{24}) in the adducted hydrocarbon was indicated. The presence of impurity was found in a preliminary investigation by gas chromatography of the hydrocarbon (see section X(b)) but insufficient material was available to permit purification.

SECTION XII(d). The origin of the high temperature anomalies.

Consideration of a model of the urea-hydrocarbon adduct system representing the packing arrangement of the constituent atoms shows the number of modes of motion available to the hydrocarbon molecules in the urea lattice are somewhat limited (see FIG 2.). Rotation of a terminal methyl group or the entire chain in the zig-zag planar configuration is permissible, but rotation of methylene groups in addition to the terminal CH_3 relative to the chain axis would be highly hindered by grating of the molecule against the urea lattice channel walls. Additional possible modes include a small degree of lateral and longitudinal translational motion and internal modes such as torsional oscillation. The latter may be enhanced by random reorientation between low energy sites. Smith[49] has proposed, from implication diagrams and electron density projections, that the whole molecule undergoes random reorientation between three low energy sites disposed at multiples of 60° to a line drawn perpendicular to the "a" axis. However this mechanism of random reorientation demands the entropy of transition per mole of occluded hydrocarbon to be given by

$$\Delta S = R.\ln W$$

where W is an integer representing the number of possible reorientational sites available to the hydrocarbon. Such a correspondance was not found for the n-hydrocarbon adducts, in the even paraffin series at least.

It is probable that the transition is associated with the onset of rotation or possibly reorientation of the included hydrocarbon molecules about their long axis. This type of motion has been shown (see section XIV(c)) to be capable of producing a rapid co-operative breakdown in the long range order existing at low temperature through coupling between adjacent molecules in the same channel and with molecules in the six neighbouring channels of the urea lattice. Simple meshing of the ends of hydrocarbon chains, within each cavity through the lattice, producing rotation as a single unit or as several long chains where a lattice defect or impurity molecule terminates its continuation would not be sufficiently co-operative to produce the sharp anomalies observed. At best a transition smeared over a large temperature range (approximately 100°) would result. This arises from the inability of one dimensional interacting systems (e.g. the Ising model for a chain of interacting dipoles)[144] at temperatures above the absolute zero to develop long range order. The existence

of a crystalline field from the urea lattice retarding rotation will also cause a further spread of the transition region.

The absence of a transition in the temperature range covered by Cp measurement for the 2-methyl-pentadecane adduct furnishes strong evidence for the proposed rotational mechanism. In this adduct the bulky side group gives rise to a large barrier to rotation as a result of steric hindrance. PLATE 4 (a) and (c) shows the relative dimensions of chains with and without a methyl side group. Also, although the constants of transition for the n-C_{15} adduct do not correspond to the series formed by the even homologues, the variation is not sufficiently large to merit a separate explanation of the transition in this case. The n.m.r. measurements of Gilson and McDowell[67] on the tridecane and hexadecane adducts confirm a similar behaviour for the odd and even series and from the decrease in second moments (see section I(h), they conclude that at room temperature the hydrocarbons have considerable rotational freedom.

Clearly an analysis of the magnitudes of the energies and associated potential barriers to rotation arising from the three possible interactions listed below must be considered before a theory explaining the transitions can be developed.

(1) Interaction of the urea lattice with the occluded hydrocarbon.

(2) Interaction between adjacent included hydrocarbon molecules in the same channel.

(3) Interaction between hydrocarbon molecules in neighbouring channels.

These interactions are discussed in subsequent sections.

SECTION XII(e) The excess energy absorption in the region 220°-250°K

A small excess absorption of the order (0.2 - 0.5)% of the total heat capacity was found in the heat capacity curves for all the adducts studied over part of the region 220°-250°K. Although this effect is small it represents several times the r.m.s.% deviation (approximately 0.1%) at these temperatures.

Hoffman and Ruehwein[127] found a similar excess energy uptake in the range 255° to 265°K when investigating the heat capacity of urea, and concluded that the melting of a saturated aqueous solution of urea was responsible. The estimated 0.052g. of water present which could not be removed by re-evacuation of their calorimeter but addition of the same weight of water showed a doubling

of the excess energy absorbed. However, Gilson and McDowell[67] from an n.m.r. study of the second moments of the C_{13} and C_{16} adducts in a fully deuterated urea lattice have reported a sharp decrease of 0.3 gauss^2 and 1.4 gauss^2 respectively at a temperature of 225-230°K. They have suggested that this results from an expansion of the urea lattice permitting a greater freedom of motion of the adducted hydrocarbon.

It is not possible to decide which mechanism is responsible on the evidence available. If, however, the melting of a saturated aqueous urea solution is responsible then on average approximately 0.01g. of water must have been present in the calorimeter during our heat capacity determinations.

CHAPTER XIII. THE INTERMOLECULAR FORCES PRESENT IN THE ADDUCTS.

SECTION XIII(a) The interaction between the urea crystalline field and the adducted n-paraffins.

From a detailed X-ray diffraction study of the n-hexadecane and 1,10-dibromodecane-urea complexes Smith[49] has shown (see section I(d)) that this class of adducts are formed between a hexagonal urea lattice and hydrocarbon mplecules in the extended planar configuration. Furthermore he concluded that the weak bonding present is of the weak van der Waals type as has been confirmed by all subsequent investigations.

In outline therefore the interaction potential and hence the rotational barrier for a given hydrocarbon molecule in the urea field may be derived from Smith's data by calculation of inter atomic separations and a subsequent pair-wise summation, assuming a central force law, based on a Lennard-Jones (6-12) potential of the form

$$\phi(r) = B\left[\tfrac{1}{2}(r_o/r)^{12} - (r_o/r)^{6}\right] \ldots\ldots (1)$$

where r is the distance between the two interacting atoms, B is the minimum value of the potential energy and ro the distance of separation at which this minimum occurs.

Smith's study[49] revealed a helical symmetry for the urea lattice and hence the intermolecular field produced ϕ will be a function of the distance along(z) and the angle θ rotated about the "c" crystallographic axis.

$$\phi = f(z,\theta)$$

However, a translation of z = 1.834 Å along and a rotation of 60° about the screw axis of symmetry reproduces the initial crystalline field at the origin ($z = o$, $\theta = o^{\circ}$). In the calculations made the plane z = o was chosen to correspond with that containing the oxygen atoms of the urea lattice; in addition the terminal carbon atom of the hydrocarbon was sited in this plane with its long molecular axis in the centre of the hexagonal channel. The plane of the paraffin carbon skeleton for θ = o was chosen as that joining carbon atoms of the type C_1 and C_4 (see FIG.1.)

Three approximations simplifying the calculation were introduced.

(1) The interactions between the hydrogen atoms of the urea, on the one hand, and the carbon and hydrogen atoms of the hydrocarbon, on the other, were ignored due to the small force constants of hydrogen

relative to those of the nitrogen, oxygen and carbon atoms of the urea and the high negative powers of r which are being considered. The location of the hydrogen atoms would also be in some doubt from the X-ray diffraction study but their separations from the hydrocarbon are similar to those for the N,O and C atoms of urea (approximately 4.1Å for the urea oxygen).

(2) Only contributions arising from molecules constituting the immediately surrounding channel of the urea lattice were considered. Contributions from atoms forming the six adjacent lattice channels add to Ø only as a second degree term owing to the larger distances involved.

(3) To reduce the time of computation, while retaining a realistic physical situation, the length of the interacting urea lattice was restricted such that, for each CH_2 element of the hydrocarbon chain interactions with urea molecules were considered provided the z-co-ordinate of the urea molecules did not differ by more than one and a half times the c-spacing(3/2 x 11.01 = 16.51 Å) from the z-co-ordinate of the element. The hydrocarbon molecules were considered to be sited centrally in the lattice channel.

Because of the helical symmetry properties of the urea lattice it is possible to evaluate the cylindrical co-ordinates of the carbon and hydrogen atoms of the included hydrocarbon by relation to those in the urea field in the plane z = o. By an appropriate rotation through the angle (α) and translation to z = o, a crystalline field identical to that existing at the original atom site is reproduced. In a computer programme this device, which reduced by one sixth the number of co-ordinates relating to the urea lattice which had to be generated, was applied to the evaluation of the potential energy of a (CH_2) unit and the total hydrocarbon interaction energy obtained as the sum of such separate (CH_2) contributions.

In the computation the bond distances of C-H, C-C, C = O and C-N bonds were taken to be 1.10Å, 1.54Å, 1.28Å and 1.33Å respectively (after Pauling)[145] and the $C\!\!<\!\!\!\diagup^{C}_{C}\!\!\diagdown$ bond angle as 109° 28′. Application of the Lennard-Jones equation required the following van der Waals radii which were taken also from Paulings' work.

	Radius(Å)
Oxygen	1.4
Hydrogen	1.2
Nitrogen	1.5
Methyl group	2.0

The Lennard-Jones equation may be written in the form:

$$\phi(r) = -A\left(\frac{1}{r^6} - \frac{r_o^6}{2r^{12}}\right) \quad \ldots\ldots\ldots(2)$$

where A is a constant which can be approximately calculated from several theoretical and empirical equations. Of these, those most widely used are:

(1) London[146]:

$$A = \frac{3}{2}\alpha_1.\alpha_2\frac{E_1E_2}{E_1+E_2} \quad \ldots\ldots\ldots\ldots\ldots(3)$$

where the α's are the polarisabilities and the E values are the characteristic energies (close to the ionisation potentials) of the interacting atoms.

(2) Kirkwood-Müller:[147][148]

$$A = -6mc^2 \cdot \frac{\alpha_1\alpha_2}{\alpha_1/\chi_1 + \alpha_2/\chi_2} \quad \ldots(4)$$

where m is the mass of an electron, c is the velocity of light and the χ's denote the diamagnetic

susceptibilities of the interacting molecules.

(3) Slater-Kirkwood[149]

$$A = \frac{3}{4} \cdot \frac{eh}{m^{1/2}} \cdot \frac{\alpha_1 \alpha_2}{\left(\frac{\alpha_1}{N_1}\right)^{1/2} + \left(\frac{\alpha_2}{N_2}\right)^{1/2}} \quad \ldots (5)$$

where e is the electronic charge, h is Planks constant and N for closed shell systems, is the number of electrons in the outer shells of the two interacting systems.

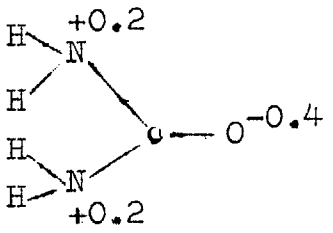
The London equation however, represents the interaction of a single oscillating electron from each atom, and consequently in systems containing several electrons the values obtained are found to be too low. The empirical modifications of the London equation by Slater and Kirkwood to deal with the case of N interacting electrons is more realistic. Tests of equation (5) have been made by Rowlinson[150] who found that plots of log A against log α for isoelectronic systems should have a slope of 3/2. Examination of the rare gases with N = 8(the number of electrons in the outermost shell) showed a crude agreement with this law and it was concluded that N varies from atom to atom depending on the polarisability. A second effect

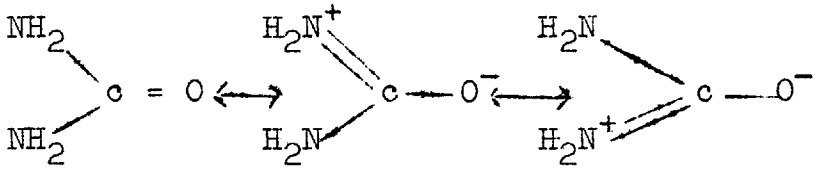
increasing the interaction energy arises from electrons in the more tightly bound shells below the outer subshell. The empirical evaluation of N from the interaction energy from the Slater-Kirkwood equation and a correlation with the actual number of electrons in the outer subshell of the complete system has been given by Pitzer[151]. He concluded that:

N = 1/2 x (total number of electrons + number of electrons in the outermost subshell)

The Slater-Kirkwood equation, with values of N as presented by Pitzer, was chosen for the present calculations.

However, in urea a charge separation as a result of resonance is found as shown below





The effective value of N for nitrogen and oxygen in the urea lattice must be modified by this value.

Therefore for nitrogen $N = 1/2(6.8 + 2.8) = 4.8$

oxygen $N = 1/2(8.4 + 4.4) = 6.4$

carbon $N = 1/2(6.0 + 4.0) = 5.0$

hydrogen $N = 1/2(1.0 + 1.0) = 1.0$

Values for the molecular polarisability α were obtained from Silberstein's work[152] and are shown below

TABLE 33

Atom	α
C	9.56×10^{-25} cm^3
H	4.33 : :
O=	8.68 : :
N	9.15 : :

The value for nitrogen is that obtained from the amine group. This data enables the attractive term in the Lennard-Jones equation to be evaluated. No reliable theoretical treatment for the repulsive interaction constant has been deduced; thus this term was calculated from the van der Waals radii estimating the equilibrium distances ro by the hard-sphere approximation giving:

$$ro = 1/2(r_1 + ro^1).....(6)$$

where r_1 and ro^1 are the respective van der Waals radii. Since Pauling does not quote a value for the

carbon radius this was estimated to be 1.6Å by extrapolation of the values for nitrogen(1.5Å), oxygen(1.4Å) and fluorine(1.35Å) with respect to the number of electrons in the system. Values of the calculated attractive and repulsive constants for the different bond types considered are given in TABLE 34.

Computation of the urea-hydrocarbon interaction potential for hydrocarbons containing 1,3,4,5,7,8,9, 10,12 and 16 carbon atoms have been made for values of θ from 0°, by 10° intervals, to 360° over values of z from 0.0Å to 1.5Å in steps of 0.3Å. This covers the entire range of variation of potential energy(ϕ) with z possible, since the helical symmetry produces a repetition of the urea lattice field after approximately a z increment of 1.8Å. The computed values of ϕ in calories per Avogadro number of hydrocarbon-urea interactions for the C_9 and C_{16} adducts are shown in TABLES 35 and 36. The results are represented graphically for various z values and the C_7, C_8, C_9, C_{10}, C_{12} and C_{16} hydrocarbons in FIGS 40 to 45. TABLE 37 shows the interaction potential for all the systems treated theoretically at z = 0.0Å, θ = 0°, the maximum potential barrier and the "envelope potential barriers" formed by the family of curves of different z co-ordinates.

TABLE 34 .- SUMMARY OF THE INTERACTION CONSTANTS USED IN THE COMPUTATION OF INTERACTION ENERGIES AND POTENTIAL BARRIERS TO ROTATION.

Interacting Atomic Pair.	Attractive Pot. ($cal.mole^{-1}$ $Å^6$.)	Repulsive Pot. ($cal.mole^{-1}$ $Å^{12}$.)
O—C	-3.73×10^5	$+1.36\times10^8$
O—H	-1.33×10^5	$+2.05\times10^7$
C—C	-3.79×10^5	$+2.03\times10^8$
C—H	-1.37×10^5	$+3.30\times10^7$
N—C	-3.63×10^5	$+1.61\times10^8$
N—H	-1.31×10^5	$+2.54\times10^7$
H—H	-5.16×10^4	$+4.93\times10^6$

TABLE 35 .- COMPUTED INTERACTION ENERGY IN CALS. FOR AN AVOGADRO NUMBER OF NONANE MOLECULES WITH THE HEXAGONAL UREA LATTICE.

θ°- Orientation in the (X,Y) crystalographic plane.

z - Displacement along the Z crystalographic axis.

	(-) INTERACTION ENERGY.		
θ°	z = 0.0Å	z = 0.3Å	z = 0.6Å
0	28,398.6	28,386.4	28,370.9
20	28,331.7	28,321.6	28,309.6
40	28,292.7	28,282.2	28,275.7
60	28,291.5	28,283.5	28,284.4
80	28,274.1	28,276.5	28,284.1
100	28,299.6	28,311.9	28,323.8
120	28,355.5	28,374.1	28,389.0
140	28,351.9	28,373.5	28,392.0
160	28,365.2	28,383.2	28,404.0
180	28,433.4	28,447.9	28,465.6
200	28,453.2	28,467.6	28,481.0
220	28,491.6	28,504.8	28,510.9
240	28,545.7	28,554.6	28,553.6
260	28,512.0	28,510.3	28,502.7
280	28,491.0	28,478.6	28,464.9
300	28,481.8	28,461.9	28,444.8
320	28,421.6	28,399.9	28,379.5
340	28,404.5	28,388.7	28,369.6
360	28,398.6	28,386.4	28,370.9

TABLE 35 (Continued).

	(-) INTERACTION ENERGY.		
θ°	z = 0.9Å	z = 1.2Å	z = 1.5Å
0	28,351.7	28,329.9	28,309.1
20	28,297.4	28,286.5	28,278.2
40	28,274.4	28,278.7	28,287.2
60	28,294.0	28,310.6	28,331.6
80	28,295.0	28,309.2	28,327.7
100	28,333.4	28,341.4	28,350.5
120	28,400.6	28,410.8	28,420.9
140	28,407.3	28,421.7	28,436.6
160	28,425.7	28,448.0	28,470.2
180	28,485.6	28,507.0	28,527.5
200	28,493.1	28,503.2	28,509.5
220	28,511.8	28,509.2	28,502.5
240	28,543.1	28,526.0	28,505.4
260	28,488.4	28,468.5	28,446.3
280	28,450.4	28,435.4	28,420.5
300	28,431.1	28,420.0	28,410.0
320	28,362.3	28,349.6	28,340.7
340	28,347.7	28,326.1	28,307.9
360	28,351.7	28,329.9	28,309.1

TABLE 36 .- COMPUTED INTERACTION ENERGY IN CALS. FOR AN AVOGADRO NUMBER OF HEXADECANE MOLECULES WITH THE HEXAGONAL UREA LATTICE.

θ°- Orientation in the (X,Y) crystalographic plane.

z - Displacement along the Z crystalographic axis.

	(-) INTERACTION ENERGY.		
θ°	z = 0.0Å	z = 0.3Å	z = 0.6Å
0	50,486.4	50,493.0	50,495.0
10	50,474.5	50,478.8	50,478.3
20	50,443.6	50,445.4	50,443.8
30	50,428.0	50,422.2	50,420.9
40	50,431.2	50,426.8	50,426.4
50	50,455.5	50,450.2	50,451.3
60	50,467.9	50,465.1	50,468.8
70	50,452.8	50,454.0	50,461.0
80	50,426.4	50,431.7	50,441.3
90	50,422.9	50,431.1	50,441.3
100	50,457.2	50,467.9	50,477.1
110	50,508.5	50,522.0	50,531.3
120	50,540.5	50,556.8	50,567.5
130	50,534.4	50,551.6	50,563.5
140	50,504.6	50,520.0	50,532.5
150	50,486.3	50,498.8	50,510.6
160	50,502.0	50,510.6	50,519.8
170	50,538.5	50,541.8	50,546.3
180	50,562.7	50,560.3	50,559.6
190	50,557.1	50,550.6	50,545.0
200	50,535.6	50,526.9	50,517.4
210	50,526.7	50,518.6	50,507.6
220	50,544.1	50,539.3	50,529.5
230	50,569.8	50,568.5	50,560.9
240	50,571.3	50,571.2	50,565.2
250	50,536.2	50,534.9	50,529.3

TABLE 36 (Continued).

	(-) INTERACTION ENERGY.		
θ°	z = 0.0Å	z = 0.3Å	z = 0.6Å
260	50,486.9	50,482.1	50,474.9
270	50,458.4	50,448.7	50,438.5
280	50,464.2	50,450.2	50,438.4
290	50,488.9	50,469.8	50,458.5
300	50,492.6	50,476.6	50,467.0
310	50,470.2	50,457.2	50,450.2
320	50,435.5	50,429.1	50,425.9
330	50,418.5	50,419.9	50,421.1
340	50,433.8	50,440.4	50,444.5
350	50,466.9	50,474.7	50,478.9
360	50,486.5	50,493.0	50,495.0

TABLE 36 (Continued).

	(-) INTERACTION ENERGY.		
θ°	z = 0.9Å	z = 1.2Å	z = 1.5Å
0	50,491.8	50,484.3	50,475.8
10	50,473.1	50,464.7	50,457.1
20	50,439.0	50,432.1	50,426.9
30	50,408.1	50,418.2	50,397.0
40	50,430.6	50,437.4	50,446.1
50	50,460.1	50,474.0	50,490.6
60	50,480.2	50,497.4	50,518.3
70	50,473.5	50,490.8	50,511.7
80	50,453.5	50,468.1	50,485.4
90	50,451.1	50,461.0	50,472.6
100	50,483.4	50,488.2	50,494.1
110	50,535.5	50,536.4	50,537.0
120	50,571.7	50,570.8	50,567.5
130	50,569.4	50,569.4	50,565.1
140	50,540.9	50,544.7	50,543.1
150	50,520.9	50,528.4	50,531.0
160	50,529.1	50,537.7	50,543.6
170	50,552.1	50,559.1	50,565.9
180	50,560.7	50,563.8	50,567.9
190	50,540.8	50,538.2	50,536,9
200	50,508.3	50,500.2	50,493.2
210	50,495.6	50,483.2	50,470.9
220	50,516.3	50,500.4	50,482.8
230	50,547.6	50,529.6	50,508.6
240	50,553.1	50,535.8	50,515.2
250	50,518.9	50,504.7	50,488.2
260	50,465.3	50,454.7	50,444.8
270	50,428.8	50,421.5	50,418.2
280	50,429.9	50,426.0	50,427.3
290	50,453.2	50,453.3	50,458.0
300	50,465.3	50,469.5	50,476.9

TABLE 36 (Continued).

	(-) INTERACTION ENERGY.		
θ°	z = 0.9Å	z = 1.2Å	z = 1.5Å
310	50,451.1	50,457.5	50,465.9
320	50,427.8	50,432.7	50,438.5
330	50,422.6	50,423.6	50,423.9
340	50,445.3	50,442.6	50,437.7
350	50,478.2	50,472.7	50,464.7
360	50,491.8	50,484.3	50,475.8

FIG.40·COMPUTED UREA–HEPTANE INTERACTION POTENTIAL.

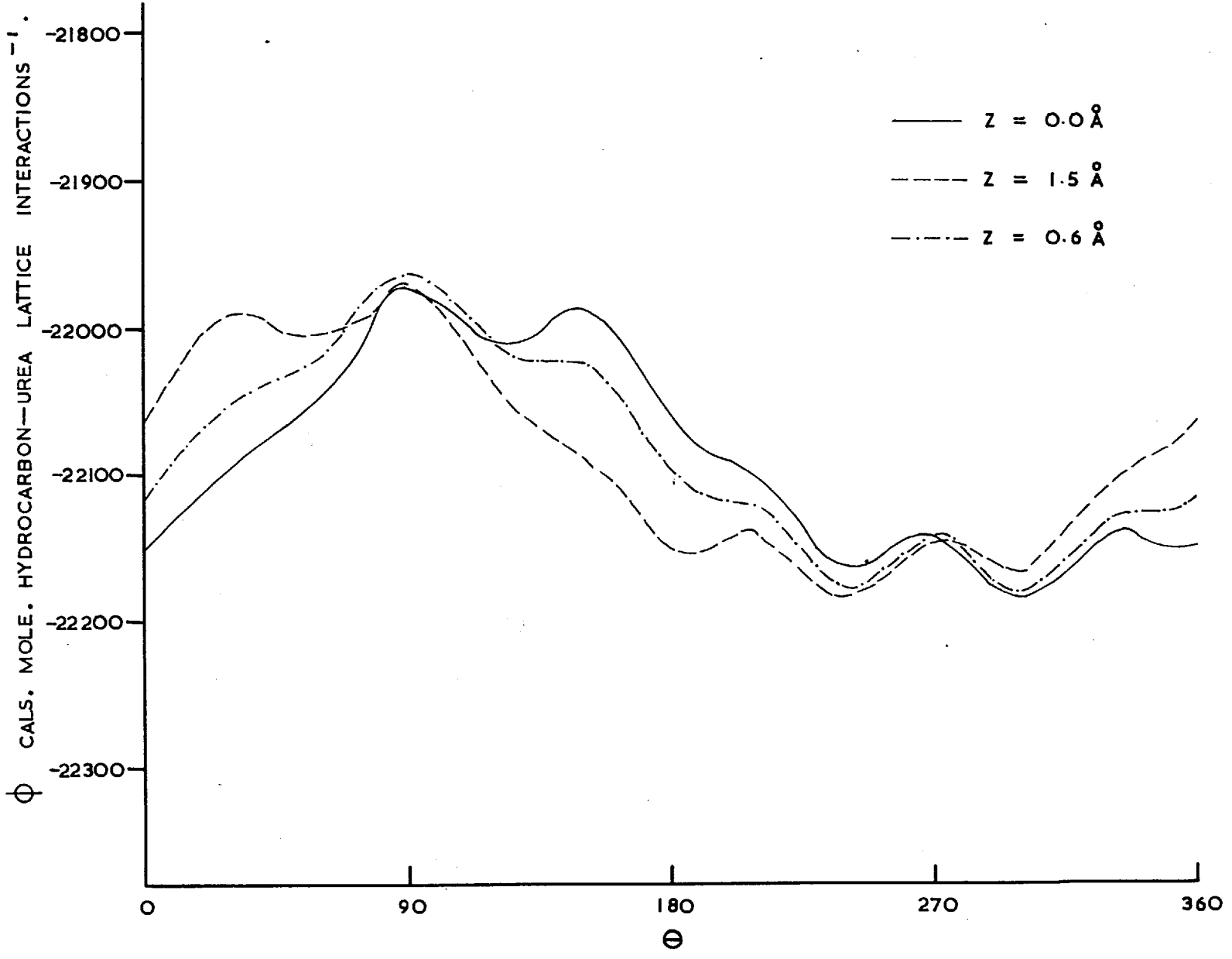


FIG.41. COMPUTED UREA–OCTANE INTERACTION POTENTIAL.

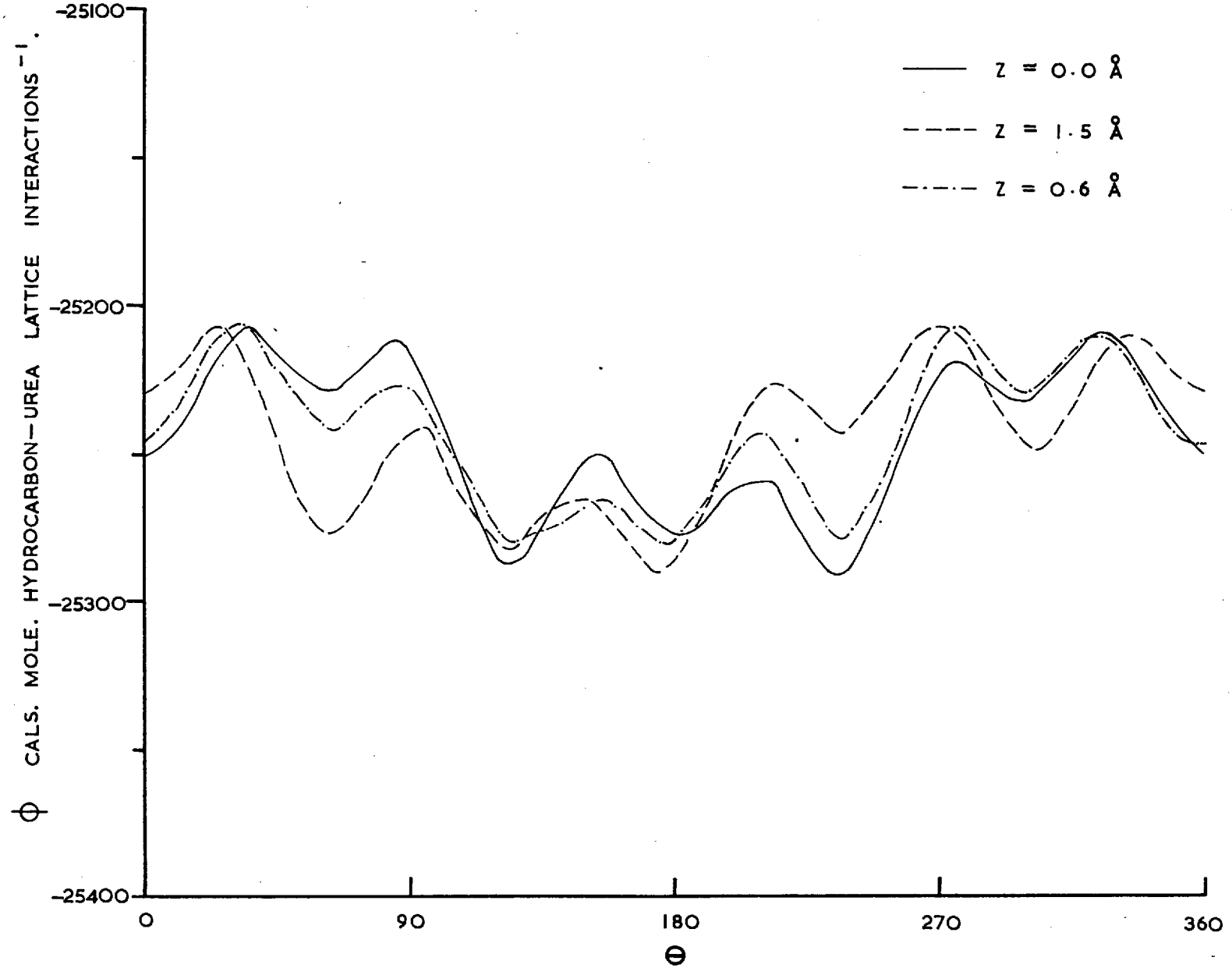


FIG.42. COMPUTED UREA—NONANE INTERACTION POTENTIAL.

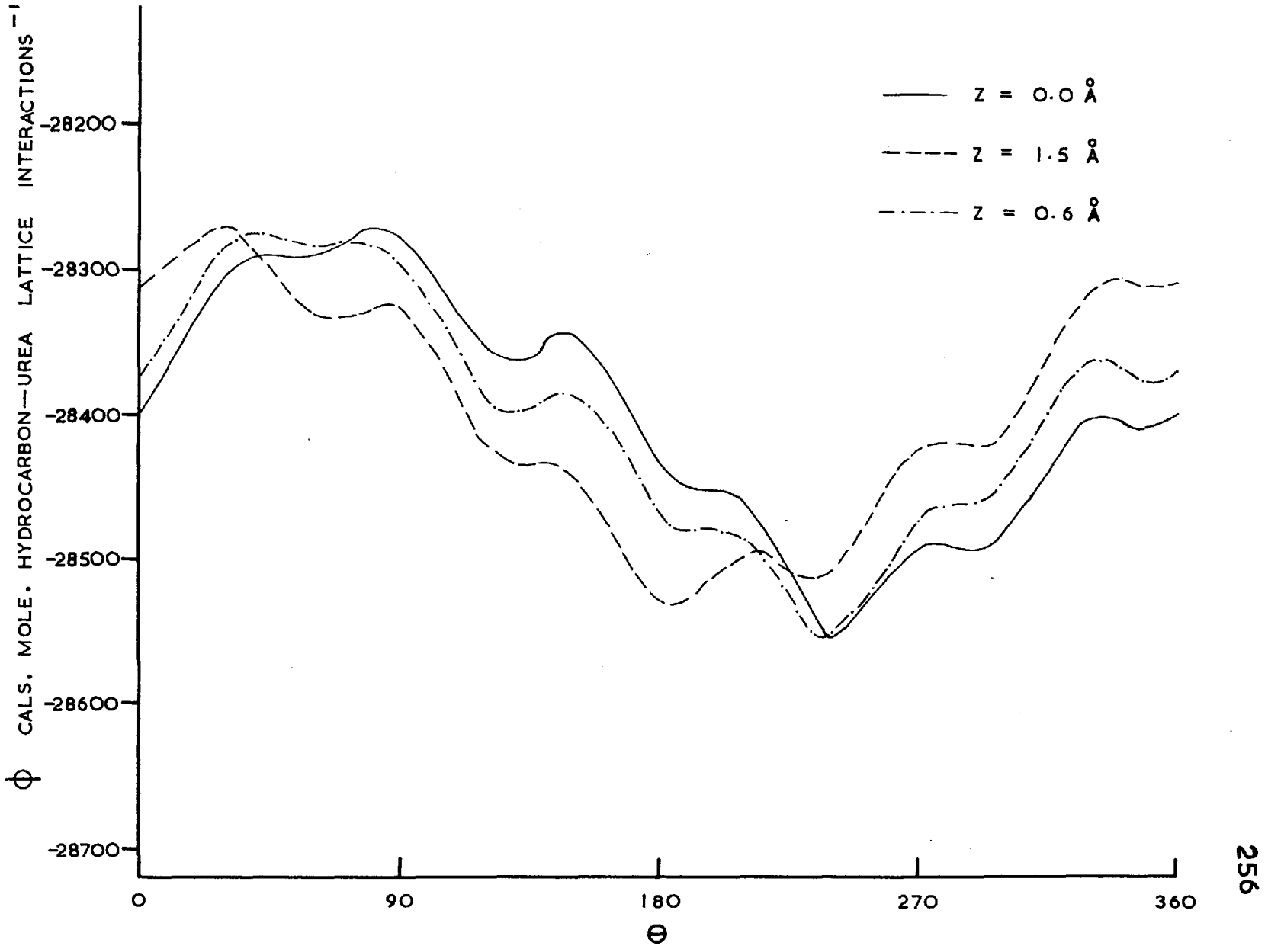


FIG.43. COMPUTED UREA–DECANE INTERACTION POTENTIAL.

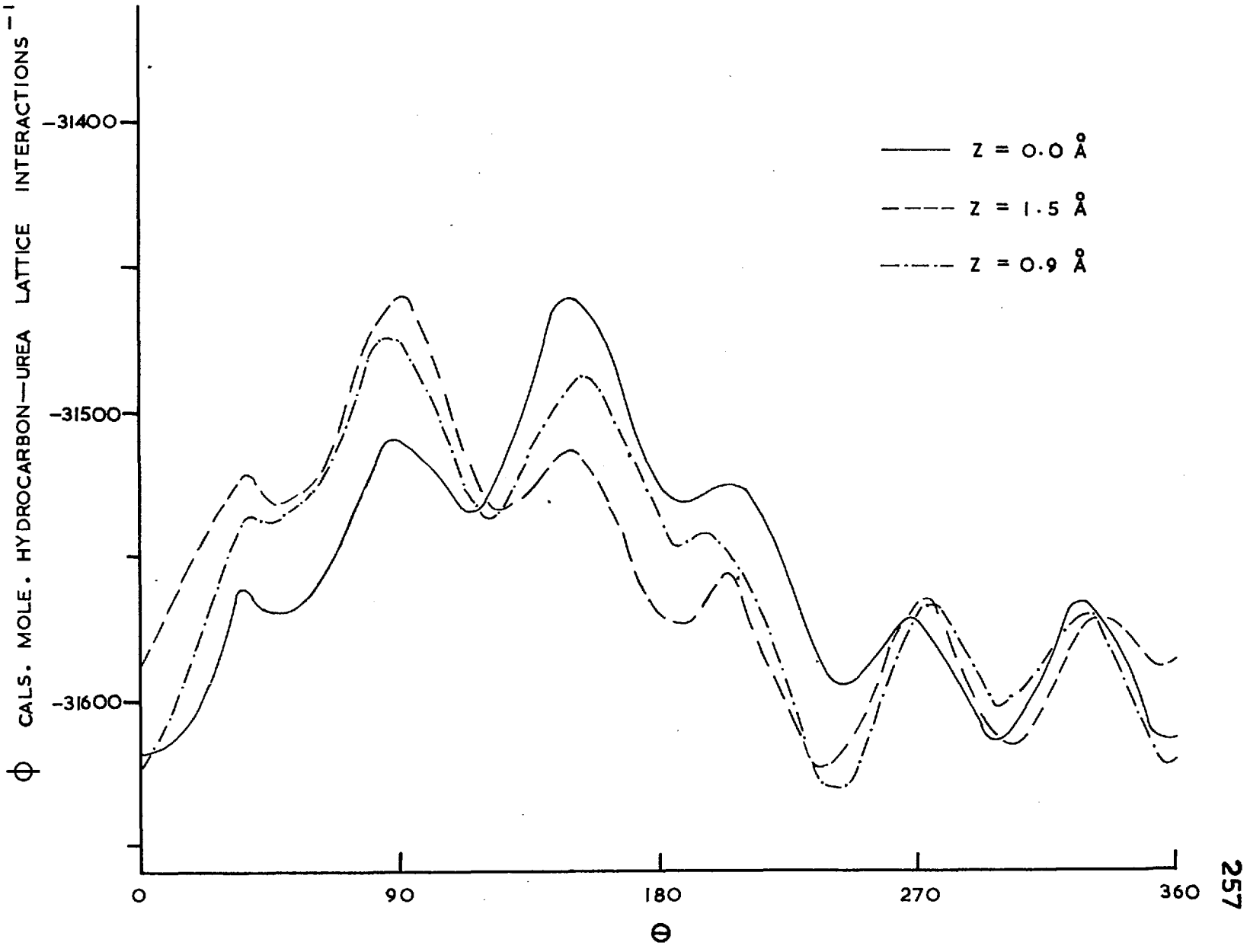


FIG.44. COMPUTED UREA–DODECANE INTERACTION POTENTIAL.

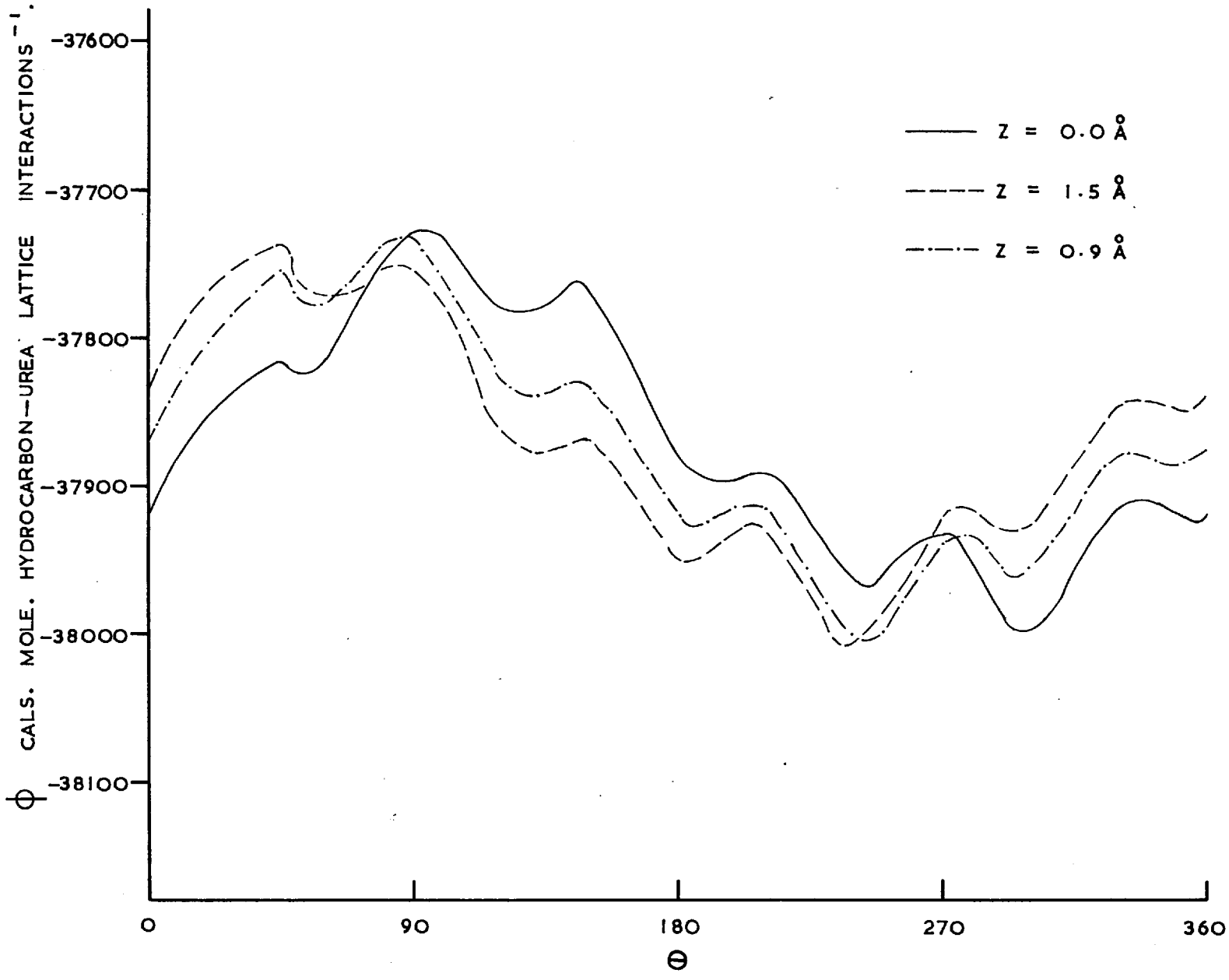


FIG .45. COMPUTED UREA–HEXADECANE INTERACTION POTENTIAL .

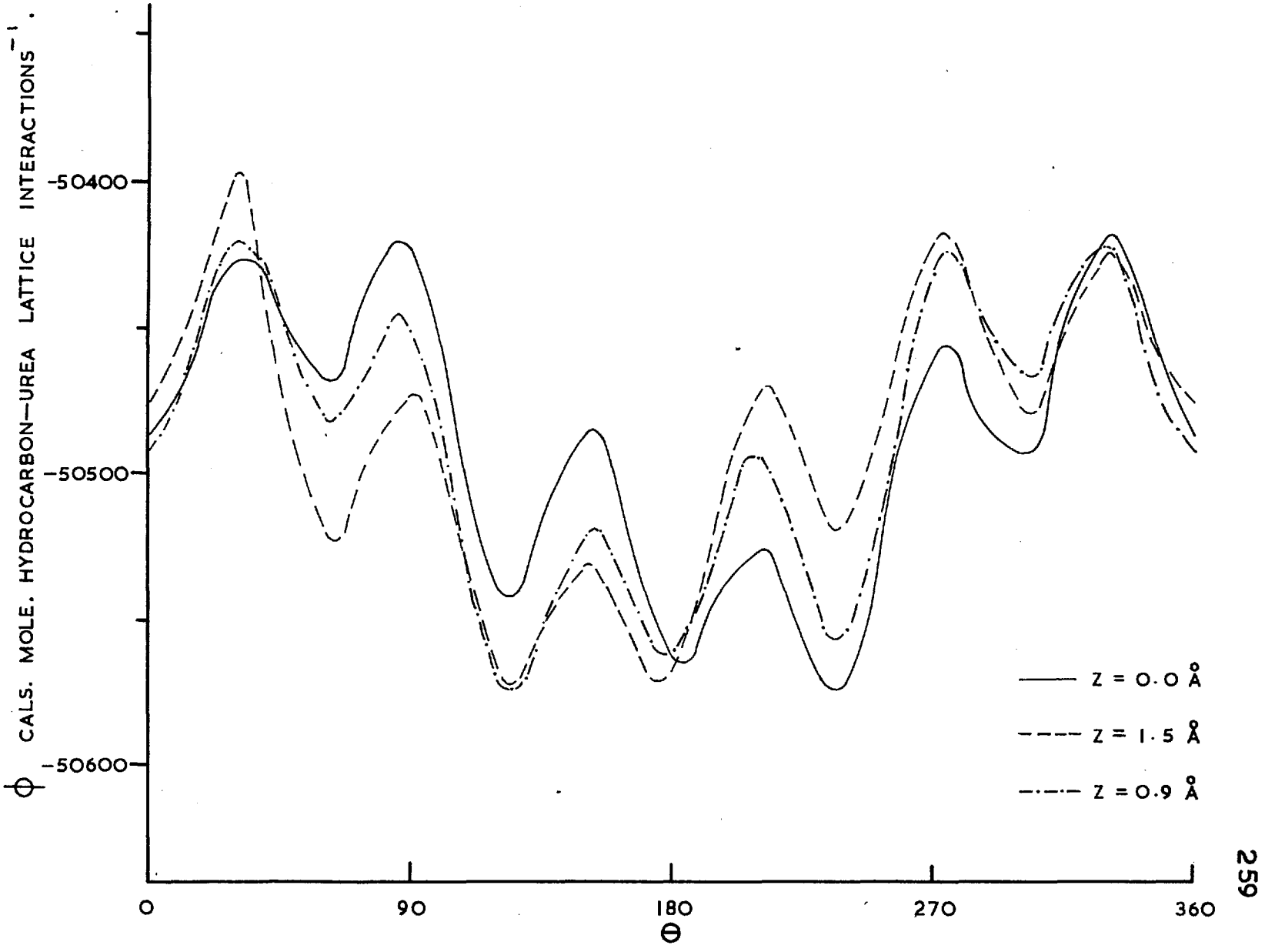


TABLE 37 .- COMPUTED POTENTIAL BARRIERS TO ROTATION FOR VARIOUS N-PARAFFINS, IN THE PLANAR ZIG-ZAG CONFIGURATION, WITHIN THE HEXAGONAL CHANNELS OF THE UREA LATTICE.

The interaction energy (at z=0.0 Å, $\theta=0^{\circ}$) and the potential barrier (both maximum and envelope values, the latter formed by the family of curves with different z constants, are shown) in cals. mole hydrocarbon^{-1} for molecules containing "n" carbon atoms.

"n"	Interaction Energy.	Maximum Barrier.	"z" value for max. barrier.	Envelope Barrier.
C_1	-3,113.0	223	0.6	210
C_3	-9,438.4	118	0.3	110
C_4	-12,630.0	272	0.9	235
C_5	-15,819.5	85	0.0	77
C_7	-22,101.9	220	0.6	210
C_8	-25,250.3	76	0.3	72
C_9	-28,398.6	273	0.3	262
C_{10}	-31,612.5	168	0.0	120
C_{12}	-37,900.3	259	0.3	255
C_{16}	-50,486.5	152	0.3	150

SECTION XIII(b) Characteristics of the computed urea-hydrocarbon potential energy.

The interaction potential increases in a linear manner with hydrocarbon chain length as expected. From the thermochemical data of Redlich[61] for heats of formation according to the equation

urea(tetragonal) + hydrocarbon(liquid) $\rightleftharpoons$ complex(solid)

and heat of vaporisation of the hydrocarbon, values of $-\Delta H$(gas) for adduct formation from gaseous hydrocarbons have been calculated and are shown below.

TABLE 38

N(no. of carbon atoms)	$-\Delta H$(liq) Kcals mole hydrocarbon^{-1}	$-\Delta H$(vap)	$-\Delta H$(gas)	δ/CH_2
7	7.3	8.7	16.0	
8	9.7	9.9	19.6	3.6
9	11.8	11.1	22.9	3.3
10	13.1	12.3	25.4	2.5
12	16.1	14.6	30.7	2.65
16	21.0	19.4	40.4	2.43

Determination of the increments in $-\Delta H$(gas) for the addition of an extra CH_2 unit to the adducted hydrocarbon produces the values shown in the last column. Taking an average value for δ/CH_2 and multiplying by the

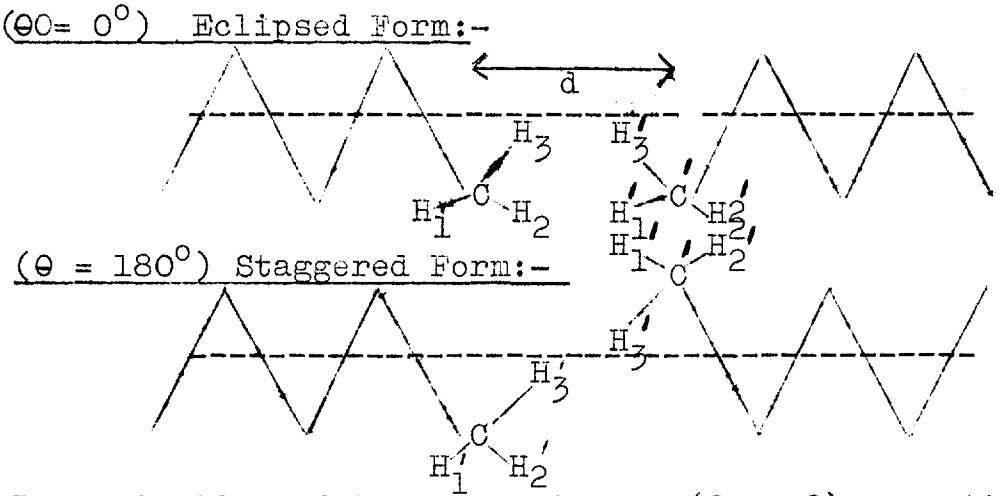
number of CH_2 units in the hydrocarbon chain gives a rough value for the urea-hydrocarbon interaction energy. For C_{12} the expected interaction potential of 32 K cals. per mole compares favourably with our calculated value of 38 K cals. assuming only Van der Waals interactions. Since the value of the heats of solution for tetragonal and hexagonal urea, of which the latter cannot be directly measured, are not expected to differ greatly (e.g. the difference in the molar heat function H for ß- and α- quinol is only 0.16 K cal per mole[153]) the agreement of the theoretical and "experimental" values for Ø indicates that the consideration of Van der Waals forces alone is a good approximation to the physical system in this case.

The form of the urea-hydrocarbon interactions may be approximated to a complex sine wave which is symmetrical in general, only about $\theta = 0^{\circ}$. The potential barriers to rotation also have the surprising property of being independent of the length of the included hydrocarbon chain. This arises from the helical urea crystaline field tending to make contributions from the various atom pairs cancel out for any given orientation θ. The effect of this form of field is also seen in the change of the plane of the maximum interaction potential with the z co-ordinate.

The nature of these results is somewhat surprising in view of the approximately linear increase of the transition temperature (Tc) with chain length but, as is shown later(section XIV(c)), the magnitude of the urea-hydrocarbon potential barrier is of little importance in determining Tc.

SECTION XIII(c). The interaction between neighbouring hydrocarbon molecules in the same channel of the urea lattice.

The dispersion energy between two hydrocarbon molecules set end to end may, as a result of the high inverse powers of r the distance separating the constituent atomic centres, be represented to a good approximation by the Van der Waals interaction of their terminal methyl groups. Further, to establish the magnitude of the barrier to rotation, it is only necessary to consider two orientations, namely the eclipsed form($\theta = 0^{\circ}$) and the staggered form generated by rotating one hydrocarbon chain about the long axis through 180° from this position. These two cases are illustrated below:



Byapplication of the Lennard-Jones(6 - 12) potential function, using the modified Slater-Kirkwood attractive interaction constants and repulsive terms derived from Van der Waals radii, as in section XIII(b), contributions to Ø from the nine H-H, six C-H and single 6-C interacting atom pairs were calculated as a function of (d), the distance separating the terminal carbon atoms. The hydrocarbon chains were assumed to have a common longitudinal axis (shown dotted above) and to be in the zig-zag planar configuration. Furthermore, the C-H and C-C bond distances were taken as 1.10Å and 1.54Å respectively and the bond angles as 109° 28′. On this basis the carbon atoms lie 0.44(4)Å from the line of molecular centres.

From his X-ray investigations Smith[49] suggested a value of 4.1Å for (d). At a separation

of 4.0 Å there is an overall attractive interaction of 610 calories per mole of interacting CH_3 groups (see the table below) with a barrier to rotation of only 12 calories.

TABLE (39).

(d) Å	θ^o	Interaction Pot. (cals.mole CH_3^{-1})	Barrier (cals)
3.70	0	+ 347.09	297.69
	180	+ 49.40	
4.00	0	- 606.29	12.08
	180	- 618.37	
5.00	0	- 188.29	6.85
	180	- 181.44	

However, if the hydrocarbon molecules pack more closely the barrier rises rapidly to 298 cals. for d = 3.70 Å but now gives a repulsive interaction of approximately + 350 cals. ($\theta^o = 0^o$). Since the attracive energy between the urea lattice and the guest hydrocarbon increases linearly with the length of hydrocarbon in the urea channel, an additional stabilising energy to offset the repulsions of the terminal methyl groups may be simultaneously generated by closer approach of the hydrocarbon chains. This is shown in the calculation below.

For the C_{16} adduct the Ø LATTICE-HYDROCARBON interaction amounts to -50,500 cals per mole of hydrocarbon. As the hexadecane molecule occupies 22Å of the lattice channel and assuming a contraction of 0.4Å in (d) over Smith's value (i.e. d = 3.70Å) the additional stabilising energy is given by:

$$\frac{-50,500 \times 0.4}{22} = -919 \text{ calories per mole.}$$

This is of the correct order to balance the repulsive interaction increase between the terminal methyl groups (approximately 950 cals/mole) resulting from their smaller separation. On energetic grounds therefore the chain end separation (d) is most probably in the region of 3.7 ±0.1Å with a rotational barrier of 300 cals.per Avogadro number of interactions. A contraction of 0.4Å in (d) for a hydrocarbon of 22Å chain length represents an increase of 1.52% of the total hydrocarbon present. This corresponds to only 0.38% of the total adduct weight and is therefore on the limit of analytical methods so far devised for accurate adduct composition determination.

SECTION XIII(d). The interaction between hydrocarbon molecules in neighbouring channels of the hexagonal urea lattice.

Calculation of the dispersion forces between saturated paraffin chains in the crystalline form have

been made by Müller[148][154] and Brandt[155][156] to obtain the theoretical value of the sublimation energy at $0^{o}K$.

The method used by Müller was to divide each molecule into sub-units, each of size small compared with the interaction distance. The separate attractive dispersion energy interactions (N^2 in number if each chain contains N sub-units) were calculated from London's inverse sixth power law and the total interaction found by addition. Müller made three estimations using as sub-units atoms, bonds and CH_2 groups, respectively, and for each he employed both the Kirkwood-Müller and London formulae in calculating the dispersion energy constant(A). Calculation of the repulsive energy however was somewhat arbitrary, the C-H bond repulsion being assumed to equal that which would be found if there were helium atoms (0.36 K cals. $mole^{-1}$ CH_2) centred at both the hydrogen and carbon atom sites. This amounted to approximately 0.36 K cals. $mole^{-1}$ per CH_2 interaction in the solid state. The energy required to remove a molecule out of the attractive force field of its neighbours was found to lie between -2.5×10^{-13} and -1.52×10^{-13} ergs per CH_2 group. The sublimation energy ΔH_s from CH_2 group

interactions and the Kirkwood-Müller equation is quoted as:

$$\Delta Hs = 2.19 - 0.36 = 1.83 \text{ K cals. per mole of } CH_2 \text{ groups.}$$

Brandt used the Lennard-Jones (6-12) potential between chain units in a more sophisticated calculation, employing a modified Slater-Kirkwood equation for (A) and obtained a value of ΔHs of 1.25 K cals. per mole of CH_2.

In view of the close correspondance of the calculated values of ΔHs with Billmeyer's (157) value for the experimental heat of sublimation (1.838 K cals. per mole of CH_2 groups) obtained from heats of fusion, vaporisation and heat capacities of hydrocarbons in all three phases, it was felt justified to apply the Lennard-Jones equation to determine the potential barriers to rotation for n-hydrocarbons at the separation 8.23Å characteristic of the urea adducts.

The model proposed was again based on Smith's X-ray studies for the geometry of the system, and involved the following assumptions:

1). The hydrocarbon molecules are assumed to be in the zig-zag planar configuration with their line of centres 8.23Å apart.

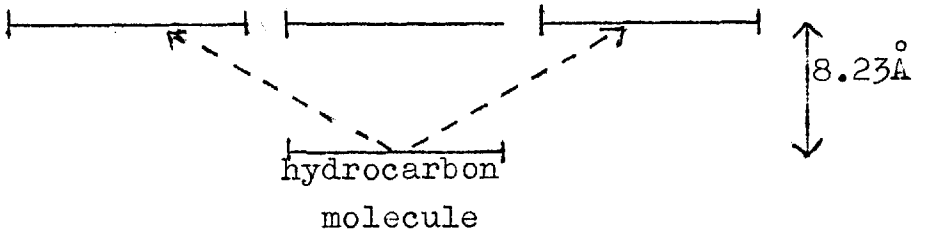
2). The interaction of a single molecule with a single nearest neighbour only was initially considered (i.e. contributions from hydrocarbon molecules at distances greater than 8.23Å in planes perpendicular to the molecular axis were ignored.)

3). Repulsive energy terms in $1/r^{12}$ were ignored due to the large inter-atomic centre separations.

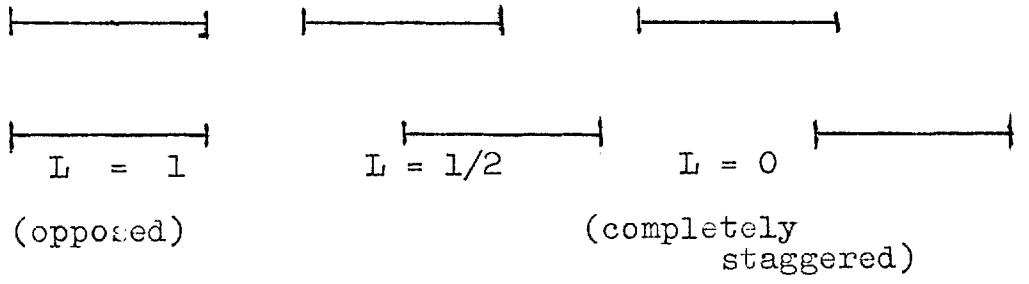
4). The total interaction with all six neighbouring hydrocarbon molecules will be given by approximately six times the interaction with a single neighbour. The associated barrier to rotation will lie between six times the maximum barrier and six times the minimum barrier since the instantaneous orientations of all six neighbours will not necessarily be identical.

5). All possible orientations for the two interacting systems will be generated by considering the variation of two angles θ and ϕ. These represent the angles made by the planes containing the hydrocarbon skeletons with respect to a plane initially containing both (denoted (X,Y) in TABLE 40) with $\theta = 0^{\circ}$, $\phi = 0^{\circ}$. The change in θ and ϕ required demands that ϕ runs from 0° to 180° while θ is constant and θ changes from 0° to 360° with ϕ constant. In the computation, performed on the London Atlas computer, intervals of $\Delta\theta = 60^{\circ}$ and $\Delta\phi = 20^{\circ}$ were used.

6). Interactions with one neighbour only in each adjacent channel were considered (i.e. the interactions shown in dotted lines below were ignored).



7). Since neighbouring molecules may not always lie in the opposed position but be displaced in the channels as shown below, calculations were initially made for the three special cases with a para-meter L = 1,1/2,0.



Further calculations for displacements increasing by 1.27Å (the CH_2 group repeat distance along the chain) were made from the fully opposed (L = 1) to the staggered (L = 0) positions.

TABLE 40 and FIGS. 46 and 47 show the variation of the interaction potential energy for variations of Θ and ϕ for the C_{15} and C_{20} adducts at constant values of $\phi = 120^{\circ}$ and $\Theta = 40^{\circ}$ respectively. The overall attractive interaction is small as is expected from the comparatively large distance of chain separation. From the computed interactions of an Avogadro number of molecules for the C_8, C_{10}, C_{11}, C_{12}, C_{16} hydrocarbons, in addition to the C_{15} and C_{20} cases, the following maximum and minimum potential barriers for L = 1 were obtained.

TABLE 41

No. of Carbon atoms in chain	MAX BARRIER cals.Mole interactions	MIN BARRIER
8	4.97	4.43
10	6.27	5.90
12	7.58	6.99
16	10.19	9.58
20	12.80	12.01
11	16.69	13.85
15	19.01	16.29

The potential barriers shown for the odd n-paraffins for L = 1 are much higher (about twice) than those for the even homologues of similar chain length.

TABLE 40 .- COMPUTED LATERAL HYDROCARBON-HYDROCARBON INTERACTION ENERGY FOR MOLECULES IN ADJACENT CHANNELS OF THE HEXAGONAL UREA LATTICE IN CALS. FOR AN AVOGADRO NUMBER OF INTERACTIONS.

θ and ϕ represent the orientations in the (X,Y) plane and L=1 the "z" co-ordinate of the second molecule with respect to the first.

	C_{15} $\theta=120^\circ$	C_{20} $\theta=120^\circ$
ϕ°	Interaction Potential cal.	Interaction Potential cal.
0	-416.10	-569.98
20	-418.53	-573.56
40	-422.63	-580.06
60	-422.68	-582.13
80	-418.82	-579.97
100	-416.09	-579.75
120	-415.25	-581.63
140	-412.23	-579.54
160	-406.69	-573.04
180	-403.74	-569.35

	C_{15} $\phi=40^\circ$	C_{20} $\phi=40^\circ$
θ°	Interaction Potential cal.	Interaction Potential cal.
0	-403.66	-567.27
60	-415.18	-579.54
120	-422.63	-580.06
180	-416.21	-568.13
240	-422.67	-580.07
300	-415.12	-579.41
360	-403.66	-567.27

FIG. 46. VARIATION OF HYDROCARBON-HYDROCARBON LATERAL INTERACTION POTENTIAL WITH ANGLE Θ.

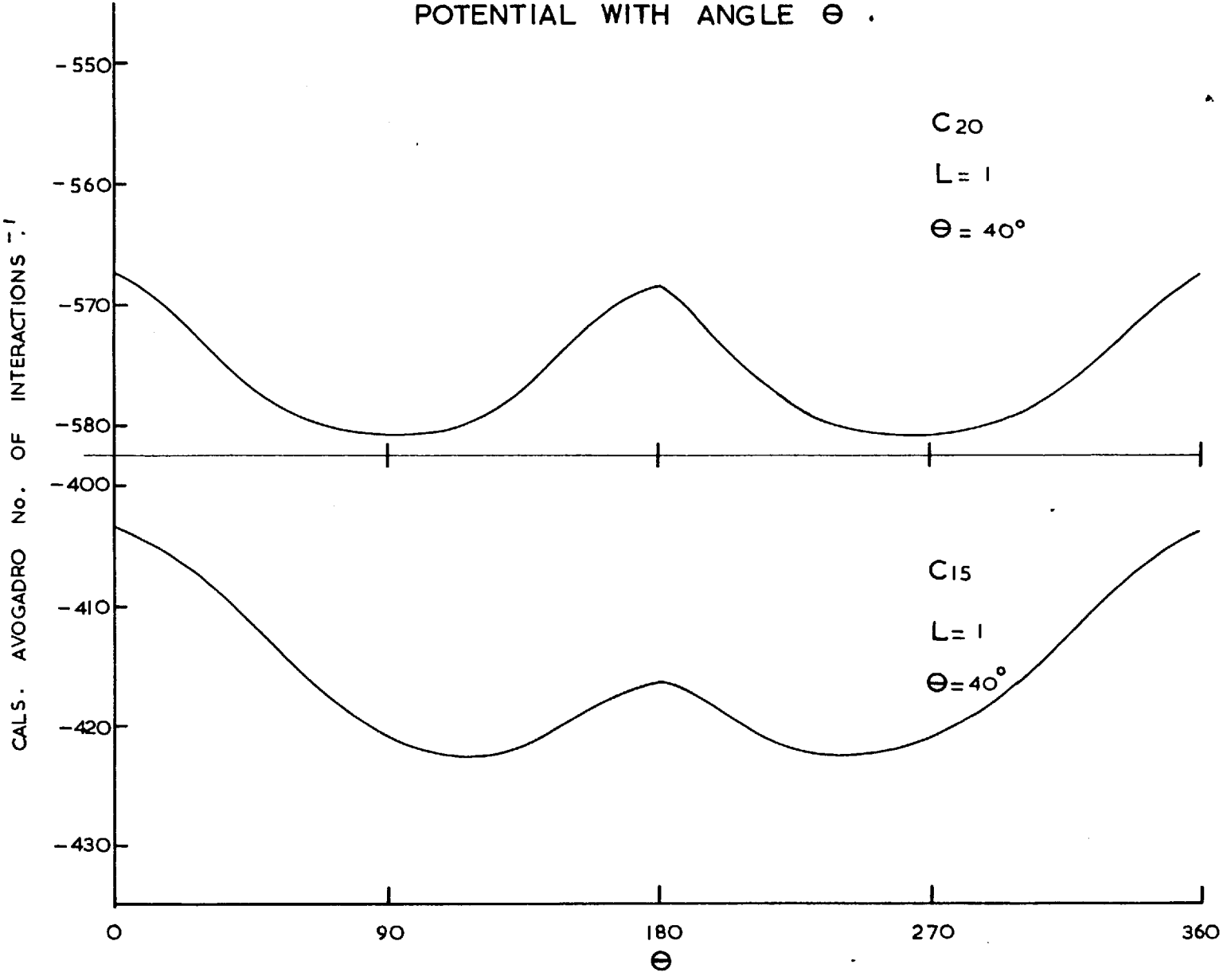
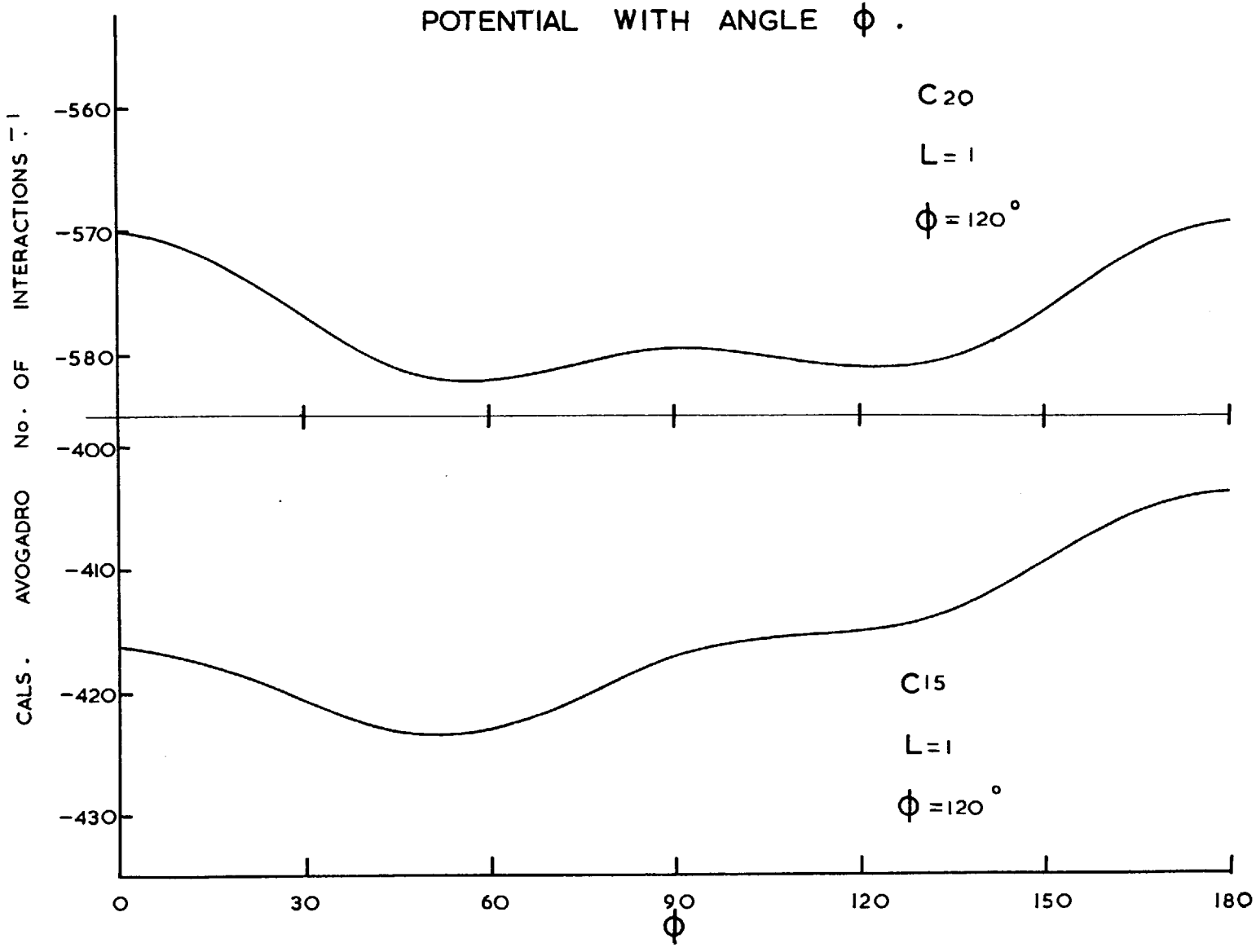
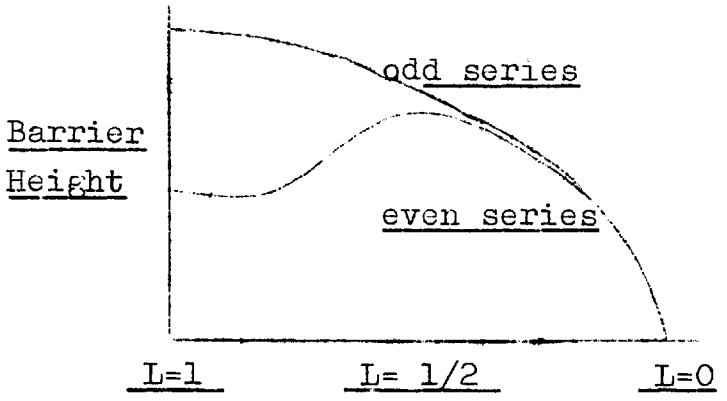


FIG . 47 . VARIATION OF HYDROCARBON–HYDROCARBON LATERAL INTERACTION POTENTIAL WITH ANGLE ϕ .



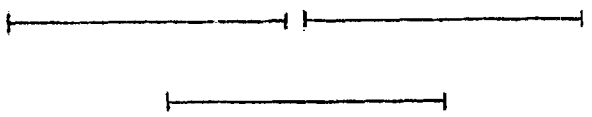
However, this is seen to be partly illusory from the more detailed calculations of barrier height as is shown in the diagram below.



For C_{15} at L = 1/2 the barrier ranges from 13.70 to 15.27 cals which is always smaller than that found at L = 1. The barrier for L = 0, 7.18 to 8.30 cals. is approximately half that for L = 1/2. On the other hand for C_{20} the barrier at L = 1/2, 14.94 to 16.35 cals. is always larger than for L = 1; for L= 0 barriers are approximately half that for L = 1/2 (7.18 to 8.70 cals.). When n, the number of carbon atoms in the hydrocarbon, is even then the barrier for L = 0 is about 7 cals. in all the cases considered, since the end group interactions is now of paramount importance.

In practice the hydrocarbon molecules pack closely together (approximately 4Å) in the channels as

shown by the studies on their composition and, although the pure opposed form of interaction with L = 1 may not be the most common case due to lattice defects, impurity molecules or other effects, the interaction of one molecule with sections of two others as shown below is expected to give a barrier to rotation similar to that for L = 1.



Consequently the rotational barriers for L = 1 were used in the theoretical treatment.

CHAPTER XIV. THE THEORETICAL TREATMENT OF THE CO-OPERATIVE TRANSITIONS.

SECTION XIV(a). Introduction.

Any realistic theoretical treatment of the co-operative transitions observed in the heat capacities of certain urea-n-hydrocarbon adducts must be based on a model incorporating the three types of interaction listed below and discussed in previous sections of this thesis.

(A) Hydrocarbon - urea crystalline field.

(B) Hydrocarbon - hydrocarbon for adjacent molecules in the same urea lattice channel.

(C) Hydrocarbon - hydrocarbon interchannel interactions.

An analogy will now be drawn between the present system and the situation found in ferro and antiferromagnetic solids, for which some explanation of the co-operative transitions observed have already been reported. A simple model of these transitions in magnetic compounds was suggested by Ising[158] in 1925. He assumed that each molecular magnetic dipole could occupy one of two possible orientations ($\mu = -1$ or $\mu = +1$) and that only nearest neighbour interactions are possible, and further that these interactions are proportional to $\mu_1 . \mu_2$. Corresponding to this situation it is here assumed that each hydrocarbon molecule can take

up only one of two possible orientations and that the interaction energy between nearest neighbours is given by a constant times the product $\mu_1 \cdot \mu_2$. The orientational influence exerted by the urea field corresponds to the presence of a magnetic field attempting to align the magnetic dipoles.

From an initial comparison of the magnitudes of the three potential barriers to rotation listed above it might be thought that (C) (approximately 10 cals. $mole^{-1}$) could be neglected relative to (A) and (B) (approximately 200 and 300 cals. $mole^{-1}$ of interactions) the system thereby becoming one dimensional. The calculated specific heat for such a linear chain of dipoles in zero magnetic field was found to exhibit a maximum value at $kT = 0.833J$, where J is the interaction energy between nearest neighbour spins, k is the Boltzmann constant and T the absolute temperature. However, this maximum in Cp is not associated with any anomalous thermodynamic behaviour characteristic of the magnetic properties of the chain. The gradual rise to a maximum in the heat capacity results from an assembly of non-interacting systems each with two independent energy levels and consequently the long range order parameter is always zero.

This arises as the presence of one incorrectly oriented spin in the chain disorganises the ability of subsequent spins to determine their correct orientation with respect to the remaining lattice array. Imposition of an external field again does not have the effect of producing a rapidly varing configurational specific heat. To obtain a co-operative break-down in long range order as exhibited in a λ shaped heat capacity anomaly it has been found essential to consider a two or three dimensional model.

The weak interactions between nearest neighbour hydrocarbon molecules belonging to different chains or channels are therefore of paramount importance in the development of three dimensional long range order throughout the adduct, since each molecule is connected thereby not only to its immediate neighbours but also with all other hydrocarbon molecules in the urea lattice.

The energy levels of a co-operative assembly are not simply related to those of its constituent microscopic systems and as a result it is not possible to treat them by the elementary methods of statistical mechanics. The problem reduces to the solution of the configurational integral for the system which is of general type:

$$Zn = \int_V e^{-U(x_1,\ldots\ldots,z_n)/kT} \cdot dx_1,\ldots\ldots,dz_n. \quad \ldots.(7)$$

where the potential energy $U(x_1,\ldots\ldots,z_n)$

depends on the location of the molecules in the available volume V. To facilitate calculations simplified models of the molecular or atomic interactions have been proposed for example, the "Weiss-type" model of a ferromagnetic where a generalised internal field produces interactions of extremely long range. Here the interaction of any two atoms in a magnetic material has the same magnitude irrespective of their separation in contrast to the Ising model where only nearest neighbour interactions contribute to the potential energy function U. Although neither model is thought to adequately represent any physical systems showing co-operative characteristics, the formidable mathematical problems associated with the evaluation of the partition function for the two dimentional Ising model have been solved. Newell[159] and more recently Domb[160] have reviewed the theory of co-operative phenomena in crystals.

Onsager[161] has produced an exact treatment of the 2-dimensional case of a ferromagnetic with Ising type interactions in a vanishingly small magnetic field. The calculated specific heat for varying degrees of anisotropy, represented by the two interaction parameters J and J' (for two directions perpendicular to each other), are shown in FIG.48.

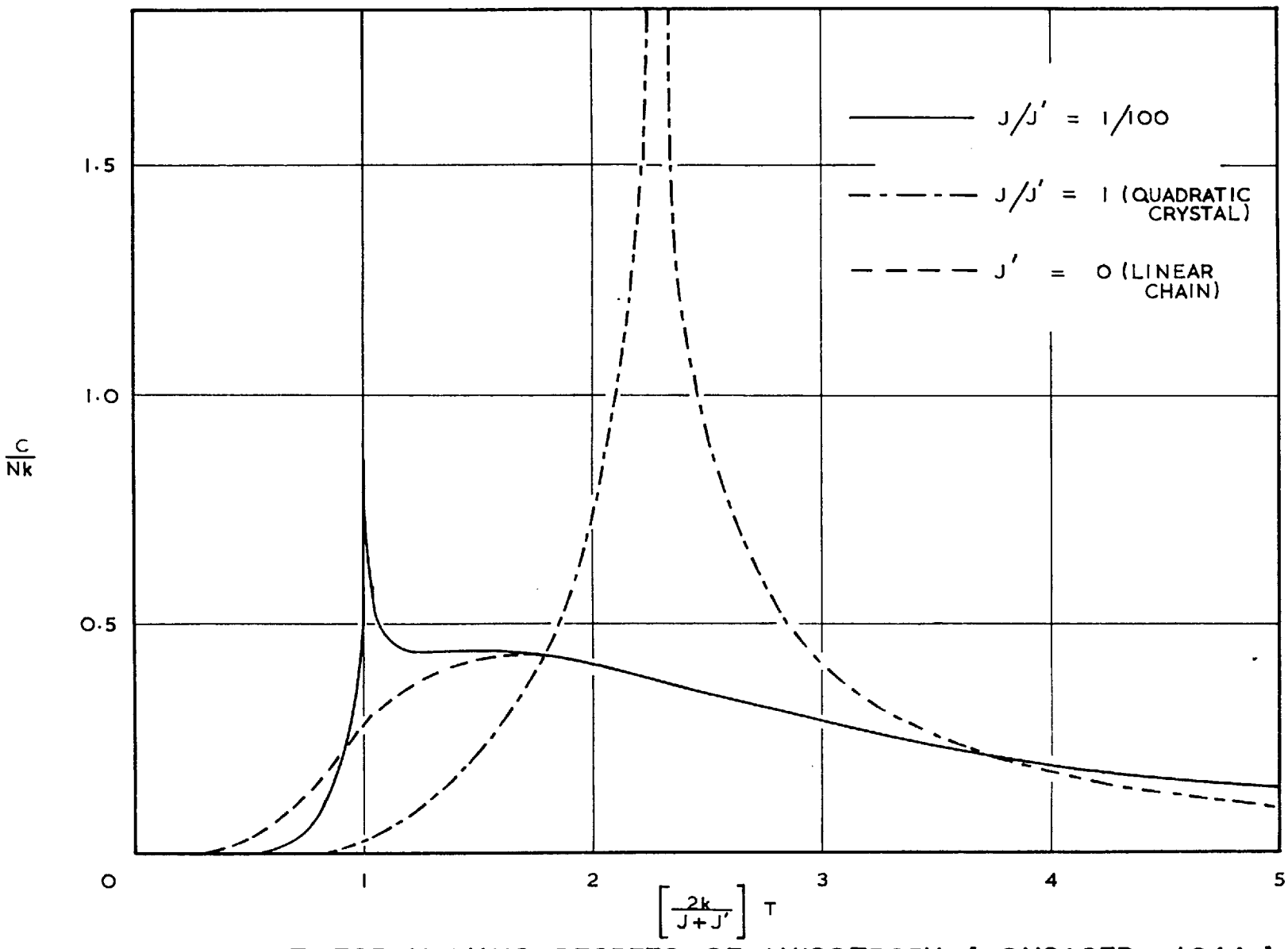


FIG.48. SPECIFIC HEAT FOR VAIRYING DEGREES OF ANISOTROPY [ONSAGER 1944].

With a decreasing value of J the breakdown in long range order occurs less readily and as a result a shift of the co-operative transition to higher temperatures occurs together with a reduction in its sharpness. In the limiting case (the linear chain) with J =0, the one dimensional case of Ising, a λ type anomaly is not found.

To date, little progress has been made in the exact solution for a three dimensional lattice.

SECTION XIV(b). The Ising-Weiss model for the n-paraffin adducts of urea.

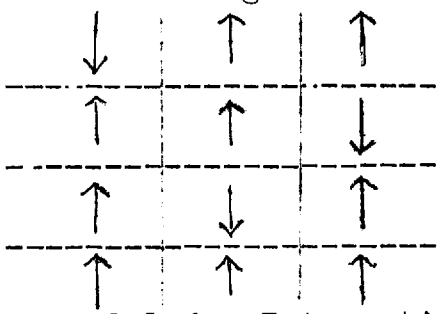
In view of the complexity of the urea-hydrocarbon adduct system a much simplified model had to be proposed. This is based on a two-dimensional combination of the Ising and Weiss models in an applied magnetic field (the urea lattice field in this case). Allowance is also made for the three dimensional nature of the system by the introduction of a numerical factor in the Weiss treatment of interactions perpendicular to the urea lattice channels. The resulting model may therefore be termed pseudo-three dimensional.

The basic assumptions for the model are summarised below:-

(1). Interactions between adjacent hydrocarbon

molecules along the urea lattice channels are treated exactly using an Ising model, the hydrocarbon molecules hereafter being regarded for simplicity as "magnetic dipoles" possesing spins. The spins are assumed capable of orienting in only two directions, corresponding to low energy re-orientational sites for the paraffin in the urea lattice. This is only a rather rough approximation to the actual situation since it will lead to an entropy of transition of $\Delta S = R\ln 2 = 1.38$ cals. $mole^{-1}deg^{-1}$, but is necessary to simplyfy the subsequent mathematics.

(2). Interactions in the plane perpendicular to the channel are treated in terms of the Weiss (Bragg-Williams) model, in which it is assumed that the interaction energy is a function of the long range order in this plane and does not require detailed knowledge of the distribution of spin orientations. These interactions are represented in the diagram below.



Ising Model for Interactions along the urea lattice channel.

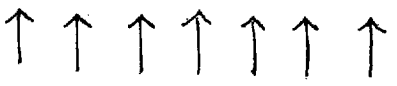
Weiss Model for Interactions perpendicular to channel.

(3). It was further assumed that the ordering effect of the spiral field of the urea lattice can be adequately represented by a term proportional to cos $j\alpha$, where j is the "index number" of the molecule and α is a constant for the lattice. For consecutive molecules along the channel j increases by unity within the range 0 to (N-1) and then returns to zero. The integer N may be explained as follows. The filling of the lattice channels in terms of the arrangement of the hydrocarbon molecules within the repeat distance of the unit cell depends on the length of the adducted hydrocarbon. Thus a cetane molecule will fill two unit cells and each molecule will therefore be in the same orienting field as its neighbours in the same channel. In the case of paraffins of lengths which are not close to simple multiples of the urea lattice "c" repeat distance (11.0 Å) several molecules along the channel may be encountered before a molecule in the same crystaline field is observed. The value N therefore defines in terms of the length of the included species the interval of occurance of molecules in an identical urea field and is given by the smallest non zero integer for which α is a multiple of 2π in the equation:

$$\cos N\alpha = 1 \qquad \ldots\ldots\ldots\ldots\ldots (7).$$

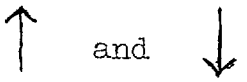
In the case of N = 1 (i.e hexadecane adduct

where each molecule is in the same urea field) the alignment of spins due to the field alone will be in a characteristic direction as is shown below:

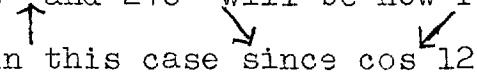


Direction of the resultant spiral urea field.

For N = 2 the repeat angle α will be 180° and two alternate directions of spin orientation will be favoured:



N = 3 corresponds to $\alpha = 120^{\circ}$ and three orientations at 0°, 120° and 240° will be now favoured :



However, in this case since cos 120° and cos 240° are numerically equal the associated long range order parameters will be equal and the case of N = 3 reduces to a form similar to N = 2.

The model discussed above was then treated by the variational method suggested independantly by Kramers and Wannier (1941)[162], Lussettre and Howe (1941)[163] and Montroll (1941)[164].

Consider the lattice model proposed above, each lattice site being occupied by a spin unit capable of two orientations A spin parameter μ, which therefore

has two permitted values +1 or -1, is assigned to these orientations.

If $P(\mu_1, \mu_2, \ldots\ldots, \mu_{n-1})$ is the probability of an arrangement of a chain containing (n-1) spins in the channel with specified values of $\mu_1, \mu_2, \ldots, \mu_{n-1}$

e.g $\mu_1 = -1, \mu_2 = +1, \mu_3 = +1, \mu_4 = -1, \ldots\ldots, \mu_{n-1} = +1$

then $P(\mu_{n-N}, \ldots\ldots, \mu_{n-1})$

the probability of spins (n-N) to (n-1) having given values will berepresented by:

$$P(\mu_{n-N}, \ldots\ldots, \mu_{n-1}) = \sum_{\mu_1=\pm1} \ldots\ldots \sum_{\mu_{n-N-1}=\pm1} P(\mu_1, \ldots\ldots, \mu_{n-1}) \ldots\ldots (8).$$

Adding a further N more spins to the system the probability that these will have specified values $P(\mu_n, \ldots\ldots, \mu_{n+N-1})$ can be written as:

$$\lambda' P(\mu_n, \ldots\ldots, \mu_{n+N-1}) = \sum_{\mu_1} \ldots\ldots \sum_{\mu_{n-1}} P(\mu_1, \ldots\ldots, \mu_{n+N-1}) \ldots (9).$$

where λ' is a normalising constant.

Since the a priori probability for any arrangement of these added N spins is the same, equation (9) may be rewritten by introducing a Boltzmann factor $e^{-E^\circ/kT}$, where E° is the potential energy of interaction

comprising three terms , each being the sum of (N-1) components:

$$P(\mu_n, \ldots\ldots, \mu_{n+N-1}) = \sum_{\mu_{n-N}} \ldots\ldots \sum_{\mu_{n-1}} P(\mu_{n-N}, \ldots\ldots, \mu_{n-1}).a.b.c. \qquad \ldots\ldots\ldots (10.$$

where:

$$a = e^{K(\mu_{n-1}\mu_n + \ldots\ldots + \mu_{n+N-2}\mu_{n+N-1})}$$

$$b = e^{C(\cos n\alpha\mu_n + \ldots\ldots + \cos(n+N-1)\alpha\mu_{n+N-1})}$$

$$c = e^{D(\langle\mu_n\rangle\mu_n + \ldots\ldots + \langle\mu_{n+N-1}\rangle\mu_{n+N-1})}$$

Here,

$$K = -E/kT$$

$$C = -H/kT$$

$$D = -L/kT$$

where T is the absolute temperature k the Boltzmann constant, E the end-end hydrocarbon interaction energy, H the field strength of the urea lattice and L the lateral hydrocarbon interaction energy.

Terms in (a) arise from the Ising type interactions between molecules in the same channel while the contributions to (b) and (c) are due to the spin interactions with the helical field H and the Weiss type spin - average spin $\langle\mu_n\rangle$ coupling between spins in

different chains respectively. The simplifying assumption has been made here that , for the ith. molecule in a channel the relatively weak lateral hydrocarbon-hydrocarbon interactions can be approximated by $D\langle\mu_i\rangle\,\mu_i$ where $\langle u_i \rangle$ is an average value of u taken over all the occupants in the urea lattice channel having the samr z-value. This is therefore equivalent to reducing the model for lateral interactions to the Weiss type system. The average spin $\langle\mu_n\rangle$ will reflect the long range order throughout the assembly of spins or molecules and in this treatment may have values from +1 to -1.

If the chain is sufficiently long (i.e if the number of spins n is large) then the same function P for the (n-N)th. to the (n-1)th. spins as for the nth. to the (n+N-1)th. may be used since the addition of a few extra spins does not alter the physical situation to any marked extent. Equation (10) may now be written in matrix form as:

$$\lambda' P(\mu_n, \ldots\ldots, \mu_{n+N-1}) = \mathbb{H} \cdot (\mu_n, \ldots\ldots, \mu_{n+N-1}, \mu_{n-N}, \ldots\ldots, \mu_{n-1}) \times P(\mu_{n-N}, \ldots\ldots, \mu_{n-1}) \quad \ldots\ldots\ldots\ldots\ldots (11).$$

where P and $\mathbb{H}$ are matrices of order 2^N x 1 and 2^N x 2^N respectively.

It has been shown by several authors[162][163][164] that in this case the partition function may be obtained by determining the largest eigenvalue of the matrix.

Reduction of the matrix leads to a quadratic equation for λ the partition function in terms of the long range order parameters $\langle \mu_o \rangle$ and $\langle \mu_1 \rangle$ in the case of N equal to 2 or 3. Here $\langle \mu_o \rangle$ and $\langle \mu_1 \rangle$ have been written for $\langle \mu_n \rangle$ and $\langle \mu_{n+1} \rangle$. Solution of this equation gives:

$$= 1/2 \left[e^{3K}(e^{2x}+e^{-2x}) + 2e^{-K}(e^{x+y}+e^{-x-y}) + e^{-K}(e^{2y}+e^{-2y}) + X^{1/2} \right] \quad \ldots\ldots\ldots\ldots (12).$$

where

$$X = e^{6k}(e^{2x}+e^{-2x})^2 + 4e^{-2K}(e^{x+y}+e^{-x-y})^2 + e^{-2K}(e^{2y}+e^{-2y})^2$$
$$+ 4e^{2K}(e^{2x}+e^{-2x})(e^{x+y}+e^{-x-y}) + 4e^{-2K}(e^{x+y}+e^{-x-y})(e^{2y}+e^{-2y})$$
$$+ 2e^{2K}(e^{2x}+e^{-2x})(e^{2y}+e^{-2y}) + 4e^{-6K}(1-e^{4K})^3$$

and

$$x = 1/2 \left(D \langle \mu_o \rangle + 2D \langle \mu_1 \rangle \right)$$

$$y = 1/2 \left(2C + D \langle \mu_o \rangle - 2D \langle \mu_1 \rangle \right)$$

Values of the order parameters may also be determined since:

$$\langle \mu_o \rangle = \frac{1}{\lambda_{MAX}} \cdot \frac{\partial \lambda_{MAX}}{\partial (D \langle \mu_o \rangle)} \quad \ldots\ldots\ldots\ldots\ldots (13).$$

and similarly:

$$\langle u_1 \rangle = \frac{1}{2\lambda_{MAX}} \cdot \frac{\partial \lambda_{MAX}}{\partial (D \langle \mu_1 \rangle)} \quad \ldots\ldots\ldots\ldots\ldots (14).$$

Writting

$$\lambda^2 - b\lambda - c = 0 \qquad \ldots\ldots\ldots\ldots\ldots\ldots\ldots\ldots \quad (15).$$

for the quadratic in λ where:

$$b = e^{3K}(e^{2x}+e^{-2x}) + 2e^{-K}(e^{x+y}+e^{-x-y}) + e^{-K}(e^{2y}+e^{-2y})$$

$$c = e^{-6K}(1-e^{4K})^3$$

Differentiating equation (15) gives:

$$\frac{2\lambda\partial\lambda}{\partial(D\langle\mu_o\rangle)} - \frac{\partial b\,\lambda}{\partial(D\langle\mu_o\rangle)} - \frac{\lambda\partial b}{\partial(D\langle\mu_o\rangle)} - \frac{\partial c}{\partial(D\langle\mu_o\rangle)} = 0 \qquad \ldots\ldots\ldots\ldots\ldots\ldots\ldots\ldots \quad (16).$$

Hence,

$$-\lambda\left[e^{3K}(e^{2x}-e^{-2x}) + 2e^{-K}(e^{x+y}-e^{-x-y}) + e^{-K}(e^{2y}-e^{-2y})\right] + 2\langle\mu_o\rangle\lambda^2 - b\langle\mu_o\rangle\lambda = 0 \qquad \ldots\ldots\ldots\ldots\ldots \quad (17).$$

Dividing by λ and simplifying gives,

$$\langle\mu_o\rangle = \frac{e^{3K}(e^{2x}-e^{-2x}) + 2e^{-K}(e^{x+y}-e^{-x-y}) + e^{-K}(e^{2y}-e^{-2y})}{(2\lambda - b)} \qquad \ldots\ldots\ldots\ldots\ldots \quad (18).$$

Similarly:

$$\langle\mu_1\rangle = \frac{e^{3K}(e^{2x}-e^{-2x}) - e^{-K}(e^{2y}-e^{-2y})}{(2\lambda - b)} \qquad \ldots\ldots\ldots\ldots\ldots \quad (19).$$

In order to evaluate the partition function and the long range order parameters $\langle\mu_o\rangle$ and $\langle\mu_1\rangle$ a computer program was written to give λ from chosen values of $\langle\mu_o\rangle$ and $\langle\mu_1\rangle$. Initially a value of +1 was

assigned to the latter two parameters and from the computed value of λ the average long range order parameters were then recalculated. A subsequent recalculation of λ then enabled the cycle to be repeated until close agreement for for succesive values of λ were obtained, By this process values of λ and $\langle \mu_o \rangle$ and $\langle \mu_1 \rangle$ were derived as a function of the absolute temperature T for values of the interaction barriers previously calculated.

From the partition function the configurational Helmholtz free energy F' of the assembly was calculated using the equation:

$$F' = -kT \ln \lambda \quad \ldots\ldots\ldots\ldots\ldots\ldots (20).$$

By graphically determining the second derivative of the free energy with respect to the absolute temperature, values of the configurational molar heat capacity at constant volume (Cv) for the adducted hydrocarbon were found.

In order to ascertain the dependance of the long range order parameters on N, the urea field strength H and both the end-end and lateral interactions between hydrocarbon molecules , a series of computations assigning a wide range of the various interaction constants was undertaken.

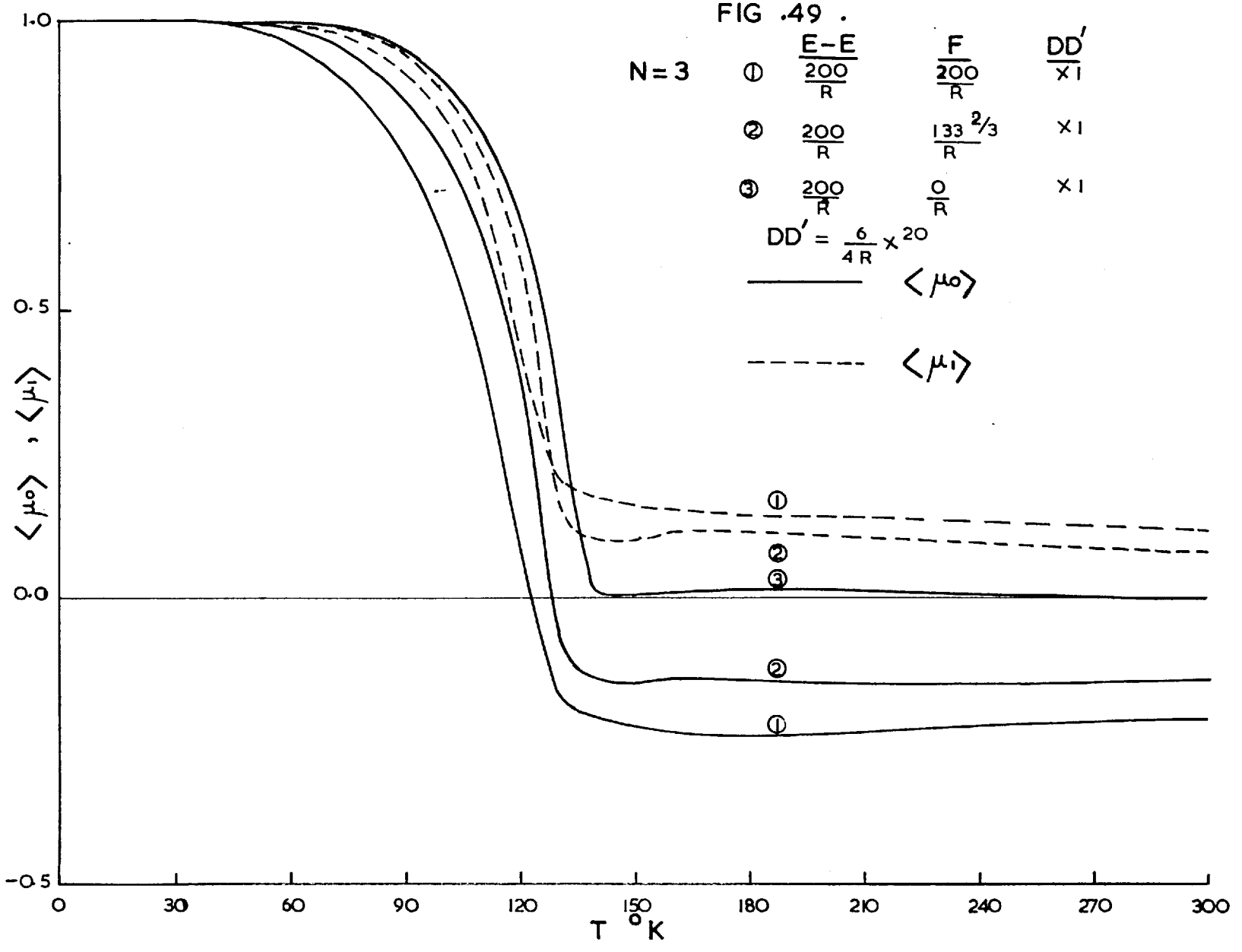
The results for a comprehensive range of these parameters are shown graphically in FIGS.49 to 68. On

these graphs the values of the parameters used in the calculations are shown numerically. The end-end hydrocarbon interactions represented by (E-E) are equal to one half the corresponding computed potential barrier. Similarly DD the lateral interaction parameter is shown as 6/2x2R times the calculated potential barrier. The factor of six is introduced as this represents the number of nearest neighbour hydrocarbon molecules, while the interaction is halved to avoid counting lateral interactions twice (i.e. A with B and B with A). R is the gas constant per mole. The important features of these plots are discussed in the following section XIV (c).

SECTION XIV(c). Computed results of the Ising-Weiss Model and Conclusions.

(1). Variation of the barrier to rotation arising from the urea field (F) (see FIG.49) shows the relatively small displacement in the order parameter curves for a range of potential barriers varying from 400 to 0 cals. per mole of interacting hydrocarbon molecules. This insensitivity to the urea barrier is in agreement with the absence of a simple relationship between the adducted paraffin chain length and the computed urea-hydrocarbon barrier. Since the values of Tc, the adduct transition temperature, increase in

FIG .49 .


N=3
E-E / 200/R
F / 200/R
DD' / ×1
① 200/R 200/R ×1
② 200/R 133 2/3 /R ×1
③ 200/R 0/R ×1
DD' = 6/4R × 20
⟨μ0⟩
⟨μ1⟩
1.0
0.5
0.0
-0.5
⟨μ0⟩ , ⟨μ1⟩
0
30
60
90
120
150
180
210
240
270
300
T °K

a regular manner (at least for the even membered paraffins)with chain length, the urea field for the model proposed is of minor consequence in determining the degree of long range order existing in this system. This independance of Tc on (F) is thought to be due to its periodic nature, the aligning effect of one section of the urea field cancelling out that of another. However, an increase in (F) does extend the temperature range - the spread of the transition - over which $\langle \mu_o \rangle$ and $\langle \mu_1 \rangle$ change most rapidly. The short range order, which still exists at temperatures above the main transition (perhaps through meshing of the ends of the hydrocarbon chains along the urea channels), will be affected by the urea field on this model. Values of $\langle \mu_o \rangle$ and $\langle \mu_1 \rangle$ are not equal to zero as is expected for a perfectly disordered system except in the case of a vanishing urea field interaction (F)=0. The residual short range order continues to decrease with increasing temperature as is shown in the graphs of $\langle \mu_o \rangle$ and $\langle \mu_1 \rangle$ against temperature at least up to T=500°K (by which temperature the adducts would infact already have decomposed).

The difference in sign of the order existing after the transition for $\langle \mu_o \rangle$ and $\langle \mu_1 \rangle$ results from the

average orienting effect of the lattice acting in the opposite direction in the two cases.

(2). The variation in the long range order with DD′ the lateral hydrocarbon-hydrocarbon interaction parameter is shown in FIG.50. Here the effect of systematically reducing the associated rotational potential barrier is significant. Large shifts in the temperature range of transition , depending almost linearly on the value of DD′ are found. Since an approximately linear relationship between the hydrocarbon chain length and the computed lateral interaction energy exists for the adducts the transition temperature appears to be directly related to DD′.

In the case where DD′ = 0 the model reduces to the one dimensional case and as expected a co-operative transition is not found (see FIG.50.). The lateral hydrocarbon-hydrocarbon interactions are also thought to be responsible for the significantly higher value of the transition temperature of the odd hydrocarbon adduct studied (see TABLE. 31) over the even series.

(3). The long range order parameters show a fairly sensitive dependence on the magnitude of E-E the end-end potential energy for hydrocarbon rotation as is shown in FIG.51. Doubling E-E while maintaining

the parameters F and DD′ constant , was found to increase the temperature at which a rapid change in $\langle \mu_o \rangle$ and $\langle \mu_1 \rangle$ occurs. (seeFIG.51). For the parameters chosen and shown on the figure a change in Tc from about 110° to 200°K was found.

The values of the transition temperatures for the various adducts, obtained from the graphs of the long range order parameters against temperature,using the computed values of DD′ and F (see sections XIII (b) and XIII (d)) with R(E-E) equal to 148and 425 cals. per Avogadro number of interactions are shown in TABLE 42 below. Here R is the gas constant per mole.

TABLE 42.

Adduct	Experimental Trans temp°K.	R(E-E)=148cals. mole int^{-1} Trans temp°K.	R(E-E)=425cals. mole int^{-1} Trans temp°K.
C_{10}	110.85	55	130
C_{12}	123.19	56	134
C_{16}	151.77	66	145
C_{20}	189.27	65	153

(4). The variation of N from 2 to 3 while maintaining (E-E), F and DD′ constant is shown in FIG. 52. This change is found to be of minor importance in determining Tc although the approximation of having

FIG . 50.

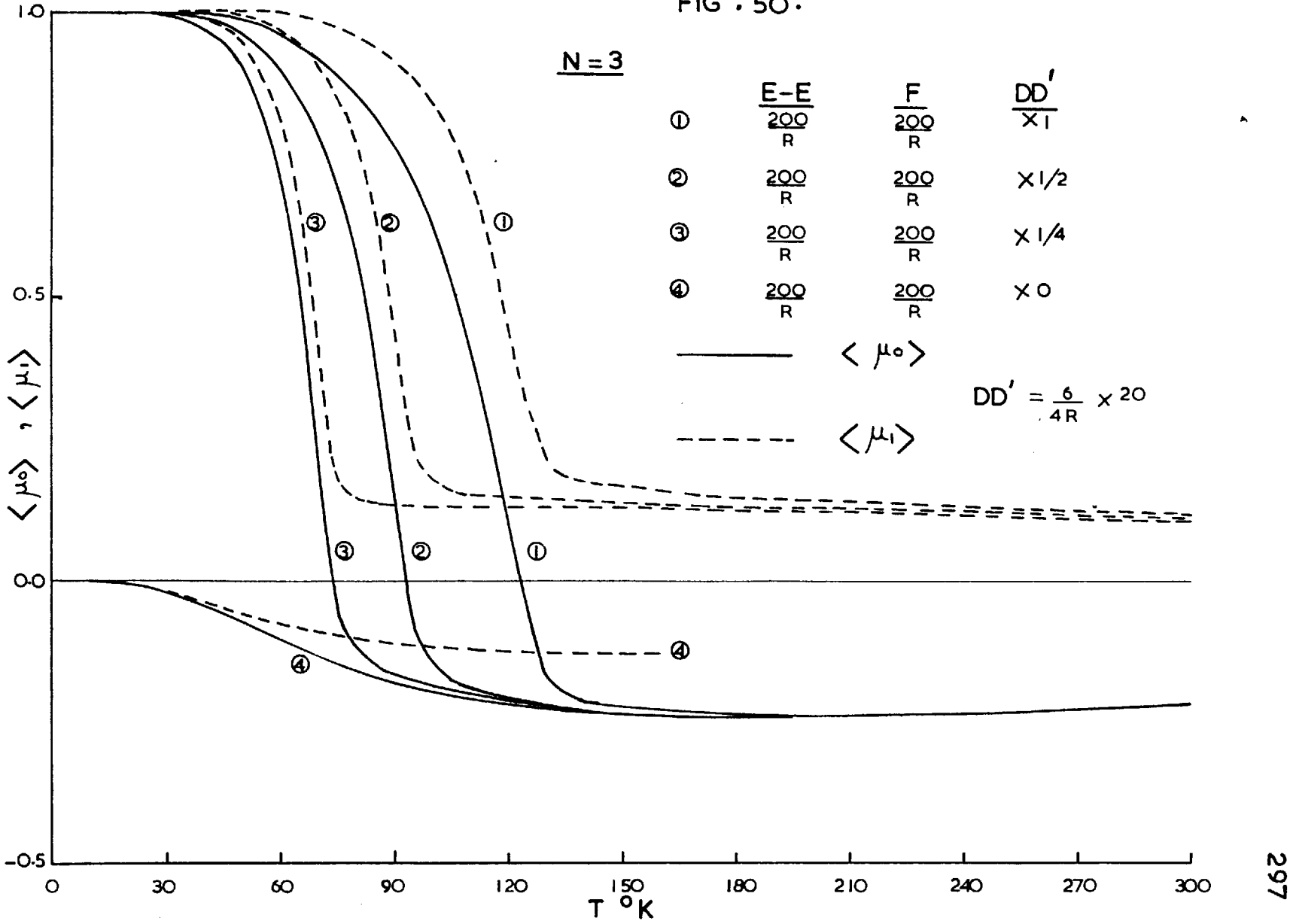

N = 3
E-E / 200/R
F / 200/R
DD' / X1
① 200/R 200/R X1
② 200/R 200/R X1/2
③ 200/R 200/R X1/4
④ 200/R 200/R X0
⟨μ0⟩
⟨μ1⟩
DD' = 6/4R × 20
1.0
0.5
0.0
-0.5
⟨μ0⟩ , ⟨μ1⟩
0
30
60
90
120
150
180
210
240
270
300
T °K

FIG . 51 .

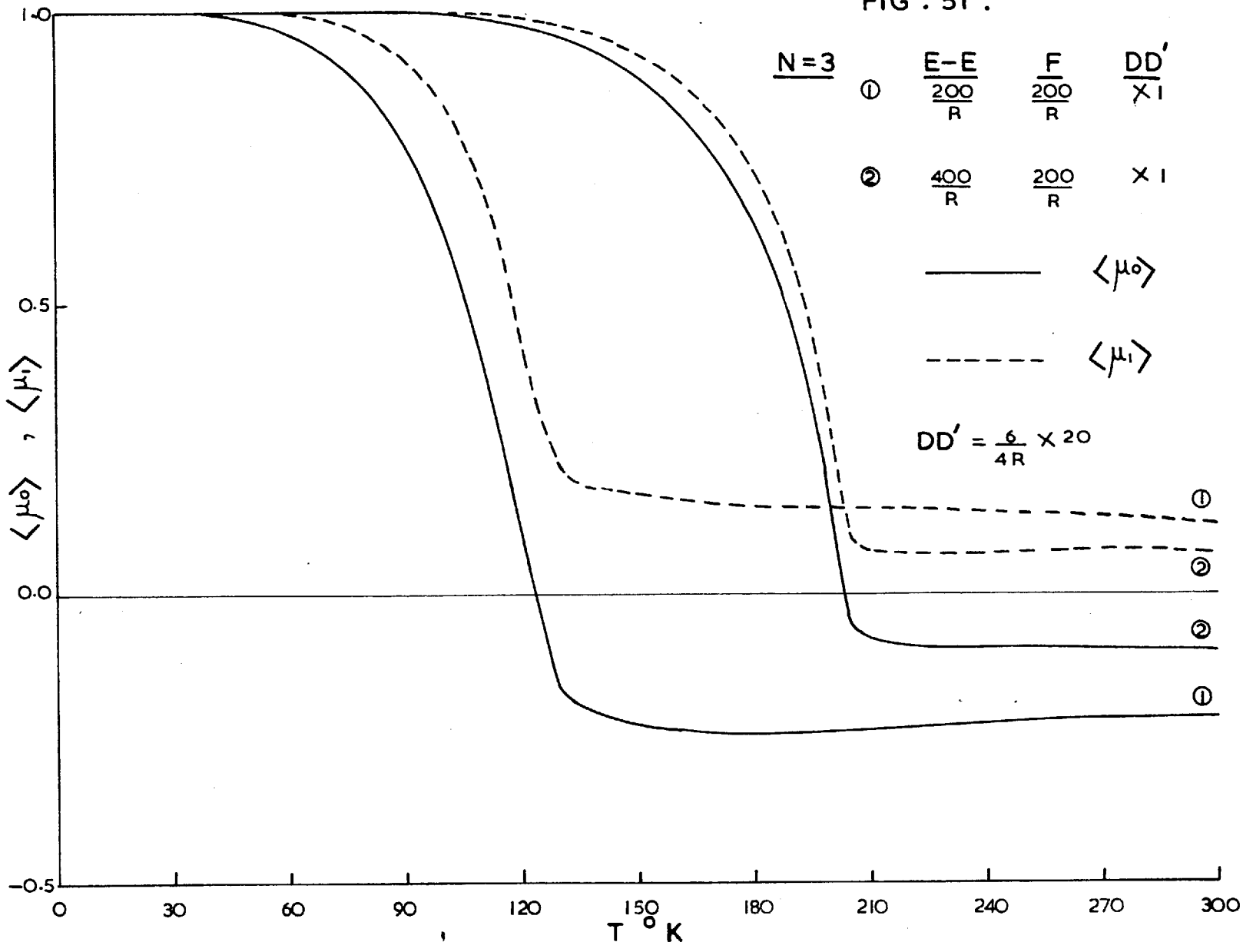
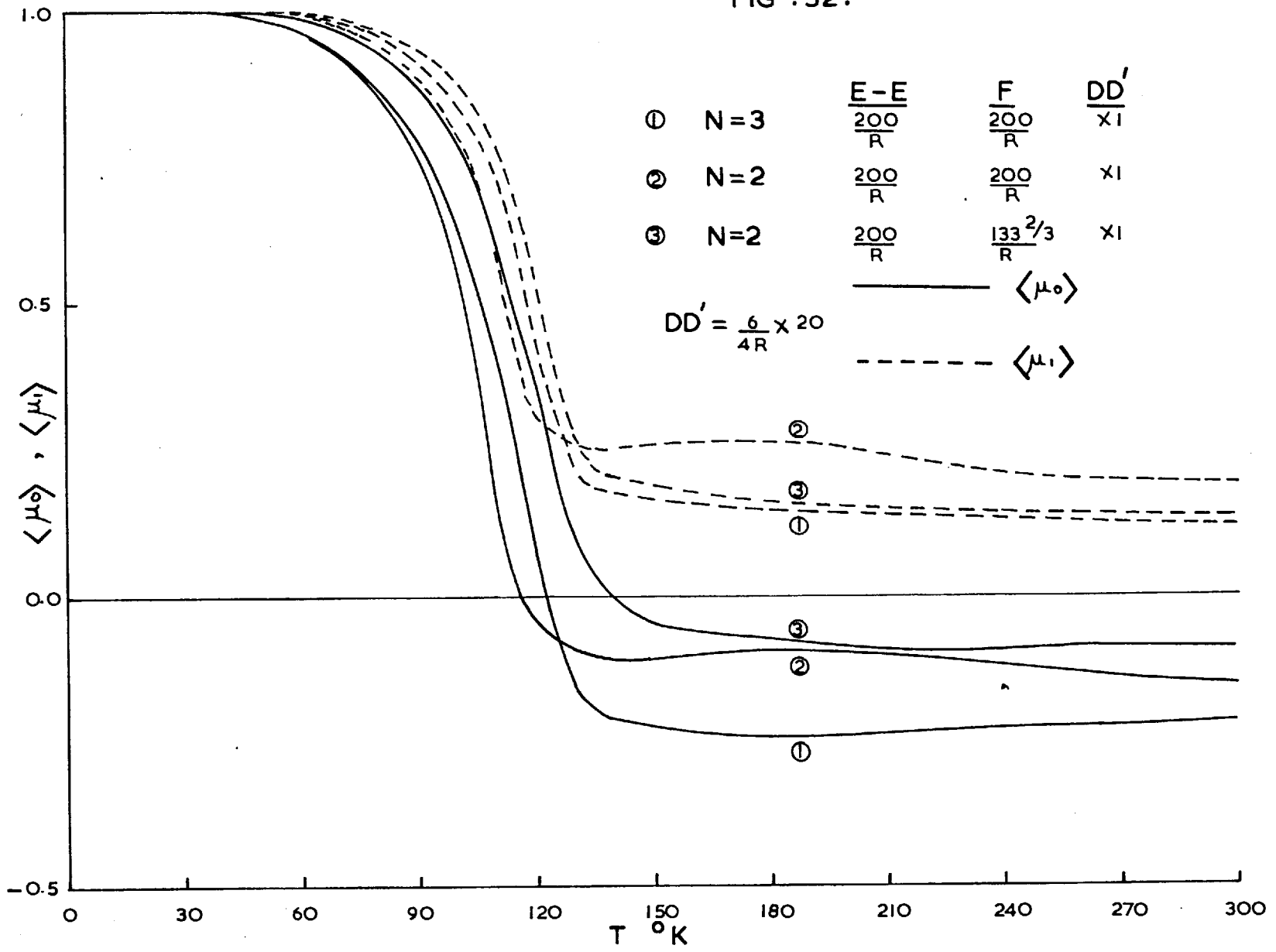

N=3
E-E / 200 / R
F / 200 / R
DD' / X1
① 400/R 200/R X1
② 400/R 200/R X1
⟨μ₀⟩
⟨μ₁⟩
DD' = 6/4R × 20
1.0
0.5
0.0
-0.5
⟨μ₀⟩ , ⟨μ₁⟩
0 30 60 90 120 150 180 210 240 270 300
T °K
①
②
②
①

FIG . 52.


1.0
0.5
0.0
−0.5
⟨μ₀⟩ , ⟨μ₁⟩
0
30
60
90
120
150
180
210
240
270
300
T °K
① N=3 E−E/200/R F/200/R DD′ ×1
② N=2 200/R 200/R ×1
③ N=2 200/R 133^2/3/R ×1
DD′ = 6/4R × 20
⟨μ₀⟩
⟨μ₁⟩
①
②
③

N small is not physically correct, except for the C_7, C_{16} and C_{24} adducts, since the number of units, each the length of the relevant hydrocarbon molecule which must be repeated before the urea field returns to its initial magnitude and direction is likely to be large.

Once the model had been shown to give a rapid breakdown in long range order over a small temperature interval the values of the interaction energies determined by the calculations reported in previous sections of this thesis, relating to the hydrocarbon adducts studied experimentaly, were used in the computation. Graphs of the variation of the order parameters together with the free energy, derived from the partition function using equation (20), with temperature are presented in FIGS. 53 to 60 and 61 to 68 respectively. From the free energy the configurational heat capacity Cv in the transition region was calculated from:

$$Cv = \frac{RT}{N} \cdot \frac{\partial^2 F}{\partial T^2} \quad \ldots\ldots\ldots\ldots (21).$$

where R is the gas constant per mole, T the absolute temperature and N the integer defining the interval, in terms of the length of the included species, between hydrocarbon molecules in an identical urea lattice field. The heat capacity plots (calculated) are shown in FIGS. 69

FIG .53.

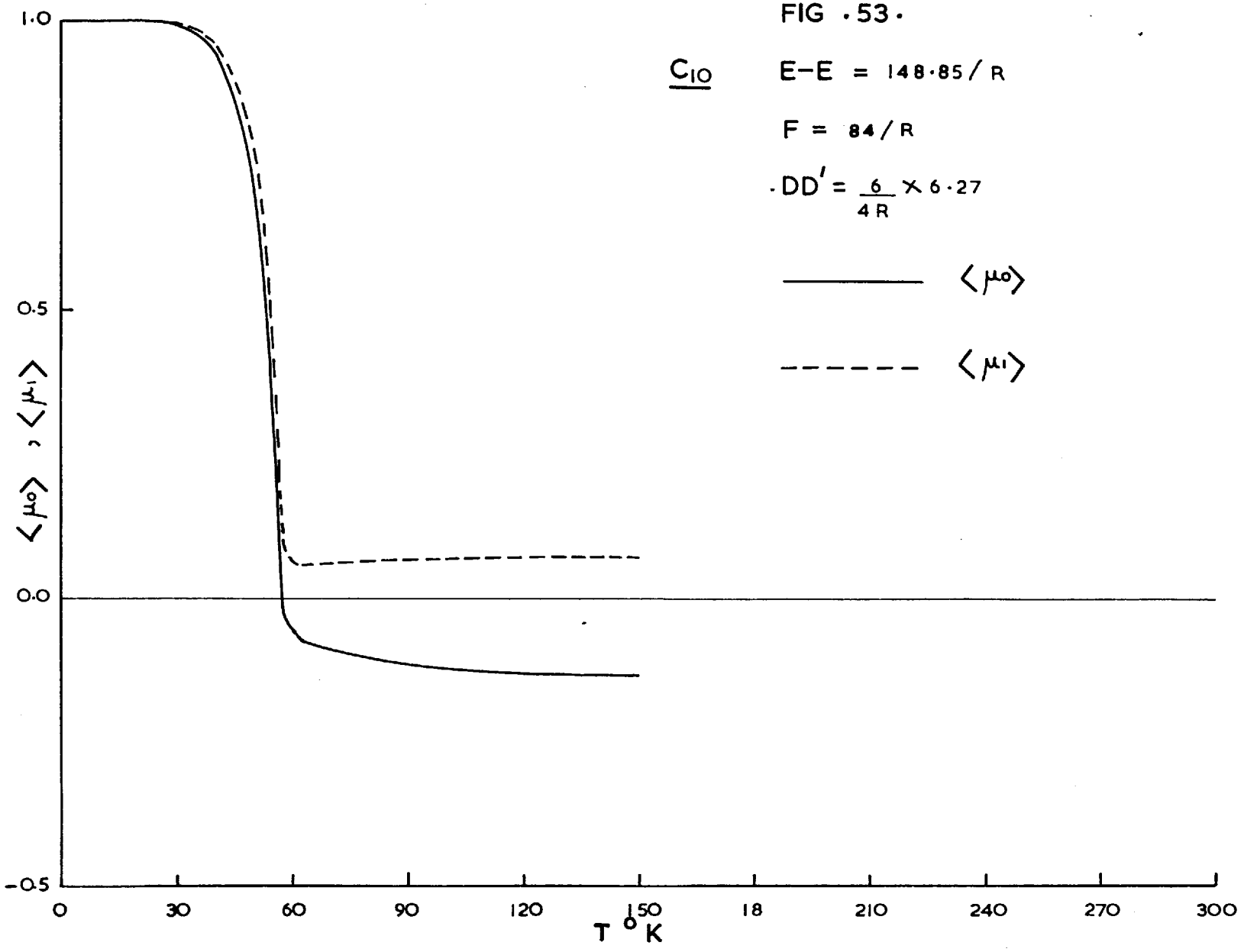
C_{10} E−E = 148·85 / R

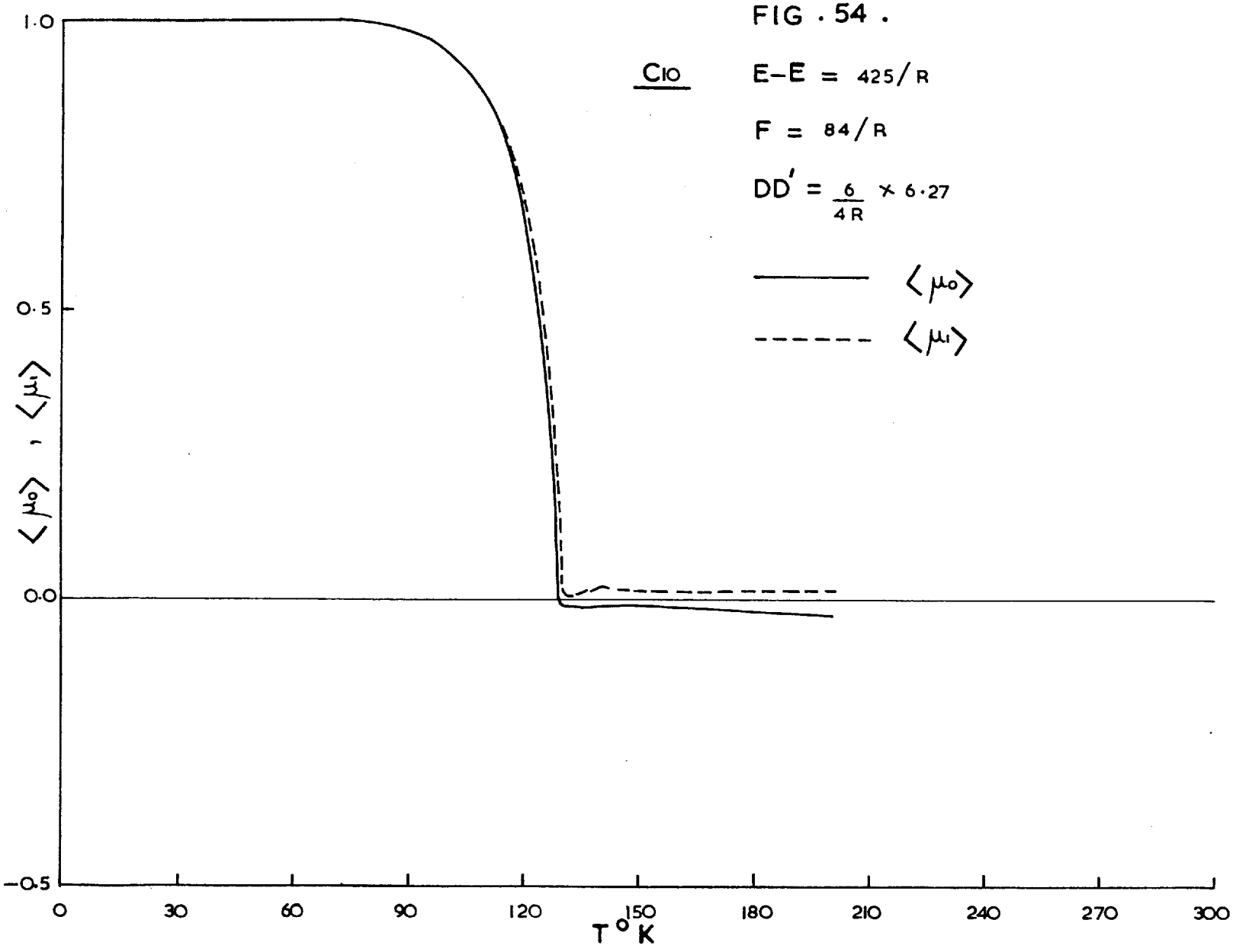
F = 84 / R

$DD' = \frac{6}{4R} \times 6 \cdot 27$

——— $\langle \mu_0 \rangle$

– – – – – $\langle \mu_1 \rangle$




FIG . 54 .
C10
E–E = 425/R
F = 84/R
DD′ = 6/4R × 6·27
⟨μ₀⟩
⟨μ₁⟩
1·0
0·5
0·0
−0·5
⟨μ₀⟩ , ⟨μ₁⟩
0
30
60
90
120
150
180
210
240
270
300
T °K

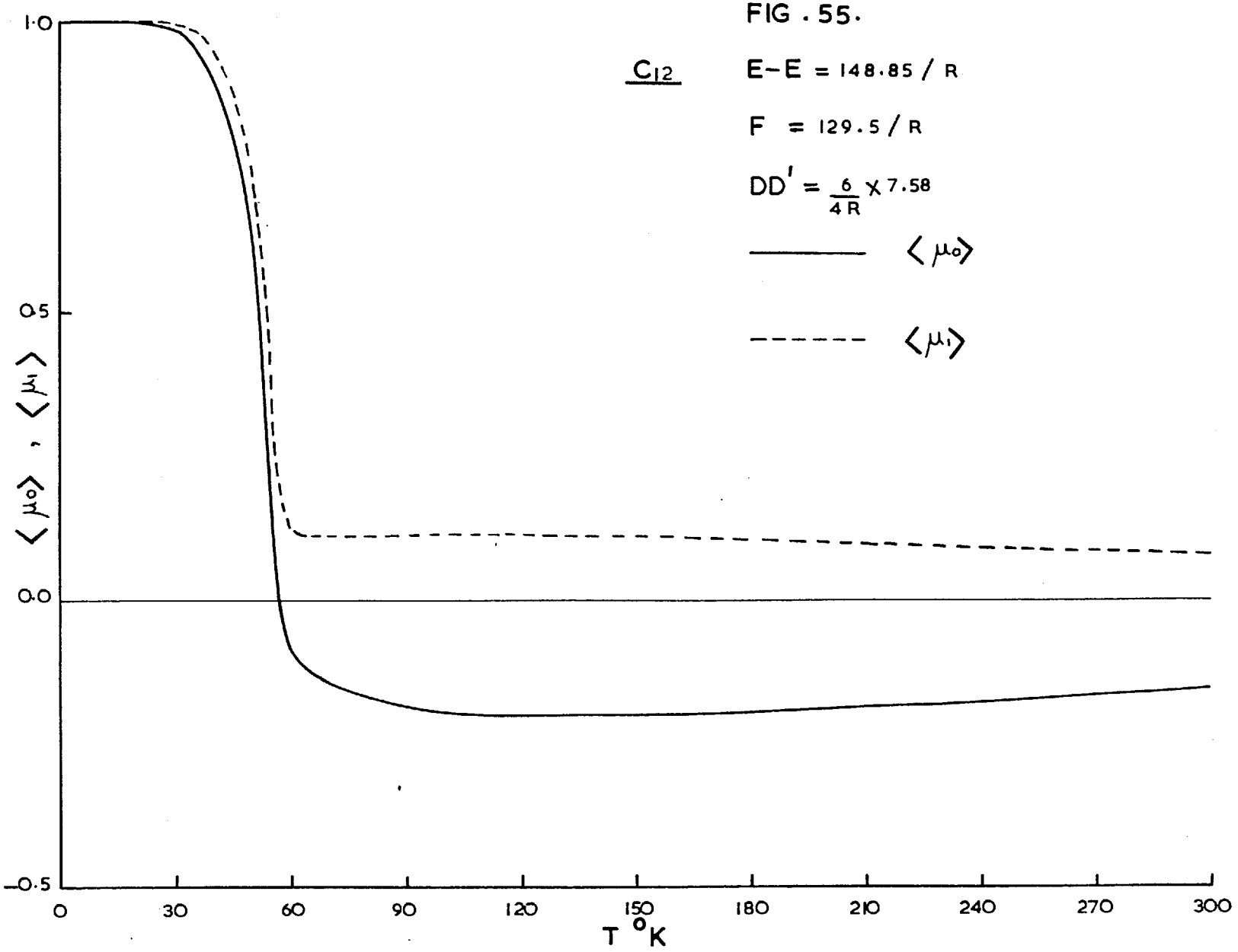

FIG . 55.
C12
E−E = 148.85 / R
F = 129.5 / R
DD' = 6/4R × 7.58
⟨μ0⟩
⟨μ1⟩
1·0
0·5
0·0
−0·5
⟨μ0⟩ , ⟨μ1⟩
0
30
60
90
120
150
180
210
240
270
300
T °K

FIG .56.

C12 E-E = 425/R

F = 129.5/R

$DD' = \frac{6}{4R} \times 7.58$

——— $\langle \mu_0 \rangle$

- - - - - - $\langle \mu_1 \rangle$

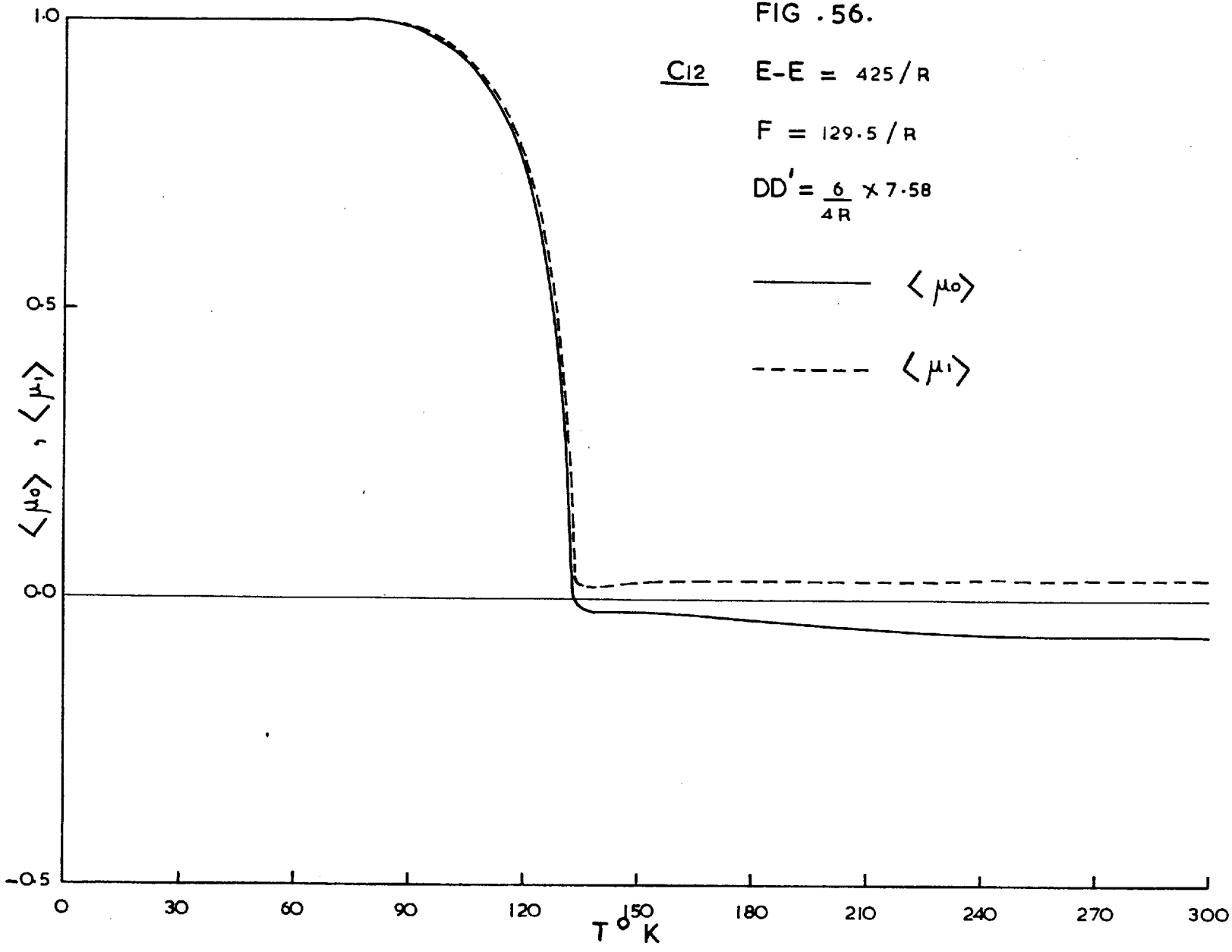


FIG. 57 .

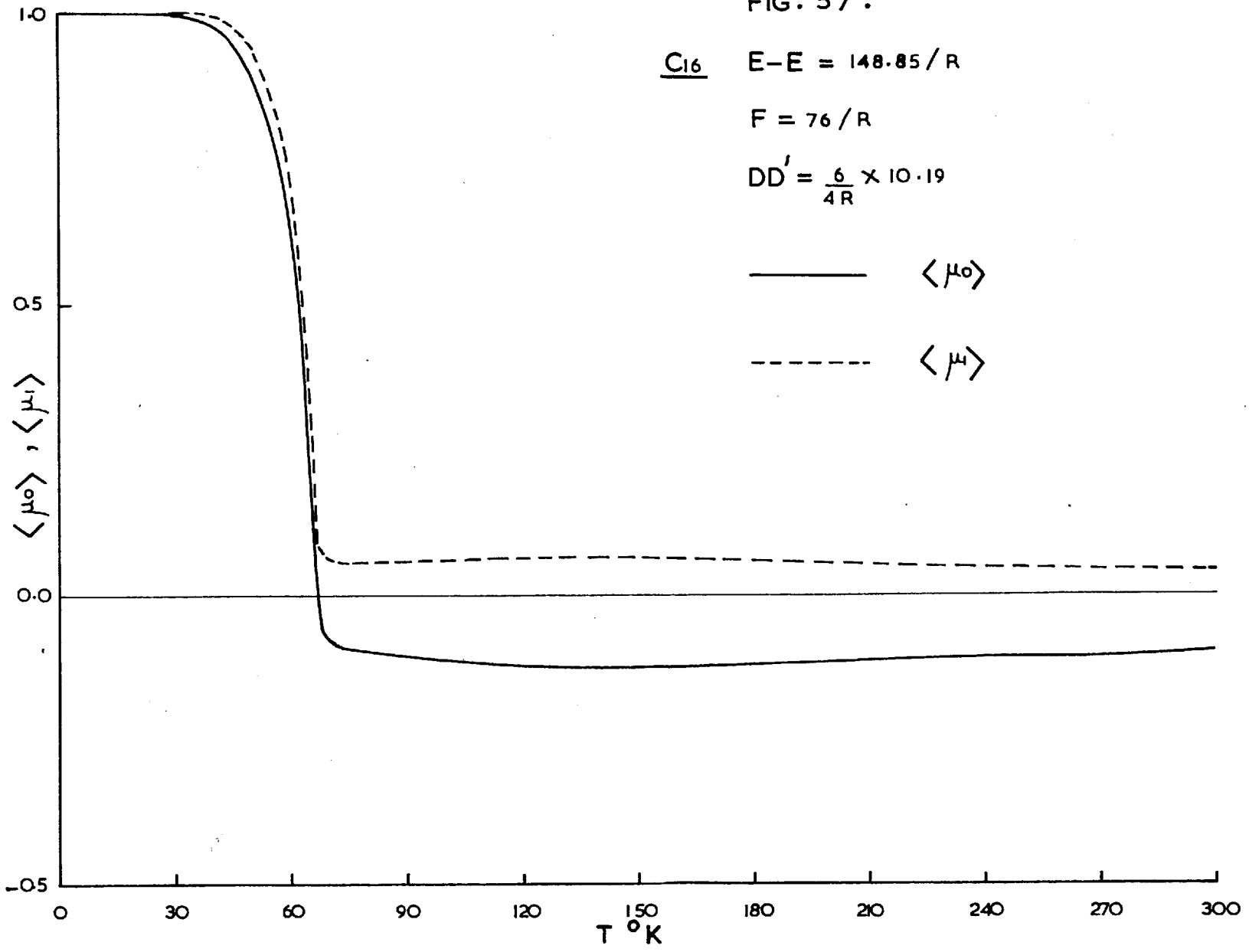
C_{16} E−E = 148.85 / R

F = 76 / R

$DD' = \frac{6}{4R} \times 10.19$

——— $\langle \mu_0 \rangle$

- - - - - - $\langle \mu \rangle$



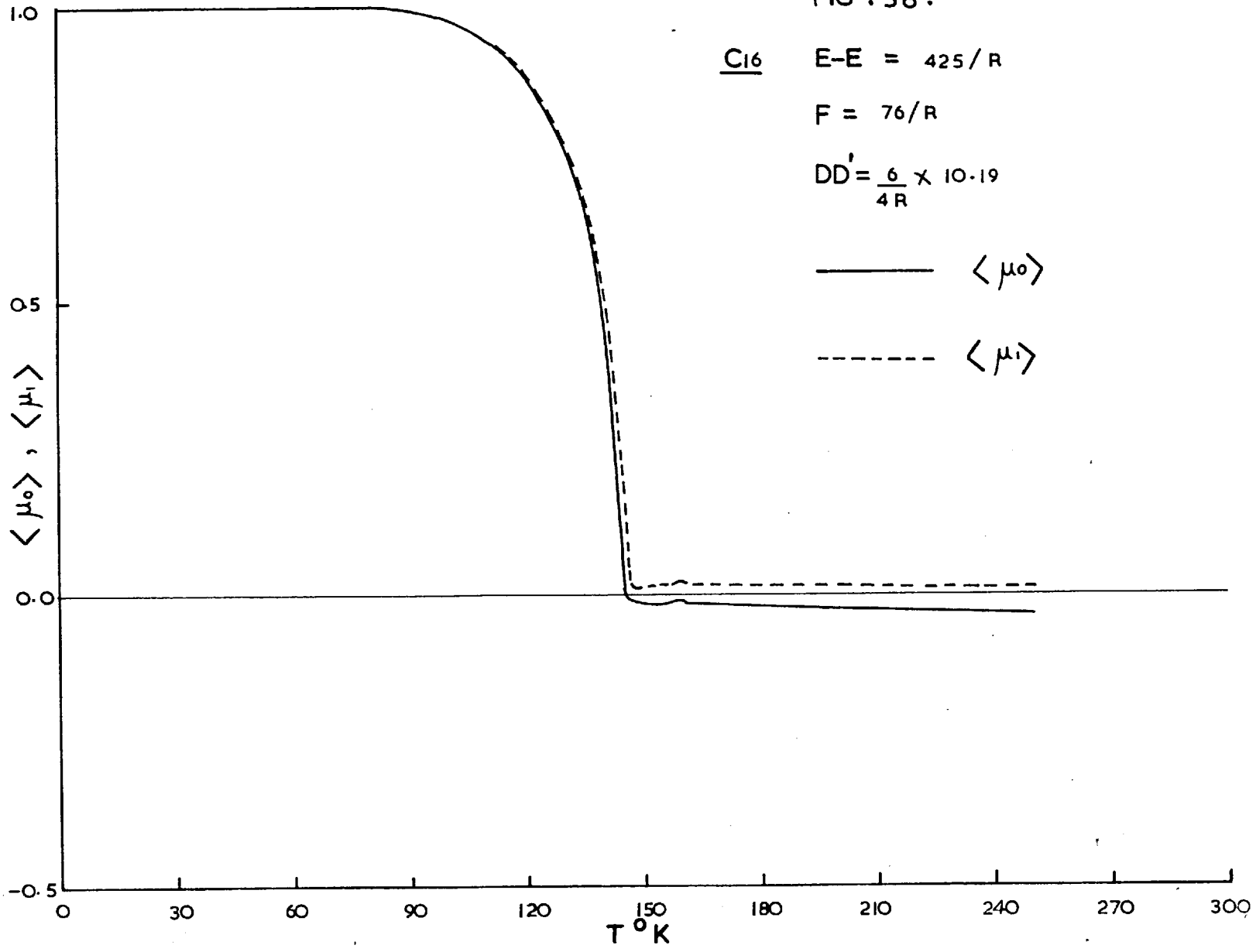

FIG . 58 .
C16
E-E = 425/R
F = 76/R
DD' = 6/4R × 10·19
⟨μ0⟩
⟨μ1⟩
1.0
0.5
0.0
-0.5
⟨μ0⟩ , ⟨μ1⟩
0
30
60
90
120
150
180
210
240
270
300
T °K

FIG · 59 ·

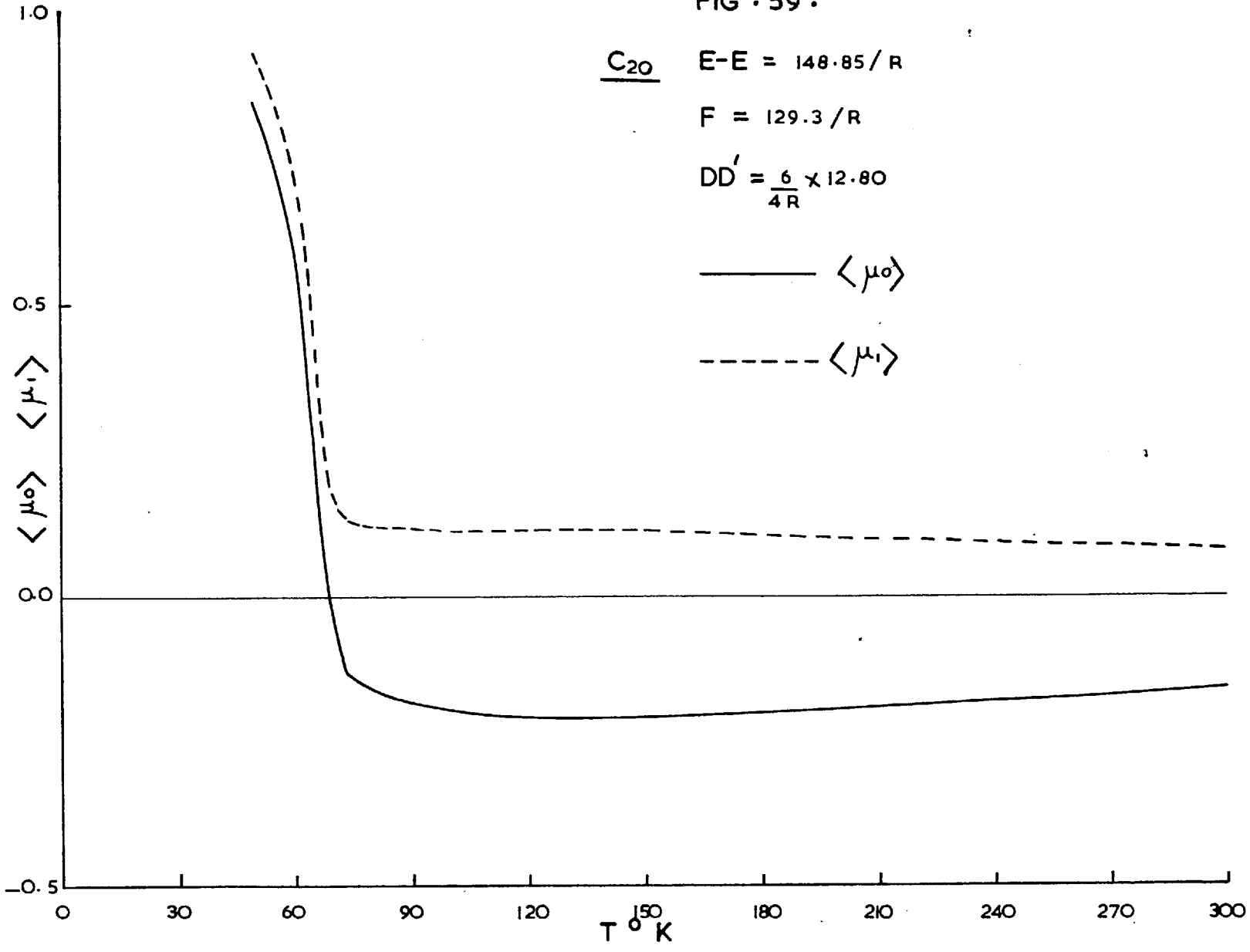

C20
E-E = 148·85/R
F = 129.3/R
DD' = 6/4R × 12·80
⟨μ0⟩
⟨μ1⟩
1.0
0.5
0.0
−0.5
⟨μ0⟩ ⟨μ1⟩
0
30
60
90
120
150
180
210
240
270
300
T °K

FIG. 60.

C20 E-E = 425/R

F = 129.3/R

$DD' = \frac{6}{4R} \times 12.80$

——— $\langle \mu_0 \rangle$

------- $\langle \mu_1 \rangle$

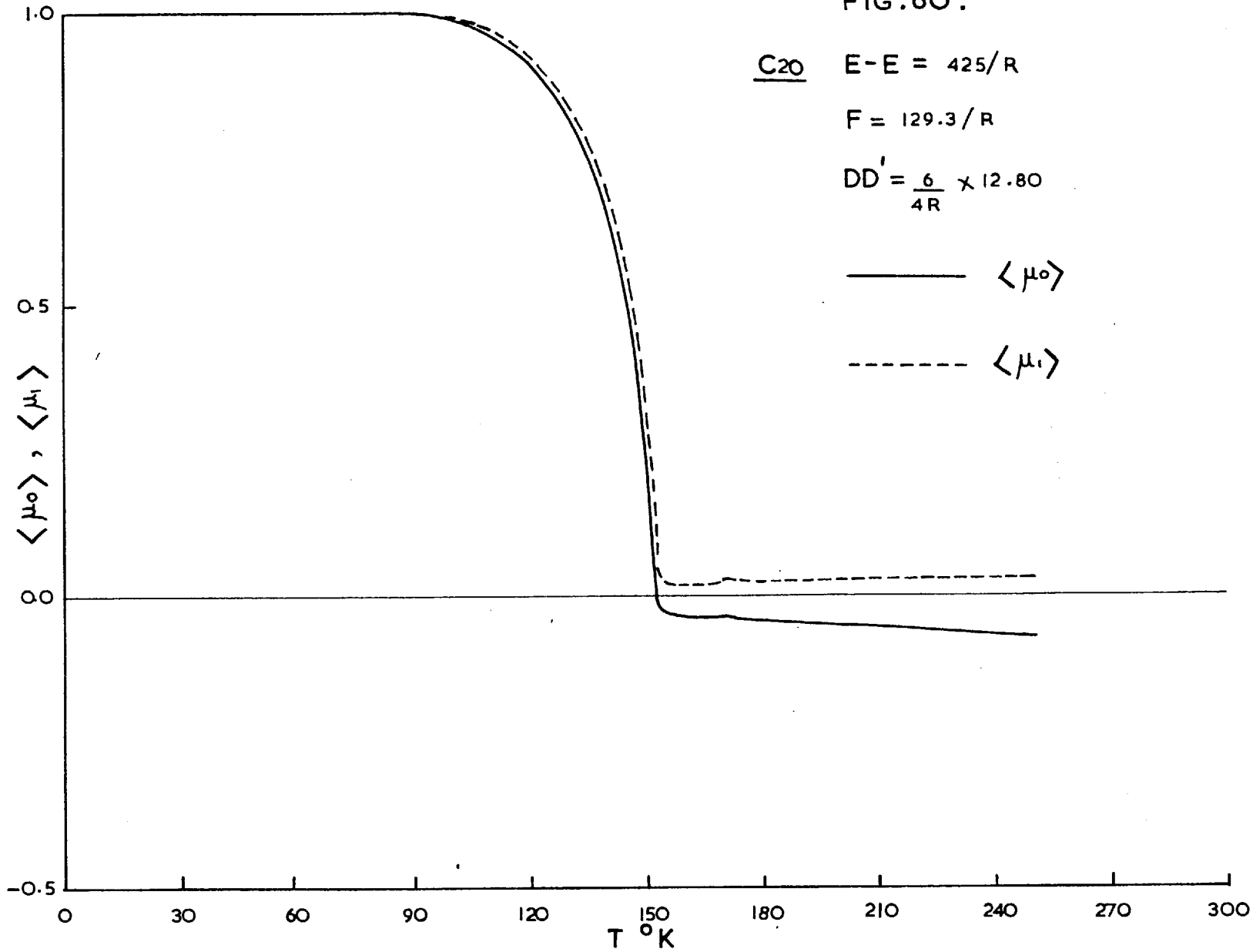


FIG. 61.

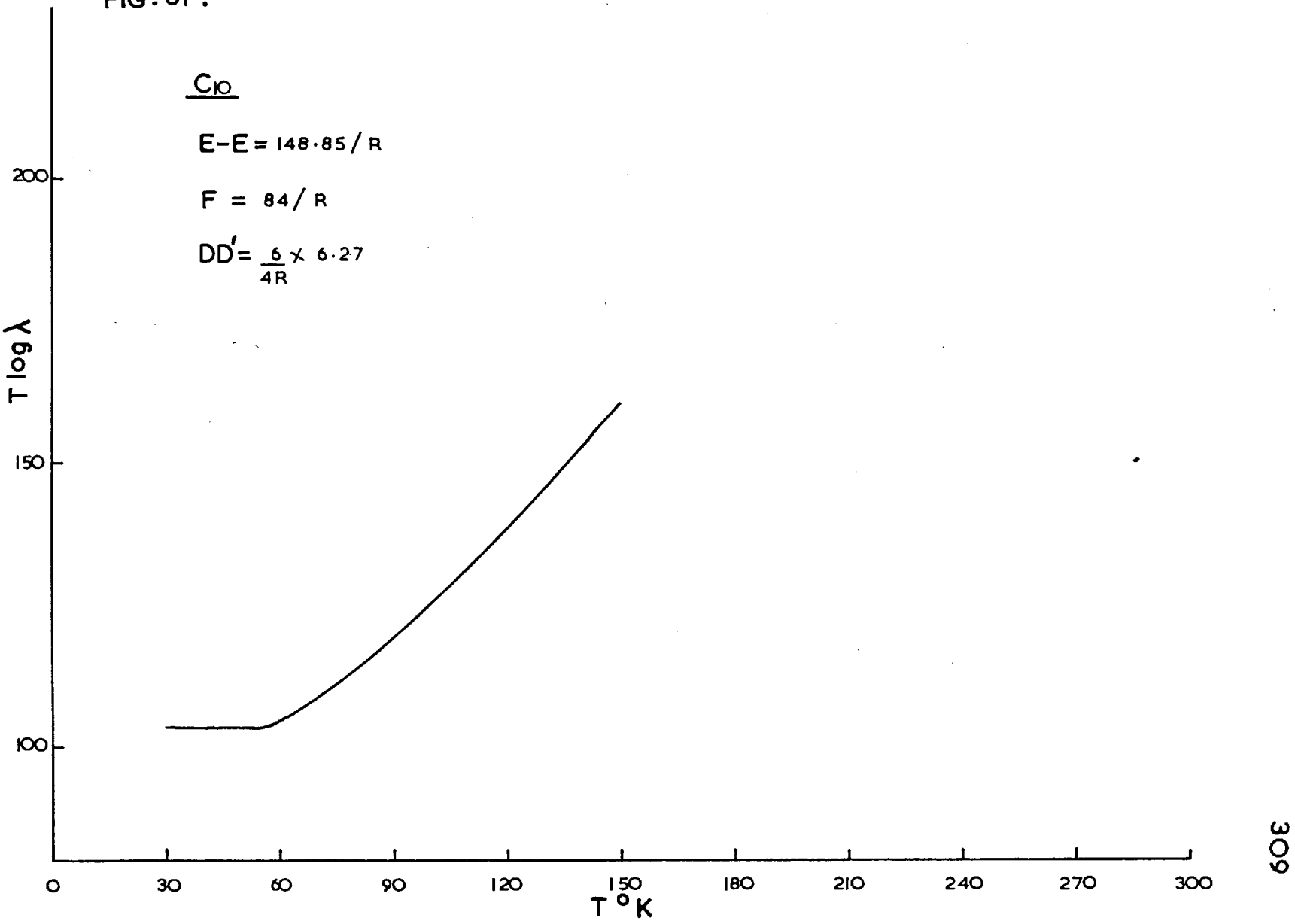

C10
E-E = 148·85 / R
F = 84 / R
DD' = 6/4R × 6·27
T log λ
200
150
100
0
30
60
90
120
150
180
210
240
270
300
T °K

FIG.62.

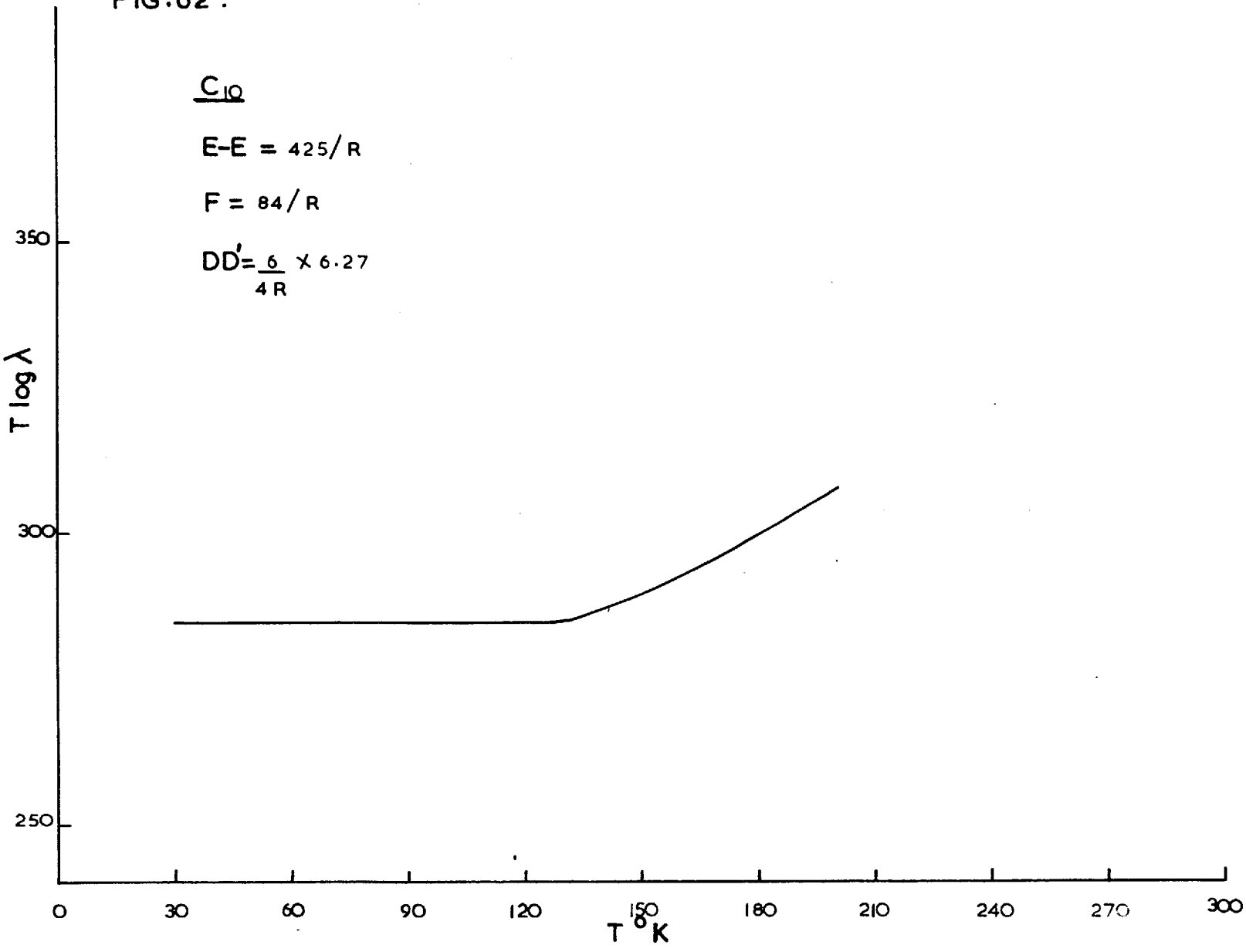

C10
E-E = 425/R
F = 84/R
DD' = 6/4R X 6.27
350
300
250
T log λ
0
30
60
90
120
150
180
210
240
270
300
T °K

FIG .63 .

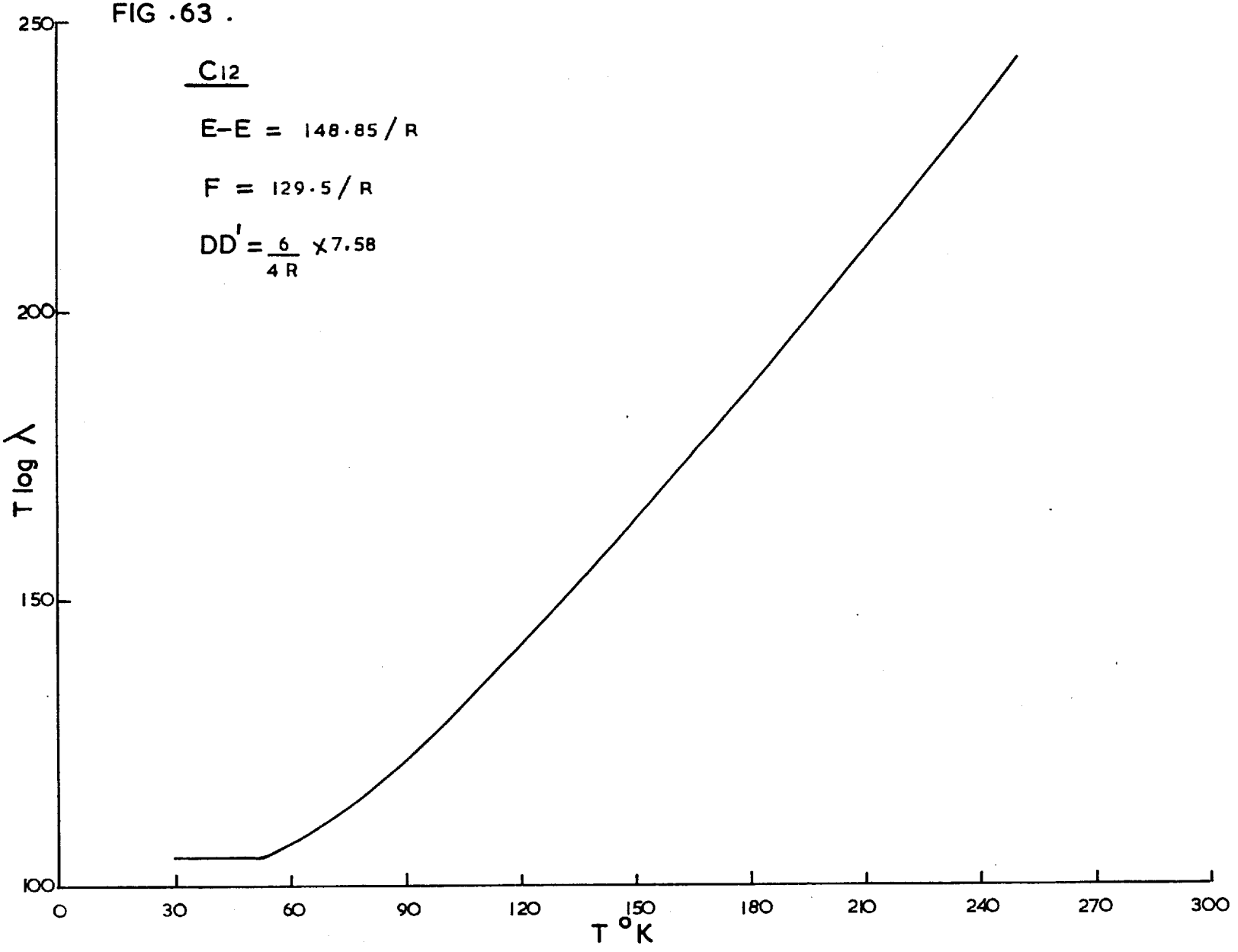

C12
E-E = 148.85 / R
F = 129.5 / R
DD' = 6/4R x 7.58
250
200
150
100
T log λ
0
30
60
90
120
150
180
210
240
270
300
T °K

FIG .64 .

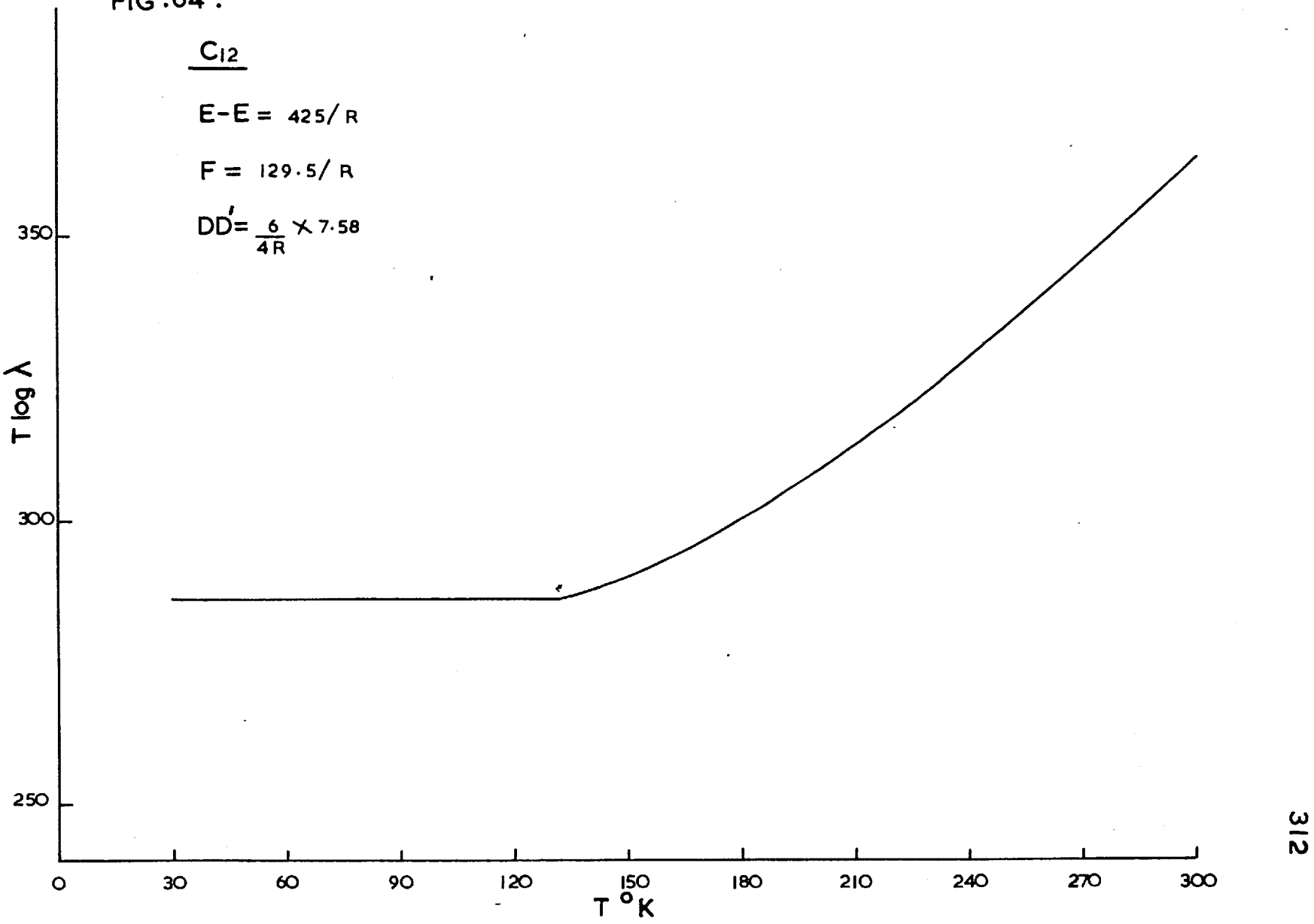

C12
E-E = 425/R
F = 129.5/R
DD' = 6/4R × 7.58
350
300
250
T log λ
0
30
60
90
120
150
180
210
240
270
300
T °K

FIG.65.

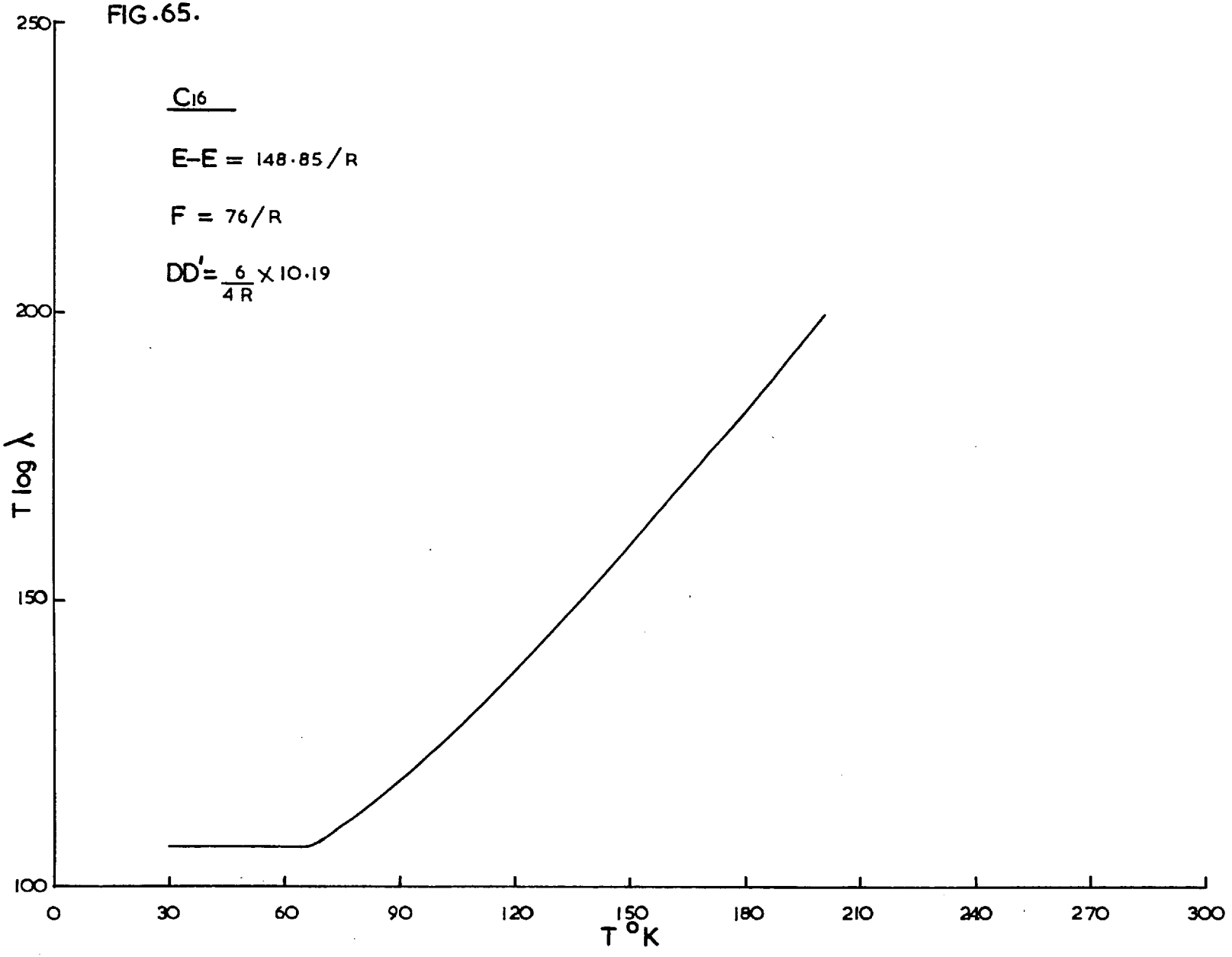

C16
E-E = 148·85/R
F = 76/R
DD' = 6/4R × 10·19
250
200
150
100
T log λ
0
30
60
90
120
150
180
210
240
270
300
T °K

FIG .66.

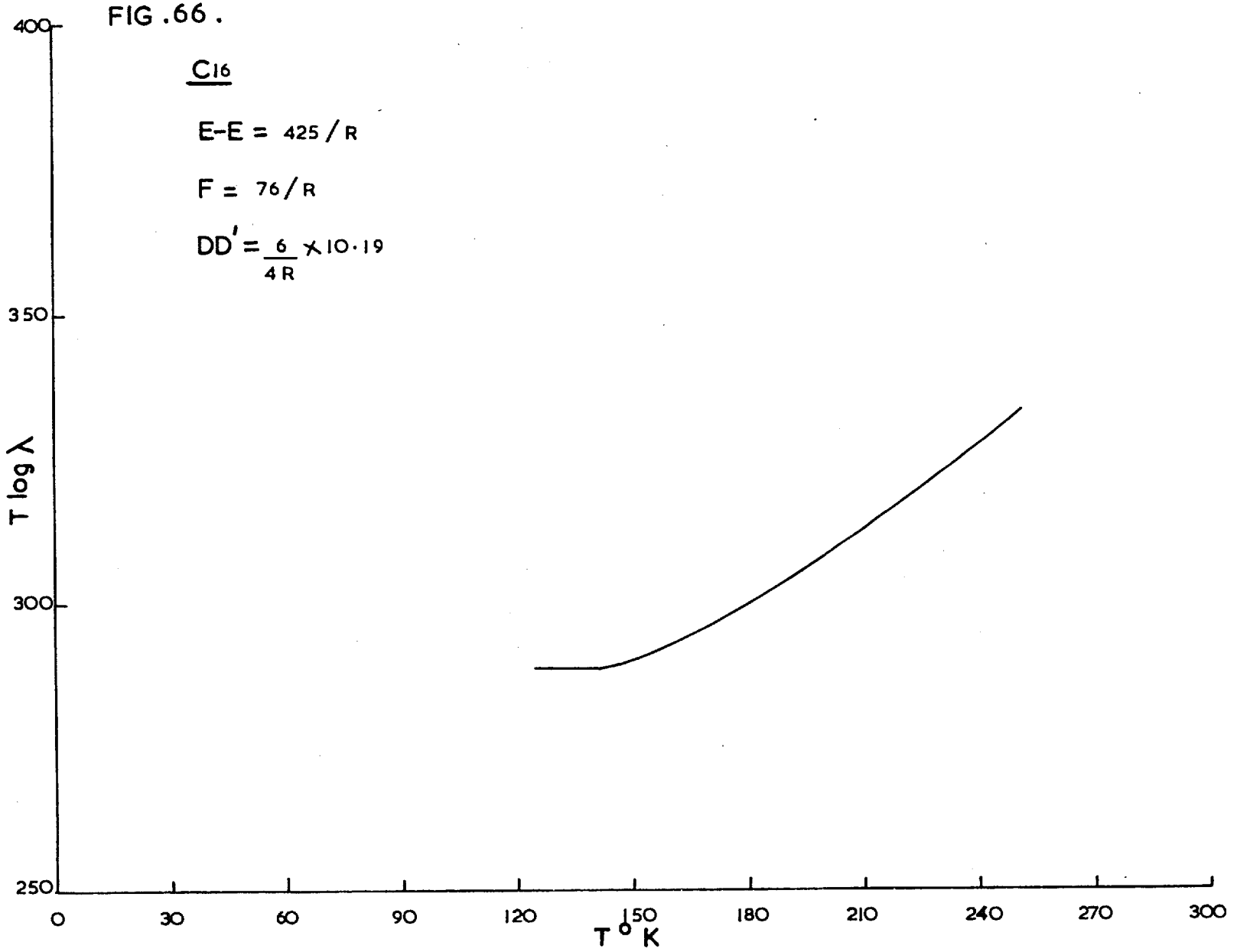

C16
E-E = 425 / R
F = 76 / R
DD' = 6/4R × 10·19
400
350
300
250
T log χ
0
30
60
90
120
150
180
210
240
270
300
T °K

FIG.67.

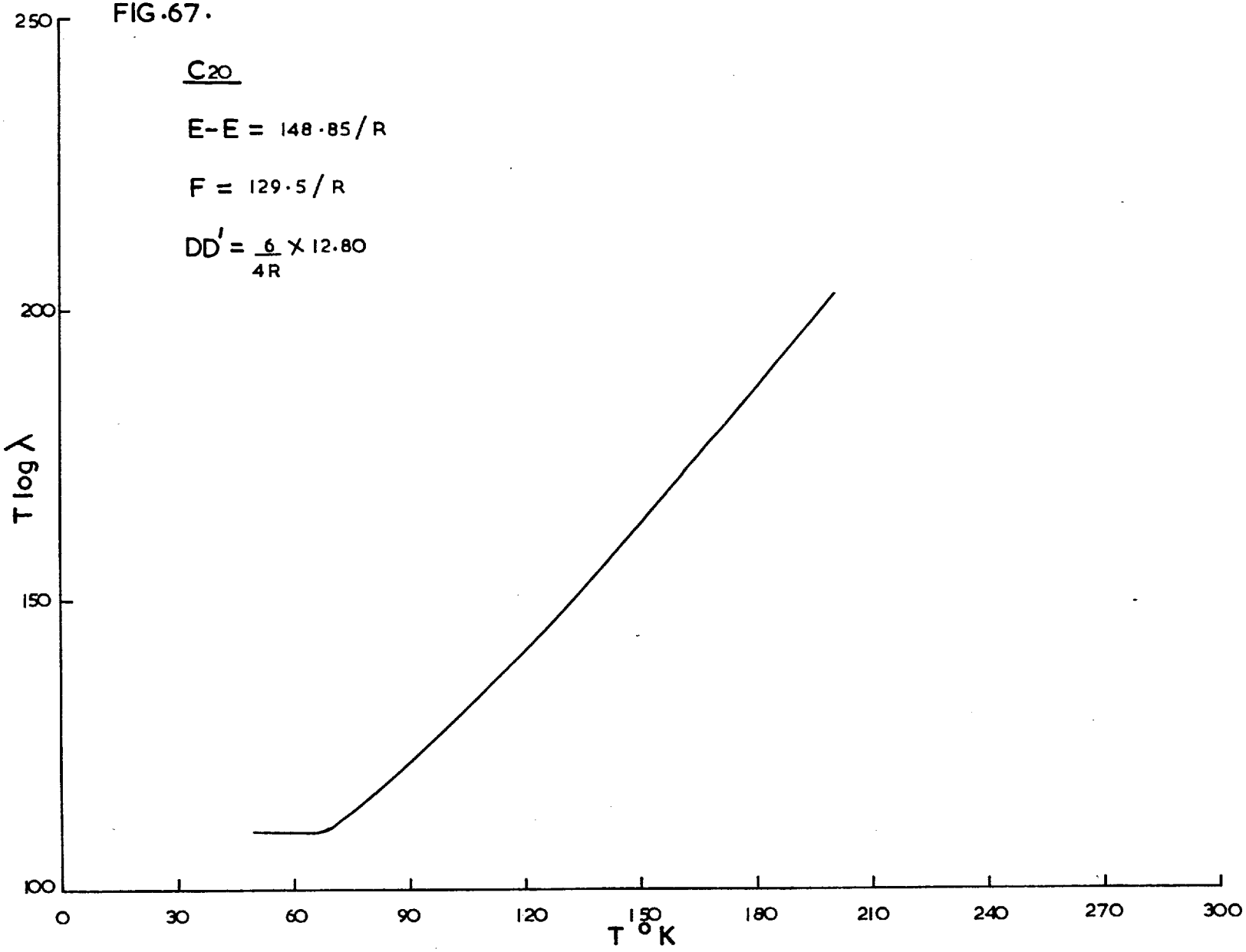

C20
E-E = 148·85/R
F = 129·5/R
DD' = 6/4R × 12·80
250
200
150
100
T log λ
0
30
60
90
120
150
180
210
240
270
300
T °K

FIG.68.

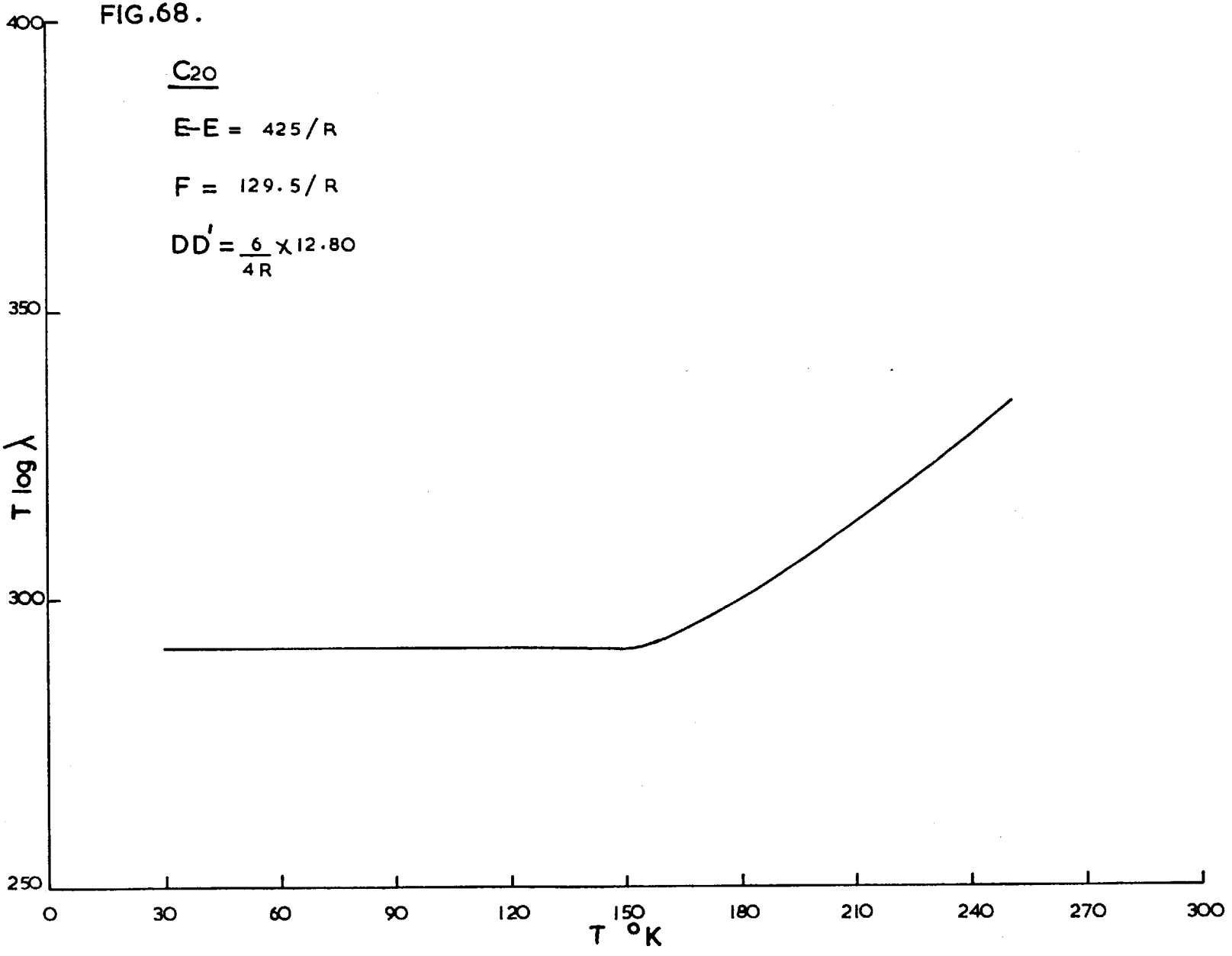

C20
E-E = 425/R
F = 129.5/R
DD' = 6/4R X 12.80
400
350
300
250
T log λ
0
30
60
90
120
150
180
210
240
270
300
T °K

FIG . 69 . COMPUTED TRANSITIONAL CONTRIBUTION TO THE HEAT CAPACITY FOR DODECANE ADDUCT.

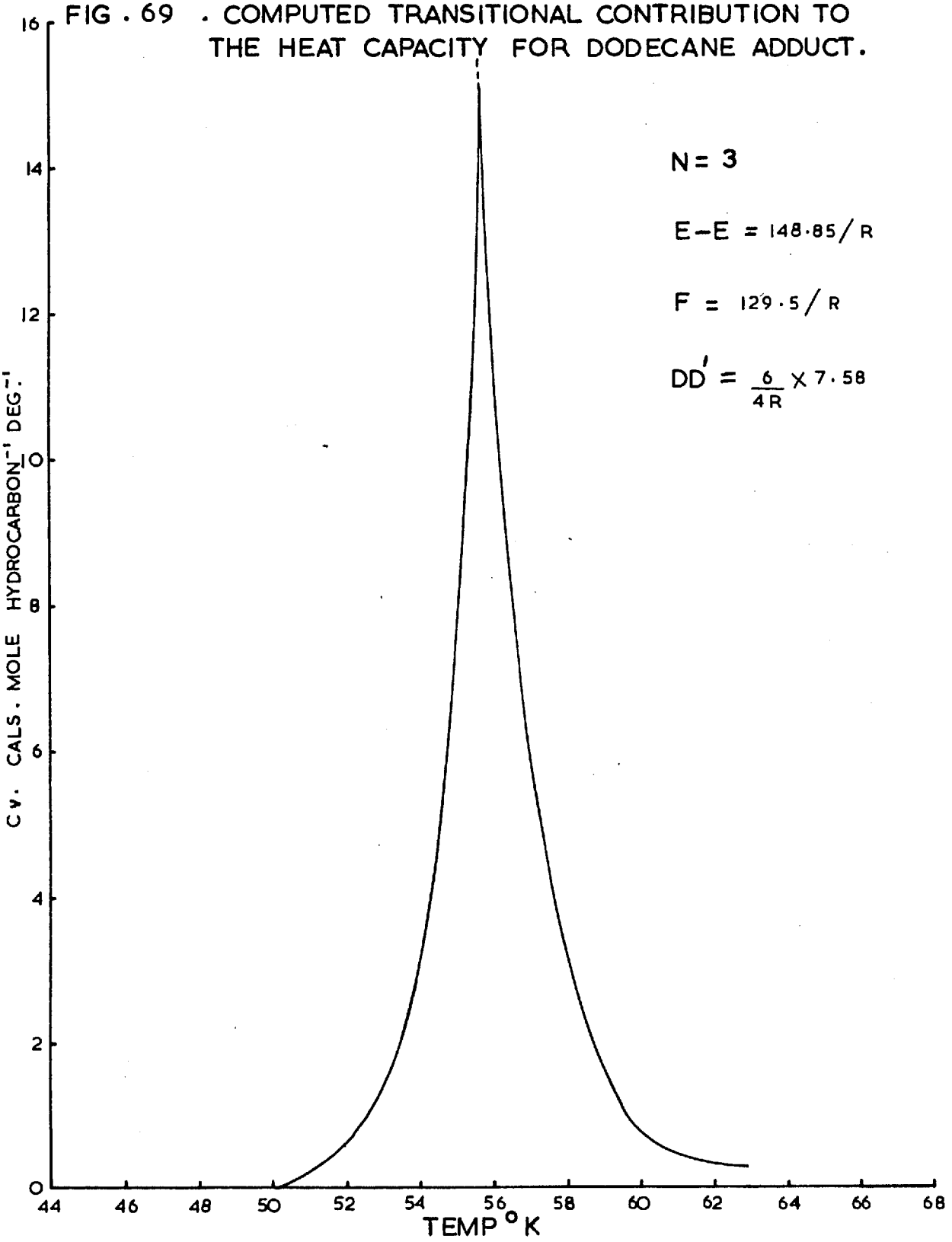


FIG . 70 . COMPUTED TRANSITIONAL CONTRIBUTION TO THE HEAT CAPACITY FOR DODECANE ADDUCT.

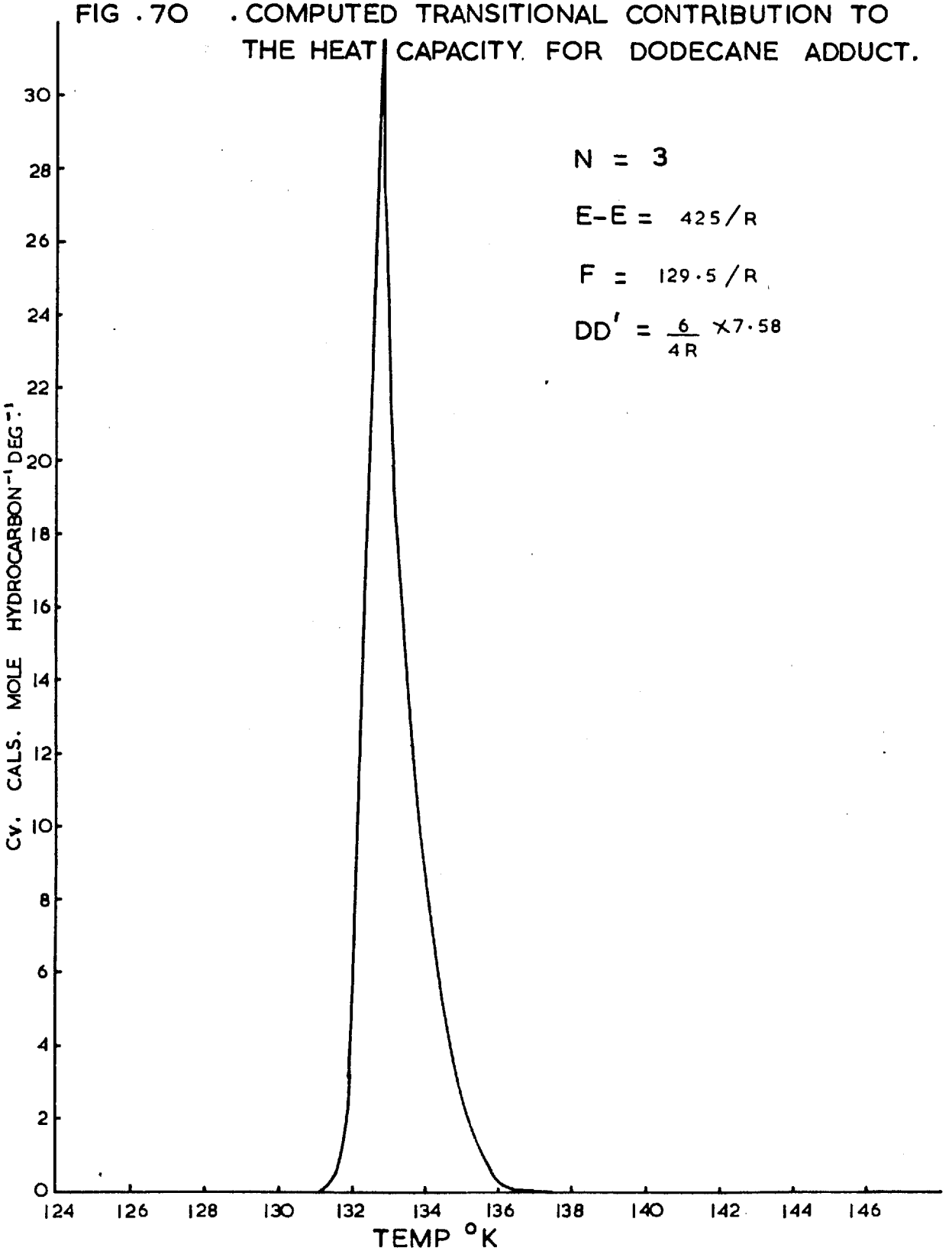


FIG. 71 . COMPUTED TRANSITIONAL CONTRIBUTION TO THE HEAT CAPACITY FOR HEXADECANE ADDUCT.

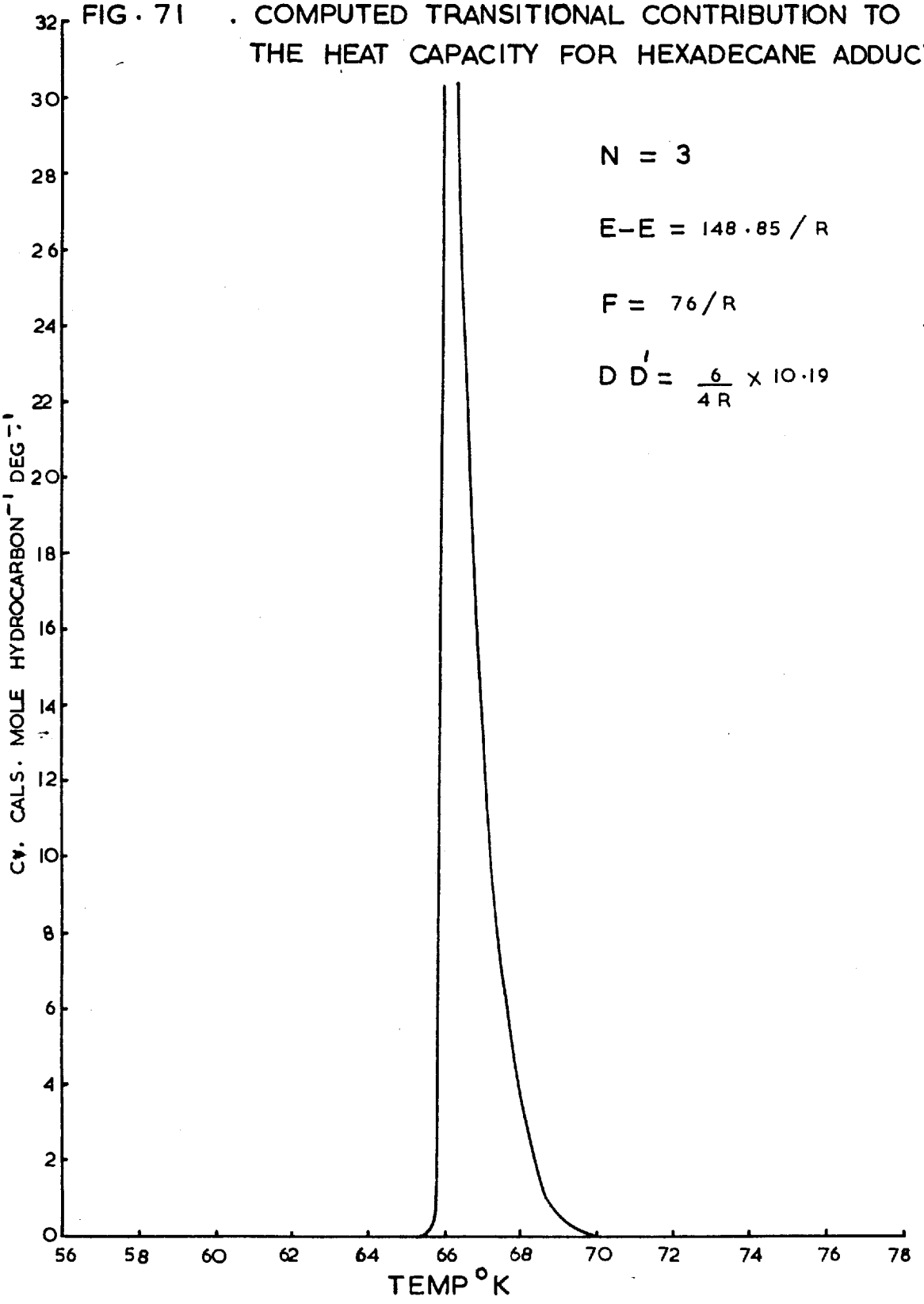
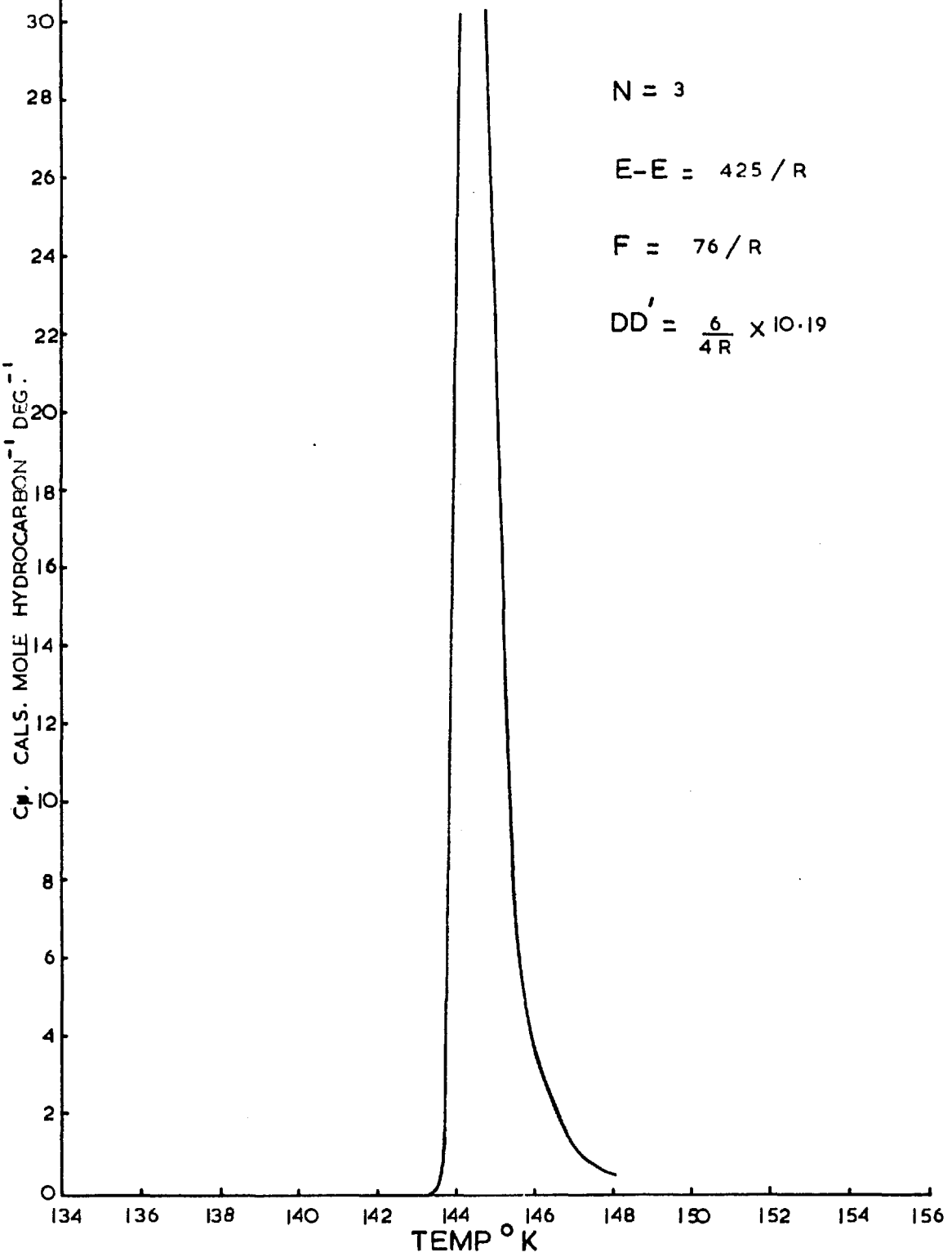


FIG. 72. COMPUTED TRANSITIONAL CONTRIBUTION TO THE HEAT CAPACITY FOR HEXADECANE ADDUCT.



to 72 for the dodecane and hexadecane adducts. A great deal of significance can not be attached to these Cv values as they were obtained graphically from the computed values of the partition function calculated at only 1° intervals across the transition region. As the computed "width" of the transition at its base is only approximately 4°-6° for all but the dodecane adduct, where a spread of 10° was found when E-E = 148.85/R (see FIGS. 69 to 72), an accurate variation of Cv with T would only result from using smaller temperature intervals in the computation. However, the "width" at the base of these computed configurational heat capacity peaks is comparable with the experimental widths (C_{10}- 5°K, C_{12}- 4°K, C_{16}- 3°K, for the higher transition peak, and C_{20}- 10°K) when only the sharply rising portion of the transitions are considered.

CONCLUSIONS.

In view of the absence of an adjustable parameter in the theoretical treatment the results obtained are in very reasonable agreement with experiment. However, the approximations introduced to simplify the calculations restrict the entropy of transition to a value of Rln2 (1.38 cals. mole hydrocarbon^{-1} deg^{-1}). In fact all the adducts studied

had entropy changes larger than this and as a series the "even" hydrocarbons show an almost linear increase in ΔS with chain length (see FIG.39). It might be possible to introduce a number (W) of allowed low energy sites, which would then lead to an entropy of transition equal to RlnW, but this would still not account for the observed increase in ΔS with hydrocarbon chain length. The onset of flexing or internal rotations in individual hydrocarbon molecules may be responsible for this "excess entropy of transition".

The theoretical treatment is also inadequate in its present form, in that it does not account for the double peak found in the heat capacity of the hexadecane adduct. This adduct is unusual however in having a chain length close to an integer multiple of the urea lattice unit cell repeat distance. To elucidate this problem investigations of the heat capacities of the n-heptane and n-tetracosane adducts, where as in the inclusion compound with hexadecane, the terminal methyl groups turn from the plane of the carbon atom skeleton to reduce the chain length to a multiple of 11.0 Å, could be undertaken.

The model may be further improved by computing an average value for the lateral hydrocarbon-

hydrocarbon interactions in place of the maximum or minimum energies used in these calculations. Higher values may also be given to N although for high N the time of computation is likely to be excessively long.

Further work on the urea adduct heat capacities is necessary. The investigation of the "odd" hydrocarbon series to determine whether the other adducts show anomalies, as was found in that of pentadecane and if the entropies of transition exhibit a similar behaviour to the "even" series would prove interesting. The adducts of the unsaturated and some further branched chain hydrocarbons, together with the large number of adducts formed by thiourea as the host lattice demand attention.

There is still much work to be done in this field of research.

———————"———————

REFERENCES

(1). Davy, Sir H., Phil. Trans. Roy. Soc. London A101, 1(1811).

(2). Wieland, H. and Sorge, H., Z Physiol. Chem. Hoppe-Seyler's 97, 1(1916).

(3). Wöhler, F., Ann.Chem. Liebigs 69, 297(1849).

(4). Clemm, A., Ann. Chem. Liebegs 110 357(1859).

(5). Mylius,F., Ber. 19, 999(1886).

(6). Hofmann, K.A. and Küspert, F., Z. anorg. u. allgem. Chem. 15, 204(1897).

(7). Evans, D.F., and Richards, R.E., J. Chem Soc. (London), p. 3295(1952).

(8). Schmidlin, J. and Lang, R., Ber. 43, 2806(1910)

(9). Gomberg, M. and Cone, H., Ann Chem. Liebegs 376 238(1910).

(10). Powell, H.M., and Guter, M., Nature 164, 240(1949)

(11). Powell, H.M., J. Chem. Soc. (London), p. 300(1950).

(12). Jacobsen, O., Ber. 20, 898(1887).

(13). Gomberg, M., J. Am. Chem. Soc. 37, 2569(1915).

(14). Nikitin, B.A., Doklady Akad. Nauk. U.S.S.R. 24 567(1939).

(15). Pauling, L. and Marsh, R.E., Proc. Natl. Acad. Sci. U.S. 38, 112(1952).

(16). Müller, H.R. and von Stackelberg,M., Naturwissenschaften 39, 20(1952)

(17). Müller, H.R. and von Stackelberg,M., J. Chem. Phys. 19, 1319(1951).

(18). Paulin, D.E. and Powell, H.M., Nature 156, 334(1945).

(19). Paulin, D.E. and Powell, H.M., J. Chem. Soc. (London) p. 815(1948).

(20). Powell, H.M., J. Chem.Soc. (London), p.61(1948).

(21). Bengen, M.F., German Patent Appl. OZ 123438 (Mar. 18, 1940).

(22). Bengen, M.F., Angew. Chem. 63, 207(1951).

(23). Fetterly, L.C., U.S. Patent 2,499,820 (Feb. 21, 1947).

(24). McLaughlin, R.L. and McClenahan, W.S., J. Am. Chem. Soc. 74, 5,804(1952).

(25). Schlief, H., J. Prakt. Chem. 2, 337(1955)

(26). Bailey, F.E., Jr. and France, H.G., J. Polymer Sci. 49, 397(1961).

(27). Gorin, E., U.S. Patents 2,681,332, -3, -4, -6 (1954).

(28). Garner, P.J., Goldsbrough, L.N. and Byers,T.B., U.S. Patent 2,518,677(1950).

(29). Kelley, C.S. U.S. Patent 2,739,144 (1956).

(30). Fetterly, L.C., Petrol Refiner 36, 145 (1957).

(31). Bailey, W.A., Jr.,Bannerot, R.A., Fetterly, L.C. and Smith, A.G., Ind. Eng. Chem. 43, 2125(1951).

(32). Fetterly, L.C., Petrol Refiner 34, 134 (1955).

(33). Holman, R.T., and Schlenk, H., J. Am. Chem. Soc. 74, 1720 (1952).

(34). Truter, E.V., "Wool Wax: Chemistry and Technology" Vol.I, p. 195, Wiley, New York, 1956.

(35). Schlenk, W. Jr., Analyst 77, 867 (1952).

(36). Brown J.F. and White D.M., J. Am. Chem. Soc. 82, 5671 (1960).

(37). Karr, C., U.S. Patent 2,912,426 (1959).

(38). Nicolaides, H. and Laves, F., J. Am. Chem. Soc. 76, 2596 (1954).

(39). Kolbe, K.A. and Domask, W G. , Petrol Refiner 34 (4), 128 (1955).

(40). Schlenk, W., Jr., Fortschr. chem. Forsch. 2, 92 (1951).

(41). Staveley, L.A.K., "Non-Stoichiometric Compounds" (L. Mandelcorn, ed.) p. 606, Academic Press, New York and London (1964).

(42). McLaughlin, R.L., "The Chemistry of Petroleum Hydrocarbons" B.T. Brooks and L. Schmerling, eds. Vol. 1, p. 241. Reinhold, New York, 1954.

(43). Mandelcorn, L., Chem. Revs. 59, 827 (1959).

(44). Child, W.C., Jr., Quart. Revs. 18, 321 (1964).

(45) Fetterly, L.C., "Resins Analysis" (C.P.A. Kappelmeier, ed.), chapter XV - B. Wiley, New York, 1959.

(46). Fetterly, L.C., "Non-Stoichiometric Compounds" (I. Mandelcorn, ed.).p. 491, Academic Press, New York and London (1964).

(47). Cramer, F.D., Revs. Pure Appl.Chem. 5, 143(1955)

(48). Smith, A.E., J. Chem Soc. p. 2416 (1951).

(49). Smith, A.E., Acta Cryst. 5 224 (1952).

(50). Hermann, C. and Lenne, H.U. von, Naturwissenschaften 39, 234 (1952).

(51). Schlenk, W., Jr. Ann. 565, 204 (1949).

(52). Lenne, H.V. von, Acta Cryst. 7,1(1954).

(53) Kutzelnigg, W., and Mecke, R.Z. Electrochem. 65, 109 (1961).

(54). Wyckoff, R.W.G. and Corey, R.B., Z. Krystallogr. 89, 102 (1934).

(55). Gorin, M.H. and Rosenstein, L., U.S. Patent 2,600,431 (1952).

(56). Mcadie, H.G. and Frost, G.B., Can. J. Chem. 33, 1275 (1955).

(57). Kyriacou, D., J. Org. Chem. 24, 987 (1959).

(58). Schlenk, W., Jr., Ann. 565, 204 (1949).

(59). Angla, B., Compt. rend. acad. sci. 224, 402, 1166 (1947).

(60). Zimmerschied, W.J., Dinerstein, R.A., Weitkamp, A.W., and Marschner, R.F., Indust. Engng. Chem. 42, 1300 (1950).

(61). Redlich, O., Gable, C.M., Dunlop, A.K., and Millar, R.W., J. Am. Chem. Soc. 72, 4153 (1950).

(62). Schlenk, W., Jr., Ann. 573 142 (1951).

(63). Zimmerschied, W.J., Dinerstein, R.A. Weitkamp, A.W. and Marschner, R.F., J. Am. Chem. Soc. 71, 2947 (1949).

(64). McAdie, H.G. , Can. J. Chem. 40, 2195 (1962)

(65) Miller, F.W., Jr., and Dittmar, H.R., J. Am. Chem . Soc. 56, 848 (1934).

(66). Gilson, D.F.R. and McDowell, C.A., Nature 183, 1183 (1959).

(67). Gilson, D.F.R. and McDowell, C.A., J. Mol. Phys. 4, 125 (1961).

(68). Andrew, E.R., "Nuclear Magnetic Resonance", p. 151, Cambridge University Press, 1958.

(69). Andrew, E.R., J. Phys. Chem. Solids. 18, 9(1961).

(70). Gutowsky, H.S. and Pake, G.E., J. Chem. Phys. 18, 163 (1950).

(71). Smith A.E., J. Chem. Soc. p. 2416 (1951).

(72). Meakins, R.J., Trans.Far, Soc. 51, 953 (1955)

(73). Dryden, J.S. and Welsh, H.K., Austral. J. Sci. Res. A. 4 , 616 (1951).

(74). Lauritzen, J.I., Jr., J. Chem. Phys. 28, 118 (1958).

(75). Hoffmann, J.D. and Pfeiffer, H.G., J. Chem. Phys. 22, 132 (1954).

(76). Fischer, P.H.H. and McDowell, C.A., Canad, J. Chem. 38, 187 (1960).

(77). Stuart, A.V., Rec. Trav. Chim. Pays-Bas, 75, 906 (1956).

(78). Barlow, G.B. and Corish, P.J., J. Chem.Soc. p. 1706 (1959).

(79). Stewart, J.E., J. Chem. Phys. 26, 248 (1957).

(80). Badger, R.M. and Waldron, R.D., J. Chem Phys. 18, 566 (1950).

(81). Durie, R.A. and Harrison, R.J., Spectrochimica Acta. 18, 1505 (1962(.

(82). Parsonage, N.G. and Staveley, L.A.K., Mol. Phys. 3, 59 (1960)

(83). Van der Waals, J.H., Trans. Far Soc. 52, 184 (1956).

(84). Van der Waals, J.H. and Platteeuw, J.C., Adv. in Chem. 2 , 1 (1959).

(85). Parsonage, N.G. and Staveley, L.A.K., Mol. Phys. 2, 212 (1959).

(86). Grey, N.R., Parsonage, N.G. and Staveley, L.A.K., Mol, Phys, 4, 153 (1961).

(87). Grey, N.R. and Staveley, L.A.K., Mol.Phys.7, 83 (1964).

(88). Meyer, H. and Scott, T.A., J.Phys. Chem. Solids 11, 215 (1959).

(89). Foner, S., Meyer, H. and Kleiner, W.H., J. Phys. and Chem. Solids 18, 273 (1961).

(90). Cooke, A.H., Meyer, H., Wolf, W.P., Evans, D.F. and Richards, R.E., Proc. Roy. Soc. A 225 112 (1954).

(91). Meyer, H., O'Brien, M.C.M. and Van Vleck, J.H. Proc. Roy. Soc. A 243, 414 (1957).

(92). Hexter, R.M. and Goldfarb, T.D., J. Inorg. and Nuclear Chem. 4, 171 (1957).

(93). Dryden, J.S., Trans. Far. Soc. 49, 1333 (1953).

(94). Edwards, J.W., Thesis, London, (1959).

(95). Edwards, J.W. and Kington, G.L., Trans. Far. Soc. 58, 1313 (1962).

(96). Southard, J.C. and Brickwedde, F.G., J. Am. Chem. Soc. 55, 4378 (1933).

(97). Davies, T. and Staveley, L.A.K., Trans. Far. Soc. 53, 19 (1957).

(98). Ginnings, D.C., Osborne, N.S. and Stimson H.F., J. Res. Nat. Bur. Stand. 23, 197 (1939).

(99). Meyers, C.H., J. Res.Nat. Bur.Stand. 9 807 (1932).

(100). Blanpied, W.A., and Powell, R.L., Nat. Bur. Stand., Circular 556,(1954).

(101). Buffington, R.M., Giaque, W.F., and Schulze, W.A., J. Am. Chem. Soc. 49, 2343 (1927).

(102). "Reference Table for thermocouples", Nat. Bur. Stand. Circular 561 (1955).

(103). Woolley, H. W., Scott, R.B. and Brickwedde, F.G. J. Res. Nat. Bur.Stand., 41, 379 (1948).

(104). Hoge, H.J., J. Res. Nat.Bur. Stand., 44, 321 (1950).

(105). Moessen, G.W., Aston, J.G. and Ascah, R.G., J. Chem. Phys. 22, 2096 (1954).

(106). Scott, R.B., Temperature, vol.II, p. 179 (1955), Reinhold, N.Y.

(107). Stimson, H.F., J. Res. Nat.Bur.Stand., 42, 209 (1949).

(108). Barber, C.R., Recent developments and techniques in the maintenance of standards Nat. Phys. Lab., (1951).

(109). Kistemaker, J., Physica II, 283 Leiden Comm. No. 268d (1945).

(110). Linder, B. The measurement of low temperatures, Westinghouse Res. Lab. Feb (1950). 2. R - 94433-2-A p. 21.

(111). Ginnings, D.C. and Furukawa, G.T., J. Am. Chem. Soc. 75, 522 (1953).

(112). Challoner, A.R., Gundry, H.A. and Meetham, A.R. Phil. Trans., A, 247, 553 (1955).

(113). Busey, R.H., (a) Ornl - 1828 (Jan. 26, 1955) (b). J. Am. Chem.Soc. 78 3263 (1956).

(114). Cole, A.G., Hutchens, J.D., Robie, R.A., and Stout, J.W., J. Am. Chem.Soc., 82, 4807 (1960).

(115). Osborne, D.W., Westrum, E.F., Jr., and Lohr H.R., J. Am. Chem. Soc., 77, 2737 (1955).

(116). Parks, G.S., Huffman, H.M., and Barmore, M., J.Am. Chem. Soc., 55, 2733 (1933).

(117). Sklyankin, A.A., and Strelkov, P.G., Znurnal Prikladnoy Mekhaniki I Tekhnicheskoy Fiziki, Moscow, 2, 100 (1960).

(118). Andon, R.J.L., Counsell, J.F., Herington,E.F.G., and Martin J.S., Trans.Far.Soc., 59, 830(1963).

(119). Martin, D.L., Can. J. Phys., 38, 17 (1960).

(120). West, E.D., J. Res. Nat. Bur. Stand., 67A, 331 (1963).

(121). Ginnings, D.C. and West, E.D., Rev. Sci. Inst., 35, 965 (1964).

(122). Coops, J., Jessup, R.S., and Van Nes, K., Experimental Thermochemistry ed. Rossini, F.D., (Interscience N.Y. 1956).

(123). Krafft, F., Ber., 15, 1698 (1882).

(124). Egloff, G., Physical constants of the hydrocarbons (1939).

(125). Physical properties of Hydrocarbons, Nat. Bur. Stand. Circular 461, (1947).

(126). Johnson, G.D., Kiser, R.W., and Shetlar, D.M., Ann. Chem., 33, 314 (1961).

(127). Huffman, H.M., and Ruehrwien, R.A., J. Am. Chem. Soc., 68, 1759 (1946).

(128). Huffman, H.M., Finke, H.L., Gross, M.E., and Waddington, G., J.Am. Chem. Soc., 76, 333 (1954).

(129). Beattie, J.A., J.Math. Phys., 6, 1 (1926).

(130). Müller, A., Proc. Roy. Soc. (Lond), A 127, 421 (1930).

(131). Bunn, C.W., Trans. Far. Soc., 35, 482 (1939).

(132). Smith, A.E., J. Chem. Phys., 21, 2229 (1953).

(133). Shearer, H.M.M., and Vand, V., Acta Cryst., 9, 379 (1956).

(134). Pinsker,Z.G. and Vainshtein,B.K., Doklady. Akad. Nauk S.S.S.R., 72, 53(1950).

(135). Oldham,A.R. and Ubbelohde,A.R., Trans. Far. Soc., 34, 282(1938).

(136). Ubbelohde,A.R. and Oldham,A.R., Proc.Roy.Soc., A176, 50(1940).

(137). Lonsdale,K., Proc. Phys. Soc., 54, 314(1942).

(138). Parsonage,N.G. and Staveley,L.A.K., Mol. Phys., 3 , 59(1960).

(139). Grey,N.R., Parsonage,N.G. and Staveley,L.A.K., Mol. Phys.,4 , 153(1961).

(140). Westrum,E.F. Jr., Symposium Lund (Plenary Lectures) p. 193,(1963).

(141). Kelley,K.K., J. Am.Chem. Soc.,51, 180(1929).

(142). Kassel,L.S., J. Chem.Phys.,4 , 493(1936).

(143). Gupta,A.K. and Staveley,L.A.K., Trans. Far. Soc., 45, 50(1949).

(144). Domb,C., Adv. in Phys., 9, 149(1960).

(145). Pauling,L., The Nature of the Chemical Bond, p.260, Cornell Univ. Press(1960).

(146). London,F., Z. Phsik. Chem. B 11, 222(1930).

(147). Kirkwood,J.G., Phsik Z., 33, 57(1932).

(148). Müller,A., Proc. Roy. Soc., A 154, 624(1936).

(149). Kirkwood,J.G. and Slater,J.C., Physic.Rev. 37, 682(1931).

(150). Rowlinson,J.S., Quart. Revs., 8, 168(1954).

(151). Pitzer,K., Adv. in Chem. Phys.,2, 59(1959).

(152). Silberstein,L., Phil. Mag., 33, 92(1917).

(153). Evans, D.F. and Richards,R.E., Proc. Roy. Soc. (Lond.)., A223, 238(1954).

(154). Müller,A., Proc. Roy. Soc.(Lond.)., A178,227(1941).

(155). Brandt,W., J. Chem. Phys., 24, 501(1956).

(156). Brandt,W., J. Chem. Phys., 26, 262(1957).

(157). Billmeyer,F.W., J. Appl. Phys., 28, 1114(1957).

(158). Ising,E., Z. Physik, 31, 253(1925).

(159). Newell, G.F., Phys. Rev., 78, 444(1950).

(160). Domb.C., Adv. in Phys., 9, 149(1960).

(161). Onsager, L., Phys. Rev., 65, 117(1944).

(162). Kramers,H.A. and Wannier, G.H., Phys. Rev., 60, 252(1941).

(163). Howe,J.P. and Lassettre, E.N., J. Chem. Phys., 9, 747(1941).

(164). Montroll, E.W., J. Chem. Phys., 9, 706(1941).